BNWL-1064
UC-80

4-
6-70

[redacted]

FFTF FUEL PIN AND SUBASSEMBLY CONCEPTUAL DESIGN METHODS AND DATA

June 1970

[redacted]

AEC RESEARCH & DEVELOPMENT REPORT

ROUTE TO	NAME	LOCATION	FILED ROUTE DATE

BATTELLE NORTHWEST
BATTELLE MEMORIAL INSTITUTE PACIFIC NORTHWEST LABORATORIES
BATTELLE BOULEVARD, P. O. BOX 999, RICHLAND, WASHINGTON 99352

BNWL-1064

LEGAL NOTICE

PACIFIC NORTHWEST LABORATORY
RICHLAND, WASHINGTON
operated by
BATTELLE MEMORIAL INSTITUTE
for the
UNITED STATES ATOMIC ENERGY COMMISSION UNDER CONTRACT AT(45-1)-1830

AEC-RL RICHLAND, WASH.

BNWL-1064
UC-80, Reactor
Technology

FFTF FUEL PIN AND SUBASSEMBLY CONCEPTUAL DESIGN METHODS AND DATA

E. G. Stevens
P. D. Cohn
R. J. Jackson
D. C. Kolesar
C. L. Mohr
A. Padilla
C. L. Wheeler

June 1970*

*Originally published in May 1969 in Draft Issue (OUO) form.

BATTELLE MEMORIAL INSTITUTE
PACIFIC NORTHWEST LABORATORIES
RICHLAND, WASHINGTON 99352

Printed in the United States of America
Available from
Clearinghouse for Federal Scientific and Technical Information
National Bureau of Standards, U.S. Department of Commerce
Springfield, Virginia 22151
Price: Printed Copy $3.00; Microfiche $0.65

FFTF FUEL PIN AND SUBASSEMBLY CONCEPTUAL DESIGN METHODS AND DATA

E. G. Stevens
P. D. Cohn
R. J. Jackson
D. C. Kolesar
C. L. Mohr
A. Padilla
C. L. Wheeler

ABSTRACT

The major technical bases for the FFTF first core fuel assembly conceptual design are presented in four general categories: (1) thermal, (2) hydraulic, (3) structural and (4) performance-manufacturing design characteristics. Recommended design values and conceptual engineering drawings of the fuel pin and subassembly are included.

TABLE OF CONTENTS

LIST OF FIGURES

FFTF FUEL PIN AND SUBASSEMBLY CONCEPTUAL DESIGN METHODS AND DATA

E. G. Stevens
P. D. Cohn
R. J. Jackson
D. C. Kolesar
C. L. Mohr
A. Padilla
C. L. Wheeler

INTRODUCTION

The major technical bases for the Fast Flux Test Facility fuel assembly conceptual design[100] are presented. The methods used to determine the design points and the recommended data for the FTR first mixed oxide core are discussed. Included are descriptions of the design point or range, the uncertainties involved and references to in-depth discussions of the data. The information is divided into four broad categories:

1. Thermal Design and Behavior
2. Hydraulic Behavior and Design Methods
3. Structural Design
4. Performance and Manufacturing Characteristics

The thermal behavior of the fuel pin and subassembly are investigated in Section 1.0 and recommended design curves for the required thermal conductivities and heat transfer coefficients are derived. Steady-state fuel and subassembly thermal descriptions are presented. Conditions that alter these nominal temperatures are treated, e.g., hot channel factors, pin touching and transient effects.

The fuel and subassembly hydraulic behavior is covered in Section 2.0 by the orificing and pressure drop analyses, the vibration and fretting as well as erosion and corrosion effects. Design considerations for the entrance and exit regions and spacer system are included.

The structural design of the pins and subassembly presented a significant challenge due to the high fast neutron fluence damage effects anticipated in the FTR. The lengthy Section 3.0 treats the swelling effects of the fuel, clad and coolant duct and gives the bases for the mechanical design of the clad and plenum. Operational considerations such as the change of clad properties with temperature and neutron exposures stresses and strains, fatigue effects and stress relaxation are presented. Core restraint, axial shielding and fuel assembly holddown design are discussed.

Section 4.0 covers many of the aspects of performance and manufacturing that must be investigated due to their influence on the fuel subassembly design. Burnup limits and anticipated fuel management schemes influenced the gas plenum sizing and orificing analyses. The core zoning and axial shielding affect the fuel enrichment with consequent thermal design considerations. Fuel cycle costs are estimated to provide the basis for determining total FTR operating costs.

The four sections, taken together, enable the core designer to establish the maximum allowed pin linear power and operating environment within the established design constraints[100] (e.g., the maximum allowed transient fuel temperature is incipient melting). Use of the nuclear radial and axial power shape factors yields the average pin power and provides the number of pins or core volume required for a given design average core power.

Document BNWL-1102, U.K. Commercial Data Employed in FFTF Fuel Pin and Subassembly Conceptual Design, was issued separately, with limited distribution.

1.0 THERMAL DESIGN AND BEHAVIOR

1.1 FUEL THERMAL PROPERTIES

The operational design basis for the fuel pins is that they be capable of continuous operation at a linear power such that a 20% increase in nominal power will raise the center-point temperature of the hottest pin just to incipient melting. Fuel thermal properties selected for use in the pin design directly affect the maximum allowable linear power to achieve incipient fuel melting. Thermal conductivity (k) and the melting point (T_m) of the mixed oxide fuels, as well as the physical behavior (sintering with central void formation) must be considered in fixing the pin design. Since k and T_m vary with fuel density, stoichiometry, enrichment and burnup, a recommended design curve of $\int k dT$ was developed[1] from recently published data for mixed oxide fuel with representative properties at the beginning-of-life [<10,000 MWd/tonne (Pu+U)] (BOL) and end-of-life [>10,000 MWd/tonne] (EOL): 20 wt% PuO_2–UO_2, 88% smeared theoretical density and an oxygen-to-metal ratio of 1.98. Figure 1.1-1 is the recommended $\int k dT$ design curve for FTR fuel design.

Recently published data[2] indicate that the reduction in the fuel melting point with burnup is less than previously determined by extrapolation to the goal burnup.[1] Figure 1.1-6 shows the effect of stoichiometry on melting point for unirradiated mixed oxide fuel. (Recent data by Aitken and Evans [GE, PA-53 program, unpublished] indicated T_m (O/M = 2.00) > T_m (O/M = 1.97). They show little change in T_m in the range of an O/M of 1.96 to 2.00. The T_m = 2860 °C for 20 wt% PuO_2–UO_2, O/M = 2.00, liquidus, is high compared to the data from the references used in Figure 1.1-6. No weight is given to this soon-to-be published information.)

Figure 1.1-7 shows the experimentally measured melting temperatures for 20 and 25 wt% PuO_2–UO_2, O/M = 2.00, as a

function of burnup. The effect of burnup on stoichiometry has not been extensively investigated although preliminary work by Christensen[3] indicates that an O/M gradient tends to develop across the radius of the irradiated fuel pellet. In general, the oxygen tends to redistribute to create a stoichiometric material (O/M = 2.00) at the cooler fuel surface. This means the hotter interior of an initially substoichiometric material will tend to lose oxygen and become further substoichiometric. Additional work is required in this area to clarify the long term effects of O/M on the fuel melting point. Craig's oral presentation of the data[2] indicated that fuel samples were taken from various radial locations across the pellet, which was ultrasonically cut in a checkerboard pattern, providing many samples per pellet. This makes the reported data lack the potential for extracting the information as to whether the central fuel melting point differs from the surface fuel value, after extended burnup. However, since the fuel was initially fabricated with an O/M = 2.00, the stoichiometry should have remained constant across the radius according to Christensen's findings.

For 20 to 25 wt% PuO_2–UO_2, O/M = 1.97 to 1.98, the melting point values recommended for design purposes are:

<10,000 MWd/tonne (Pu+U)	2810 ± 30 °C
>10,000 MWd/tonne (Pu+U)	2715 ± 63 °C

For hot channel analyses a melting point value of 2680 °C (4850 °F) has been selected. It is judged as being compatible with the probability of occurrence of the other parameters.

In-reactor sintering or densification of the fuel in the high temperature regions is accounted for in the SINTR design program[4] in determining the operational power required to produce melting. The resultant central hole formation lowers the peak fuel temperature for a given linear power. A sintering correction factor (SCF) is applied to the nominal power to calculate the larger operational power to achieve melting.[5]

Figure 1.1-2 plots the required nominal pin linear power to achieve incipient melting (no hot channel effects considered), the SCF and the nominal $\int kdT$ versus pin smeared density.

Safety analyses require the Heat of Fusion and Specific Heat of the mixed oxide fuel as input parameters. Based on the work of Hein[6] and Epstein,[7] a heat of fusion for PuO_2—UO_2 of 18.1 kcal/mole (280 j/gm) is recommended for FTR use. Since the specific heat (C_p, at a constant pressure) varies considerably with temperature, Figure 1.1-3 is recommended for use, based on the experimental work of Hein,[6] Ogard[8] and Godfrey.[9] The heat of fusion enables the transient model to take advantage of the "thermal arrest" period just prior to melting during which the peak fuel temperature does not significantly change, while an energy input (enthalpy rise) occurs that is equivalent to approximately a 380 °C temperature rise.

The thermal expansion of mixed oxide fuel has been measured by Roth[10] and Berggren.[11] Roth's X-ray diffraction measurements of the change in the lattice parameter with temperature for 20 wt% PuO_2—UO_2 fuel appear too high when compared with his thermal expansion coefficient (α) data. The reported oxygen-to-metal ratio was 2.10 which should have tended to lower rather than raise the α.[12] Figure 1.1-4 presents Berggren's data, which agrees with Roth's reported α, and is recommended for design purposes.

The expansion is reasonably isotropic in the fuel temperature regions of interest and the following relationship applies for unrestrained pellets:

$$\Delta V/V = 3\ \Delta L/L, \text{ where } \Delta L/L \simeq \Delta D/D$$

The effective in-reactor radial and axial thermal expansion are affected by plastic flow and the central void formation resulting from high temperature sintering. Asamoto's work[13] indicates that the axial expansion of flat-ended pellets is governed

by the maximum fuel temperatures up to approximately 1000 °C; for higher peak temperature the value at approximately 40% of the radius was found to be required to match the out-of-reactor, centrally heated fuel pellet stack expansion. These experiments produced a hyperbolic thermal gradient, while the FTR in-reactor case will have a parabolic gradient, making the data of limited usefulness. However, for a common peak temperature, the in-reactor effective axial expansion temperature would be approximately the volumetric average temperature, which is recommended for FTR design purposes between 1000 to 1800 °C. The diametral expansion characteristics observed by Asamoto[13] were similar to the axial expansion of the flat-ended pellets, although the radial slot to the pellet center hole may have affected his results. It is recommended that the volumetric average temperature also be used as the effective radial expansion temperature between ambient and 1800 °C. At higher temperatures the fuel is assumed to crack or plastically flow into the central void region. A previous analysis,[14] using a fuel linear expansion curve similar to Figure 1.1-4, indicated that the peak power pin could be expected to expand the fuel column height by ∿1%, due to the thermal effects from ambient to full power conditions. Further analysis is required to relate an average core expansion to possible physics effects. See Section 3.2 for thermal expansion and end effects.

A typical thermal expansion curve of 316 SS clad material is also shown in Figure 1.1-4 to permit determination of the expected operational, beginning-of-life fuel-clad gap and pin diameter for hydraulic considerations.

The volume expansion of mixed oxide fuel on melting has not been measured and reported in the literature. Data for UO_2 have been published by Lyons[15] and Christensen.[16] Both sets of experiments had rather large uncertainties associated with their results. A value of 8 ± 4% volume expansion on melting

covers both references and is recommended for FTR design use. This assumes the mixed oxide behaves in a manner similar to UO_2.

Fuel restructuring occurs as the temperature is increased,[17] as shown in Figure 1.1-5. The resultant growth of equiaxed and columnar grains tends to cause the initial, cold assembly gap between the fuel and clad to close and the characteristic annular fuel configuration to be formed in the higher temperature regions. The heat transfer characteristics are favorably altered by these changes. This yields a lower peak fuel temperature for a given power at equilibrium operating conditions as compared to the initial conditions with new fuel. A startup procedure which allows restructuring to occur will minimize peak fuel temperatures as full power is achieved.

Optimized startup procedures for the initial core loading and subsequent partial reloadings must still be determined. For the probable peak fuel temperature in the core of approximately 2200 °C (4000 °F), unirradiated fuel will take ∿7 hours for columnar grain growth to occur.[17] It is anticipated that fuel restructuring startup considerations will be no more restrictive than the thermal shock considerations which limit the rate of change of system temperature on approach to full power.

1.2 GAP SELECTION AND FUEL-CLAD GAP COEFFICIENT

The specification of the design fuel-clad diametral gap is based on operational as well as fabrication considerations. Since the temperature drop across the gap contributes directly to the peak fuel temperature, it is desirable to maximize the gap conductance. At beginning-of-life conditions, the as-fabricated gap and backfilling gas determine the gap heat transfer coefficient. However, in-reactor operation soon distorts the initial physical arrangement. A review of recent fast reactor fuel pin irradiation data concluded that the gap closes early in life for initial diametral gaps of 0 to 4 mils.[18]

The French have reported that an initial 9 mil diametral gap was fully closed at 10,400 MWd/tonne for pins operating at >10 kW/ft.[19] Hence, the gap or gap heat transfer coefficient is a dynamic quantity early in life, probably reaching an aysmptotic value at approximately 10,000 MWd/tonne in the high power regions of the core. This tends to indicate that a fuel-clad gap allowance for accommodating fuel irradiation swelling is not necessarily beneficial as earlier hypotheses indicated. Additionally, fast reactor clad damage analyses indicate the possibility that fuel swelling contributes only a minor fraction of the total pin diametral swelling observed at 45 to 60,000 MWd/tonne.[20] Transient overpower design considerations place requirements on the fuel smeared density which are independent of the fuel-clad gap.[18] Hence, the operational requirements for gap size are minimal and appear to affect only the required burnup to achieve gap closure.

The selection of the fuel-clad diametral gap is more strongly influenced by fabrication and safety considerations. To assure that assembly clearances exist between the pellets and clad tube under production scale manufacturing conditions, the readily achievable tolerances for the pellet OD and clad ID must be considered. An additional factor is the minimum acceptable fertile-to-fissile ratio [FTFR] (a major influence on the core Doppler coefficient). Since the critical mass fixes the fissile requirements for a given core size, the smeared density and FTFR are determined by the amount of fertile diluent. Hence, the permissible gap range is constrained by the pellet density which can be readily manufactured for a reasonably well defined smeared density, as set by the fertile-to-fissile ratio considerations. Therefore, core safety and fabricability are the principal governing requirements on gap size within the range of smeared densities being considered for the driver fuel (80 to 90% TD).

A smeared fuel density of approximately 88% TD is required to satisfy the safety, fabrication and operational considerations.[18,21] A consistent set of related parameters, using a pellet density which is readily achievable on production runs, (see Section 4.4) is:

Smeared Density	88% TD
Pellet Density	93 ± 2% TD
Pellet OD	0.194 ± 0.0015 in.
Clad ID	0.200 ± 0.001 in.
Fuel-Clad Gap	6 ± 1.8 mils

The design gap heat transfer coefficient (h_{gap}) associated with a nominal 6 mil diametral gap in based principally upon extrapolation of experimental data since analytical methods to predict gap coefficients have been relatively unsuccessful.[18] Figure 1.2-1 shows h_{gap} as a function of initial, cold diametral gap. Baily's (GE-APO) experimental data[22] for beginning-of-life, or lightly irradiated conditions, were obtained from relatively high power capsules (∿20 kW/ft), while Cohen's (Bettis) data[23] were for lower power conditions (∿3 kW/ft); Ross's (Canadian) out-of-reactor work[24] deals with interfacial pressure and temperature and serves mainly to fix the zero gap condition at 200 psi pressure. As noted earlier, in-reactor operation tends to close the initial gap. An analysis of fast reactor data with burnups of 50,000 MWd/tonne indicated that gap coefficients of 2000 to 3000 must have existed to result in the observed fuel postirradiation conditions.[25] The initial gaps were <2 mils, making the data of little value for the 6 mil gap coefficient. However, recent RAPSODIE data[19] indicated full gap closure at 10,400 MWd/tonne and fuel stuck to the clad at 20,000 MWd/tonne at powers >10 kW/ft in pins with initially 9 mil gaps. This suggests a gap coefficient of at least 2,000 Btu/hr-ft^2-°F for this latter condition, based on Ross's work.[24] The upper curve of Figure 1.2-1 therefore

appears reasonable for burnups greater than 20,000 MWd/tonne. Figure 1.2-2 is the recommended design gap coefficient for the nominally 6 mil gap pins.

Helium is recommended as the backfill gas, at 1 atm, based on its chemical inertness and comparatively good heat transfer characteristics.

1.3 CLAD SURFACE TO COOLANT HEAT TRANSFER COEFFICIENT

The average surface heat transfer coefficient is predicted to range between 25,000 to 50,000 Btu/hr-ft^2-°F. This results in only a small contribution to the average total temperature level, i.e., 0 to 20 °F and is thereby considered unimportant. Local depression of the energy transfer rate as well as the heat transfer coefficient due to various geometric asymmetries can result in local hot spots. To date, only the local effect of a 30 mil wire in an infinite array[26] has been considered. The method of solution involved a graphical method due to Dwyer[27] modified to incorporate the wire after a technique employed by Deissler and Taylor.[28] Update of this problem, as well as the consideration of pins on the outer periphery of the bundle and imperfectly positioned fuel pellets, should be considered for the present design.[29,30] Computer codes are being developed at BNW to expedite the necessary calculations. The most important application of these data is to bowed and touching pins. Reduction of the surface heat transfer coefficient where the wire wrap traverses the pin-pin closest approach point may cause an additional 25 to 60 °F peak in the cladding temperature at those points. This estimate of the peaking is conservative both in the design analyzed and assumptions made.

The h_f recommended design value is 37,500 ± 12,500 Btu/hr-ft^2-°F. Experimental verification during preliminary design is required to reduce this uncertainty.

1.4 HOT CHANNEL FACTOR ANALYSIS

Operational design limits are set on the maximum allowable fuel and clad temperatures to enable fuel pin safety and lifetime requirements to be met. Incipient fuel melting (∿4850 °F) at the hottest point in the core during an overpower condition is the fuel limit specified in the Basic Design Requirements.(100) The clad will be designed to operate at a local maximum temperature of ∿1150 °F for 12 months continuous operation, which has been fixed as a Firm Design Choice.(100)

Temperature distributions throughout the core can be calculated for the nominal steady-state or overpower conditions. However, the actual temperatures in the operating core will probably vary from these idealized, nominal temperatures due to the allowed manufacturing tolerances in the core components (fuel fissile content, pin OD, etc.), prediction uncertainties (coolant flow or neutron flux distribution, heat transfer coefficients, etc.) or operational considerations (instrumentation error, control band, etc.). The hot channel factors are the link between the nominal calculated temperatures in the core and the probable and maximum expected temperatures. Since the upper operational design limits are fixed, the hot channel factors effectively serve to establish the nominal operating conditions, including the nominal or allowable average pin linear power. Although safety and reliability considerations indicate large hot channel factors are desirable, practical considerations dictate that realistic values be determined which will give only a reasonable degree of confidence that the design limits will not be exceeded. Otherwise, core performance will be penalized, resulting in an unnecessarily large core volume and a proportionately low flux for a given core power.

Determining the Hot Channel Factors or Hot Spot Factors is not a task which lends itself to an exact solution. The literature contains numerous articles expounding equally as many

approaches to the treatment of this problem. Fenech and Gueron recently reviewed the principal methods of core design uncertainty analysis.[31] They proposed still another method of combining the many subfactors which contribute to the uncertainty to be assigned to the nominal maximum design conditions.

The FERMI fast reactor was designed by assuming each hot channel contributor had a normal distribution about its nominal design value with the uncertainty limits being taken as three standard deviations (3σ) (the statistical method).[32] Each contributor resulted in a change in the nominal ΔT's from the core inlet temperature to the point of maximum fuel temperature. These were statistically combined to produce an overall resultant change in the nominal design peak fuel temperature which was claimed to have a probability of occurrence associated with a 3σ limit.

The EBR-II fast reactor was initally designed by treating each of the ΔT's from the core inlet temperature to the point of maximum fuel temperature as a separate item with its associated hot spot factor (the deterministic method).[33] The various contributors to the ΔT uncertainty were multiplied together to find the combined effect. However, it was recognized that there was some probability of the various contributors all occurring simultaneously at the same location with the maximum magnitude, so a rather arbitrary $\times$ 2/3 factor was applied to the predicted deviations from nominal conditions.

The hot channel analysis presented by Combustion Engineering in their 1000 MW_e study combined both of the approaches used in FERMI and EBR-II by treating some items as direct contributors ("...because they could not be expected to be normally distributed about a nominal value") and others as statistical contributors.[34] The product of these two resultant sub-factors was taken as the hot channel factor to be applied to the appropriate ΔT (e.g., $\Delta T_{coolant}$, ΔT_{film}), in a manner similar to the EBR-II approach.

Each of the methods cited above were applied to the nominal maximum temperature point of interest to determine the more restrictive hot channel temperature. No realistic probability of occurrence was assigned to this condition. Both EBR-II and Combustion Engineering implied a certainty of occurrence. FERMI's 3σ limit was quite arbitrary, and considered only the maximum power pin. The possibility that a large number of pins, running at a slightly lower power level, could have a combined probability greater than the 3σ limit of operating at some temperature very near the calculated peak hot channel temperature was not treated.

The "best" method of hot channel analysis is not readily apparent. The most serious deficiency in this realm of nominal maximum design conditions as compared to actual operating conditions is that there is no published data comparing theory to experiment for an operating reactor system. The methods are certainly adequate as attested to by the many operating reactors; that they are or were overly conservative is indicated by the fact that large commercial reactors being designed today are using hot channel factors which have continually decreased with each core design and are now approximately half of the values used for the YANKEE-ROWE reactor (startup in 1961).[35] Experience has apparently shown that the magnitude of the controllable uncertainties (e.g., fissile content, instrumentation control band, etc.) could be reduced or that the combined effects of the individual uncertainties was less than initially calculated.

1.4.1 Method of Analysis

The FTR Hot Channel Factor (HCF) analysis treats each of the ΔT's from the reference core inlet temperature (ΔT of coolant, surface film, clad, gap and fuel) as a separate item with its associated hot channel factor. Deviations from the nominal design parameters are evaluated in terms of percent

change in the affected nominal ΔT. Parameters which contribute to the HCF are divided into two categories:

1. Direct Contributors - deviations from the nominal design parameters which are certain to occur (a probability of occurrence of 1.0) at some time during the fuel lifetime and in a given direction (e.g., power control band allowance + 2%, intra-subassembly flow maldistribution + 15%, etc.).
2. Statistical Contributors - deviations which can be expected to have a probability of occurrence over some defined range. A normal distribution is assigned to the uncertainties about the nominal value and the limits are chosen to include all reasonably expected extremes (the 3σ limit with a probability of occurrence of 0.0013) (e.g., fissile fuel content ±3.3%, power level measurement ±9%, etc.).

Table 1.4-1 summarizes the Hot Channel Factor contributors and their magnitudes. Bases for their selection are presented in the following section.

Combining the contributors to determine the net effect is accomplished by recognizing that each of the individual contributors can act independently of all others, but that there is dependence between the temperature drop regions for any single contributor. The combined effect of the direct contributors is multiplicative in any ΔT region and when applied to the nominal temperature rise, yields the PROBABLE peak ΔT. The statistical effects cannot be so easily related to individual ΔT regions due to their ± nature and dependence. Application of the maximum value of the statistical contributors to the probable ΔT yields the MAXIMUM EXPECTED peak ΔT, with some probability of occurrence. The following mathematical treatment is used to calculate the FTR peak fuel and clad hot spot temperatures (See Table 1.4-1 for regions i and contributors j).

TABLE 1.4-1. Hot Channel Factors

Radial Factor = 1.40
Axial Factor = 1.24
Overpower Factor = 1.20

CONTRIBUTOR	i = 1 Coolant	2 Film	3 Clad	4 Gap	5 Fuel
A. Direct					
j = 1. Inlet Flow Maldistribution	1.05	1.02	-	-	-
2. Intrasubassembly Flow Maldistribution	1.15	1.06	-	-	-
3. Interchannel Coolant Mixing	0.99	-	-	-	-
4. Power Control Band	1.02 (a)	1.02 (a)	1.02 (a)	1.02 (a)	(1.011) (a,c)
5. Wire Wrap Temp. Peaking	-	2.00	-	-	-
a_i = Product	a_1 = 1.219	2.206	1.02	1.02	(1.011) (c)
B. Statistical ($3\sigma_{ij}$ Limit)					
j = 6. Fissile Fuel Maldistribution	±2.3% ($3\sigma_{16}$ = .023)	±3.3%	±3.3%	±3.3%	(±2.39%) (c)
7. Power Level Measurement	±9.0%	±9.0%	±9.0%	±9.0%	(±6.48%) (c)
8. Burned Fuel Reload	±1.2%	±1.2%	±1.2%	±1.2%	(±0.84%) (c)
9. Rod Diameter, Pitch and Bow (b)	±2.0%	±0.9%	-	-	-
10. Film and 11. Gap Coefficient	- -	±33.0% -	- -	- ±40.0%	- -
12. Fuel and 13. Clad Conductivity and Tkns.	- -	- -	±12.0% -	- -	- (±7.22%) (c)
$\left[\sum_{j=6}^{13}(3\sigma_j)^2\right]^{1/2}$ = Statistical Combination	±9.58%	±34.40%	±15.41%	±41.15%	(±10.03%) (c)

a. Value goes to 1.0 at overpower.
b. Bow not considered yet.
c. Equivalent ΔT_{fuel} contributor at 12.2 kW/ft as used in calculations (varies with power).

In general:

$$T = T_o + \sum_i a_i \, \Delta T_i + \sum_i a_i \, \Delta T_i \sum_j X_{ij}$$

where i = 1 through 5 for fuel peak T, and 1 through 3 for clad peak T

j = 6 through 13

T = temperature of interest

T_o = coolant inlet temperature

a_i = product of direct contributors, j = 1 through 5, in ΔT region i

ΔT_i = nominal temperature change in region i

X_{ij} = any magnitude of the statistical contributor j in region i, within the maximum ± limits specified.

The X_{ij} have a joint normal distribution with parameters:

expected value $E(X_{ij}) = 0$

variance $V(X_{ij}) = (3\sigma_{ij})^2$

and covariance $Cov(X_{ij}, X_{i'j'}) = \rho_{ij\ i'j'} \, 3\sigma_{ij} \, 3\sigma_{i'j'}$, (where ρ = 1 for dependence and zero for independence among the X_{ij}, $i < i'$ and $j = j'$).

T is taken to be a normally distributed random variable with parameters:

$$\text{expected value } E(T) = T_o + \sum_i a_i \, \Delta T_i$$

$$\text{and variance } V(T) = \sum_i a_i^2 \, \Delta T_i^2 \sum_j V(X_{ij}) + 2 \sum_{\substack{i<i' \\ \text{and } j = j'}} a_i a_{i'} \, \Delta T_i \, \Delta T_{i'} \, Cov(X_{ij} \, X_{i'j'}).$$

The PROBABLE temperature is E(T) and the MAXIMUM EXPECTED temperature is $E(T) + V(T)^{1/2}$. Figures 1.4-1 through 1.4-4 plot hot spot peak fuel and clad temperatures as a function of steady-state peak pin power. The design limit of incipient

fuel melting at 4850 °F at end-of-life defines the pin linear power limit and hence total core power as shown in Figure 1.4-1. The nominal, non hot channel temperatures, and peak power subassembly coolant mass flow used in this analysis are presented in Figures 1.4-5 and 1.4-6. Orificing was taken to produce a nominal coolant temperature rise of 360 °F in the peak power subassembly. The total core ΔT was nominally 300 °F, varying with pin power to accommodate orificing and the maximum core power produced. Adjusting the inlet temperature and total core mass flow rate may be required in preliminary design to achieve approximately the maximum expected temperatures with the 300 to 350 °F core ΔT desired.

Figure 1.4-7 schematically depicts the interrelationship between pin power, peak temperature and frequency of occurrence. Although the direct contributors are assigned a relative frequency of occurrence of 1.0, the statistical contributors have some probability of occurrence. If they are individually chosen to represent 3σ confidence limits and are normally distributed, their combined effect will represent a 3σ limit. Figures 1.4-8 through 1.4-11 show the relative frequency of occurrence and the probability that the peak power pin fuel or clad temperature is greater than a given temperature. For the design limit of the fuel, which is incipient melting at overpower, the maximum expected temperature becomes the limiting constraint. However, for the clad limit of an 1100 to 1200 °F upper operating range, with no well defined cutoff point, the relative frequency of occurrence becomes an important consideration in assessing the design conditions.

The HCF contributors were assumed to be normally distributed with values fixed at 3σ limits. The effect of this assumption on Figures 1.4-8 through 1.4-11 should be checked in preliminary design. Use of a distribution-free approach may be desirable. The analysis should also be further developed to include larger

groups of pins operating at less-than-peak conditions which will have a greater relative frequency of occurrence at the slightly lower maximum expected temperature.

1.4.2 HCF Contributors

The individual contributors considered in this analysis, which affect one or more of the five separate ΔT regions, are listed below. The magnitudes of the deviation from the nominal ΔT's are given along with the bases for selection. Table 1.4-1 summarizes the contributors.

Direct Contributors

1. Inlet flow maldistribution (+5% resultant $\Delta T_{coolant}$ and +2% ΔT_{film})

   Basis: engineering judgement, since the centerline peak power fuel assembly is located at the farthest distance from the coolant inlet pipes into the high pressure plenum. The actual mass flow distribution to the various assemblies across the core would have to be verified by a hydraulic mockup of the plenum region. Deviations would be less for assemblies closer to the inlet pipes (e.g., zoned peak power pins). The ΔT_{film} effect reflects the resultant lower than nominal velocity. For an orificed core which compensates for the high pressure plenum flow maldistribution, this contributor represents the uncertainty in actual orificed flow.

2. Intra-subassembly flow maldistribution (+15% $\Delta T_{coolant}$ and +6% ΔT_{film})

   Basis: engineering calculations using the nominal design pin bundle and flow duct dimensions with loose packing. Experience gained in constructing a full scale hydraulic test subassembly of wire wrapped pins has indicated that the long, slender pins are supple enough so that the as-built pin bundle nearly fills the space allowed inside

of the flow duct. Idealistic tight bundle packing, with the radial assembly clearance maintained, will result in a calculated +20% $\Delta T_{coolant}$; optimistic loose packing results in a +12% change for a central pin. Peripheral pins in the bundle will experience a larger mass flow rate, reducing these contributors, depending on the degree of loose packing.

Intrachannel coolant mixing effects which tend to offset the flow maldistribution is treated in the following section.

3. Interchannel coolant mixing (-1% $\Delta T_{coolant}$)

   Basis: engineering calculations using a mixing factor $\beta = 0.01$ in the COBRA thermal-hydraulic program with a negligible power profile across the fuel assembly (centerline core location). All subassemblies other than the one at the core centerline considered here will have power gradients across them with enhanced coolant mixing which will tend to reduce this $\Delta T_{coolant}$; peripheral pins in each fuel bundle will also have significantly enhanced cooling; the acting of other hot channel subfactors creates a radial temperature gradient between coolant subchannels which is counteracted by enhanced mixing. Hence, the magnitude used for this subfactor is a "worst case" since little credit is assigned to the interchannel mixing which does occur to varying degrees.

4. Power control band (+2.0% on all ΔT's)

   Basis: Nuclear instrumentation provides an extremely sensitive tool for reactor control. Large power reactor

operating experience at Hanford indicates that <±2.0% at a given power level is a normal capability. This contributor is treated as "direct" since it has a high probability of occurrence at either extreme at some time during the total core lifetime. The items contributing to the control band include power overshoot, instrument tolerance, shim rod stepping increment and minor system instabilities (thermal, burnup, etc.). Automatic power cutback will be used at the upper control band. Uncertainty in the absolute power level is treated under No. 7, Power Level Measurement.

This contributor is considered to be zero in the overpower condition since the core is not intended to operate continuously at this power level which represents an absolute upper design limit, i.e., the overpower factor is applied to the nominal, hot channel power condition.

5. Wire Wrap Temperature Peaking (+100% equivalent on the film ΔT).

   Basis: Engineering calculations have indicated the clad region near the point of contact between the wire wrap spacer and the pin is elevated above the nominal clad temperature.[36] Since the wire is a heat sink cooled by the sodium, the effect is relatively minor. It is treated as a factor of 2 increase in the nominal film ΔT, for the 56 mil wire system. The effect of this is negligible on the temperatures in the inner fuel regions and it is assumed to go to zero when the peak fuel temperature is calculated.

Statistical Contributors

6. Fissile Fuel Maldistribution (±3.3% on all ΔT's at any elevation and ±2.3% on upstream coolant ΔT).

Basis: Allowable manufacturing tolerances permit deviations from the nominal design values of several parameters:[37]

Parameter	Deviation	Fissile Deviation
a. PuO_2 weight percent	±0.4%	±2.0%
b. Pellet density (25% PuO_2)	±2.0%	±2.0%
c. Pellet diameter ($\Delta V/V = 2\ \Delta D/D$, where $\Delta L/L = 0$)	±0.8%	±1.6%
d. Homogeneity hot spot (Estimated net effect)	--	nil
Statistical Combination		±3.25%

Assurance of a normal distribution of these parameters about the design mean can only be gained after the manufacturing process has been firmed and typical production-run lots of feed material and finished pellets examined. Since the tolerances are demanding, many rejects could conceivably occur, providing a truncated distribution or making the fissile deviations some unknown number less than three standard deviations (99.7% confidence level). Assuming 1σ, 31.7% rejects are expected; 2σ, 4.45% rejects are expected; 3σ, 0.272% rejects from a normal distribution. The 3σ tolerance limit assumption used for this contributor should be checked against the inspection data on the feed material and pellets actually used to build fuel rods.

The foregoing treated a single pellet, while the $\Delta T_{coolant}$ up to the axial location of interest is involved with many pellets ($\sim$72 up to the core midplace and $\sim$144 up to the clad peak temperature location). All pellets cannot be treated individually since single manufacturing lots can reasonably be expected to have the same enrichment and probably the same density and pellet diameter (since they

will not be individually ground to size). Therefore, a rod filled with pellets from a given lot can be expected to have an uncertainty in the resultant axial $\Delta T_{coolant}$ of exactly the same magnitude as the single pellet (current specifications require a single lot per rod). However, the six rods surrounding the rod of interest share the same coolant and contribute to the coolant temperature rise, as well as the twelve rods surrounding these seven, to a lesser degree, as determined by the coolant mixing.

Most likely, all rods will not be from the same pellet lot and hence the $\Delta T_{coolant}$ should not be treated with that associated uncertainty.

Deviations of the nominal $\Delta T_{coolant}$ as a function of the equivalent number of fuel lots contributing to the temperature rise are:

No. of Fuel Lots	3σ, $\Delta T_{coolant}$
1	±3.25%
2	±2.30%
4	±1.63%
6	±1.33%

Taking two equivalent pellet lots will reduce the fissile fuel maldistribution effect on the coolant temperature change, making $\Delta T_{coolant}$ ±2.3% up to the axial location of interest.

The number of pellet manufacturing lots used in a typical fuel pin bundle should be determined at the time of fuel assembly construction to verify this assumption of at least 2 lots per fuel assembly, randomly spaced.

7. Power Level Measurement (±9.0% on all ΔT's)*

Basis: There are three contributors to the uncertainty in power level measurement by means of an out-of-reactor heat balance system (using temperatures and coolant flow rates). These contributors and their associated deviations as considered in this analysis are:

Item	3σ Deviation, %
1. Flow measurement	
a. primary coolant flow	±7.5
b. drift in flowmeter	±2.0
c. flow field uniformity	±1.0
d. readout error	±0.5
e. as-installed calibration variation	±1.5
Total	±8.1
2. Temperature measurements	
a. temperature	
(1) inlet	±0.5
(2) outlet	±0.8
b. temperature uniformity	
(1) inlet	±1.67
(2) outlet	±1.67
c. drift	±nil
d. readout error	±0.2
Total	±2.5
3. Sodium material properties	
a. Specific heat (experimental data)	
(1) inlet	±1.35
(2) outlet	±1.35

* *These values are considered to be conservative and are for hot-channel calculations only; values for the FTR have not yet been firmed but ±5% on absolute power level is the desired measurement goal.*

b.	Specific heat (temperature error)	
	(1) inlet	±0.1
	(2) outlet	±0.1
c.	Sodium density (experimental data)	±1.0
d.	Sodium density (temperature error)	±0.2
	Total	±2.2
Statistically Combined Effect		±8.8

Power drift between calibrations is due principally to the burnup effects and compensating reactivity changes. The magnitude depends directly upon the frequency of calibration and the on-line power level indicators being used. The calibration routine has not yet been worked out. However, if a ±2% power drift is assumed between on-line power meter recalibrations, then the absolute power measurement at any time is:

Power measurement	±8.8%
Drift between measurements	±2.0%
Total	±9.0%

The power calibration routine of the as-built system should be checked against this item to determine the required frequency to achieve less than the desired absolute power drift (e.g., ±2.0%).

Note that the sodium material properties are included in this contributor. Therefore, they are not treated as a separate contributor to the local $\Delta T_{coolant}$ since it is unlikely that they will vary from assembly to assembly.

8. Burned Fuel Reload (±1.2% on all ΔT's)

Basis: Irradiation experience at BNW indicates an uncertainty in fuel burnup of approximately ±5% is not uncommon. Reshuffling of the fuel during a proposed one quarter core reloading schedule can expose this abnormally burned fuel to a "normal" flux, resulting in a local hot spot. For

25 wt% PuO_2 fuel with an irradiation goal of 80,000 MWd/tonne (Pu+U), and a breeding ratio of 0.5, an uncertainty in the remaining fissile fuel could range from ∿0.5 to 2.1% (the latter value assumes the first 60,000 MWd/tonne burnup in one location at ±5% uncertainty). In this analysis half of the goal burnup is assumed to occur at ±5% before reshuffling, resulting in an equivalent power uncertainty of ∿±1.2%.

This item should be re-evaluated as the fuel management scheme is firmed. New fuel reload flux peaking is considered in the maximum expected nuclear peak-to-average power radial factor and therefore is not accounted for in the hot channel analysis.

9. Rod Diameter, Pitch and Bow (±2% on $\Delta T_{coolant}$ and ±0.9% equivalent on ΔT_{film})

Basis: Changes in the unit-cell flow area associated with a fuel rod will result in deviations from the nominal coolant temperature rise and possible hot spots at localized constrictions.

The allowable clad diameter tolerance of ±1 mil results in a unit cell flow area change of ±1.3%. In a manner similar to the fissile fuel maldistribution, the adjoining six pins also have a clad OD tolerance and will influence the $\Delta T_{coolant}$ to a degree depending upon the number of lots of tubing used in the region of interest. The flow area uncertainty is directly related to the coolant temperature rise because the individual flow channels are interconnected, making the ΔP change negligible, the velocity decrease, and the coolant mass flow rate most likely to decrease. The effects are:

No. of Clad Lots	3σ, $\Delta T_{coolant}$, %
1	±1.3
2	0.92
4	0.65
6	0.53

Taking two equivalent clad lots will reduce the rod diameter effect to approximately ±1%.

A similar analysis on the wire diameter tolerance varies the rod pitch and contributes an additional ±1%.

Clad erosion, corrosion or crud build-up effects are small* and are neglected in this analysis.

Rod bow is a localized effect and does not alter the coolant temperature rise to a significant degree. The proximity of two heat sources due to pitch variations will raise the local temperature, the extreme being pin touching as treated in "Pin Touching".** No current analyses are available to quantify these effects. Future analyses in this particular area are warranted and estimates should be added when they become available.

10 and 11. Film and Gap Coefficients (±33% on ΔT_{film} and ±40% on ΔT_{gap})

Basis: Uncertainty in the experimental heat transfer coefficient for a given set of conditions and uncertainty in the actual in-reactor operating conditions dicates that the nominal design values be assigned some deviation. The range of coefficients were treated previously.† Use of the mid value for h_{film} gives a ±33% uncertainty in ΔT_{film} and ±40% for the ΔT_{gap}.

---

* *Refer to Section 2.2, "Clad Erosion and Corrosion."*

** *Refer to Section 1.7, "Pin Touching."*

† *Refer to Section 1.3, "Clad Surface to Coolant Heat Transfer Coefficient" and Section 1.2, "Gap Selection and Fuel-Clad Gap Coefficient."*

12 and 13. Fuel and Clad Conductivity and Thickness (±10% on ΔT_{fuel} and ±12% on ΔT_{clad}).

Basis: Uncertainty in the experimental thermal conductivity (k) of the fuel and clad as a function of temperature and uncertainty in actual in-reactor operating temperature dictate that the nominal design values be assigned some deviation. An additional factor is the change in k with burnup since irradiation swelling of both fuel and clad will occur.

The thermal conductivity of mixed oxide fuel has been measured in the higher temperature regions of interest with very little deviation about the mean and has shown reasonably good agreement between laboratories.[38]* However, uncertainties in k exist due to the initial fuel density and stoichiometry and in-reactor changes due to pellet cracking, fission product effects and fuel structural changes (sintering and the sintering temperature, grain growth, particle migration, stoichiometry changes, etc.). The combined effect on the integral conductivity curve, which is used to relate power to ΔT, is assigned an uncertainty of ±10%. This item should be re-evaluated as more fast reactor irradiation data become available since they have very significant effects upon the maximum expected fuel temperature.

The thermal conductivity of unirradiated 316 SS clad material has been measured to a high degree of accuracy. However, no data currently exist on the effect of irradiation on the thermal conductivity. Although it is expected to be small, this unknown, plus an allowance for lot-to-lot variations indicates a reasonably large

---

* *Refer to Section 1.1, "Fuel Thermal Properties."*

uncertainty of ±10% be assigned to the clad k. Additional work is required in this area on a low priority basis since the ΔT_{clad} is a small contributor to the peak temperatures.

The allowable manufacturing tolerance on the clad thickness is ±6.7% which reflects directly as a change in the temperature drop. Potential material gain or loss due to erosion, corrosion or crud buildup are small* and are neglected in this analysis. The combined effect of the clad conductivity (±10%) and clad thickness (±6.7%) uncertainties is ±12.0%.

1.5 TRANSIENT BEHAVIOR

A sufficient safety margin must be provided to minimize the possibility of fuel failure for expected operational transients. Since no fuel failures have been observed until fuel melting has occurred, incipient fuel melting has been set up as the upper limit for the fuel temperature during power transients. The safety margin between normal operation and incipient fuel melting is specified by the overpower factor (OPF), which is defined as that multiple of the nominal (steady-state) core design power, exclusive of control deadband, which will cause the hot channel fuel pin to reach incipient fuel melting at its hottest point. Thus, the OPF determines the maximum allowable equilibrium operating condition which is the base point from which transient effects are estimated. Since the OPF and transient overpower is not meaningful in transient analyses (large power increases of short duration can be experienced without much increase in fuel temperature), a fuel internal energy parameter called the overheating factor (OHF)[41] which can be related to fuel failure thresholds beyond incipient fuel melting has been used in previous safety analyses.

---

* *Refer to Section 2.2, "Clad Erosion and Corrosion."*

Parametric studies[39,40,42] compatible with an OPF of 1.20 to 1.25 have been performed to provide bases for design of the safety scram system. The power transient which can be tolerated depends not only on the magnitude of the power transient itself and the fuel design parameters but also on safety system characteristics such as:

- Trip setting on flux monitor
- Time delays in flux monitor, safety circuitry, and safety rod mechanism
- Acceleration of safety rods
- Reactivity worth of safety system.

In addition to these safety system parameters, several negative nuclear feedbacks can be taken into account during the power transient:

- Fuel Doppler effect
- Density changes in fuel, clad, coolant, structural material
- Thermal expansion effects including deformation and bowing.

However, the analyses take credit for only the fuel Doppler effect because it is considered to be the only reliable reactivity feedback.

Figure 1.5-1 shows some typical results. The reactivity ramp insertion to produce incipient fuel melting in the hot channel fuel pin was determined for various combinations of safety system delay time, rod acceleration, and safety system worth.

As an example, consider a 5$/sec reactivity ramp which occurs when the reactor is at full power. When the neutron flux increases to 15% over the value for normal operation, the flux monitor detects the excursion and initiates scram. However, the time delays in the flux monitor itself, the safety circuitry, and the safety rod latch mechanism add up to 100 msec

after the flux has increased to 115% of its normal value. If the fuel Doppler coefficient is $(T \frac{dk}{dT})$ is -0.0035 and the safety system worth ($\delta K/K$) is 0.02, Figure 1.5-1 shows that a safety rod acceleration of 2 g's is required to prevent fuel melting in the hot channel fuel pin.

Since the magnitude of the OPF inversely affects the permissible average linear heat rate which, in turn, affects the required number of fuel pins or total core power, a balance between a reasonable safety margin and core power must be made. Additional transient analyses were performed to determine the possible reduction in the OPF as a function of safety system parameters.

Since the reactor safety system must be conservative enough to accommodate changes in core design and to allow for uncertainties in design analysis, a conservative power excursion consisting of a 4$/sec reactivity ramp with a total insertion of 4$ was assumed. This ramp rate is the maximum rate of reactivity increase which has been identified to date resulting from a single unlikely fault and corresponds to the gravity compaction of the upper 1/3 of a single driver fuel assembly or open loop assembly near the center of the core into the middle 1/3. However, this fuel collapse gives a total insertion between 1 to 2$ and therefore the assumed total insertion of 4$ is conservative by at least a factor of two.

Figure 1.5-2 shows the required OPF to preclude fuel melting as a function of safety rod acceleration for two different safety system time delays. The safety rod accelerations were calculated using a bundle of 37 boron carbide rods and considering the inertial and frictional effects of the coolant. The 1- and 2-g scram assists were implemented by use of springs and the actual initial accelerations were 2 and 3 g's, respectively.

The results show that for a free-fall scram and a time delay of 100 msec, increasing the safety system worth from 0.02 to 0.03 and decreasing the trip setting from 1.15 to 1.10 results in decreasing the required OPF from 1.25 to 1.17. Decreasing the time delay from 100 to 50 msec or increasing the rod acceleration to a 1-g assist decreases the required OPF further from 1.17 to approximately 1.12.

In loss-of-coolant accidents, coolant boiling will be reached before fuel or clad melting. Since sodium boiling will result in rapid voiding of coolant from the core followed by clad and fuel melting, emphasis must be placed on insuring that the coolant does not reach its boiling point. Various types of loss-of-coolant accidents such as flow coastdowns, fuel assembly inlet blockages, pipe ruptures, and local coolant subchannel blockages within the core have been considered to determine whether such occurrences can be detected in sufficient time to take action and avoid coolant boiling.[40]

Figure 1.5-3 shows the core outlet coolant temperature for the hot channel fuel pin for instantaneous flow reductions due to gross flow blockages. For flow reductions greater than 80%, it is impossible to prevent the coolant from reaching 1700 °F (the normal boiling point for sodium is approximately 1620 °F) even if reactor scram were initiated instantaneously. Flow reductions less than 50% will not result in boiling but the response of the fuel assembly instrumentation will determine the length of time that components are subjected to excessive temperatures. Therefore, the speed of instrumentation response is important in determining whether coolant temperatures required for boiling are attained for flow reductions between 50 and 80%. Flow reductions beyond 80% must be eliminated by design since coolant boiling temperatures cannot be avoided.

Local blockages within the fuel bundle are extremely difficult to detect. For example, complete blockage of six coolant subchannels along the entire length of the fuel bundle would result in a flow decrease of only 0.8% and an increase in the coolant outlet temperature of only 3 °F. Fuel assembly instrumentation would not be capable of detecting such a blockage although excessive clad temperatures and even local coolant boiling could occur. An experimental program under Task 12151/CTH-2 is planned to determine the effects of blockage of one or more coolant subchannels.

1.6 FUEL PIN THERMAL DESCRIPTION

1.6.1 Standard Subassembly Thermal Description

Figures 1.6-1 through 1.6-5 provide temperature distributions within subassemblies located in the center of Zone I and in the hottest region of Zone II. Effects of flow suppression and departures from the tightest bundle packing due to non-straightness of individual members are not included in this section (see Section 1.6.2). The core is assumed to be orificed such that all assemblies have a mixed mean temperature rise of 300 °F. The bundles are fixed at the center of the subassembly. Slightly larger local temperatures and temperature gradients can result from bundle misalignment. The hot rod referred to in Figure 1.6-5 is regarded as representative of the hottest pin in the core but cannot be directly identified with a pin immersed in a specific coolant domain illustrated in Figures 1.6-1 and 1.6-3.

1.6.2 Flow Suppression at Duct Perimeter

Figure 1.6-6 shows the effectiveness of four methods to reduce subassembly enthalpy peaking. These data were generated using a tightly packed model of the fuel pin bundle. The peak enthalpy rise predicted for the standard bundle using the tightly packed model is probably conservative. Therefore, an

alternate model was considered. The loosely packed model with the diametral tolerance is taken up in the interior channels such that the pitch is increased from 0.286 to 0.288 in. and there is zero spacing between the wire wraps of the peripheral pins and the duct wall. These two models are compared in Figure 1.6-7 for the standard bundle. Figure 1.6-8 summarizes the effectiveness of the four methods in reducing subassembly peak enthalpy rise for both models. Table 1.6-1 summarizes the enthalpy rise and relative change in bundle pressure drop for the 5 cases studied, viz:

Case #1 - Standard bundle, no flow suppression.

Case #2 - 50% area reduction of peripheral channels along first inch of bundle.

Case #3 - Scalloped liner along the duct wall for complete bundle length.

Case #4 - Reduction of peripheral channel area by using 0.028 in. wire on the outer row of fuel pins.

Case #5 - All pins wrapped with 0.028 in. wire 180° apart, viz, two wires per pin.

TABLE 1.6-1

	Case Number				
	1	2	3	4	5
(Peak/average) Enthalpy Rise-Tight Bundle	1.19	1.17	1.10	1.10	1.07
(Peak/average) Enthalpy Rise-Loose Bundle	1.11	1.10	1.03	1.03	1.01
% Change in Pressure Drop	-	0	+15	+16	-19

Duct-pin bundle differential growth leads to no signifi- change in enthalpy peaking if the bundle can be described throughout the entire core lifetime by a loose packed model of the non-straight pins. However, if a tight bundle model is appropriate as burnup progresses, significantly larger peaking

can be predicted from expected swelling rates (e.g., 1.3 at 55,000 MWd/tonne and 1.5 at 80,000 MWd/tonne). The uncertainty in differential swelling includes even larger peaking or virtually none at all. The effect of the thermal and the radiation environment on the ability of the bundle to expand due to pin springiness is unknown. Therefore, the correct model of the bundle as a function of burnup is uncertain. It is probable that this environment will lead to a bundle that can be described by a model which falls between a tight and loose configuration of straight pins. Uncertainty in bundle porosity (bundle model) and in swelling as functions of burnup are of critical importance. Both phenomena are not sufficiently understood for confident thermal hydraulic design purposes, hence, they must be experimentally studied.

1.7 PIN TOUCHING

Fuel pin bowing may lead to the contact of two or more pins. The effect would be worsened should relocation of one or more wire spacers occur. In order to estimate the consequences of this phenomenon, preliminary analysis was conducted on the contacting of two fuel pins along their entire axial length. A model employing the concept of a "cell" about each pin was assumed where a fixed amount of coolant was associated with every pin in the bundle and this value was assumed unchanged upon pin contact. Flow distribution about the pin(s) were based upon a constant surface friction. Coolant mixing and conduction were neglected as was the presence of the wire spacer.

The TIGER computer program was used to determine the radial and axial temperature distributions for two fuel pins (0.25 in. OD, 0.016 in. clad wall thickness and 0.030 in. pin separation) in contact with the problem boundary limited to these two pins.

The geometry of the fuel pins used in this analysis had 32 in. of pin containing fuel. The pins were divided into 16 two-in. sections, and an analysis was performed at the center of each 2-in. section beginning at the 13 in. level and continuing on to the 31 in. level. The slice used at each of these levels was 0.12 in. thick. The geometry for each slice was determined using the SINTR subroutine of the TIGER-5 code. Thus, the nodal boundaries were varied accordingly to accommodate the void core, sintered, and unsintered interfaces within each slice.

In order to provide a basis of comparison, the results of the pin touching temperature distribution were compared to that of a "free" pin. Both pairs of average and of hot pins were studied. The heating rate and average flow rate for the hot pins were 14.2 kW/ft and 770 lb/hr per pin, respectively.

A summary of the results are provided in Figures 1.7-1 and 1.7-2.

It is concluded that an average pin will have its inner cladding temperature increased by 100 °F if it is in contact with another similar pin. The corresponding temperature increase for a hot pin (14.2 kW/ft versus 9.74 kW/ft maximum power) was 140 °F.

1.8 EFFECT OF FUEL SMEARED DENSITY ON SAFETY

The influence of fuel smeared density on safety is both direct and indirect. High fuel smeared densities directly influence the magnitude of overpower transients which can be tolerated before fuel pin cladding failure occurs and low fuel smeared densities increase the potential for wet fuel slumping. The fuel smeared density indirectly affects the magnitude of the Doppler coefficient because it changes the fertile-to-fissile ratio. Even if the Doppler coefficient remains unchanged, a lower fuel smeared density increases the magnitude

of the Design Basis Accident (DBA) energy release because it provides more void within the core for expansion of fuel prior to disassembly of the core and termination of the nuclear excursion.

1.8.1 Radial Expansion During Overpower Transients

For overpower transients which do not result in fuel melting, the effect of fuel smeared density (either directly by radial expansion or indirectly through the magnitude of the Doppler coefficient) is not significant. For overpower transients where a significant amount of fuel melting has occurred, experimental data for transient testing of irradiated fuel[43] has indicated that the cladding would be expected to fail from pressures generated by sudden release of fission gases when 50 to 70% of the radial cross-sectional area of the fuel reaches the melting point. A fuel smeared density to accommodate melting beyond this failure point is unnecessary and, therefore, an upper limit to the fuel smear density can be determined by allowing sufficient radial expansion within the cladding up to 50% areal melting. For a 9.6% increase in fuel volume during melting, this upper limit is 95% TD at the melting temperature, or 93% TD at room temperature. This limit is considerably in excess of the proposed value of 88% TD.

1.8.2 Fuel Slumping

Transient fuel slumping (designated "wet slumping") can occur during an overpower transient and the reactivity effect is a direct function of the center void which, in turn, is dependent upon the fuel smeared density. For a fuel smeared density of 88% TD, it was found that wet slumping within a single driver fuel subassembly could result in a reactivity increase of 1.4¢.[44] A similar analysis was carried out for fuel smeared densities of 85 and 80% TD[45] which showed little difference from the results for 88% TD. However, the potential for adverse slumping effects is greater for lower smeared density fuel because of the larger available central volume.

1.8.3 Doppler Coefficient

The Doppler coefficient is primarily dependent upon the fertile-to-fissile fuel ratio and has a significant effect on core response to accident conditions. Although the Doppler coefficient is not directly affected by a reduction in fuel smeared density, optimization of core design performance requires a change of enrichment to compensate for the reduced performance and thus the magnitude of the Doppler coefficient is adversely affected. For example, a reduction from 89 to 80% results in a Doppler coefficient decrease from -0.004 to -0.003 Tdk/dT. The Doppler coefficient is the major parameter in determining the consequences of a startup accident, the energy release from the DBA, and the inherent stability of the reactor.

1.8.4 Effect of Doppler Coefficient on the Startup Accident

For a nuclear power transient initiated during startup (or refueling), the very low initial fuel temperature provides for a much more significant Doppler effect compared to a power transient starting from full power. Scoping studies have shown that the Doppler effect by itself (not accounting for radial and axial fuel expansion) would be able to terminate a step reactivity insertion of approximately 2$ before fuel damage. A more detailed analysis will be carried out as part of the safety analysis for the Preliminary Safeguards Analysis Report (PSAR).

1.8.5 Effect of Doppler Coefficient on DBA

The energy release for the DBA increases as the Doppler coefficient is reduced. The DBA energy release as a function of Doppler coefficient has been determined for accidents initiated from both shutdown conditions and full power conditions[46] and is shown in Figures 1.8-1 and 1.8-2. For the startup accident, it was found that the DBA energy release was

more than doubled when the Doppler coefficient was decreased from -0.004 to -0.003 Tdk/dT corresponding to decreasing the fuel smeared density from 89 to 80% TD. The energy release for both cases is quite sensitive to the Doppler coefficient in the range of -0.0015 to -0.002. Although the Doppler coefficient for the reference design is approximately -0.004 (±25%) reduction of the Doppler coefficient does not seem to be a prudent course of action until further information, particularly physics critical tests, become available.

Another effect of fuel smeared density on the DBA energy release is the additional void within the core available for expansion. This increased void delays the generation of the high pressures required for disassembly of the core and termination of the nuclear excursion. Theoretically, a reduction of the fuel smeared density will increase the magnitude of the DBA energy release even if the Doppler coefficient remains unchanged.

1.8.6 Effect of Doppler Coefficient on Stability

Because of the interrelationship of a number of temperature-dependent reactivity feedback mechanisms, the inherent nuclear stability of the core must be ascertained. A preliminary analysis taking into account six reactivity feedback mechanisms (Doppler effect, axial expansion, radial expansion, pin bowing, tube sheet bowing, and sodium void) showed that the reactor was unconditionally stable according to Nyquist and Bode criteria.[47] However, a more detailed analysis[48] showed that one combination gave unstable behavior: when the Doppler coefficient is zero. Since a Doppler coefficient of -0.004 and -0.002 gave unconditional stability, the point of initial instability lies somewhere between a Doppler coefficient of -0.002 and zero. Although more analysis will be required to ascertain the point at which inherent nuclear instability occurs, reduction of the Doppler coefficient to below -0.002 would not be advisable until such verification is obtained.

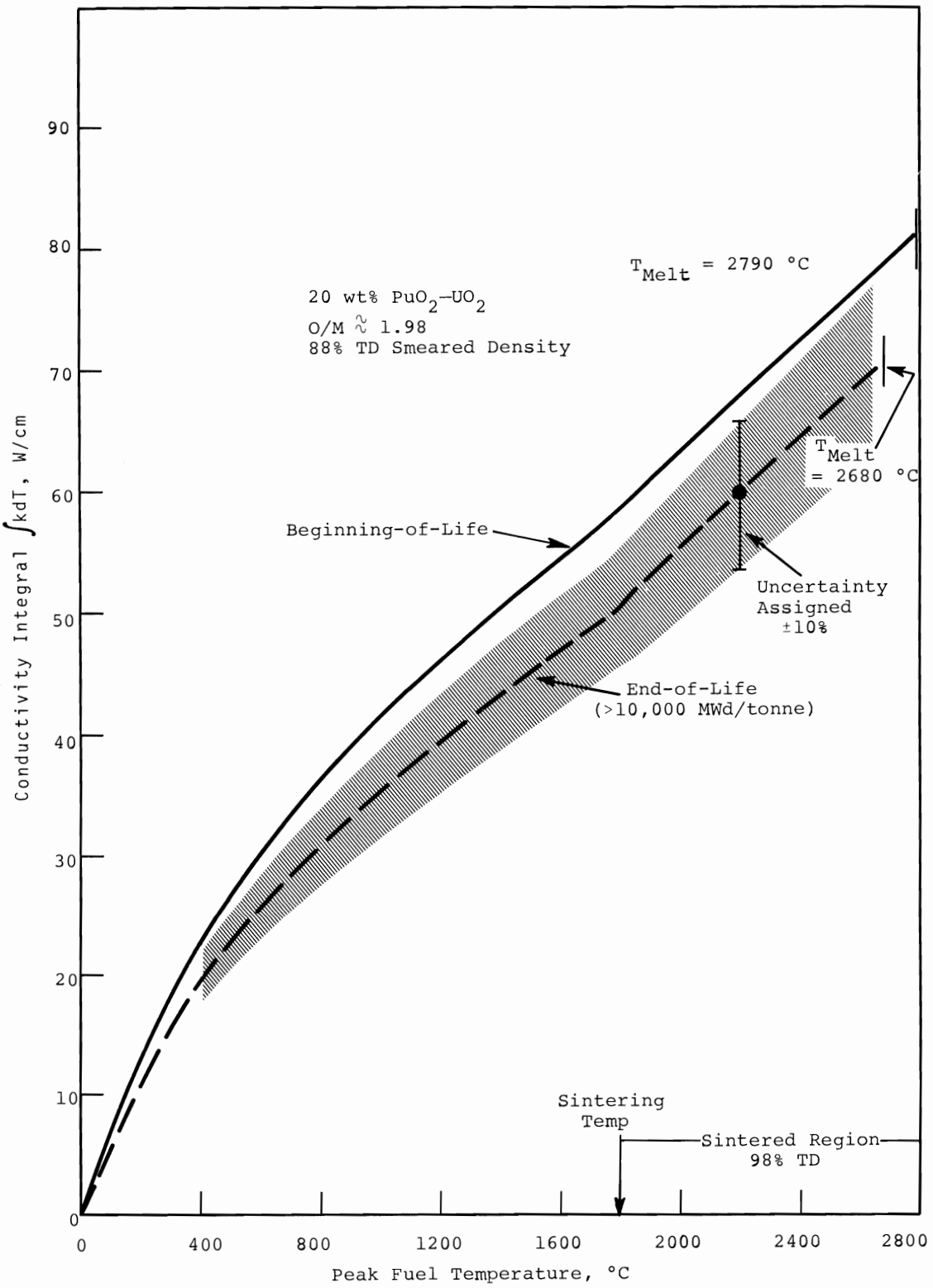

FIGURE 1.1-1. Conductivity Integral Versus Temperature

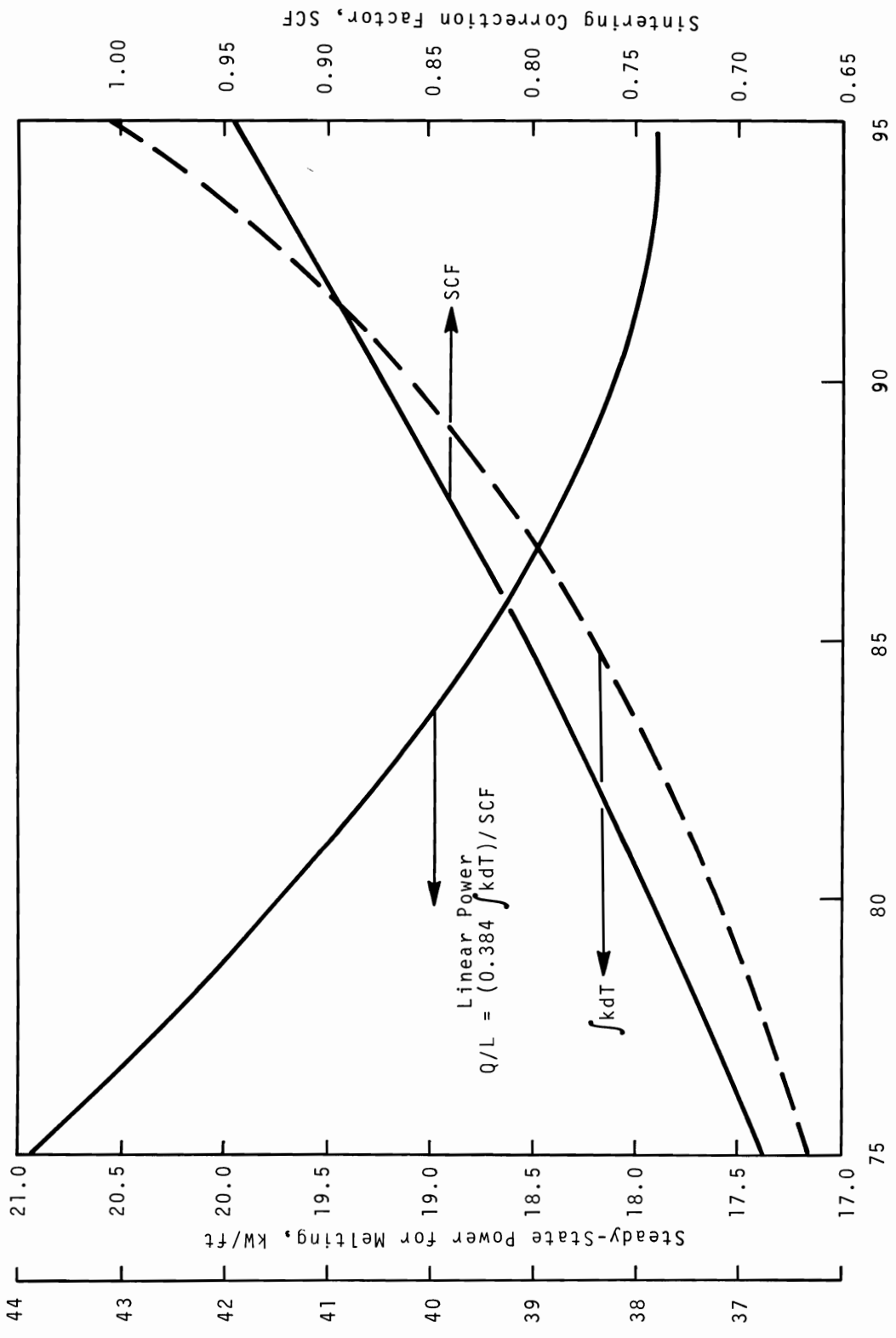

FIGURE 1.1-2. Linear Power Required for Incipient Fuel Melting Versus Fuel Smeared Density

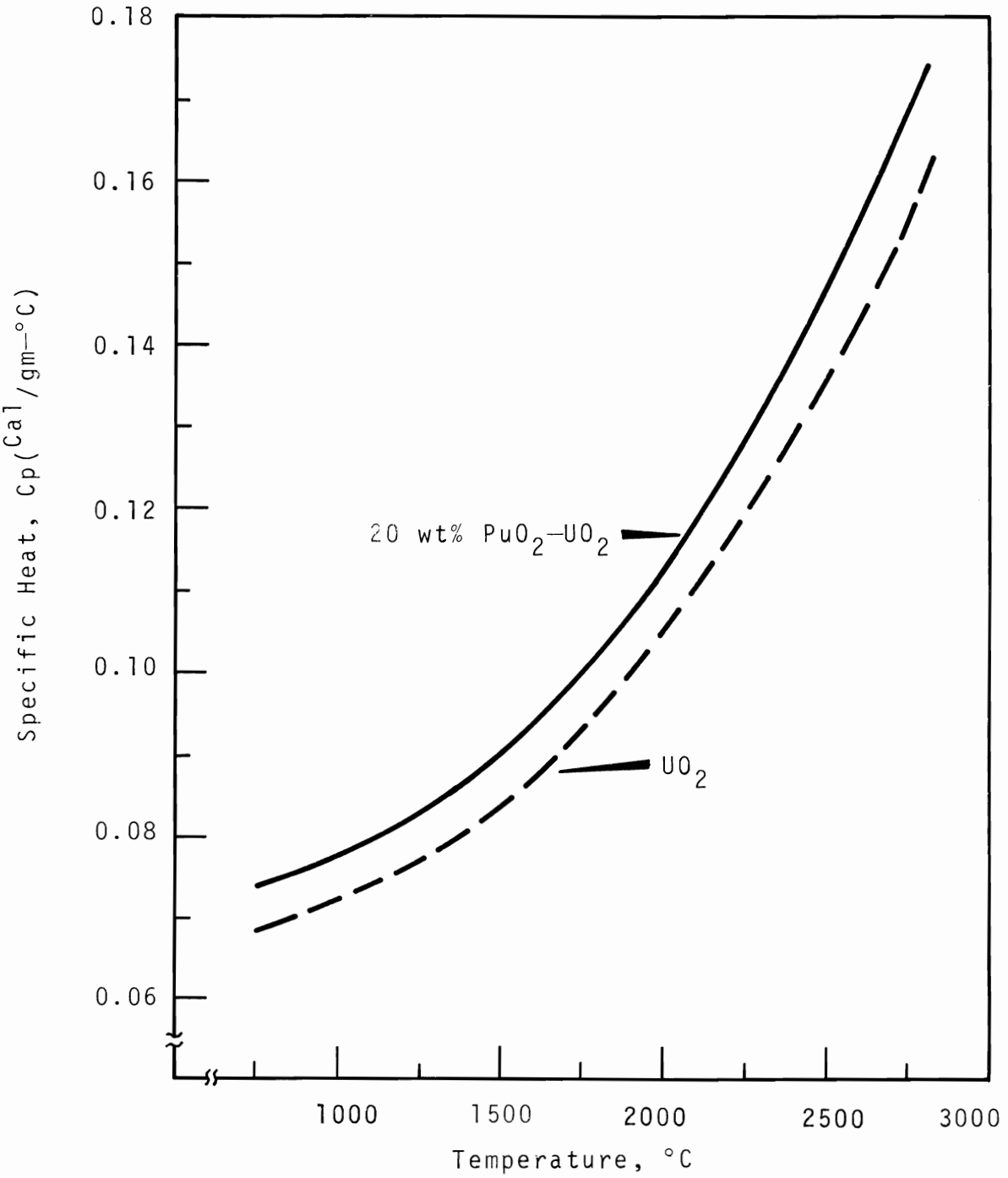

FIGURE 1.1-3. Specific Heat of UO_2 and PuO_2—UO_2 Versus Temperature

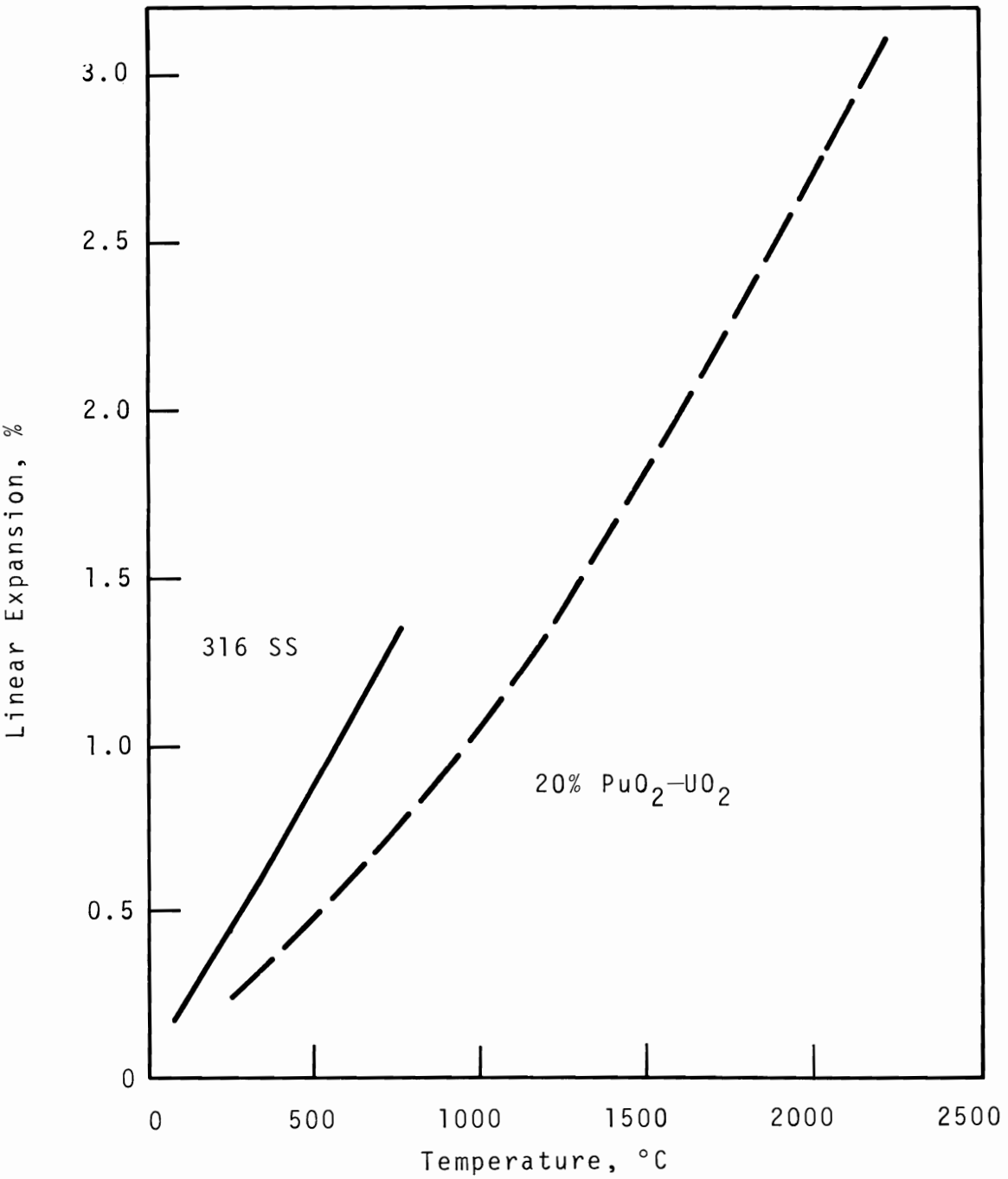

FIGURE 1.1-4. Mixed Oxide Fuel and 316 SS Clad Thermal Expansion Versus Temperature

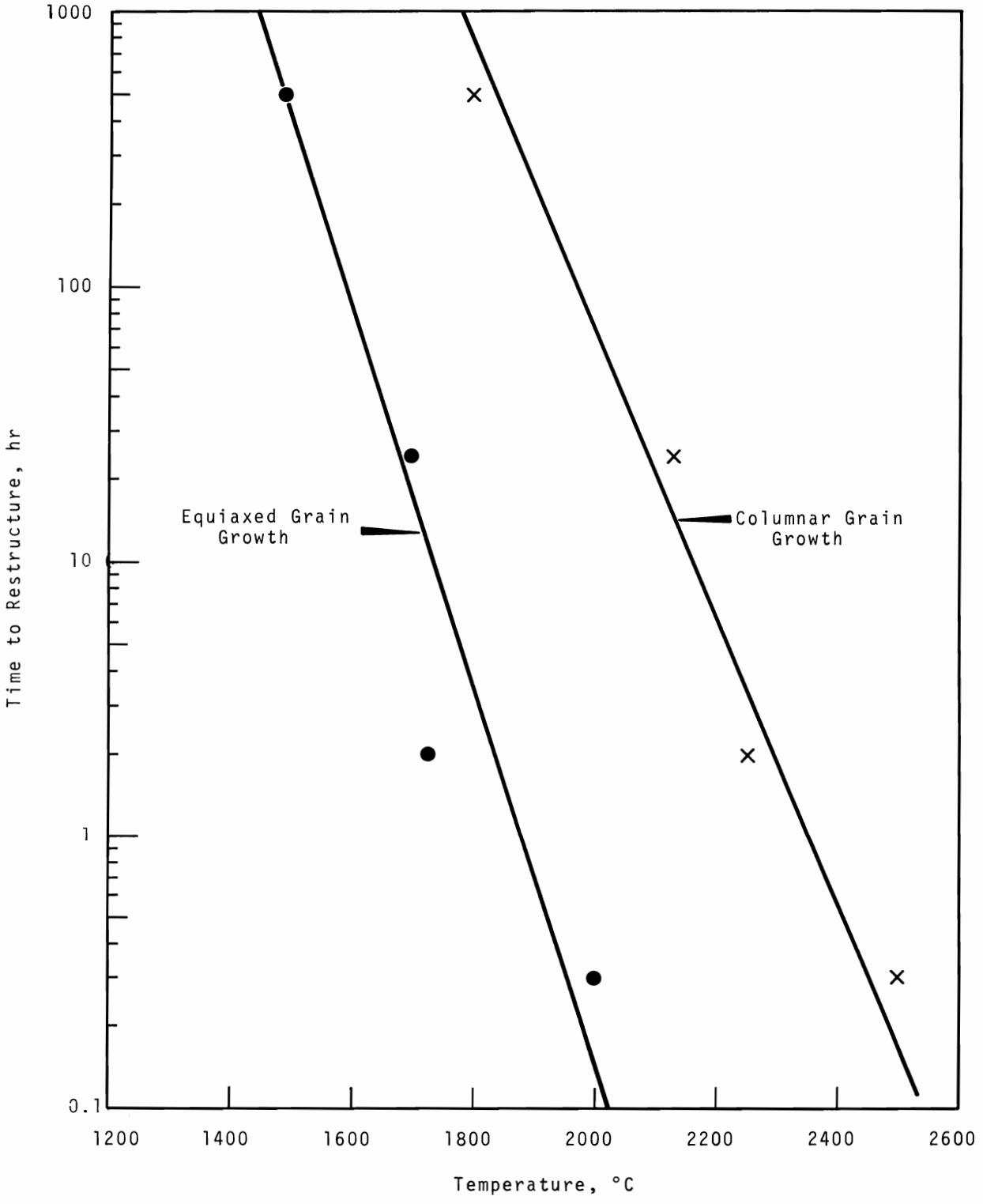

FIGURE 1.1-5. Time to Restructure UO_2 Fuel Versus Temperature

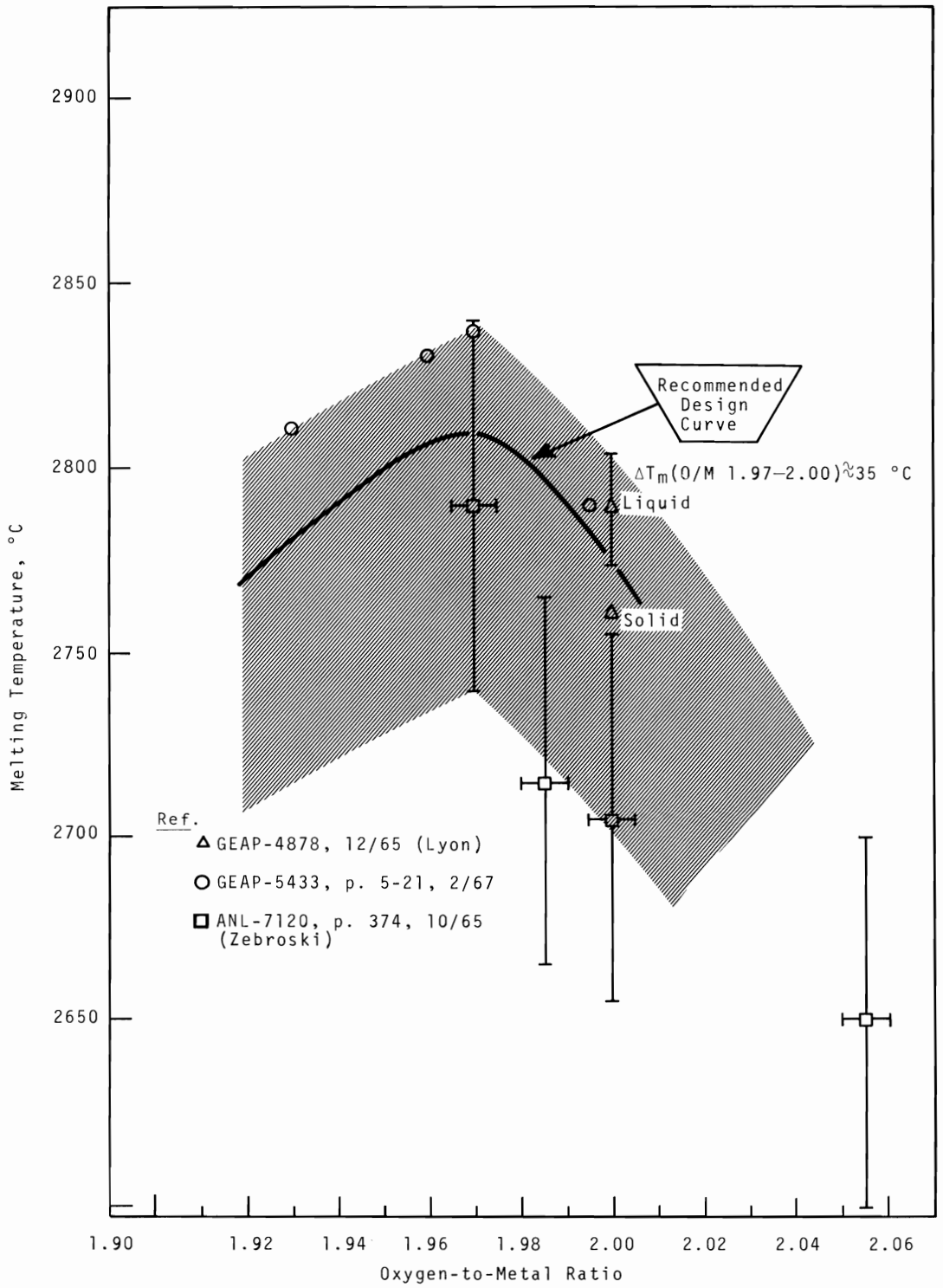

FIGURE 1.1-6. Melting Temperature of $(Pu_{0.20}U_{0.80})O_{2\pm x}$ Versus Oxygen-to-Metal Ratio

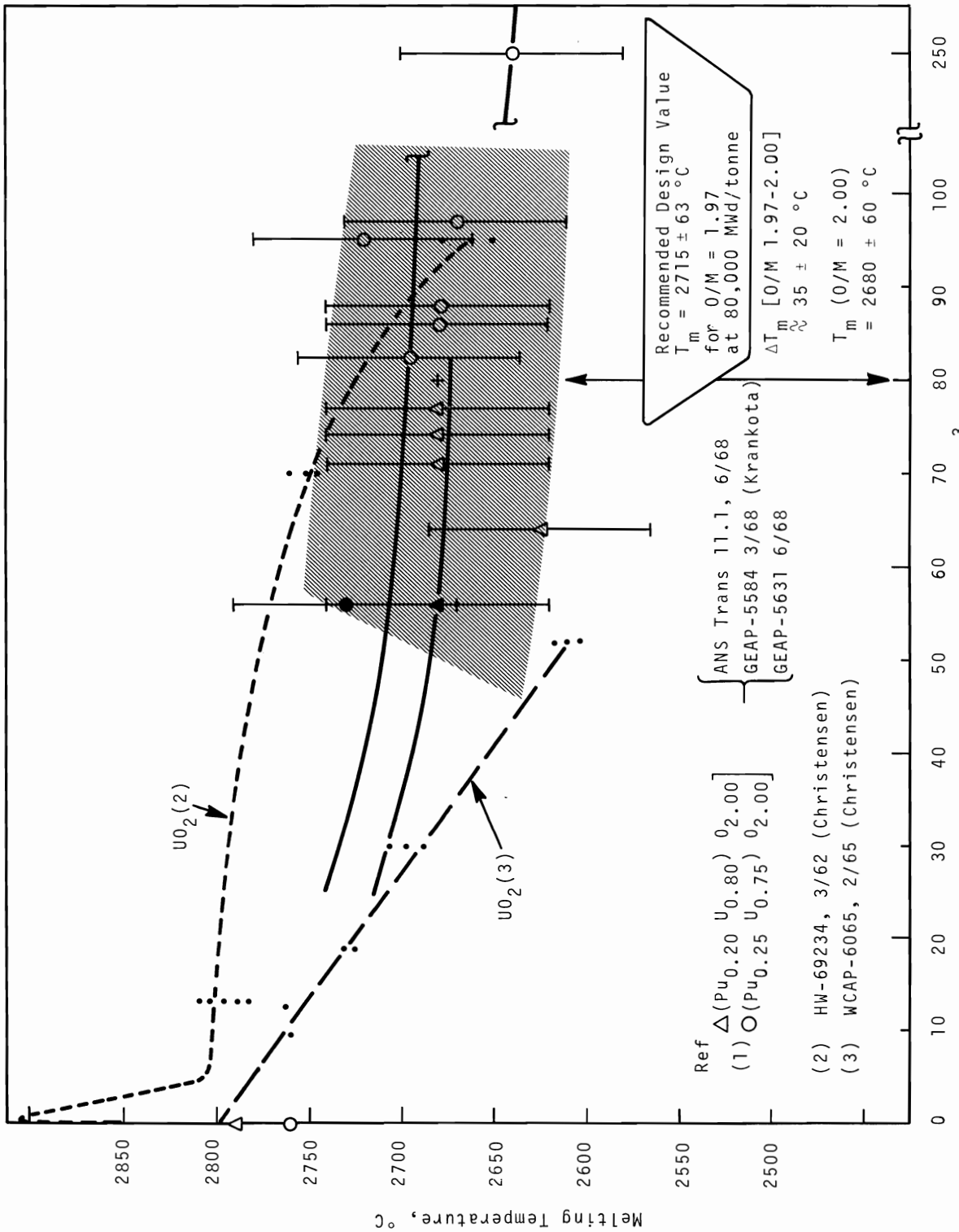

FIGURE 1.1-7. Melting Temperatures of 20 to 25 wt% $(PuU)O_{2.00}$ Versus Burnup

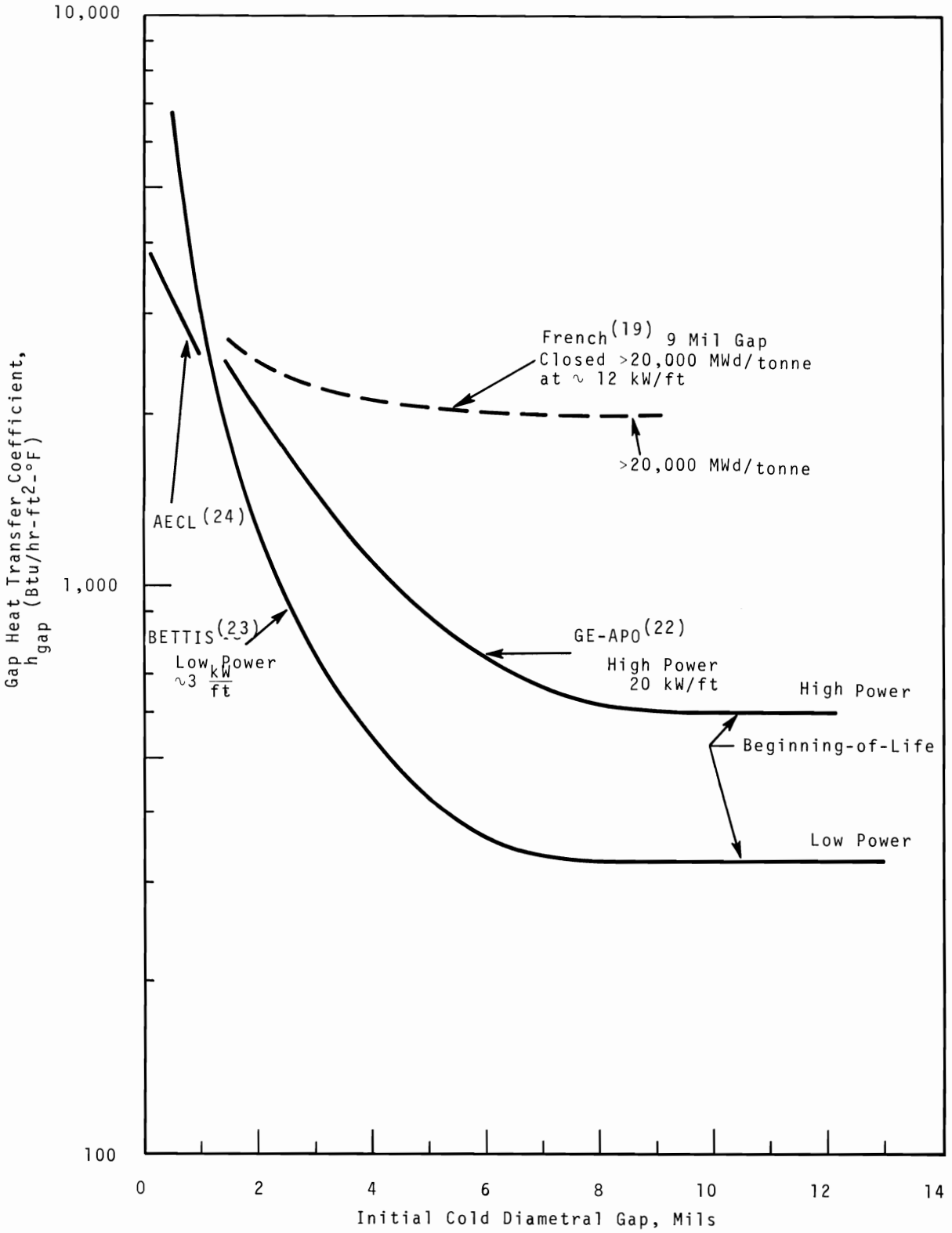

FIGURE 1.2-1. Gap Coefficient Versus Initial Diametral Gap

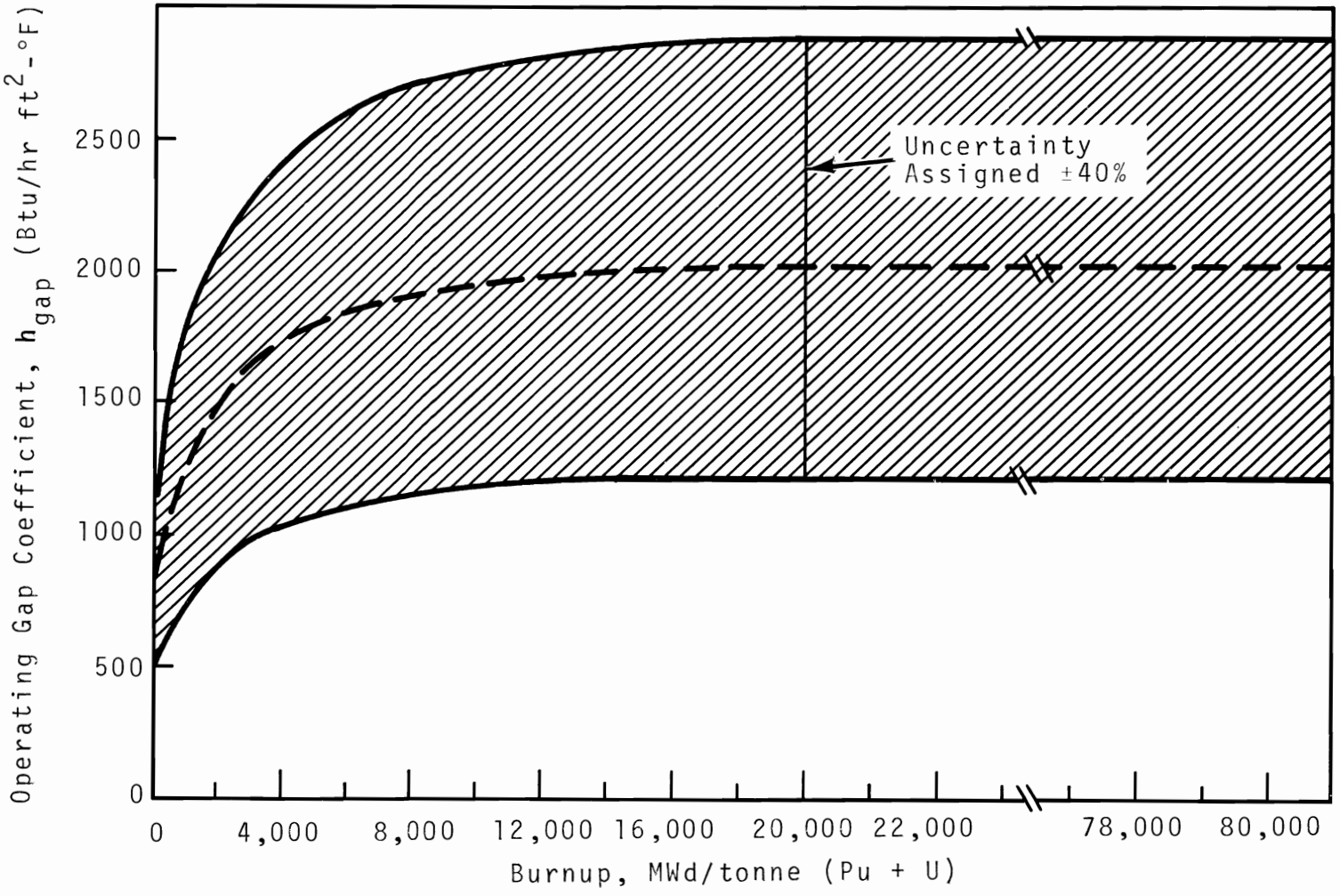

FIGURE 1.2-2. Recommended Design Gap Coefficient Versus Burnup for Peak Pin with an Initial 6 mil Diametral Gap (cold)

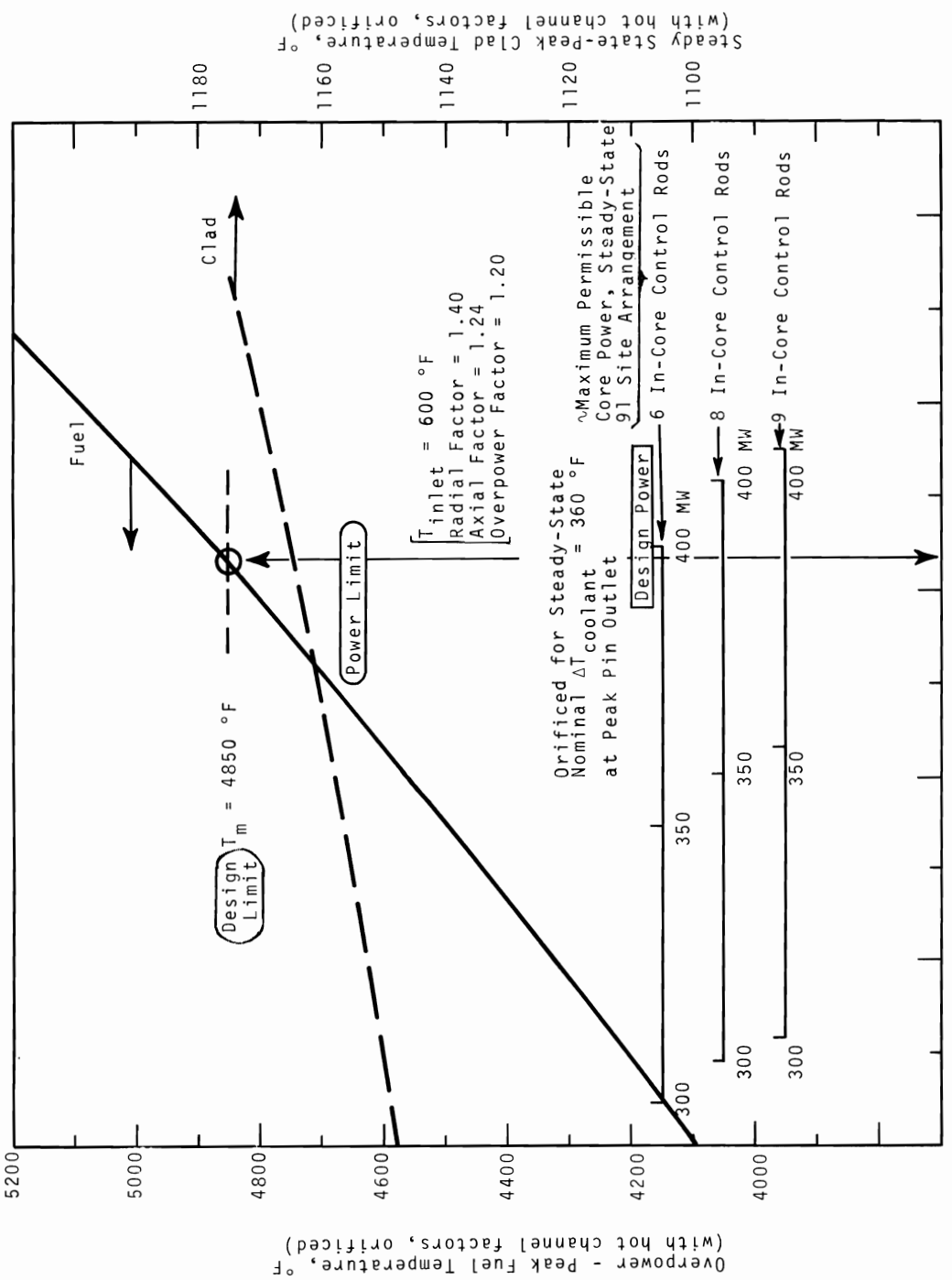

FIGURE 1.4-1. Maximum Expected Peak Hot Channel Fuel (at overpower) and Clad (steady-state) Temperatures Versus Peak Pin Linear Power

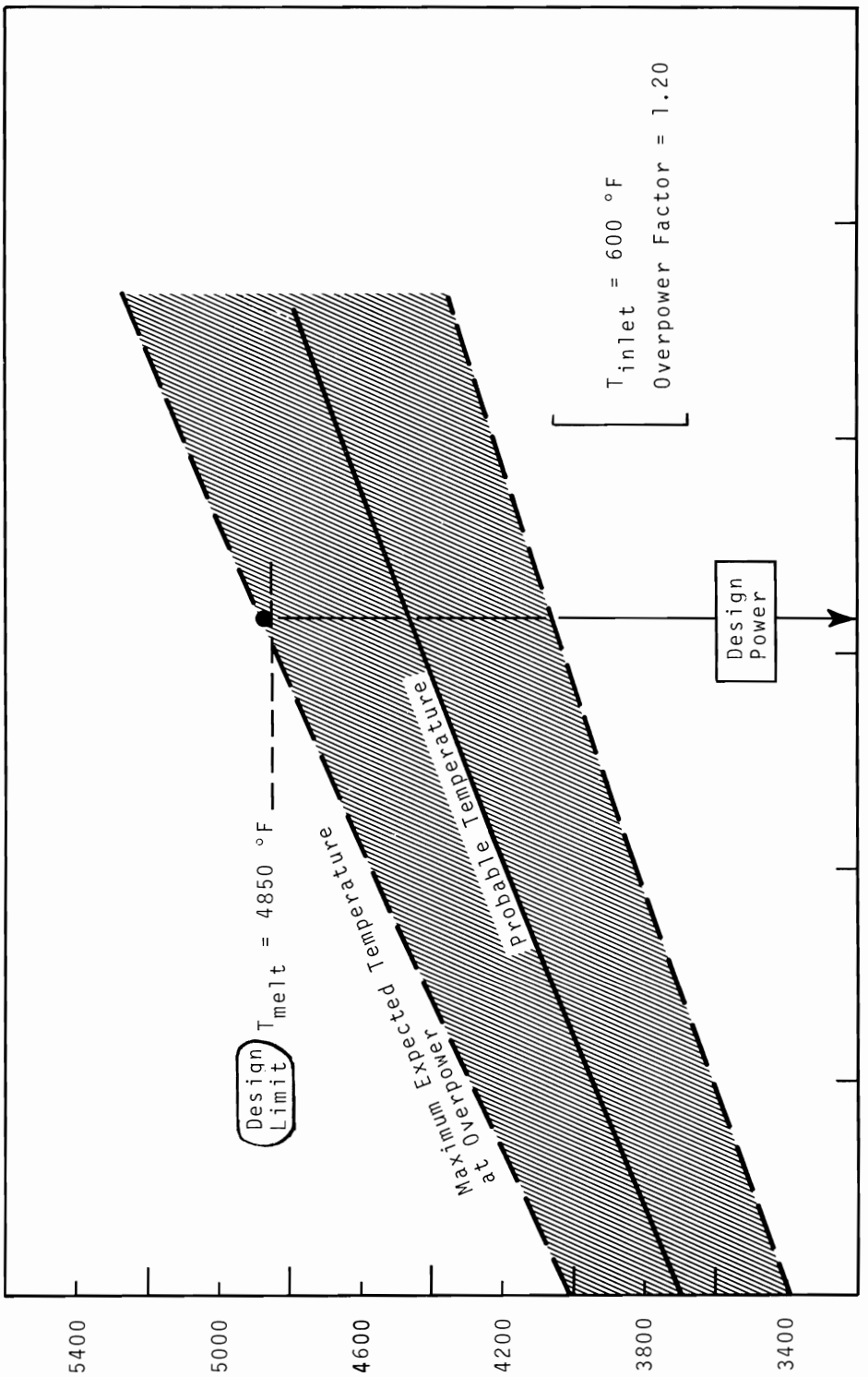

FIGURE 1.4-2. Peak Hot Channel Fuel Temperature at Overpower Versus Peak Pin Linear Power

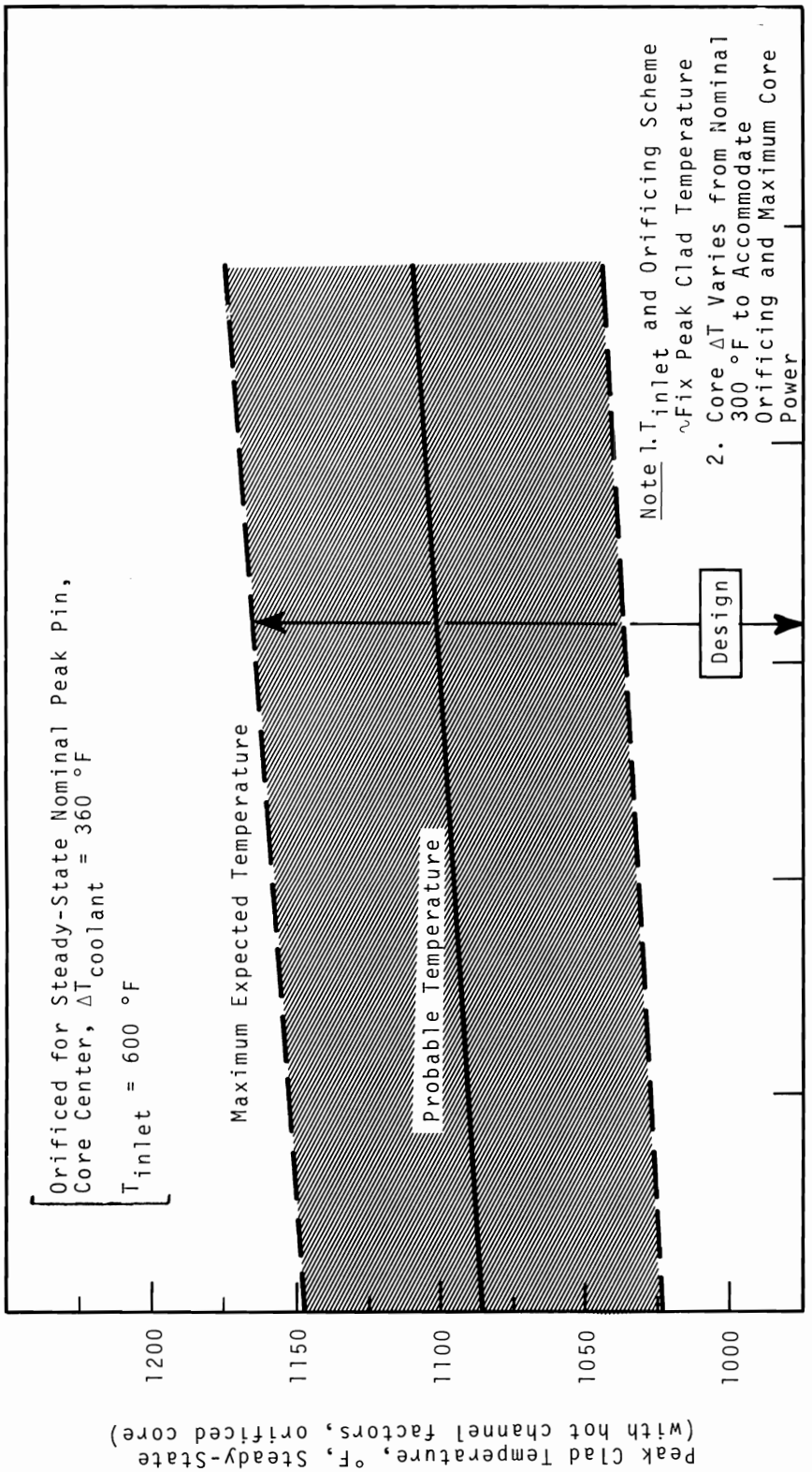

FIGURE 1.4-3. Peak Hot Channel Clad Temperature (Steady-State) Versus Peak Pin Linear Power

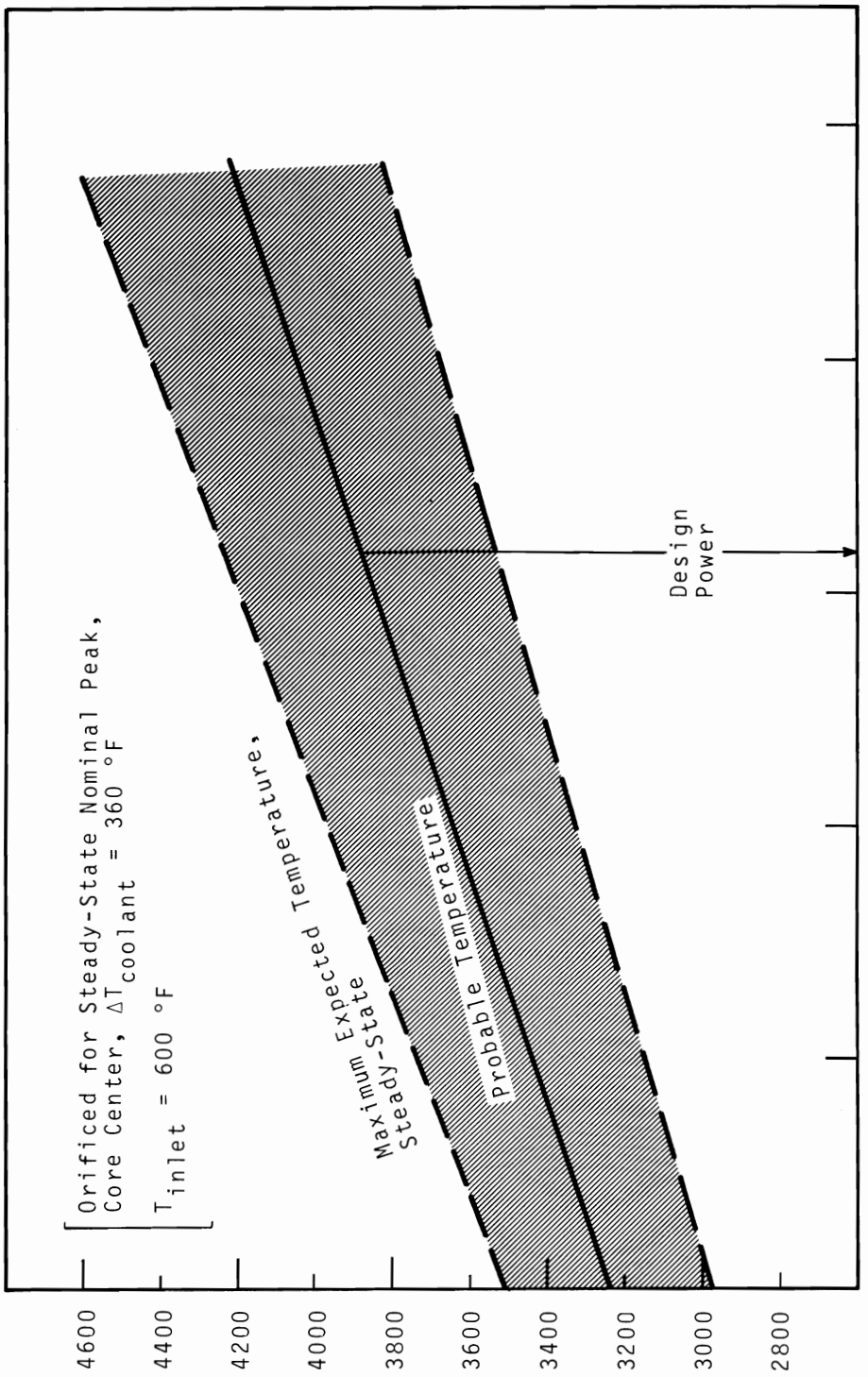

FIGURE 1.4-4. Peak Hot Channel Fuel Temperature (Steady-State) Versus Peak Pin Linear Power

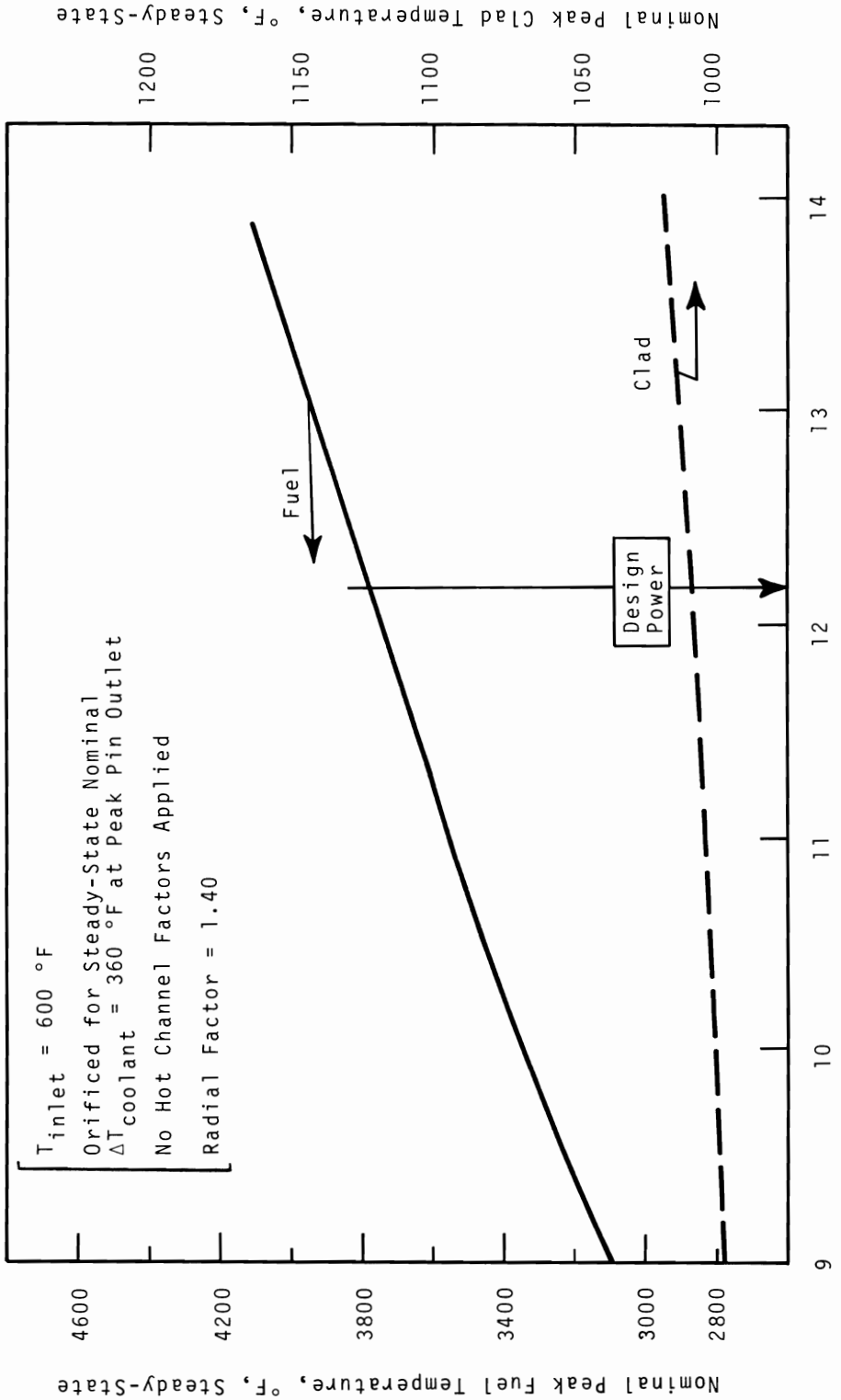

FIGURE 1.4-5. Nominal Peak Fuel and Clad Temperatures (Steady-State) Versus Peak Pin Linear Power

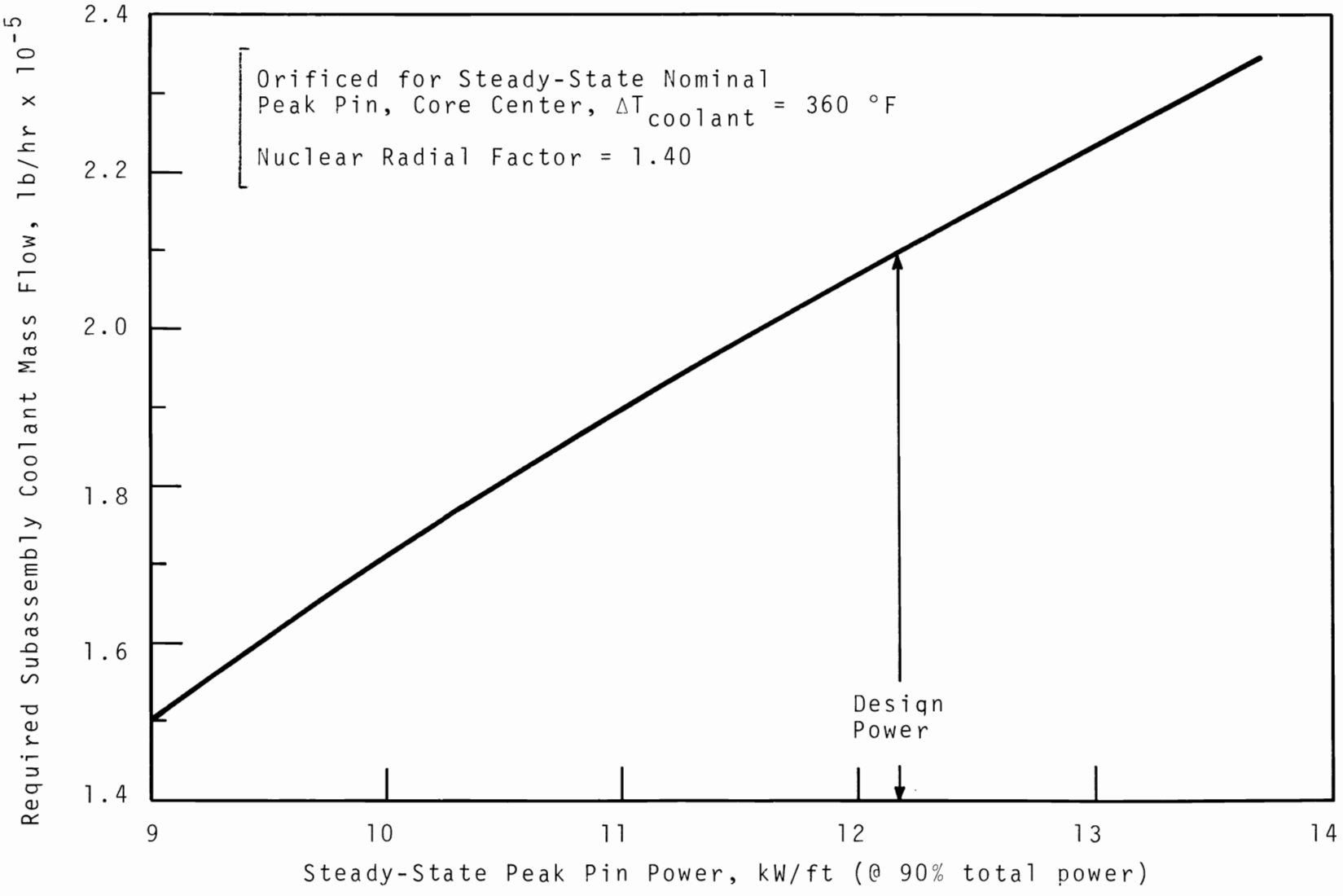

FIGURE 1.4-6. Maximum Required Subassembly Coolant Flow (Orificed Core) Versus Peak Pin Linear Power

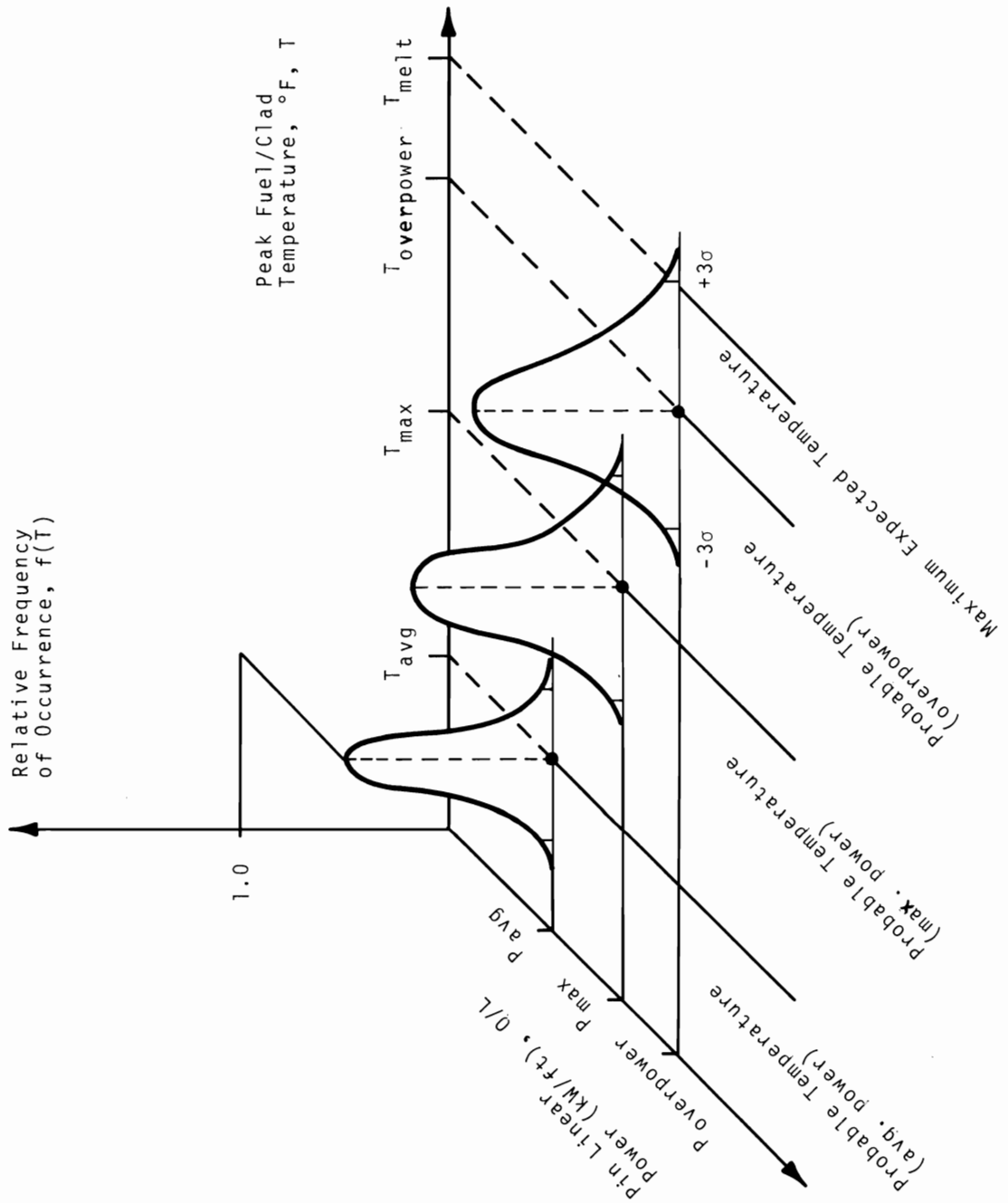

FIGURE 1.4-7. Typical Plot of Pin Power Versus Peak Fuel/Clad Temperature Versus Frequency of Occurrence

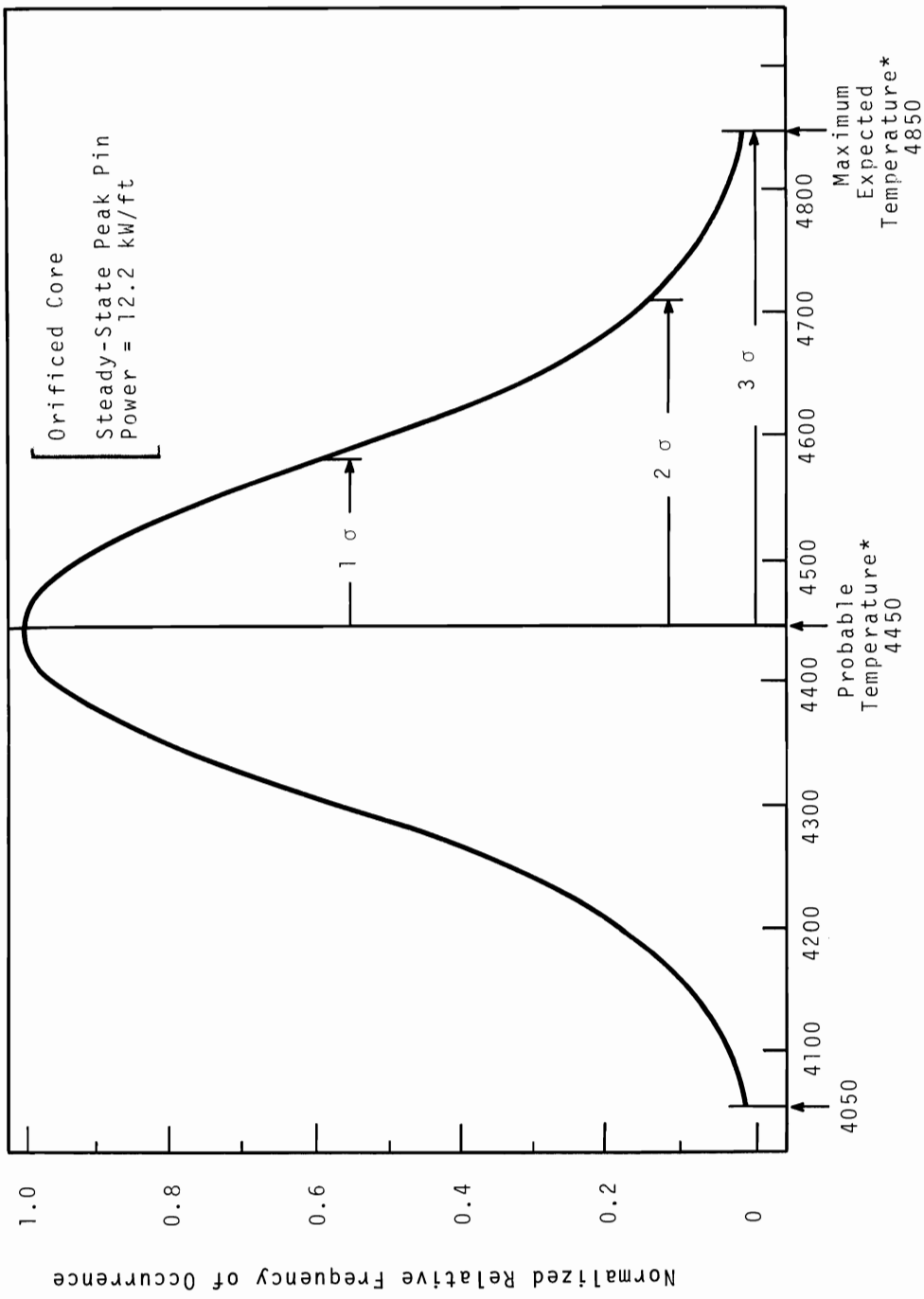

*NOTE: $T_{nominal}$ - (3770 °F) - No hot channel factor (HCF) effects considered
$T_{probable}$ - (4450 °F) - HCF direct contributions included
$T_{max.\ expected}$ - (4850 °F) - HCF direct and statistical contributions

FIGURE 1.4-8. Peak Hot Channel Fuel Temperature at Overpower Versus Frequency of Occurrence

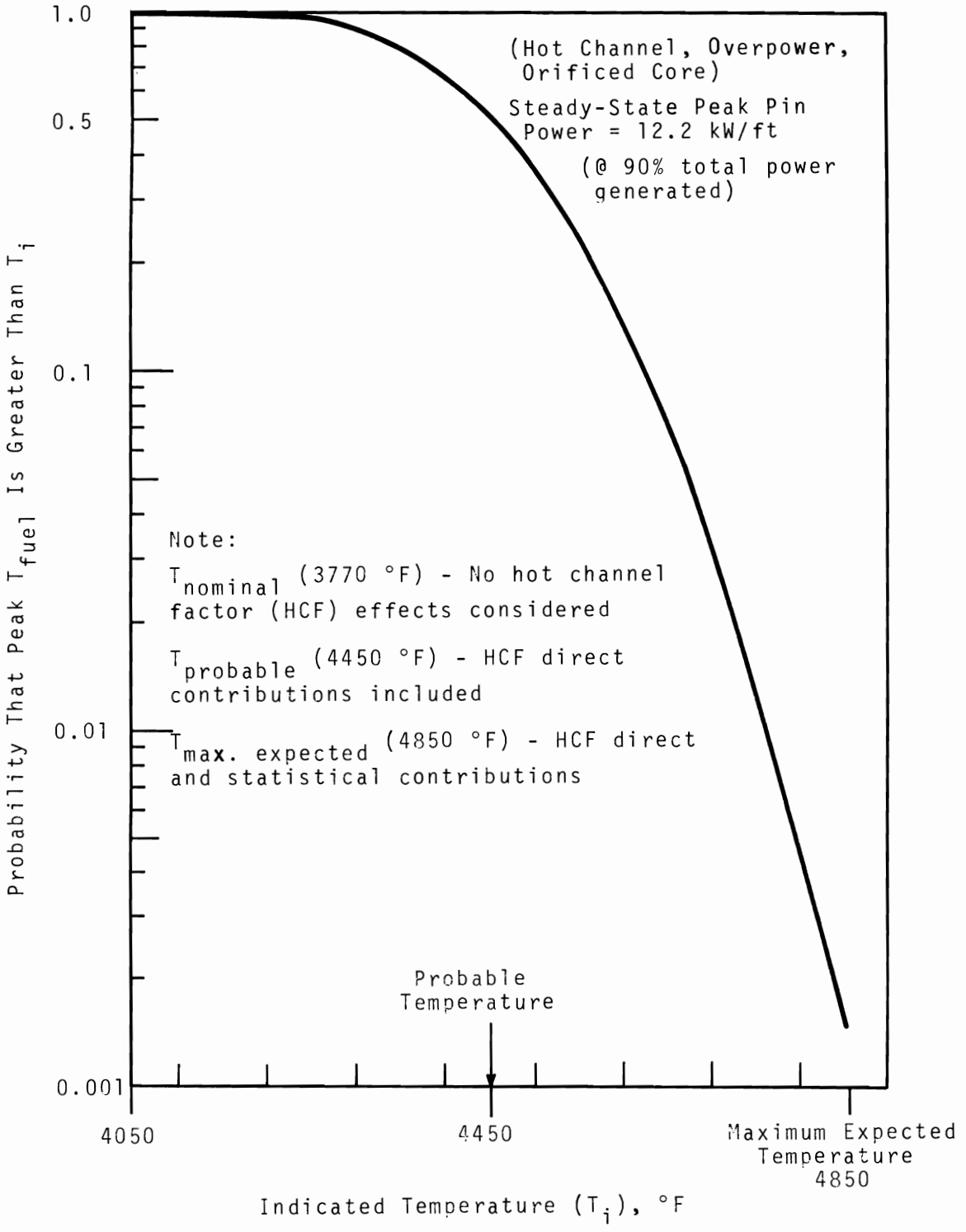

FIGURE 1.4-9. Peak Fuel Temperature Versus Probability That T_{fuel} Is Greater Than $T_{indicated}$

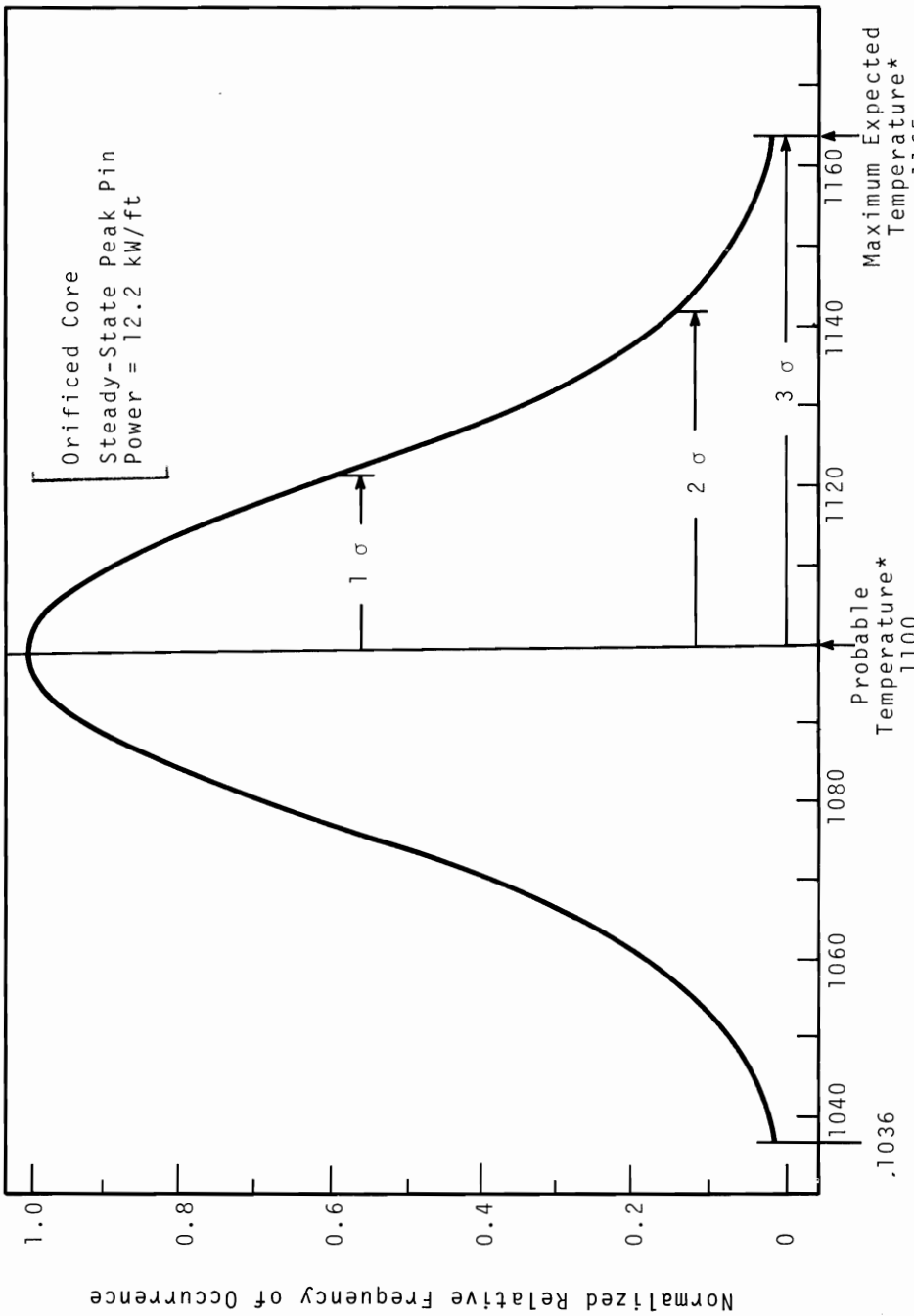

*NOTE: $T_{nominal}$ - (1010 °F) No hot channel factor (HCF) effects considered

$T_{probable}$ - (1100 °F) - HCF direct contributions included

$T_{max.\ expected}$ - (1165 °F) - HCF direct and statistical contributions

FIGURE 1.4-10. Peak Hot Channel Clad Temperature (Steady-State) Versus Frequency of Occurrence

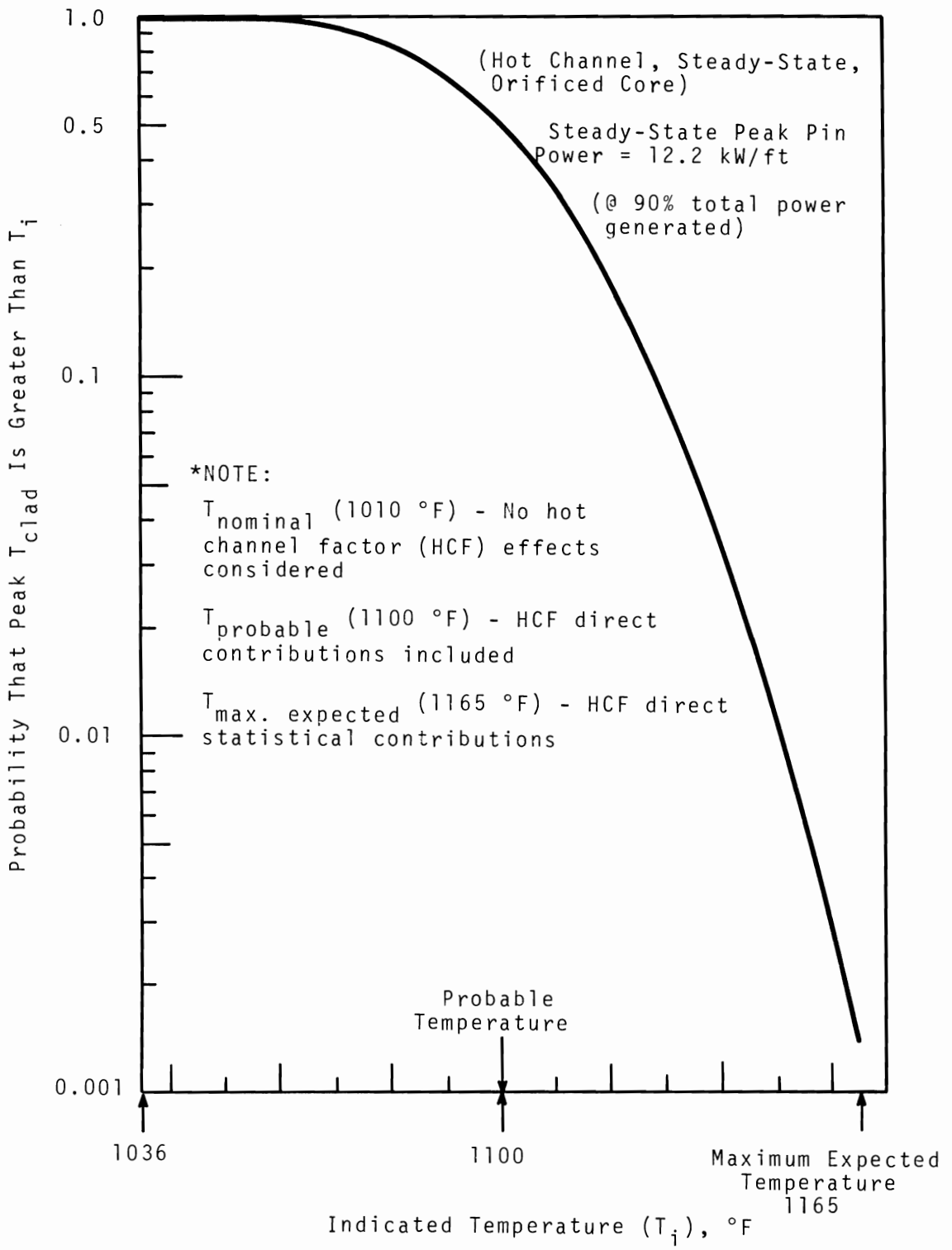

FIGURE 1.4-11. Peak Clad Temperature Versus Probability That T_{clad} Is Greater Than $T_{indicated}$

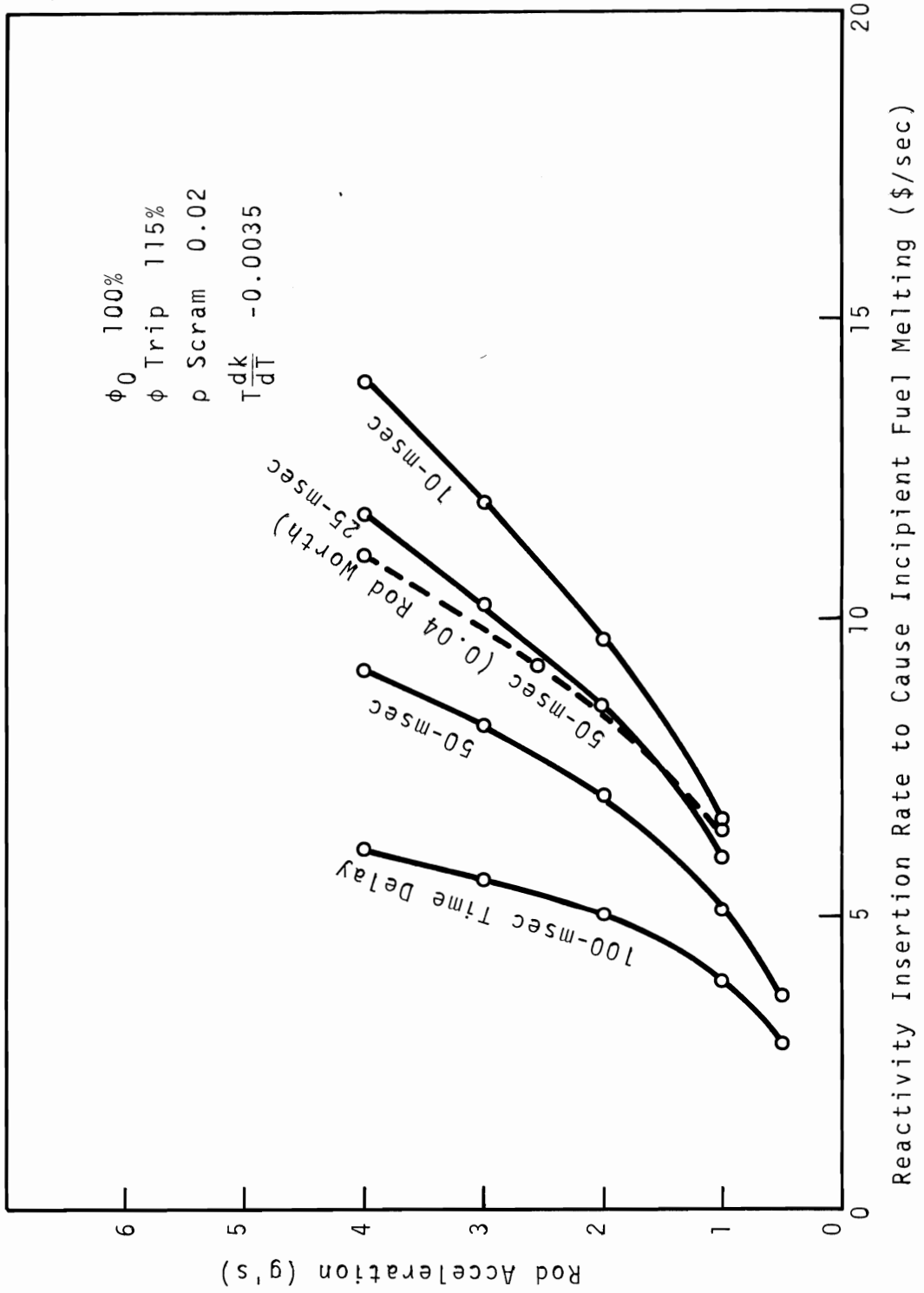

FIGURE 1.5-1. Safety Rod Acceleration Required to Prevent Fuel Melting in Hottest Fuel Pin

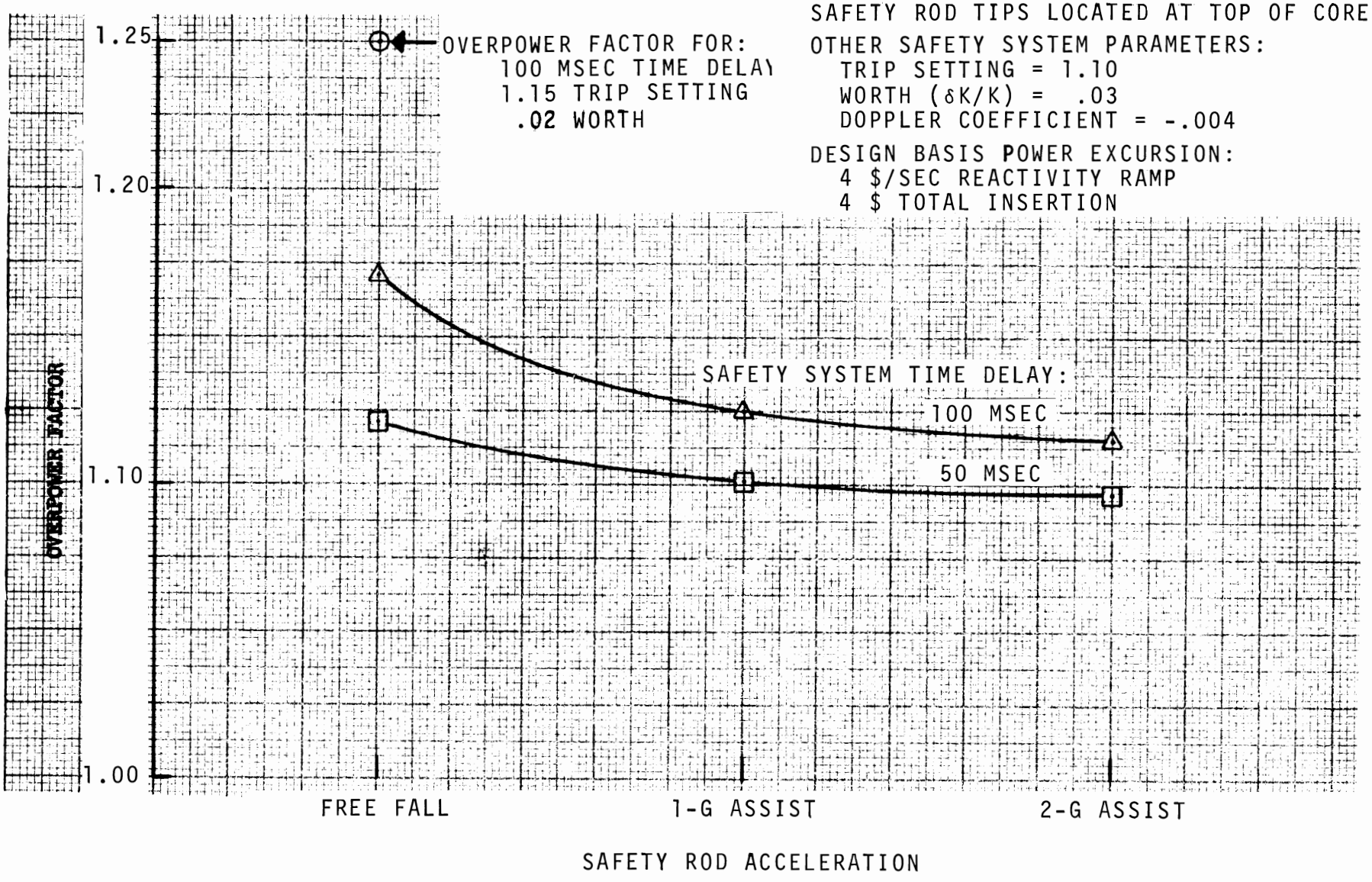

FIGURE 1.5-2. Effect of Safety System Time Delay and Rod Acceleration on Overpower Factor

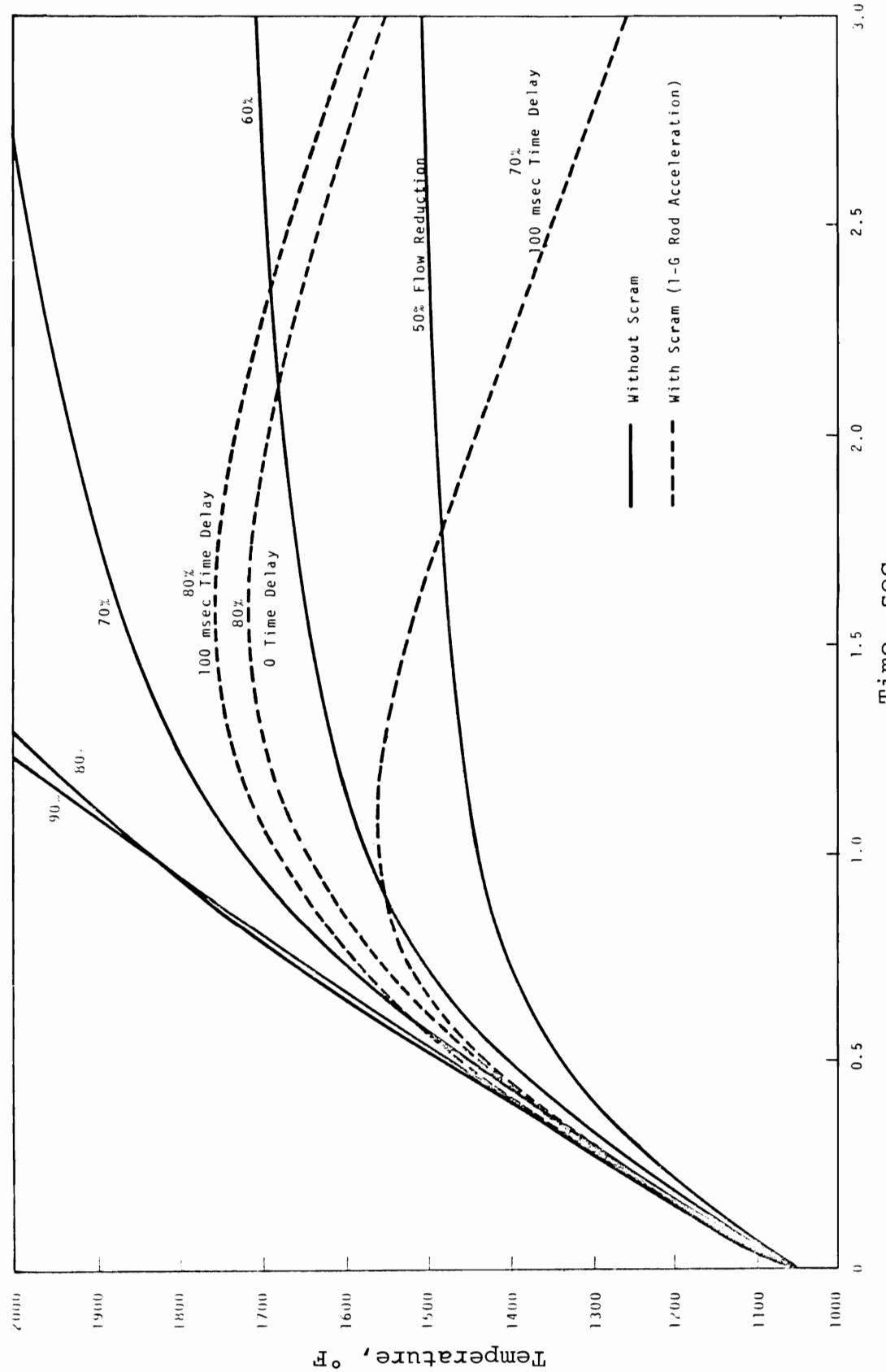

FIGURE 1.5-3. Coolant Temperature Response to Instantaneous Flow Reduction: 14.4 kW/ft Hottest Fuel Pin

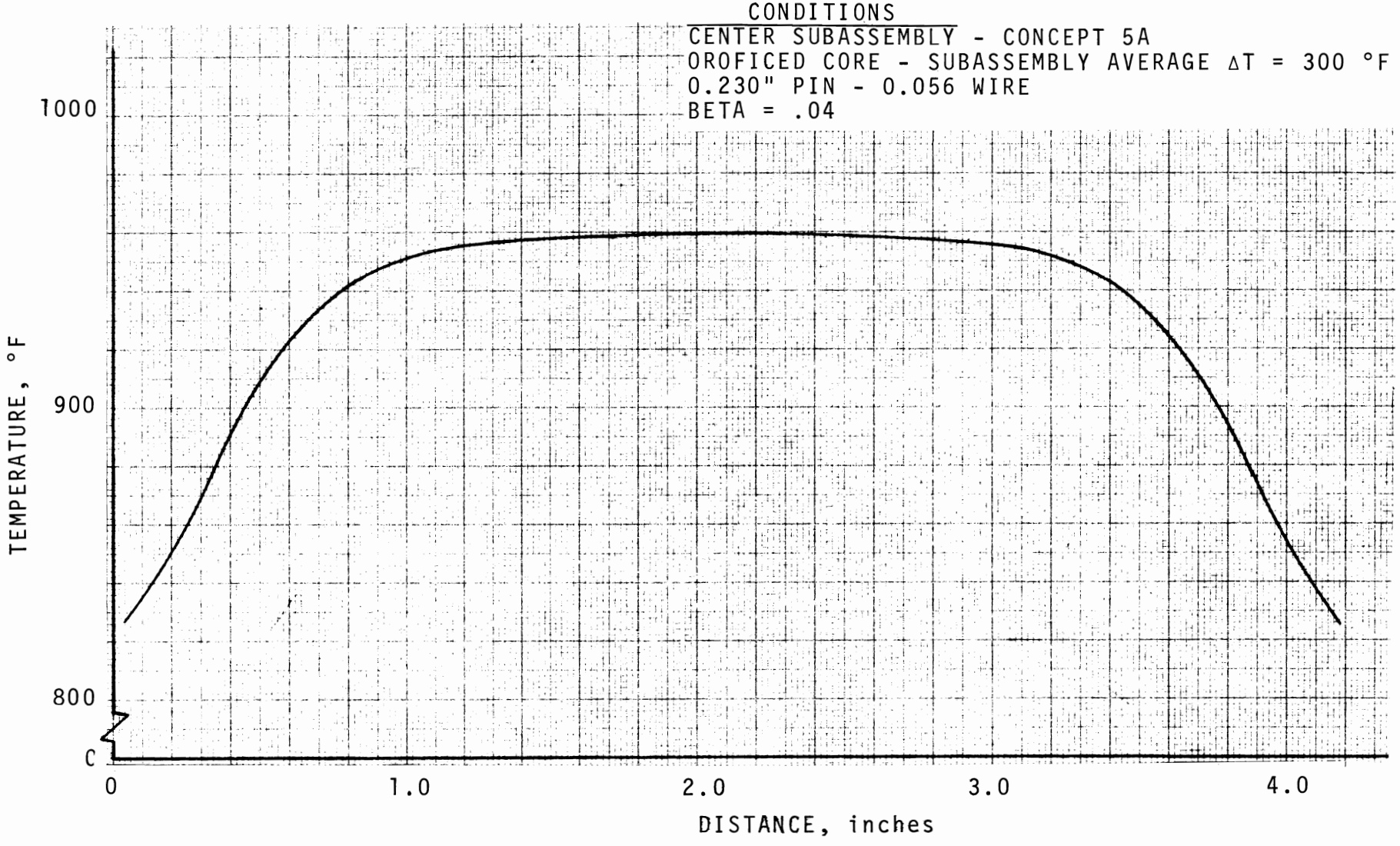

FIGURE 1.6-1. Subassembly Radial Temperature Profile at Top of Active Core

BWNL-1064

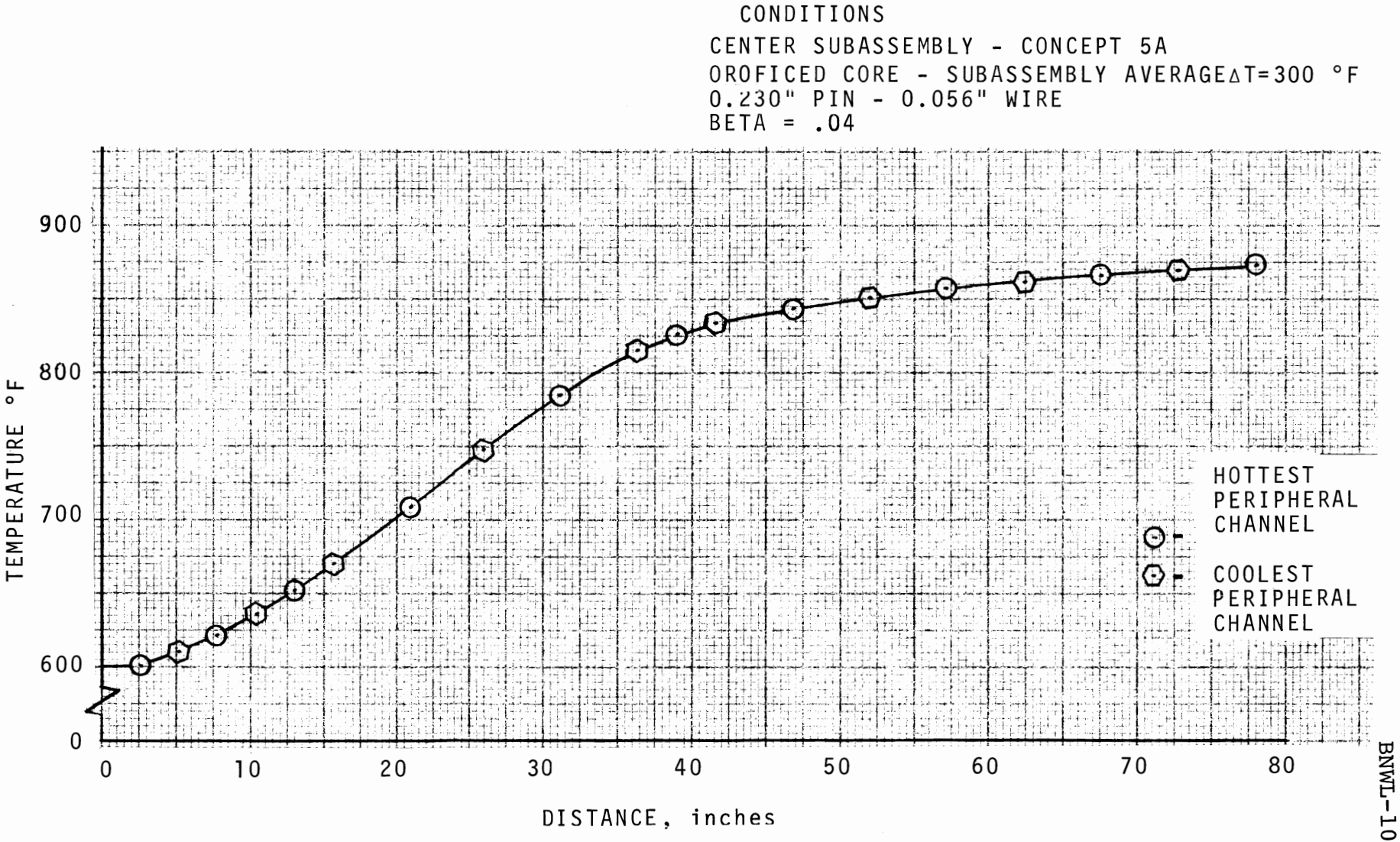

FIGURE 1.6-2. Subassembly Axial Temperature Profile

BNWL-1064

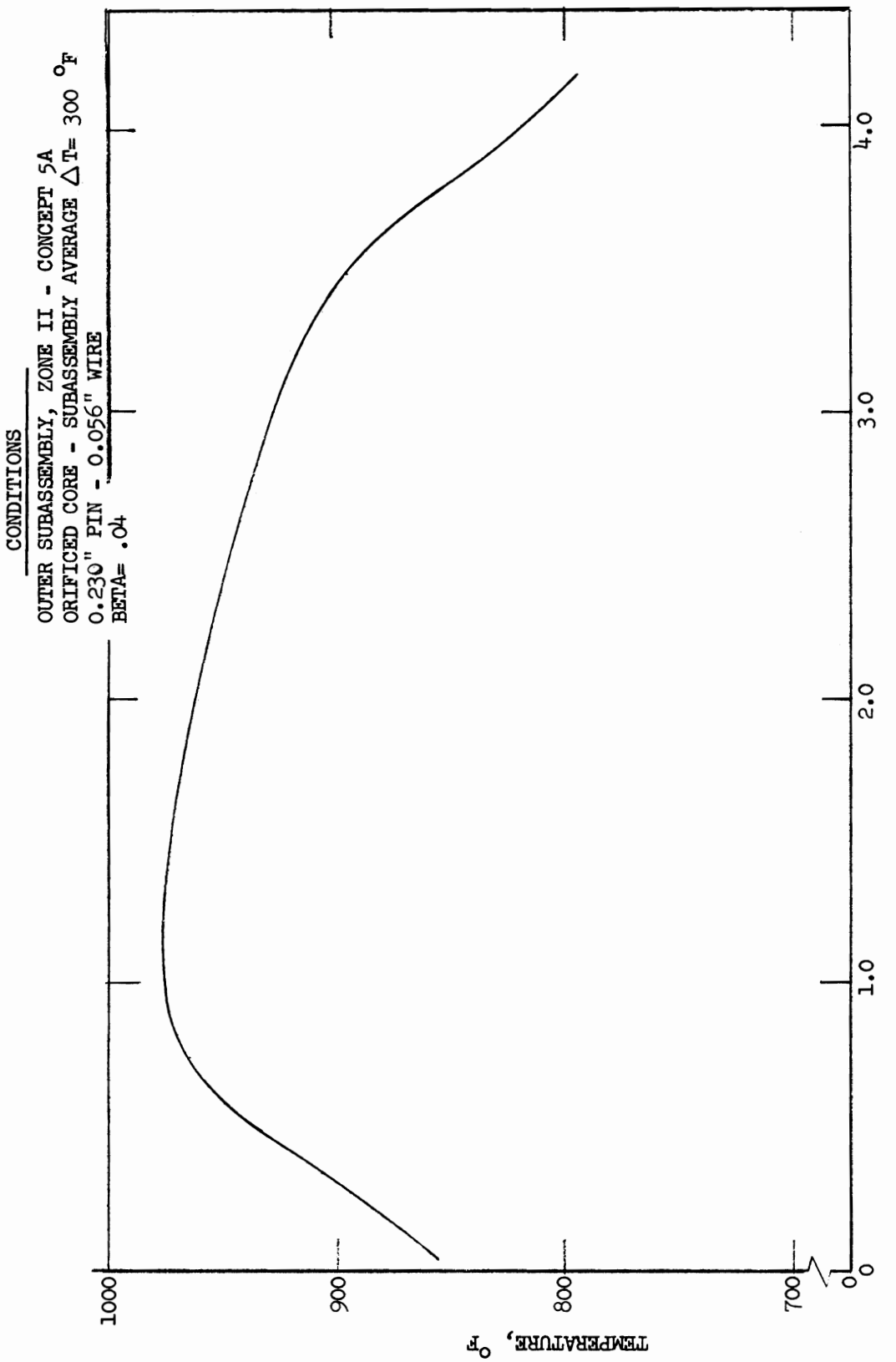

FIGURE 1.6-3. Subassembly Radial Temperature Profile at Top of Active Core.

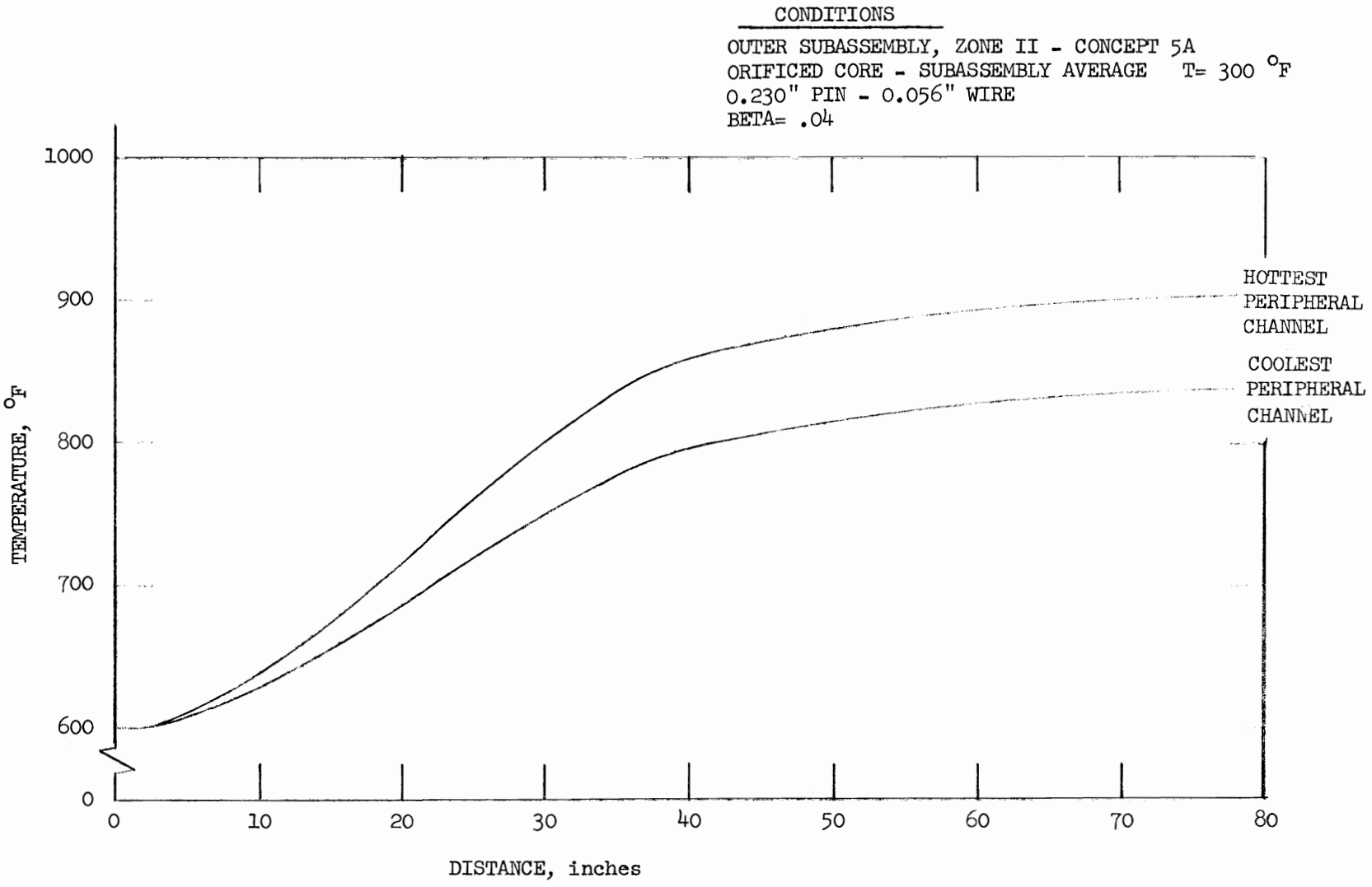

FIGURE 1.6-4. Subassembly Axial Temperature Profile

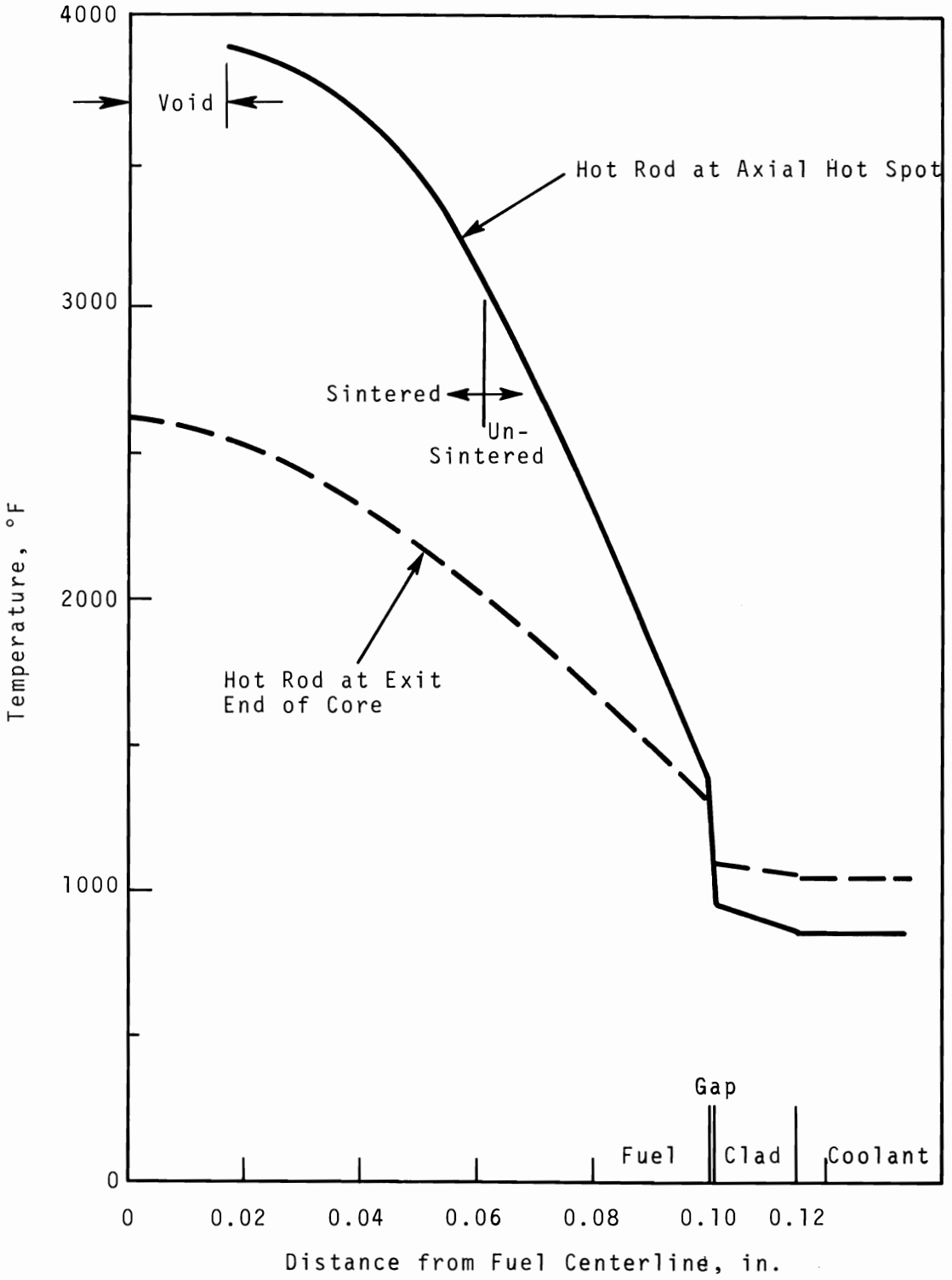

FIGURE 1.6-5. Temperature Distribution in Hot Fuel Pin (steady-state, with hot channel effects, probable temperature)

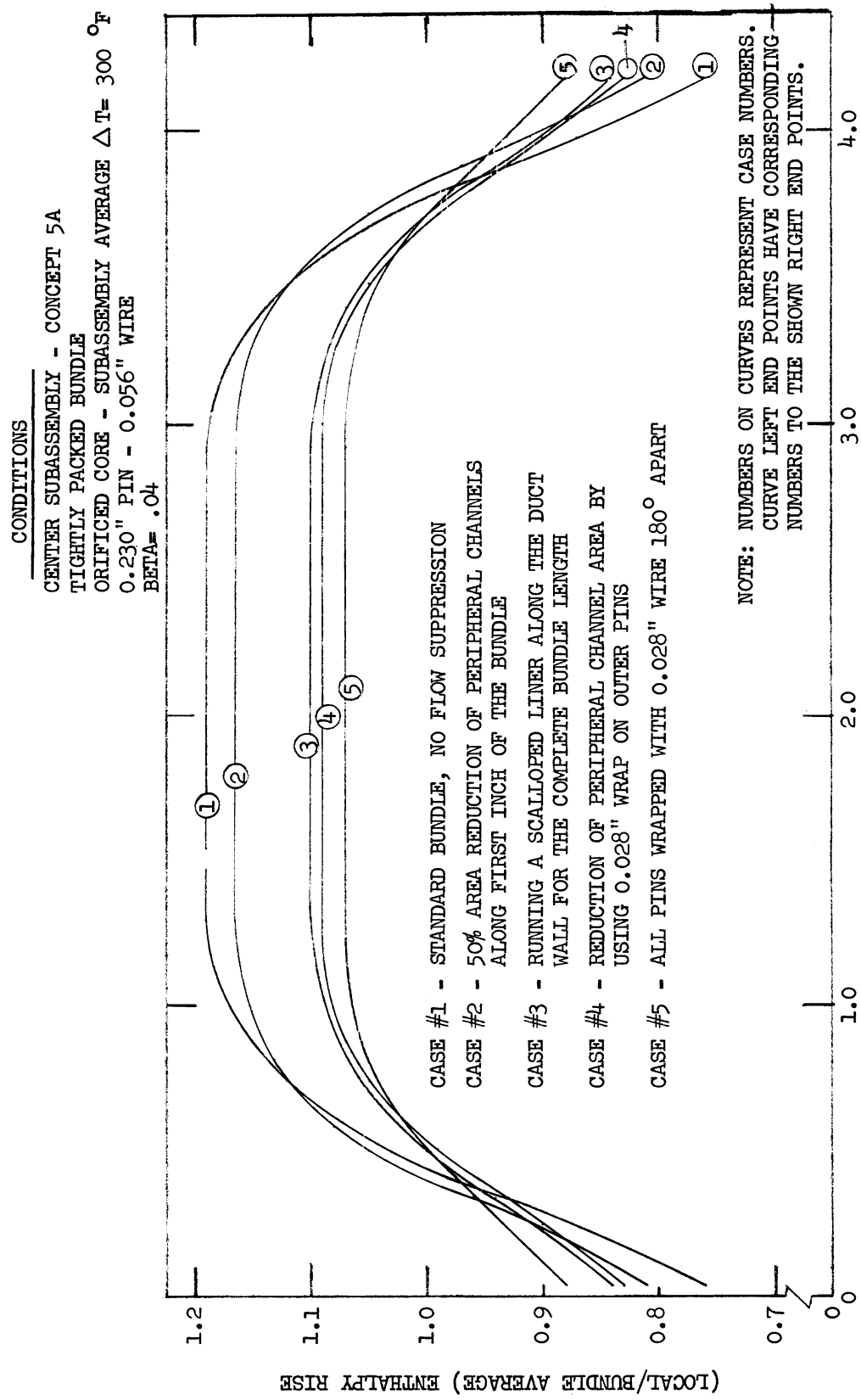

FIGURE 1.6-6. Comparison of Peripheral Flow Suppressors

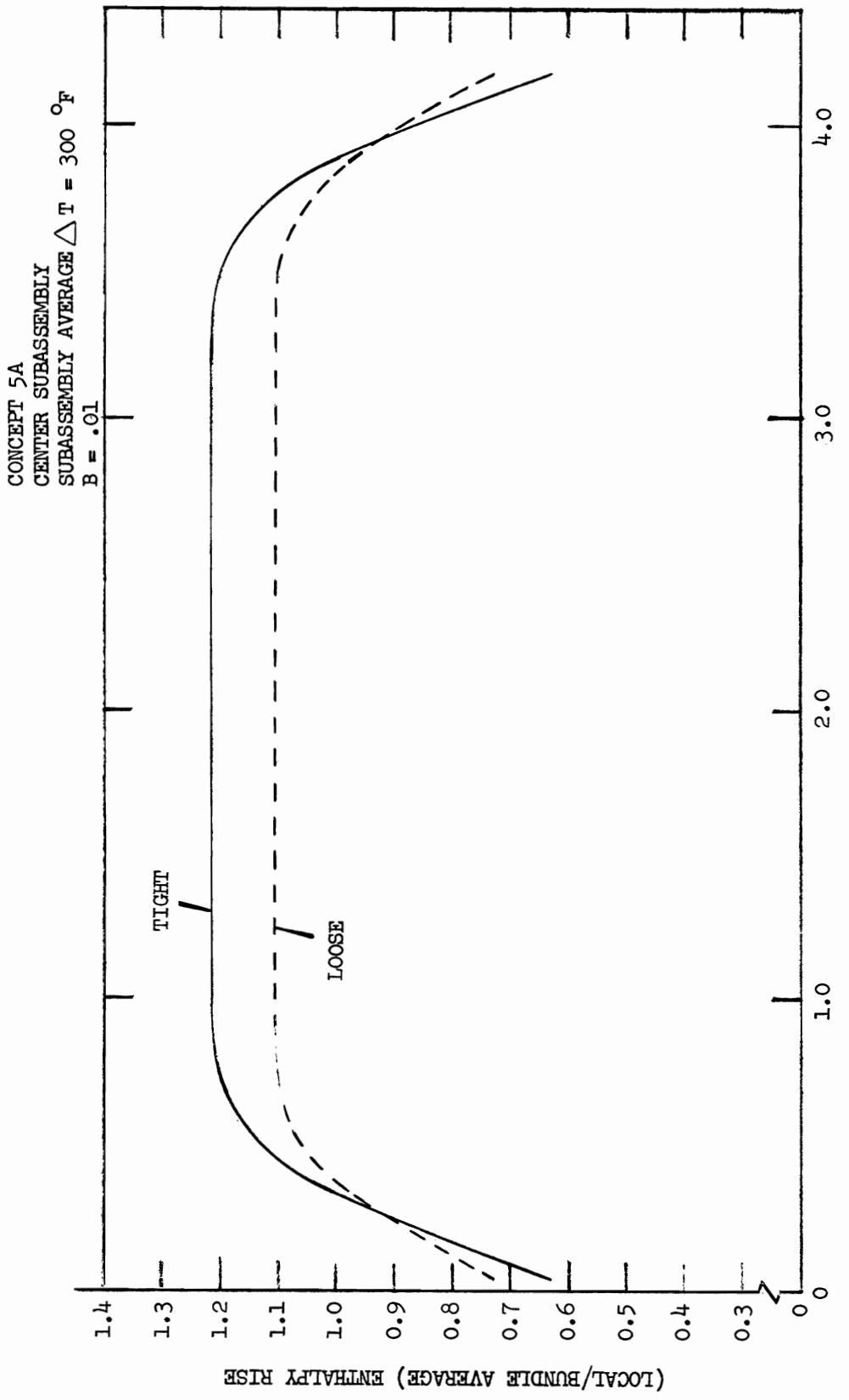

FIGURE 1.6-7. Comparison of Enthalpy Rise for Loose and Tight Packed Rod Bundles at Top of Active Core

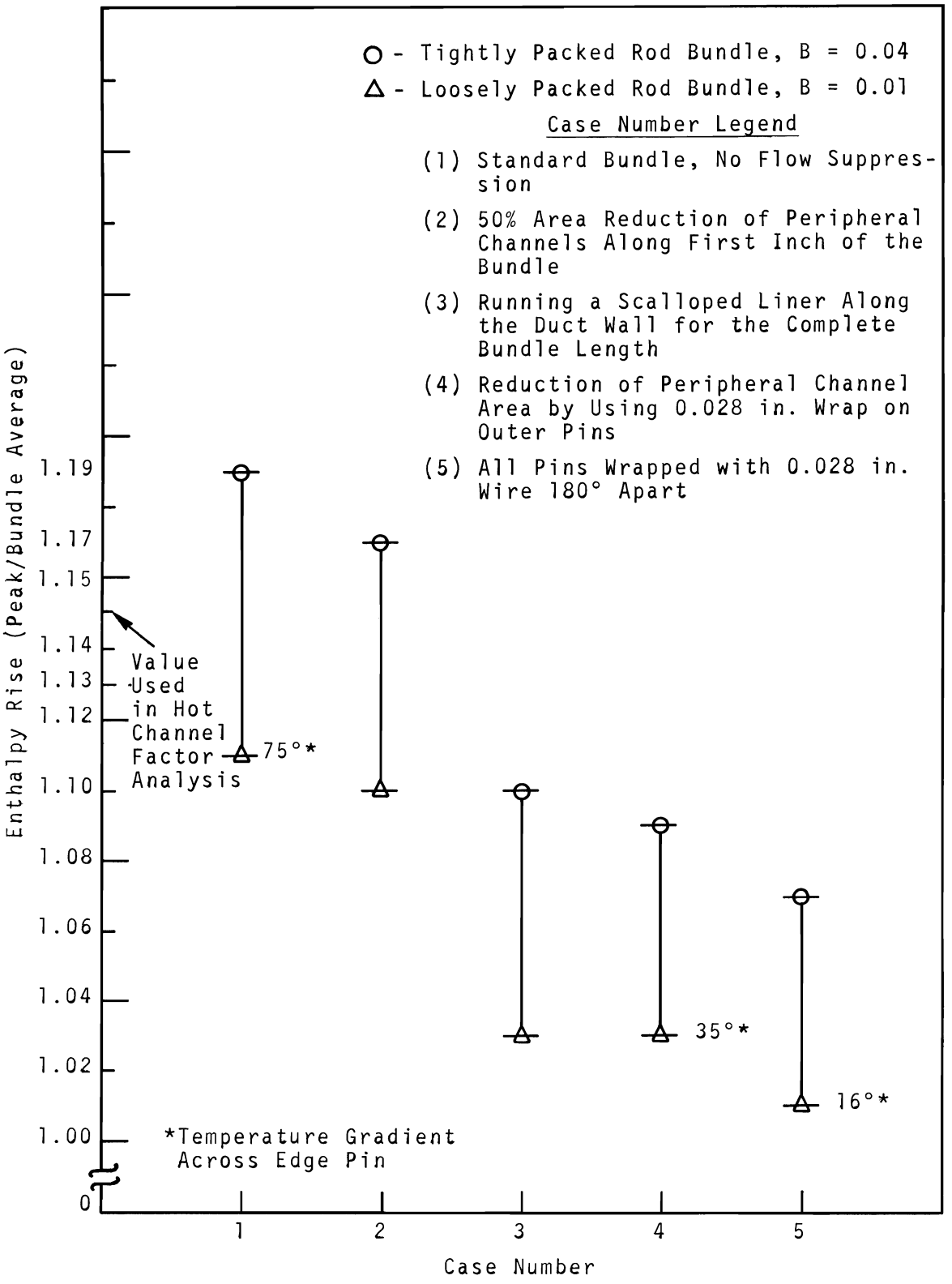

FIGURE 1.6-8. Comparison of Peripheral Flow Suppressors

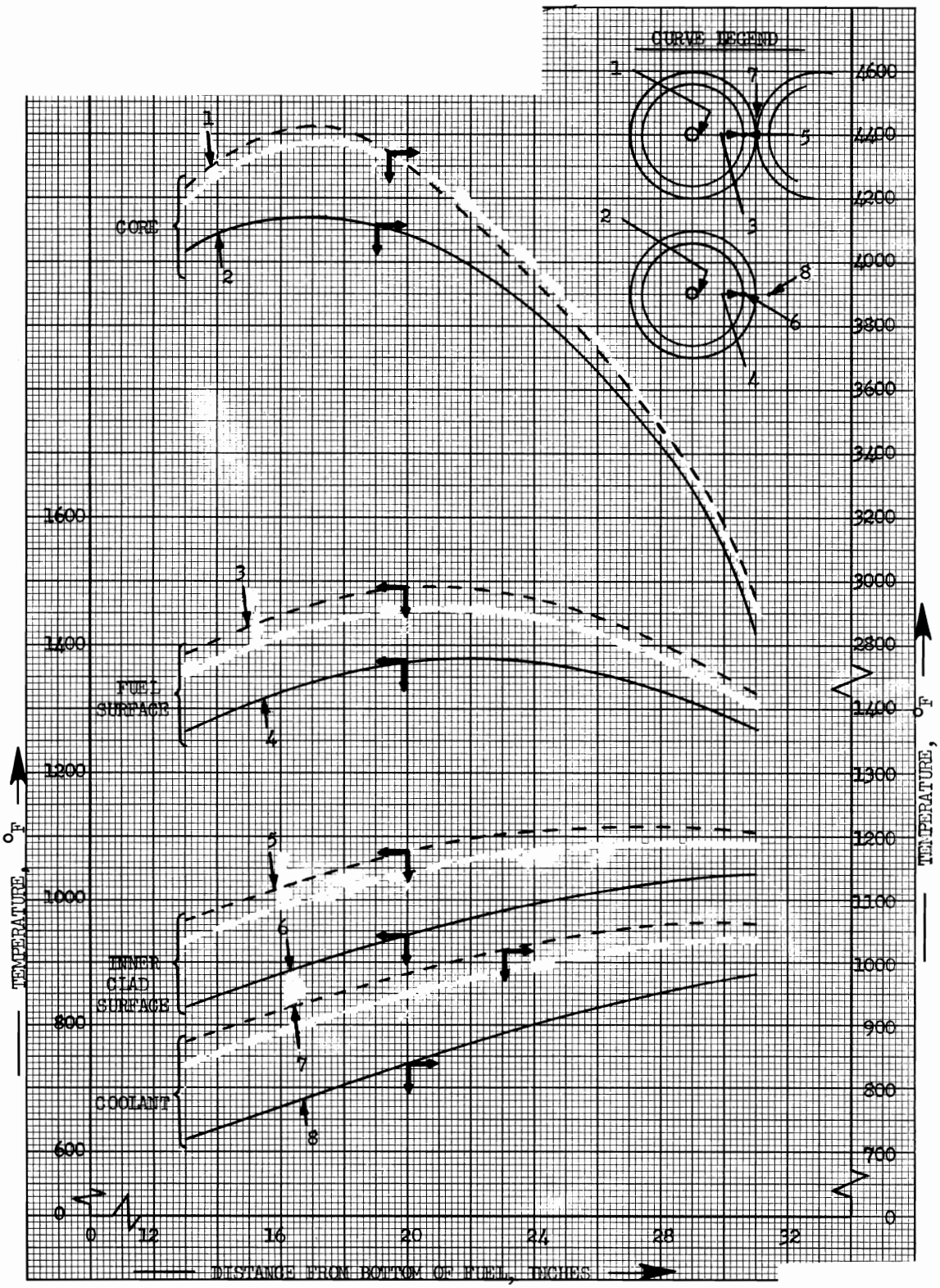

FIGURE 1.7-1. Summary of Hottest Pins (Touching and Non-Touching) Axial Profile Temperature Distributions

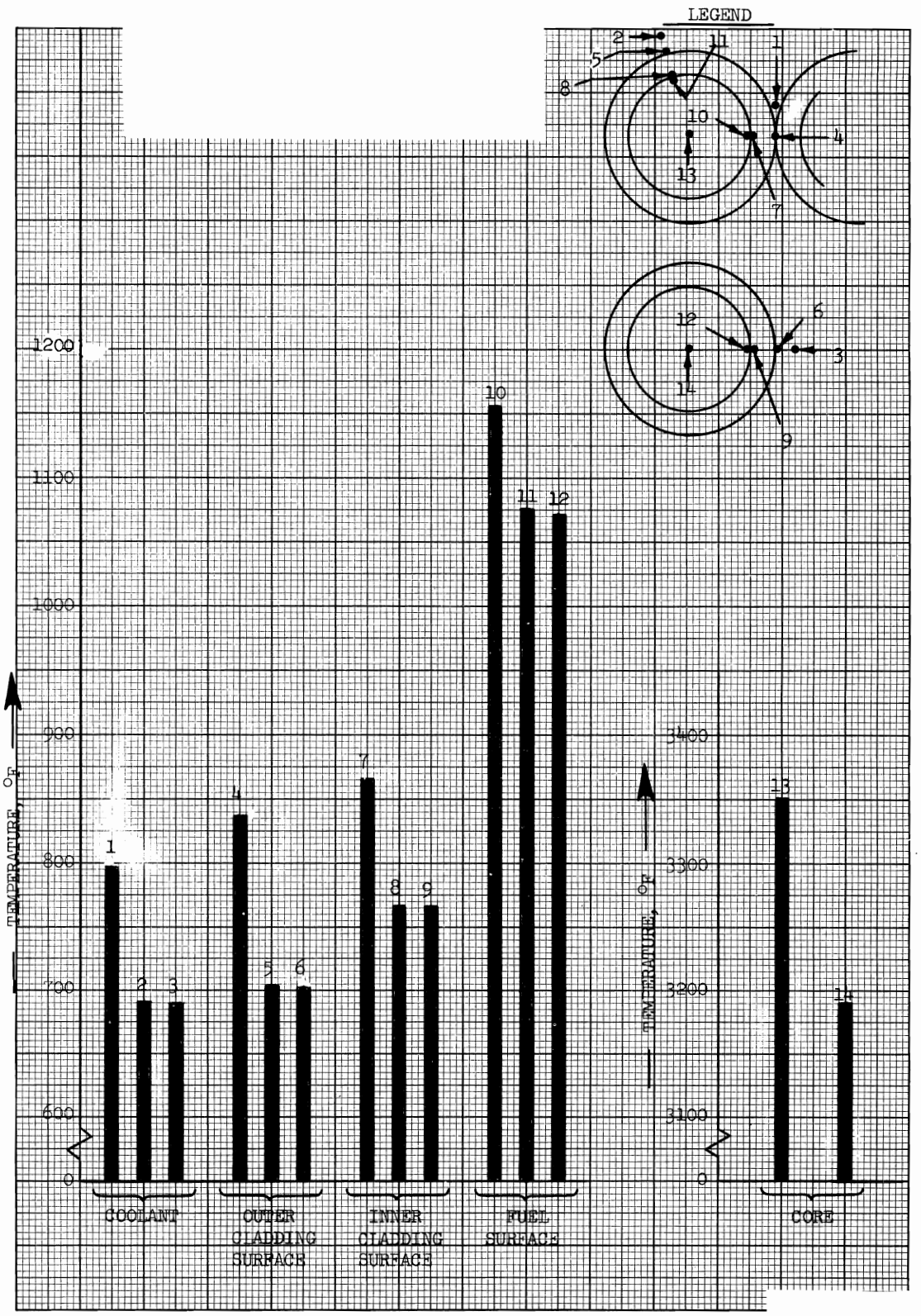

FIGURE 1.7-2. Average Pin's (Touching and Non-Touching) Temperature Distribution at Midplane of Fuel

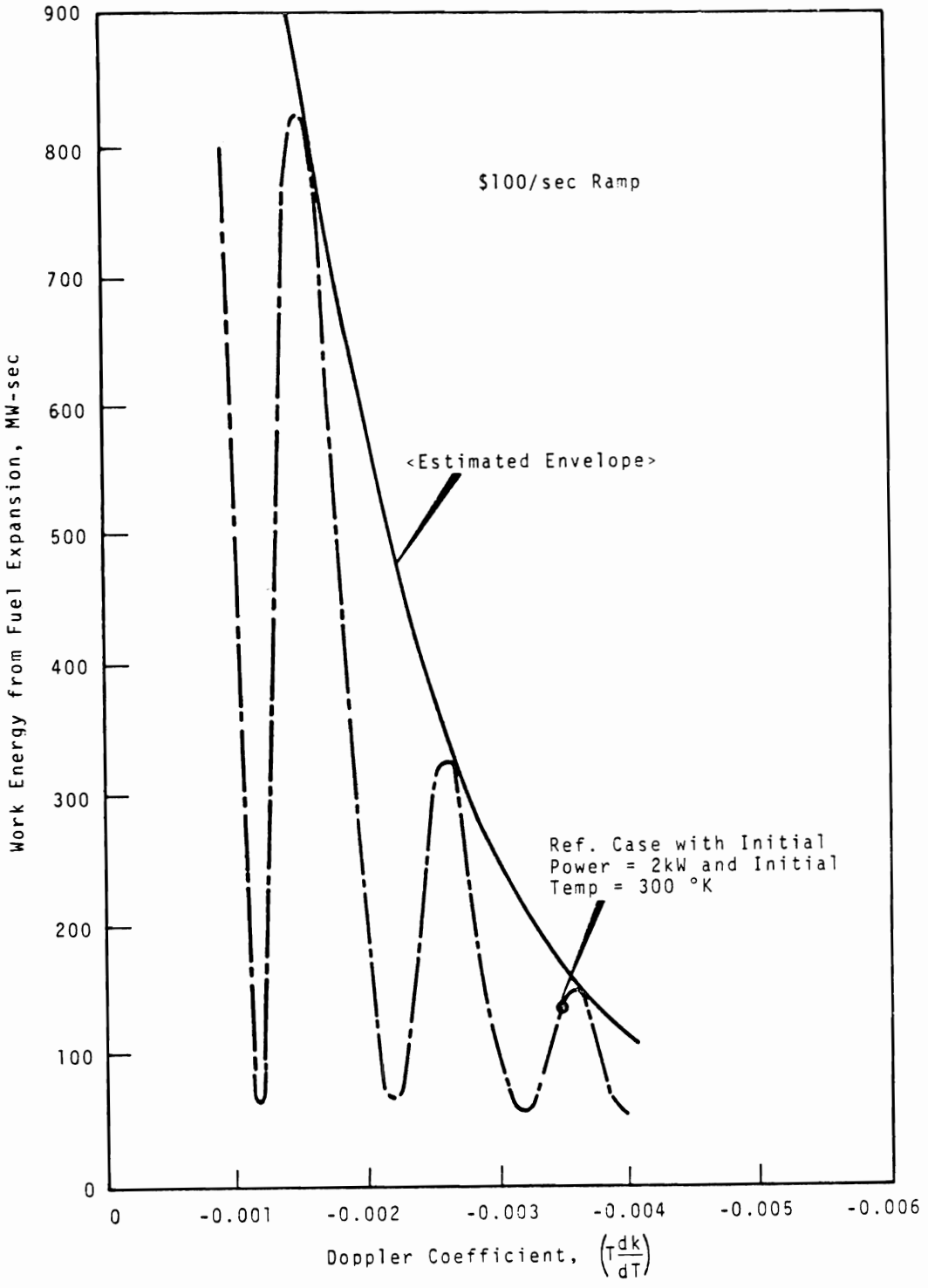

FIGURE 1.8-1. Effect of Doppler Coefficient on Energy Release for Shutdown Accident

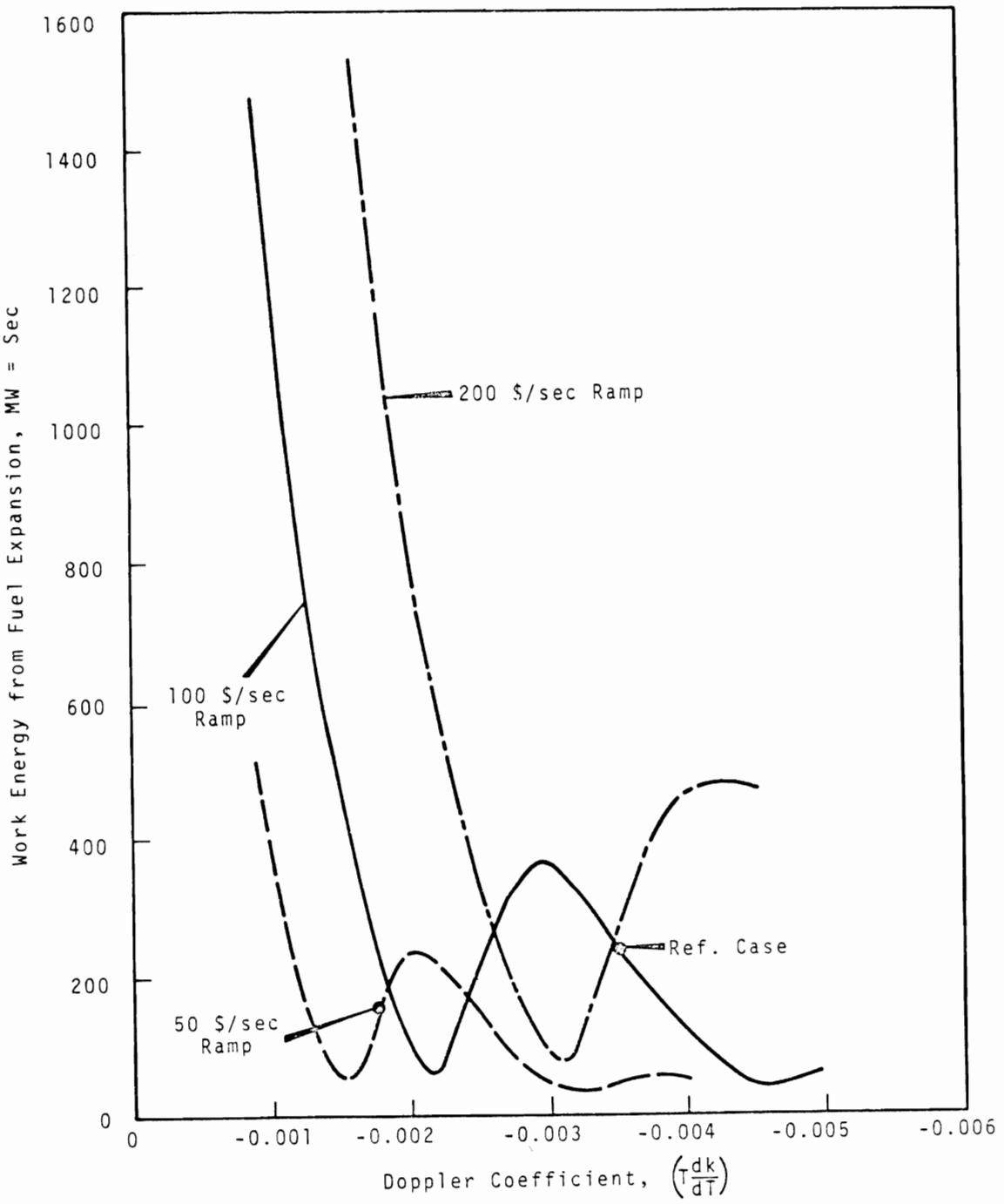

FIGURE 1.8-2. Effect of Reactivity Ramp, and Doppler Coefficient on Energy Release for Full Power Accident

2.0 FUEL AND SUBASSEMBLY HYDRAULIC BEHAVIOR AND DESIGN

2.1 ORIFICING AND PRESSURE DROP

Reference Design: 145 psi maximum pressure drop through vessel.
120 psi fuel assembly design limit.[100]

The required subassembly flow rates for two types of orificing schemes are shown in Figure 2.1-1. The flow rates are based on currently available BNW power distributions and are subject to change as better nuclear data become available. The bundle fluid average velocity for both 50 and 56 mil wrap is shown in Figure 2.1-2. Pressure demand curves for the pin bundle are given in Figure 2.1-3 and 2.1-4 for 56 mil and 50 mil wrap, respectively. The frictional pressure drop across the bundle was computed using the standard Darcy equation with the wire wrap effects included in the friction factor. The pin bundle friction factor is shown in Figure 2.1-5. The subassembly entrance and exit losses are shown in Figure 2.1-6. Other subassembly pressure drops which include all interior expansion and contraction losses and all frictional losses except bundle losses are shown in Figure 2.1-7.

The frictional losses were computed using the Darcy equation and a smooth tube friction factor. The expansion and contraction losses are computed by:

$$\Delta P_c = \frac{K M^2}{288\ p\ g_c A^2}$$

where K = Dimensionless resistance coefficient
M = flow rate, #/sec
p = density, #/ft^3
A = smaller flow area, ft^2.

The pressure drop through the instrument package was determined by assuming that the required tangential velocity in the vortex generator is 15 ft/sec and that the straightening

vains can recover 70 to 80% of the rotational energy. Instrument package ΔP is shown in Figure 2.1-8. Total subassembly ΔP as a function of flow rate is given in Figure 2.1-9 and an axial map of the subassembly pressure drop for the expected maximum and minimum flow rates is shown in Figure 2.1-10.

Present pressure drop calculations are good to about 16%. An error of ±5% is the desirable range. Water and sodium flow tests are being conducted at BNW and ANL, respectively, which will eventually verify the pressure drop.

2.2 CLAD EROSION AND CORROSION

The rate of stainless steel surface material loss in a flowing sodium environment is sensitive to the temperature and coolant oxygen content and broadly insensitive to the velocities of interest for FTR design. Figure 2.2-1 plots the loss rate as a function of temperature for various velocities and oxygen contents.[49] Experimental data obtained from zero pin heat flux, out-of-reactor weight loss tests in the velocity range of 8 to 23 fps were analyzed to yield the following equation:

$$R = 0.006 \exp. (12.8 + 0.88 \ln V - [23{,}827/T] + 1.16 \ln \theta)$$

where R = loss rate, mils/yr
V = coolant velocity, ft/sec
T = clad temperature, °R
θ = coolant oxygen content, ppm

The loss rate is the steady-state value and it is assumed that the "downstream factor"[49] does not apply to the in-reactor condition since the temperature of the coolant, and hence its solubility limits, increase as it moves downstream through the core. The data apply to 316 SS, both cold worked and solution treated.

Also plotted for comparison are some British data[50] which agree reasonably well with the GE data for 25 ppm oxygen content but not so well with the 10 ppm data in the lower temperature regions.

Additional interactions occur which affect the equivalent clad thickness for strength considerations. The surfaces exposed to sodium in the hotter portions of the pins will revert to ferrite due to the leaching of nickel and chromium. Decarburization to the cold-trapped coolant sodium system also occurs. During in-reactor operation, with a thermal gradient across the clad, carbon migrates toward the higher temperature zone of the inner clad surface where measurable grain boundary precipitation occurs.

Sodium purity requirements have not yet been firmly fixed and must be set during preliminary design. An oxygen limit of 10 ppm and a carbon limit of 20 ppm are recommended preliminary valves for design.

Considering a peak (hot channel) design clad surface temperature of 1100 °F, the nominal expected metal loss during the pin lifetime of one full power year is ∿0.1 to 0.3 mil for a coolant system with 10 ppm oxygen. This agrees reasonably well with the BNW experimental data obtained with flowing sodium at 30 fps, 1060 °F for 375 days where an erosion of <0.4 mil was reported.[51] The additional interactions will also contribute some equivalent clad thickness loss which has not yet been completely investigated. Assuming a value equivalent to the measured metal loss data, an expected erosion-corrosion allowance of ∿0.6 mil is indicated and recommended for FTR design purposes.

2.3 FLOW-VIBRATION EFFECTS, FRETTING (see also Section 3.6)

The effects of vibration, fretting, and self-welding are being investigated by current analytical and experimental

efforts which are defining the behavior of the FFTF subassembly during operation in the FTR.[53] Uncertainties existing in areas of vibrational behavior will be resolved by experimental studies of individual fuel pins and complete subassemblies in hydraulic and vibrational test facilities.

These tests will be complemented with visual examinations of complete subassemblies tested in the CCTL. These tests will provide an isothermal proof test of the pin and subassembly design and permit assessment of potential vibration, fretting, and self-welding.

Probable limits are about 1 mil per year material removal. Irradiation effects on the material subject to fretting corrosion is presently also unknown. Risks involved in not doing the analysis and tests include anomalous fuel element behavior, design deficiencies, and possible in core failure.

Table 2.3-1 lists the experimental and calculated vibration characteristics of the fuel pin. A complete discussion of vibration characteristics and tests are given in BNWL-750.[53]

2.4 ELEMENT SPACER EFFECTS

Greater operational experience relative to the complete environment suggests that the first core driver design should employ wire wrap spacing rather than grid spacers. Further, investigation of the wire spacer has disclosed no major operating problems. Material, mechanical and thermal-hydraulic problem areas which have not yet been fully investigated exist in both spacer designs. A convincing scientific comparison of the two spacer system would require consistent and complete designs.

Full size subassembly ex-reactor hydraulic and environmental tests of the wire wrap spacers are being conducted in water at BNW and sodium flow loops (CCTL) at ANL.

TABLE 2.3-1. Calculated and Test Vibration Data for Clad Tubes, Fuel Pins, and Solid Rods

Mode	Hollow Tube,[a] cps		Fuel Pin, cps					Solid Rod,[a] cps		
					Theoretical Lumped Mass				Theoretical	
	Experimental	Theoretical	Experimental (No F-F Wires)	Experimental (Fixed-Fixed)	Fixed-Fixed	Fixed-Pinned	Pinned-Pinned	Experimental	Exact	Lumped Mass (20)
1	7.2	9.5	6.3	6.3	6.29	4.77	2.82	8.5	8.04	8.05
2	37	26.1	20.5	19.5	19.9	16.5	13.1	32	22.1	22.2
3	39	51.2	21.5	20.5	38.1	32.1	27.7	35	43.5	43.5
4	105	84.8	35	35	62.8	56.8	49.8	87	71.8	71.9
5	110	126	37	37	92.4	84.9	77.6	91	107	107.4
6	210	176	52	51	132.0	123.4	113.2	160	149	149.9
7	220	235	54	53	164.9	151.8	145.0	175	199	199.4
8					200.7	199.0	188.0			255.6
9					265.7	244.5	244.3			318.5
10					323.1	313.6	313.6			387.4

a. Same dimension as reference fuel pin

Tests of the wire wrap spacer configuration in the BNW sodium loop have proven fully satisfactory. Spacer performance problems include potential loosening, damage, breakage, etc. of the spacers during operation. No operating limits are presently established for spacer other than they must remain integral during fuel life and material loss will be less than 1 mil during the fuel life. As in the previous items, the sodium and water flow test will yield data necessary for prediction of spacer behavior analysis and dictate needed design modifications.

2.5 COOLANT ENTRANCE REGION

The entrance region of the subassembly inlet plenum and receptacle have been designed to minimize identified potential problem areas (See Drawing SK-3-14581, Appendix).

Based on an experimental analysis of various seat arrangements using water,[54] acceptable tolerances and flow leakage rates were established. Further study is needed to fully evaluate these numbers in terms of the needs of the actual environment.

Prevention of flow blockage in a subassembly has received a great deal of attention. There are three major screening devices that have been employed to eliminate potential problems. The outer removable inlet plenum has 1 in. diam holes. Therefore, particles greater than 1 in. in diameter are trapped here. Particles smaller than one in. can pass into the inlet plenum where they can either fall to the bottom or pass on into a subassembly inlet receptacle. Particles of greater than 0.5 in. will be trapped here. When flow is reduced the particle will then be free to fall back down into the inlet plenum chamber. Obstructions of under 0.5 in. diam. will be carried on into the subassembly. Particles smaller than 0.5 in. and larger than pin spacing will be stopped by a particle trap positioned

in the lower subassembly inlet region. The design of this member and its exact location must be investigated further in preliminary design.

The mechanical requirements of the receptacle and subassembly inlet present potential problems. The experimental investigation of bypass flow indicate that a diametral clearance in the range of 0.030 to 0.040 in. can be tolerated. It must be established by further tests scheduled to be performed at LMEC whether this is sufficient clearance to allow easy insertion and withdrawal of the subassembly. Actual tests under sodium at temperature will help to establish these design limits. Additional precautions to prevent galling such as hard surfacing will be experimented with.

2.6 COOLANT EXIT REGION

The coolant exit region places many difficult requirements on the instrument tree interface. The design outlined in Section 2.2.12 of the Reactor Core Design Description[95] (which is in the process of being updated) allows for deflection of the outer subassembly rows. This is accomplished by allowing sufficient clearance between the instrument probe and the duct, and will prevent the duct from transmitting any moment loading to the instrument tree.

Temperature gradients which might be experienced in this region could create high thermal stresses in the instrument tree support plate. In order to reduce this problem a laminated or honeycomb structure is being proposed which would not be sensitive to thermal gradients.

The inability to provide support for the individual subassemblies in the core center is not considered a problem. It has been pointed out that potential bridging between subassemblies

will make it impossible to tighten the subassemblies in the center. It has also been thought that these loose subassemblies would provide trouble in fretting on the instrument probe. This problem does not exist in the actual core in the at power condition. There is only a potential for this problem to exist in the early stages of operation when the reactor is shut down. For any other time the thermal gradients and swelling will cause the ducts to bow and therefore provide a tight lattice throughout the core.

In the actual case the potential does exist for generating restraint forces above an acceptable limit due to these mechanisms. Careful design of the duct and restraint mechanisms must be used to reduce these forces to a minimum value.

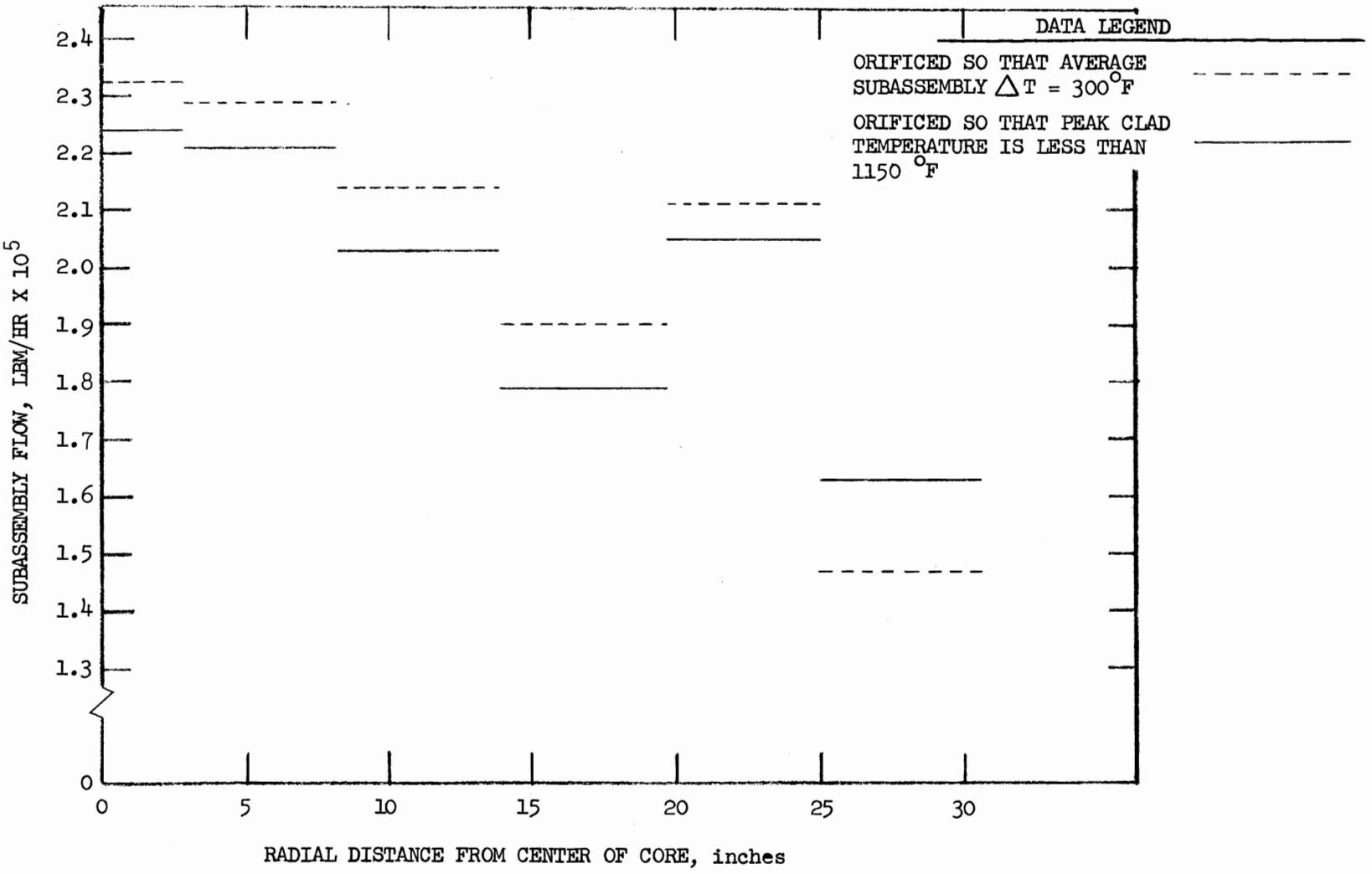

FIGURE 2.1-1. Coolant Flow Rate in Driver Fuel Subassemblies (LBM*/HR) as a Function of Radial Distance from the Center of the Core

* *M = Mass*

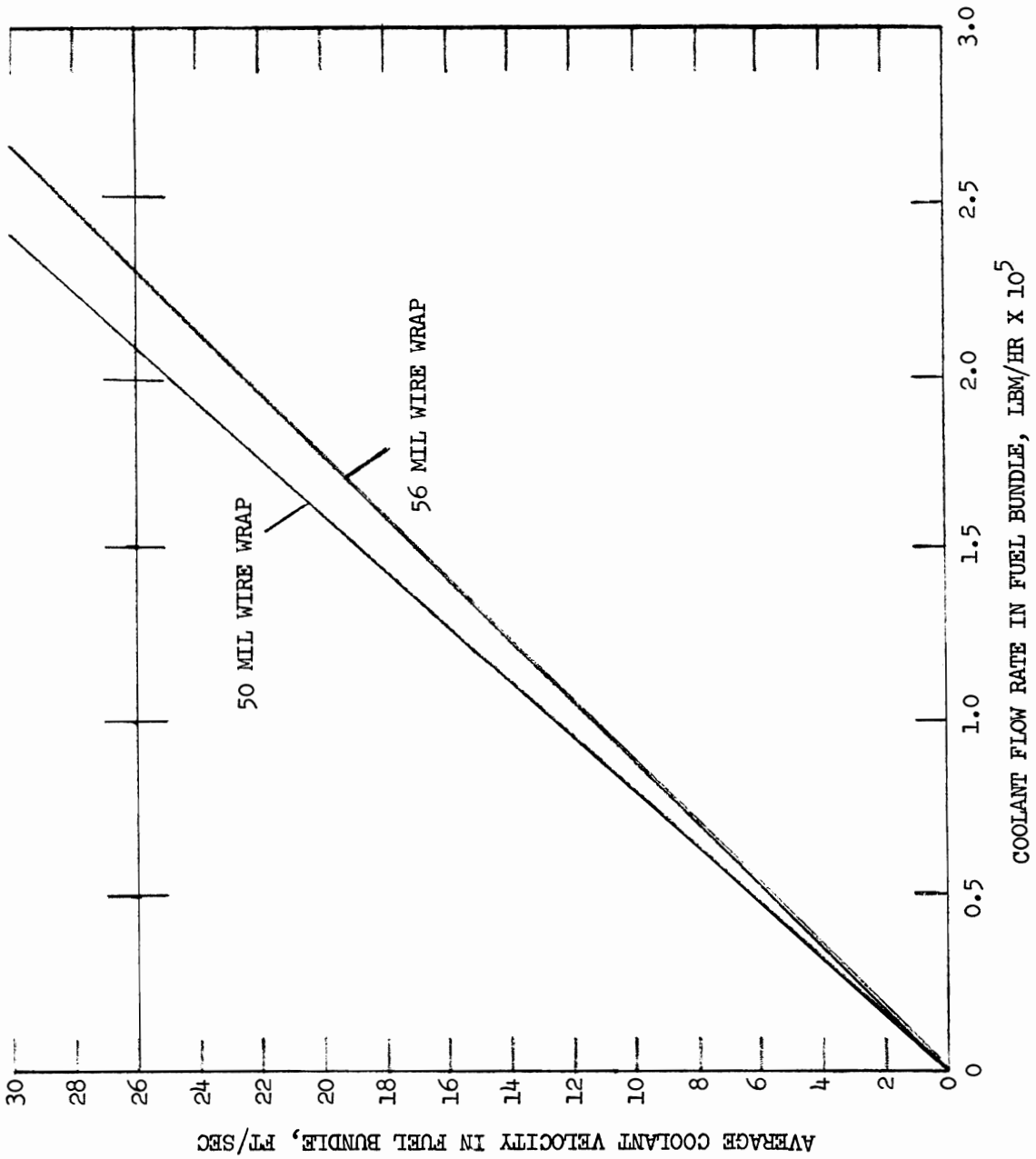

FIGURE 2.1-2. Average Coolant Velocity in the Fuel Bundle (ft/sec) as a Function of the Coolant Mass Flow Rate in the Fuel Bundle (LBM/HR)

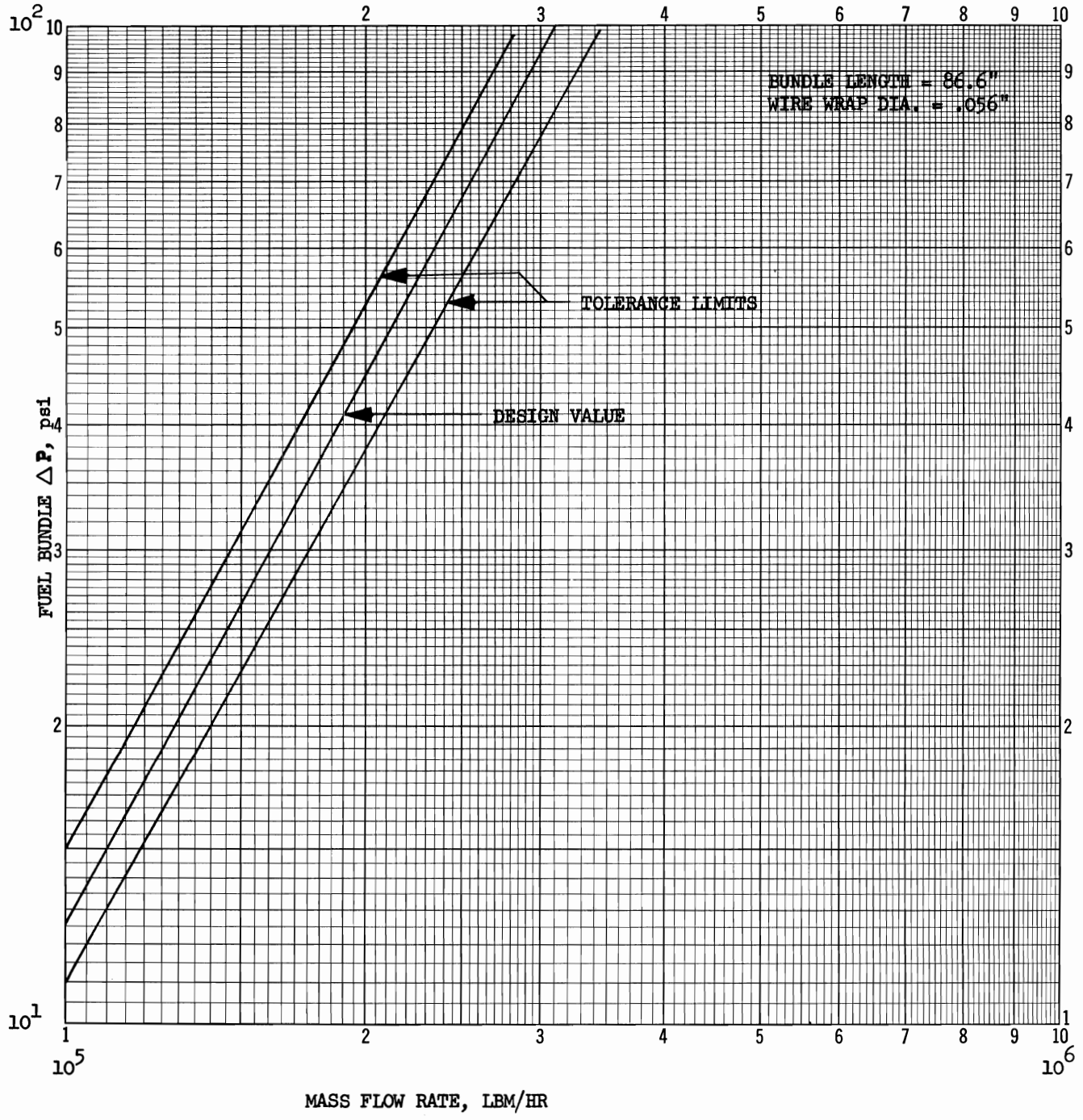

FIGURE 2.1-3. Fuel Bundle ΔP, as a Function of the Mass Flow Rate (0.056 in. Wire)

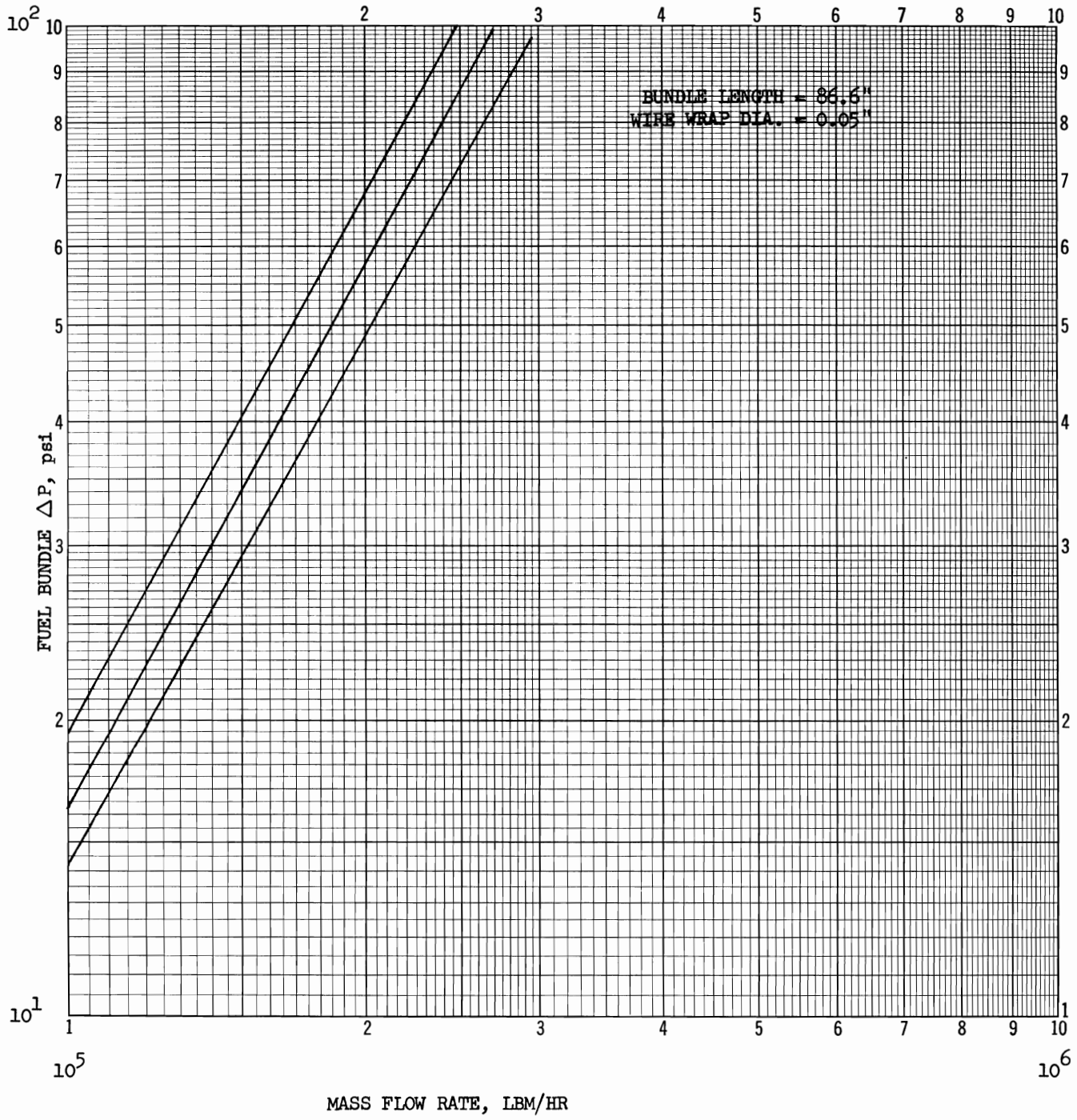

FIGURE 2.1-4. Fuel Bundle ΔP, as a Function of the Mass Flow Rate (0.050 in. Wire)

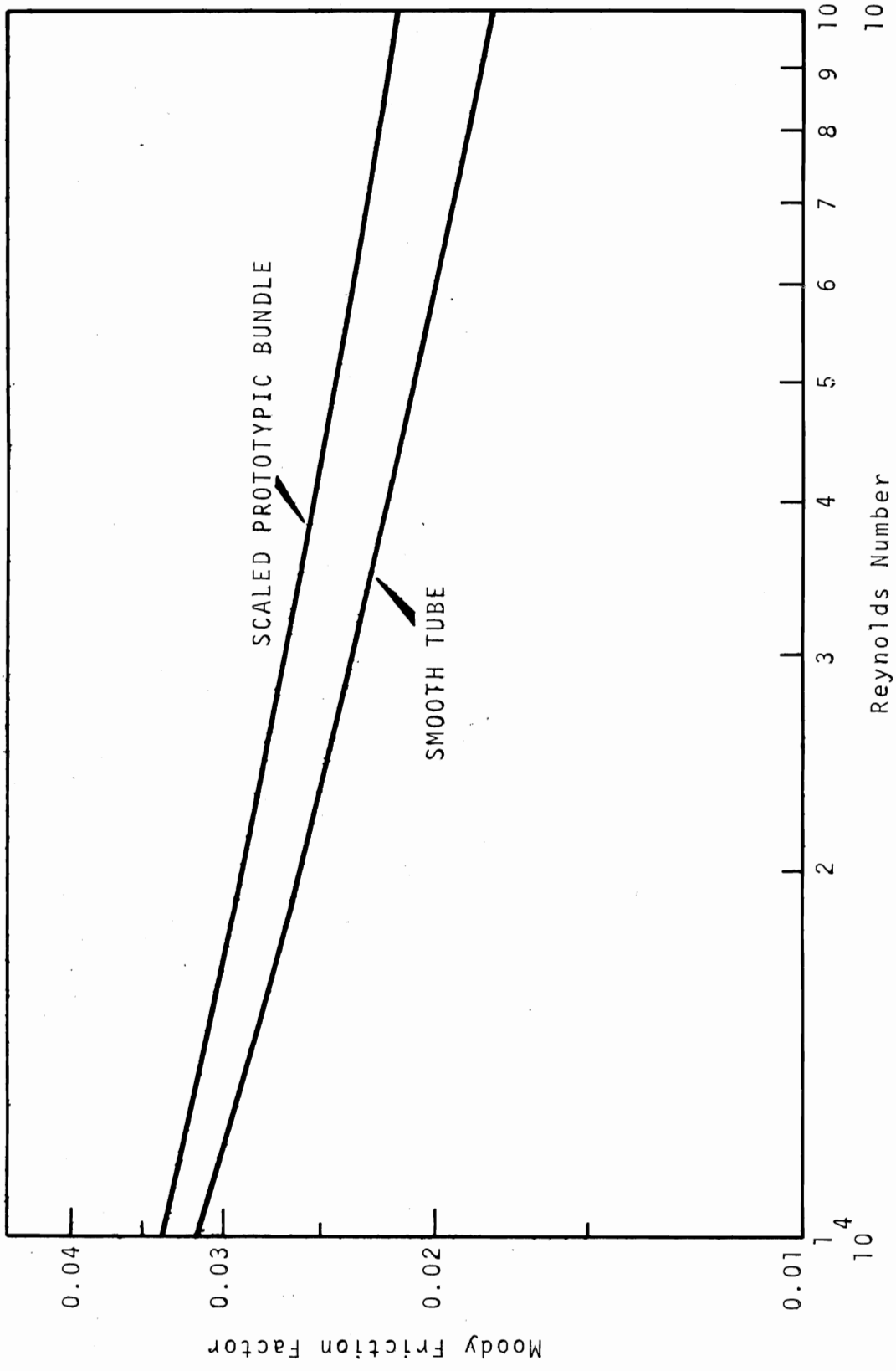

FIGURE 2.1-5. Friction Factor Versus Reynolds Number for 217 Pin Prototypic Bundle; 0.230 in. Pin Diameter, 0.056-0.050 in. Wire Wrap Diameter and 12 in. Wire Pitch

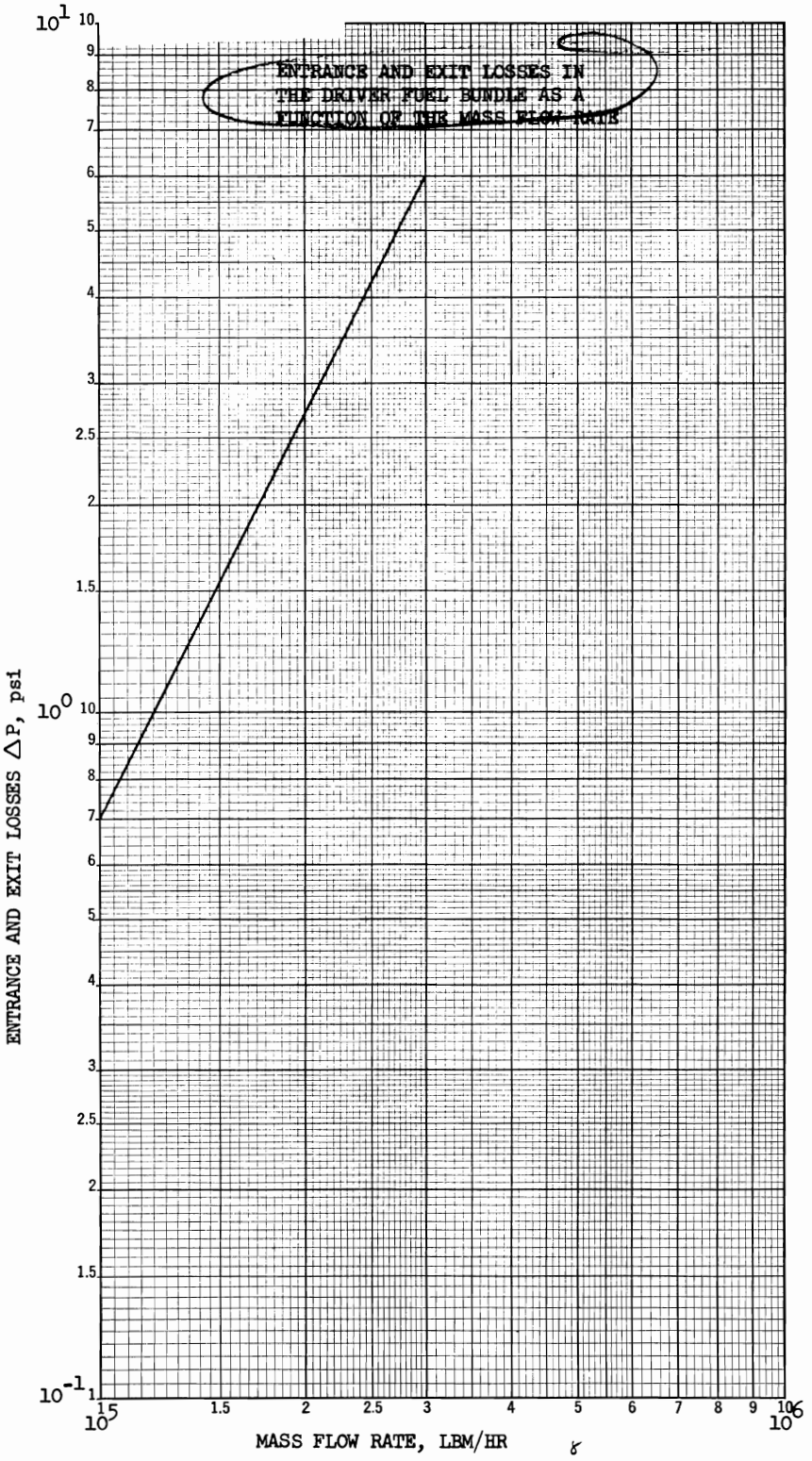

FIGURE 2.1-6. Entrance and Exit Losses in the Driver Fuel Bundle as a Function of the Mass Flow Rate

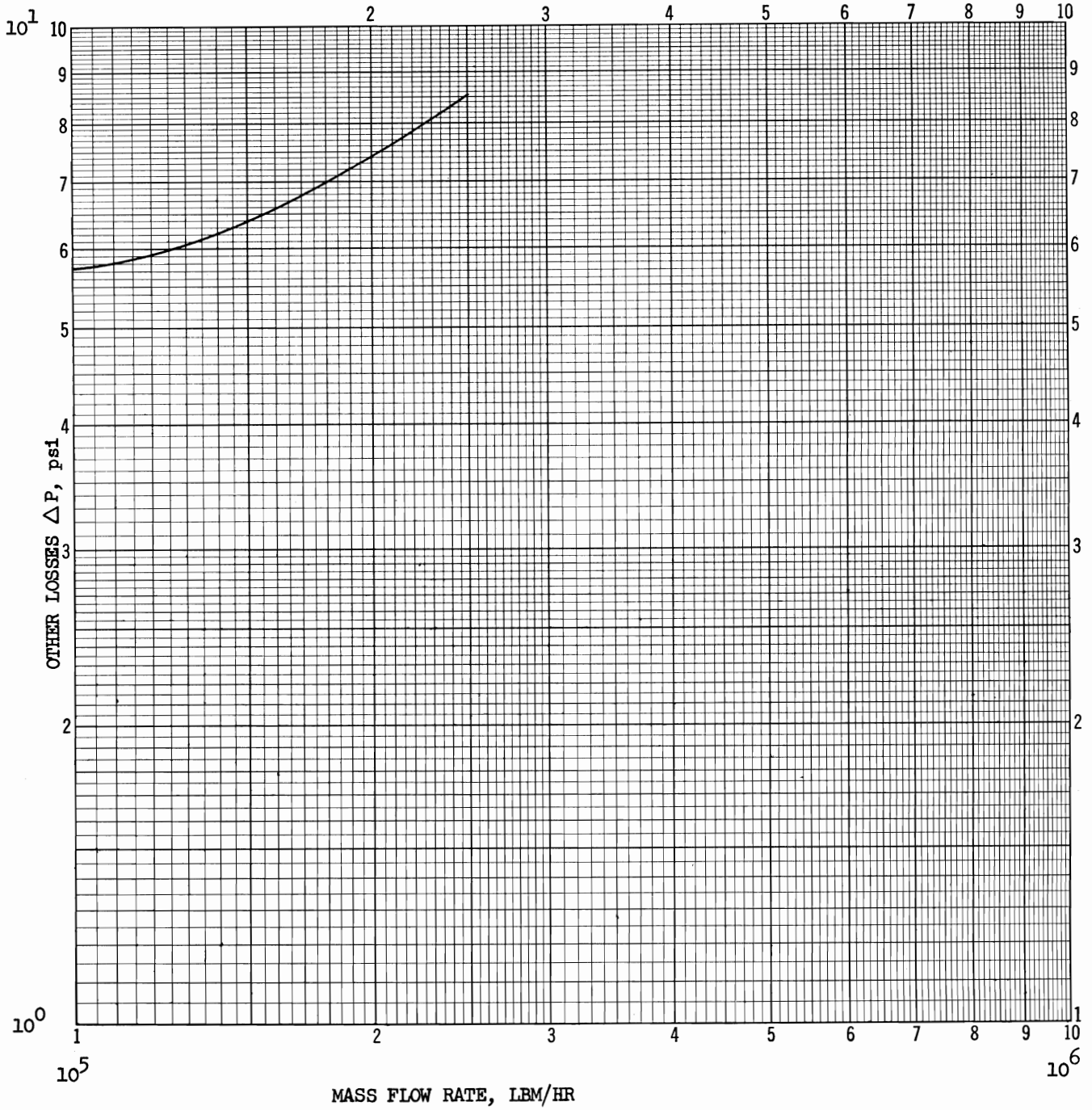

FIGURE 2.1-7. Other Losses in the Driver Fuel Subassembly as a Function of the Mass Flow Rate

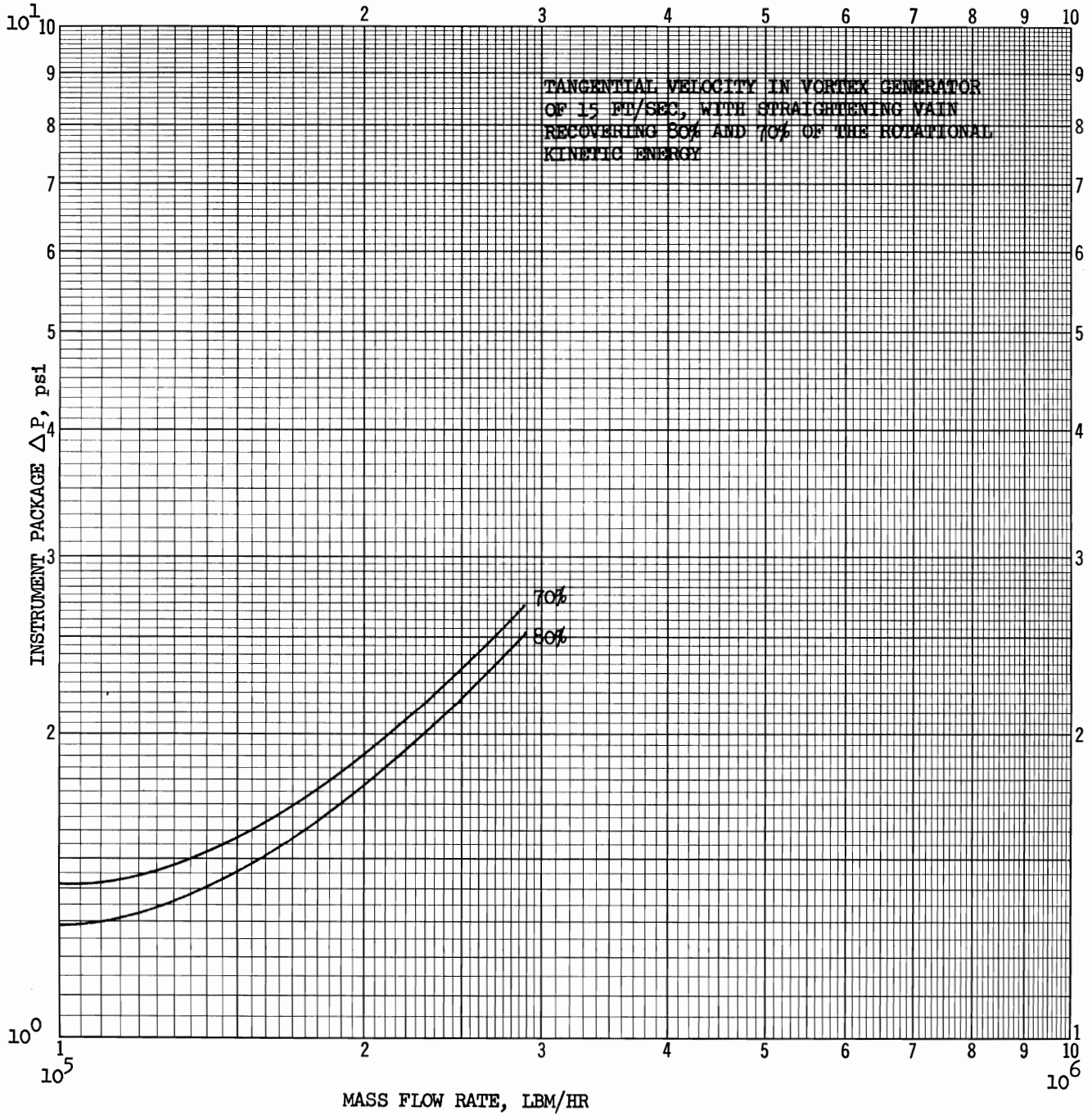

FIGURE 2.1-8. Instrument Package ΔP, as a Function of the Mass Flow Rate

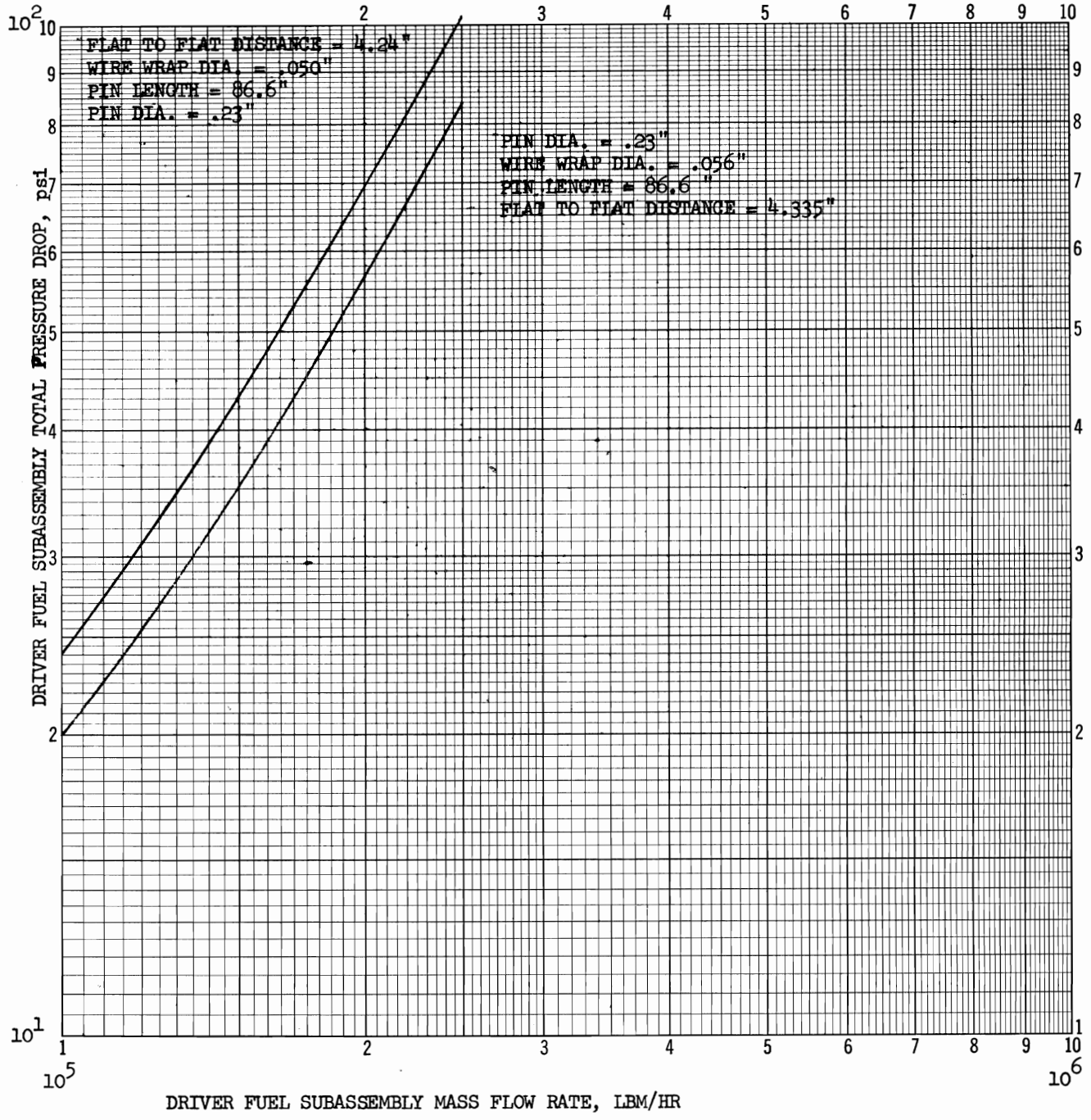

FIGURE 2.1-9. Driver Fuel Subassembly Pressure Drop as a Function of the Mass Flow Rate for Fuel Pin Bundles with 0.056 and 0.050 in. Diameter Wire Wrap

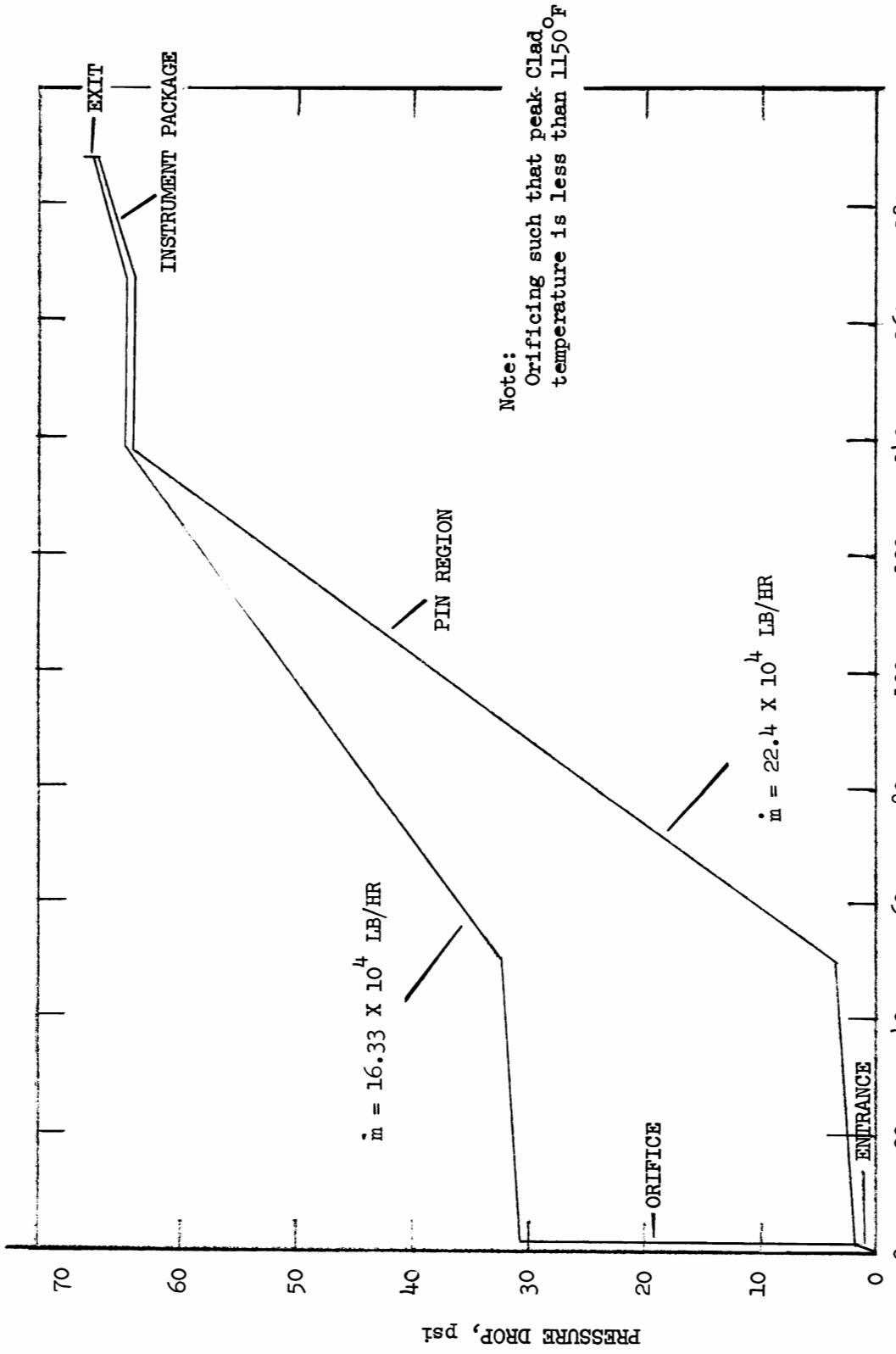

FIGURE 2.1-10. Pressure Drop (psi) as a Function of the Driver Fuel Subassembly Length

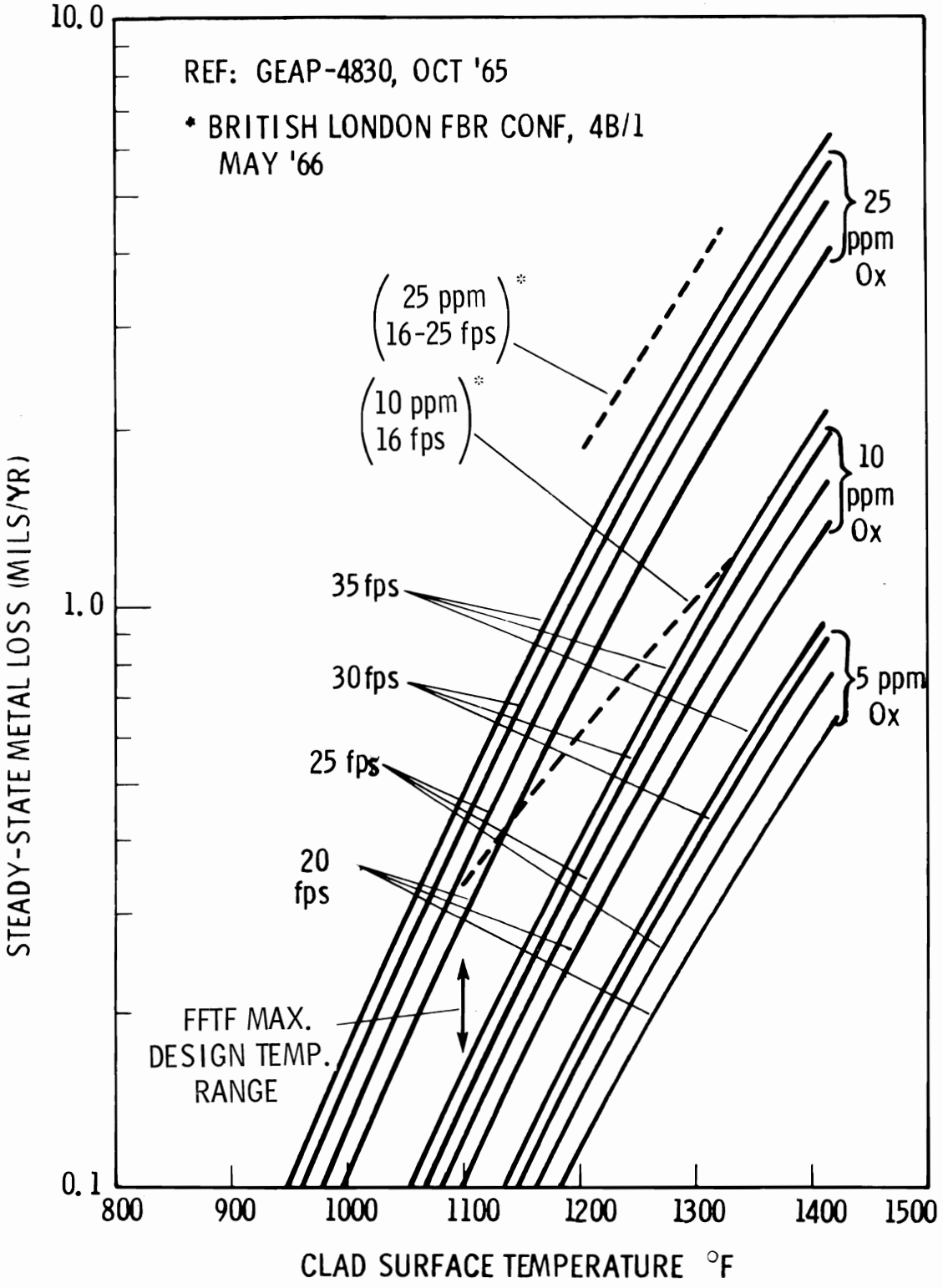

FIGURE 2.2-1. Stainless Steel Corrosion Rate Versus Temperature

3.0 FUEL ELEMENT AND SUBASSEMBLY STRUCTURAL DESIGN

3.1 FUEL RELOCATION - STEADY-STATE AND TRANSIENT

Radial redistribution of the fuel within a pin occurs during steady-state conditions in those regions operating above the recrystallization temperature (∿1600-1800 °C), resulting in the formation of a central void. Additionally, the fuel-clad gap tends to close at burnups beyond 20,000 MWd/tonne in pins operating at linear power levels above ∿10 kW/ft, as discussed in Section 1.2. The operating thermal gradient across the fuel pellet and the thermal cycling which occurs during startup, shutdown or scrams tends to crack the initially solid pellet.

The fuel pin is designed to withstand a 20% overpower condition at the hottest point in the core, with the peak fuel temperature just reaching incipient melting. Postulated accidents above this overpower, or equivalent over-temperature factor, as considered in safety analyses, result in potential melting of portions of some pins but not necessarily clad failure. Axial relocation of molten fuel within the central void region, due to the influence of gravity ("wet slumping") or the fuel expansion during the melting phase change, has been observed in high specific power irradiation tests.[55] The need for fuel motion restrictors, internal to the cladding has been evaluated.[56] Based upon safety considerations, it was concluded that the postulated maximum reactivity gain from wet slumping of all pins within a subassembly, up to the point of peak pin clad disruption from molten fuel, is within the available safety system control capacity. Therefore, restrictors are not recommended, based upon their marginal safety benefits and the penalties which they impose on the operation and safety considerations.

Another potential for fuel motion during transient conditions has been identified by Hanson[57] as the sudden release

of retained fission gases. Since the higher temperature regions of the core release a larger fraction of the generated fission gas, this phenomenon would occur mainly during a severe transient which results in melting of "colder" regions of the core.

3.2 RIDGING AND PELLET END CONFIGURATION

Circumferential clad deformation ("ridging") has been observed to occur at pellet interface locations, during both in-reactor[58,59,68] and out-of-reactor tests.[60,61] Calculations have shown that finite elastic cylinders in a radial thermal gradient have a greater diametral expansion at the ends than in the center;[62,67] also the effective axial expansion has been experimentally shown to be a function of the fuel central temperature in flat-end pellets up to the point at which plastic flow begins to occur (750-1000 °C),[62] i.e., the ends "mushroom." However, clad ridging has not been reported in recent high burnup, stainless steel clad, fast reactor irradiations (flat pellet ends),[63] (annular),[64] (unknown pellet and configuration)[65] which produced measurable clad diametral increases. Therefore, ridging was not a significant problem. The fine structure observed in the profilometer traces of pins from recent EBR-II irradiations to 58,000 MWd/tonne,[66] could possibly be interpreted as the beginning of the ridging phenomenon.

The out-of-reactor thermal gradient experiments have shown that ridging can result from temperature effects alone. "Ridges" probably existed at the start of irradiation of the fast reactor fuels cited above. But since the stainless steel clad thermal expansion is 3X that of Zircaloy, they did not deform the clad as reported in the high pressure coolant, Zircaloy systems.[58,59] However, with time and temperature, microstructural changes occur in the fuel which tend to close

the fuel stainless steel clad gap in a reasonably uniform manner. A contributing factor to explain the conflicting data might be that the Zircaloy-high pressure coolant systems cause the clad to grip the fuel and thus impede the initial axial expansion, which is then manifested by deformation of the ends of the pellets. Ridal investigated this hypothesis[58] with one deliberately defected specimen to equalize pressure across the clad and concluded that axial loading did not play a significant part in ridging in his experiment, i.e., ridge heights were independent of the external coolant pressure.

Dishing the pellet ends has been observed to increase in-reactor ridging.[59,68] However, ridging may be reduced by use of lower fuel smear densities.[59,66,68] The use of bevelled or chamfered pellet edges would also reduce the extent of ridging as shown in out-of-reactor tests.[69] A short time in-reactor investigation with aluminum clad specimens irradiated in a hydraulic rabbit system did not show any reduction of ridging with bevelled edge pellets. However, Notley has questioned the usefulness of these high intensity, short duration irradiations for obtaining information on the in-reactor thermal expansion behavior.[62]

The relationship of the observed reactivity effects during the initial low power operation of RAPSODIE to the flat ended pellet configuration was investigated. The lack of specific analysis data on this phenomenon preclude a direct correlation. However, Stachura's[70] general observations indicated that axial expansion of the fuel column probably caused the reactivity changes. As the power level was raised, fuel central temperatures increased with resultant pellet cracking, central fuel plasticity and central void formation due to sintering. After operations at full power, the initial reactivity effects apparently were no longer observed.

The conclusion which might be drawn from this experience in the realm of pellet end configuration is that the degree of the observed reactivity effect might possibly have been reduced by the use of dished-end pellets (since the initial fuel column expansion would have been less).

Comparing the manufacturing differences of flat and dished-end pellets leads to the conclusion that there is no significant cost difference for large scale pellet production.

Comparing the two end configurations from the overall core Doppler coefficient produces some potential differences which must be further investigated in preliminary design. To accommodate dishing requires either removal of some fuel material or the production of denser pellets. The former approach would decrease the fertile-to-fissile ratio (since the constant core volume requires approximately a constant fissile loading and only fertile material may be removed) and therefore decrease the Doppler coefficient. This provides less inherent negative reactivity feedback for shutdown during transients. Additionally, the lesser degree of axial fuel expansion, when compared to flat end pellets, also provides less negative reactivity feedback. The flat-end pellets can be qualitatively classed as possessing a higher degree of self shutdown capability. The higher density pellet affects burnup potential as well as other design areas which have strong requirements to maintain the density within certain bounds.[21] More investigation in this area is required before the tradeoffs can be determined.

Many pressurized water, thermal reactors have been built with dished-end pellets (built by W, B & W and CE) while many boiling water reactors have flat end pellets (GE). No specific reasoning for the choice was given in the literature. The principal consideration appears to have been the relative axial expansion characteristics between the two types of pellets for long fuel columns.

Other considerations pertinent to the pellet-end configuration have been presented in a BNW monthly progress report.[71] This concluded that the minimal advantage of dishing (initially reduced fuel column expansion as presented in Section 1.1) are outweighed by the increase in potential for ridging.

Based on a relatively larger Doppler coefficient and the reduced potential for clad ridging, flat end pellets are recommended for use in FTR fuel pins.

3.3 CLAD THICKNESS SELECTION

The clad effective thickness is determined by subtracting thickness increments from the actual clad thickness. These thickness increments are:

Erosion, corrosion,* and fretting**	1 mil
Scratch Depth†	1 mil
Na-clad diffusion	1 mil
Fuel-Clad Diffusion	1 mil
Manufacturing Tolerance	1 mil
TOTAL	5 mils

For a 10 mil effective clad thickness this requires a 15 mil actual clad thickness.

3.4 GAS PLENUM

3.4.1 Gas Plenum Location

The positioning of the fission gas plenum region greatly affects the core performance interims of thermal and material swelling. Thermal gradients and flux gradients across the core cause uneven expansion in the subassembly duct walls. The uneven expansion from side to side of a fuel duct will cause these members to bow.

By placing the fission gas plenum down below the core region the thermal gradient zone along the length of the subassembly can be greatly reduced. This reduction in turn causes a much smaller free thermal bowing deflection of a subassembly.

In terms of core restraint the reduction in thermal bowing means a great reduction in radial restraint force requirement.

---

* *Refer to Section 2.2.*
** *Refer to Section 2.3.*
† *Reference 100, Section 2.2.3, Table IV.*

There is also a great reduction in free bowing caused by material swelling which far overshadows the thermal effects as high burnups are approached.

An additional advantage in placing the plenums down is that the fission gas plenum will operate at a much lower average temperature. A reduction in temperature of 300 °F would allow the fission gas volume to be reduced based on a reduction in gas pressure as well as a reduction based on an increase in clad material properties. By reducing the fission gas volume a significant reduction in pressure drop as well as a significant length reduction of the subassembly could be achieved.

Figures 3.4.3-1, 3.4.3-2 and 3.4.3-3 show the bowing caused by relative thermal expansion and radiation induced material swelling for both designs.

It can be seen from these figures that placing the fission gas plenums down reduces the displacement of the subassembly. The results indicate that in terms of free displacements only, it would be desirable to locate the fission gas plenums below the core.

The magnitude of the swelling induced deflection and thermal deflections need further qualification. It can be seen that the thermal deflection curves have been calculated for 100 °F max. T. This was done so that any other temperature deflection could be easily scaled from these results. The temperature difference presently being quoted is in the range of 60 to 70 °F.

The swelling curves shown were calculated using the latest BNW swelling model with a duct ΔT of 65 °F max. These curves show the magnitude of deflection if no creep (thermal or radiation) were present. For the design temperature of 800 to

865 °F the thermal creep will be greatly reduced. However, the initial radiation transient creep law will be in effect.

For the first reactor cycle the effect will be very beneficial in terms of deformations and core restraint. This creep mechanism will allow the at-power thermal stress to be relaxed to almost zero. Since this happens first in the core center a "plastic hinge" area will be developed in this region. The result will be that the thermal deflection (Figure 3.4.3-6) will approach zero at power and will become opposite or negative of the initial thermal profile when the reactor is shutdown. This shift in the state of stress in the subassembly core region provides additional room for motion due to material swelling during the first reactor cycle. The result can be seen in Figure 3.4.3-4. Very low deflections will be obtained at the first reactor cycle in the down condition. The end deflection shown in Figures 3.4.3-2 and 3.4.3-3 would be reduced to approximately one sixth of the value shown for 20,000 MWd/tonne burnup.

Figure 3.4.3-5 shows the displacement that would be obtained if the subassemblies in the outer rows were rotated after each reactor cycle. This figure does not include the effect of stress relaxation in the first reactor cycle. This effect is shown in Figure 3.4.3-4. The results are that the duct will be allowed to remain in place longer than the first reactor cycle, probably to 30,000 MWd/tonne. From this time on, deflections of the order of magnitude shown in Figure 3.4.3-5 will be obtained. If smaller deflections are desired, the ducts will have to be rotated more often than at one reactor-cycle interval.

The confidence placed in these results should be biased by the uncertainty of the swelling equation. For the range of burnup shown, 20,000 to 80,000 MWd/tonne the 95% confidence

band ranges from ±80 to ±114%. With this in mind it becomes very hard to make meaningful calculations. Trends and effects can be shown but absolute magnitudes are very uncertain.

The advantages of placing the fission gas plenums down for the restrained conditions have not yet been determined. The location of support points for the core becomes very critical in establishing deflection patterns and restraint forces. From the results obtained to date it was obvious that acceptable radial restraint forces could not be obtained with support directly above and below the core for the below core fission gas plenum design. Further work is needed to investigate the placement of support pads to fully evaluate this concept.

It appears that for the first reactor cycle there is not a significant advantage in terms of the radial restraint alone to place the fission gas plenum down below the core.

3.4.2 Safety Considerations in Fission Gas Plenum Placement

Summary

The location of the fission gas (f.g.) plenums in the FTR fuel pins - either above or below the core region - presents somewhat conflicting effects related to safety. It is reasonable to expect that the frequency of random cladding failures which release quantities of fission gases to the primary coolant would be reduced with lower f.g. plenums. The increased reliability would be primarily due to the lower temperatures below the core (coolant inlet temperature) allowing possibly reduced internal operating pressures and/or increased margins to cladding failure stresses. However, the conse quences of cladding failure with lower f.g. plenums once it occurs (which even with lower plenums, would be expected with some finite probability) could be quite severe through propagation of the failure by the effects of:

- Positive core reactivity feedback by passage of the bubbles through core regions with spatially positive coolant void coefficients.
- Vapor blanketing of additional fuel pins leading to subsequent melt-through of the cladding.

These effects can occur even with upper f.g. plenums, but on a more limited basis since normal flow will oppose the entry of bubbles released above the core by cladding failures.

The gross consequences of the effect of bubbles passing through the core are quite tolerable provided any single failure is confined to a single fuel assembly. However, the limit of propagation due to progressive vapor blanketing of fuel pins is not evident and will depend to a large extent upon the results of experimental programs now in progress. Because the limits of failure progression are not explicitly defined, it is not evident that the gross consequences of fission gases passing through the core can be limited to the allowable severity of an "Operational Accident."

Since the potential consequences of fission gases released below the core are intolerable, and will remain so until positive experimental data are available, the design of the FTR should continue to incorporate upper fission gas plenums.

Discussion

The most obvious means of preventing f.g. bubbles or vapor blanketing within the core is by assuring that the cladding always maintains its integrity as an effective fission product barrier. This requires that sufficient conservatism be provided by the design to reduce the probability of random failure to acceptable level based upon the expected damages resulting from such an occurrence. Application of lower f.g. plenums in the FTR would probably allow a greater margin to failure depending upon the design since the lower temperature at the core inlet region will result in less effect upon the internal f.g. pressure and less degradation of the cladding mechanical properties. However, even with a greater margin, it is not evident that the expected failure rate of the cladding in these regions can be reduced to the

extent that such failure may be classified as an "Unlikely Fault" or "Major Fault" rather than an "Anticipated Fault."

Since it cannot be guaranteed that cladding failures below the core with lower f.g. plenums will not occur, the damage allowed for such an occurrence must be limited to that of an "Operational Incident" which allows no fuel damage (outside the effected fuel assembly which contains the initial failure).

The effect of f.g. bubbles upon core reactivity by displacement of sodium is limited by the magnitude of the coolant void reactivity coefficient. Preliminary analyses indicate that the peak reactivity which would be possible by voiding within any single fuel assembly channel is less than 0.10$. Even if this reactivity were inserted as a step input, no fuel damage would be sustained with normal operation of the primary protective system. The effect of vapor blanketing is not as straightforward and failure modes can be postulated which result in damage beyond the initially affected fuel assembly. The limiting effects depend upon the phenomena associated with sodium expulsion and subsequent re-establishment of flow sweeping out the vapor-blanketing fission gases. Data are not available to conclude that damage cannot progress autocatalytically well beyond that allowed for an "Operational Incident."

Experimental programs are established at ANL to investigate these interactions and progressions. Specifically, programs are investigating the phenomena of fuel-sodium interactions which may occur with failure of the cladding and eventually prototypic in-pile tests will be performed with pins designed to fail during operation to establish the upper bound of failure propagation. However, sufficient results from these programs will not be available in time to remove the risk associated with lower f.g. plenums.

The location of the f.g. plenum in the Na-2[72] reactor is specified to be below the core which they state reduces the overall pin length by 20 cm and considerably reduces the thermal stress and bowing effects. It is also stated that the potential release of f.g. bubbles upon cladding rupture is not expected to cause serious safety problems. However, their reference[73] for this conclusion states that the possibility that cascade failures of this type cannot be ruled out, but are very unlikely. Again, it appears that conclusive evidence must await completion of the ANL-Fuel Failure Propagation Program.

The effects of cladding failures in the core region are essentially the same in either design. However, the fuel matrix material is expected to limit the rate of f.g. release and thus prevent the consequences of extensive vapor blanketing.

The uncertainties associated with evaluation of the consequences of f.g. bubbles in the core emphasizes that a conservative approach be taken in the design of the FTR. Therefore, it is concluded that the location of the f.g. plenums should remain above the core as shown in the conceptual designs until it can be shown that the consequences associated with lower plenums result in no fuel damage for any release of retained fission gases below the core.

3.5 CLADDING PROPERTIES VERSUS EXPOSURE AND TEMPERATURE

Data required for design include radiation induced swelling, in reactor creep, mechanical strain limits, fatigue strength, tensile and impact properties of the clad material, all as a function of radiation exposure at the appropriate temperatures.[102]

Postirradiation data are available and summarized on uniaxial strength and ductility for specimens irradiated up to 1.7×10^{22} nvt. These data, while sparse, clearly show that ductility decreases with exposure at all temperatures. Some data are available on swelling of austenitic stainless as a function of fluence and temperature. Most data are from solution treated material. The data are too scattered to permit unequivocal determination of the fluence and temperature dependence of this swelling phenomena. However, the best guess model is shown in Figure 3.5-1 for solution treated austenitic stainless steel. A somewhat similar model has been developed for 20% cold worked M-316 as shown in Figure 3.5-2.

The cold worked swelling model is based upon only seven data points[74] and is subject to considerable change as additional information becomes available.

Programs have been started to obtain these data by irradiating specimens in EBR-II. Postirradiation examination and testing is planned. Tests will be conducted to determine the effect of flowing sodium on the strength properties of the clad material. The strength tests will be run in an inert atmosphere. If necessary, the strength property tests will be determined at the appropriate elevated temperatures in samples

exposed to flowing sodium. TREAT tests will be performed to provide some information on the high strain rate behavior and low cycle fatigue behavior of irradiated fuel cladding as well as the transient behavior of the fuel within the cladding.

It is felt that to do a meaningful design analysis, material properties such as ductility, creep and strength properties of the irradiated 316 cold worked stainless must be known. The alternative of using a solution treated material would provide more data to work from. The selection of this material, however, would incur a flux penalty due to the associated increase in beginning-of-life clearance between pin bundles and duct to allow for increased swelling of the fuel pin.

3.6 BUNDLE AND PIN VIBRATION, FATIGUE

Vibration limitation will be either the strength, ductility, and fatigue properties of the irradiated clad, or fretting corrosion. The factors affecting flow induced vibration stress, in their approximate order of importance, are: coolant velocity, system damping, fuel pin length, fuel pin stiffness, and the density/velocity ratio of the coolant. Attempts to relate the variables theoretically have failed because of the unknown nature of the forces between the fluid and the vibrating fuel pin. Attempts to determine the correlation between different experimental data have been only partially successful. Addal[75] has found the experimental loop geometry and the amount of pump noise to be extremely significant variables. The most successful correlations are those of Paidoussis[76] and Burgreen.[77] These correlations will be used to obtain "order of importance" information regarding trade-offs. Vibration proof tests are necessary; these are described in Section 2.3.

Experimental data obtained in flowing sodium at 28 fps, 1060 °F for 100 days using a 217 pin bundle in the Core Components Test Loop (CCTL)[78] as well as data from the seven rod life test (30 fps, 1060 °F sodium, 375 days)[51] showed no mechanical instabilities. Therefore, a maximum allowable pin bundle design velocity of 30 fps is permissible from vibration considerations. Section 2.2 indicates this is an acceptable velocity from erosion and corrosion considerations.

3.7 THERMAL AND SUPPORT STRESS, STRAIN, BOWING, ETC.

The limits on these factors will be determined by the clad and the support material properties. The limits must be established by determining both strain and stress distributions.

Strains leading to reactivity effects and strains leading to fracture must be considered. The strains leading to reactivity effects include thermal bowing of a pin bundle. Strains leading to fracture include those from fuel swelling, fission gas pressure, and thermal stress.

The stress analysis program must consider stresses leading to stress rupture, fatigue, and overload failure. The contributions to stress rupture include steady-state thermal stress, fission gas pressure, fuel swelling, and any mechanical stress from misalignment. The factors contributing to fatigue include all the preceding plus the thermal stresses resulting from reactivity transients, scrams, and normal shutdowns. The factors contributing to an overload failure include all the preceding in addition to overpower transients.

Temperature distributions along fuel pins and tubes are calculated by the SINTER[79-82,26] or NUTIGER[79-82,26] programs. Thermal stresses are calculated by SEAL SHELL[79-82,26] 2. A code, AXISOL,[79-82,26] has been developed to combine mechanical and thermal stresses and to calculate the stress distribution as a function of time and

position for surfaces of revolution. SAMOS[79-82,26] calculates the stress distribution in the structural members using the theory of elasticity. These codes will be used to calculate the appropriate stress and strain distributions with consideration being given to thermal racheting, creep and fatigue life.

Because of these mechanical forces imposed on the subassembly, the grid at the top of the fuel assembly is designed to interface with a slotted pin end cap allowing independent axial expansion of each fuel pin while restraining lateral movement. Independent axial expansion for each fuel pin is necessary to ensure that the thermal expansion, thermal gradients, mechanical differences, and fuel induced swelling do not mechanically distort the entire assembly which would be the case in a pin array which was restrained at both ends. Section 3.13 discusses "Fuel Bundle Support."

The duct design method is presented in Section 3.9. The normal operating conditions used consisted of a pressure difference across the duct wall of 80 psi and a temperature of 600 °F at the core inlet, and 40 psi and 1100 °F at the core outlet. The ratio of calculated maximum stress to allowed stress is 73% at the core inlet and 51% at the core outlet.

The duct must also maintain its integrity under design accident conditions. However, these design accidents will be defined in the "Design Safety Criteria for the First Core Fuel Assembly Component" which is currently being revised.[83]

3.7.1 Wire Wrap-Pin Interaction

The stress distribution (assuming no stress relaxation) in the spiral wire spacer both with lower reflector and without is shown in Figure 3.7.1-1. These values are based upon a 0.235 in. diam fuel pin with 10 lb tensile force and a 0.040 in. diam spacer wire. The maximum temperature difference

between wire and cladding is 58 °F. There is very little difference between the peak wire stress value for the applicable range of friction factors of 0.5 to 1.0.[84] The effect of stress relaxation is being investigated. It appears that it will reduce these stresses to very low values. However, there will be residual deformation in the pin. This deformed shape will be approximately the same as the pin when it went to the first full power. (See Section 3.10.) The wire stress in the end cap region is 8000 to 10,000 psi from the unrelaxed tensile force. There is an additional stress in the wire and a corresponding bending moment where the wire bends to form the junction with the end cap.

The helical deformation pattern of the fuel pin caused by the loading of the wire wrap is shown in Figure 3.7.1-2. The assembly helical radial deformation for 10 lb of wire tension is 0.0047 in. at room temperature. The effect of relative material thermal expansion between the wire and clad could increase this value by 0.007 in. Additional relative neutron radiation material swelling could increase by an additional deformation of 0.010 in. The effect of temperature gradients across the pin is shown in Figure 3.7.1-3. The gradient is considered to be taken from one side of the pin to the other on the diameter. This corresponds to a pin in the outside of a fuel bundle.

Both the stress concentration and the bending moment in the wire could be eliminated by welding the wire to the surface of the end cap. However, this would create a stress concentration and a bending moment in the weld area. This is considered less desirable than having this bending moment and stress concentration in the wire. Therefore, the attachment is designed to reduce these to a minimum consistent with

maintaining reasonable dimensions as shown on SK-3-14583 in the Appendix. By attaching the wire at 45° from fuel pin axis instead of at 90° the bending moment is reduced about two thirds. This also permits a slightly greater radius of curvature, thus also reducing the stress concentration.

The magnitude of wire stress depends greatly upon the wire tension during the pin fabrication. The lower limit on the required tensile force is that force required to make the wire lie properly on the pin. The magnitude of this lower limit is currently being evaluated. It is anticipated that a tensile force only slightly higher than this lower limit will be specified for the FTR core spacer wire.

3.7.2 Wire Attachment

Both the stress concentration and the bending moment in the wire created at the attachment point could be eliminated by welding the wire to the surface of the end cap. However, this would create a stress concentration and a bending moment in the weld area. This is considered less desirable than having this bending moment and stress concentration in the wire. Therefore, the attachment is designed to reduce these to a minimum consistent with maintaining reasonable dimensions as shown on SK-3-14583 in the Appendix. By attaching the wire at 45° from fuel pin axis instead of at 90° bending moment is reduced about two thirds. This also permits a slightly greater radius of curvature, thus also reducing the stress concentration.

The wire will then be welded from the other side. The weld must be inspected to ensure proper penetration into the parent material. If proper penetration cannot be easily obtained, the weld area in the cap could be counter sunk slightly to allow deeper weld penetration.

3.8 FUEL RATCHETING

Fuel ratcheting, the axial relocation, and segregation of fuel due to thermal cycling, are being experimentally assessed at this time for the FTR fuel as part of the FFTF and LMFBR irradiation test programs. Analysis may not be able to determine the ratcheting phenomenon effectively. It may be demonstrated that the plenum spring maintains the fuel column in compression during the time while the fuel column retains axial mobility without interference from the cladding. The fuel irradiation tests will have to be examined for ratcheting after the above burn-in period.

3.9 DUCT DESIGN

The duct for the driver fuel subassembly must be designed such that credible accidents within the subassembly will not propagate to adjacent subassemblies. This is particularly important if the adjacent subassembly is a safety rod because the ability to scram the reactor must not be impaired.

There are two major sources for stress in the flow duct wall: internal pressure, and temperature and flux gradients across the duct. These cause changes in shape of the hexagonal shaped duct and induce bending deformations along the length of the duct. An additional deformation mechanism is differential metal swelling which will also distort the cross section and cause duct bending.

The first step was to determine the necessary wall thickness based upon elastic stress analysis.[85] The allowable stress values were taken from ASME Section VIII and modified as specified by ASME Code Case 1331-4.

The selection of allowable stress was based upon the environmental conditions outlined in Figure 3.9-1. By using the procedure outlined in the ASME Code, it is possible to make an evaluation of the duct design.

If the loads are broken down into three categories--primary stresses, bending stress and secondary stress--the following rules apply:

primary stress + bending stresses <1.5 Sm

and

primary stress + bending stress + secondary stress <3 Sm

where Sm is the allowable stress at a particular temperature.

The following table, 3.9.1-1 shows the stress and Sm value for the inlet and the point of maximum bending stress.

TABLE 3.9.1-1. Duct Stress

	Primary-σ_p	Bending-σ_β	Secondary-σ_s	Sm
Inlet Region	3000	375	28,750	14,900
Above Core Region	1550	8,239	18,750	13,400

Using the values shown in Table 3.9.1-1 and the equations previously listed, it can be seen that

(Inlet Region)

$$3000 + 375 < 1.5(14,900)$$

and

$$3000 + 375 + 28,750 < 3(14,900)$$

(Above Core Region)

$$1550 + 8,239 < 18,100^*$$

$$1550 + 8,239 + 18,750 < 3(13,400)$$

* *Based on ASME Code Case 1331-4 for temperatures above 800 °F.*

This analysis applies only for the initial startup period. It does not include the effects of radiation on properties, stress relaxation, or material swelling. These elastic calculations and techniques are believed valid for unirradiated material. The limit of their validity to in-reactor performance will be assessed as more data becomes available.

Additional calculations which considered the effect of thermal creep has indicated less than a mil change in the dimensions across the flats of the hexagon.[86] This is accompanied by redistribution of stresses such that the effect of the stress concentration at the inside corner of the hex essentially disappears.[87] A creep experiment of a section of unirradiated hexagonal duct material indicated that up to 10 mils increase in dimensions across the flats may be expected at 85 psi internal pressure at 1050 °F for 0.150 wall thickness.[86] This deformation results from a calculated stress of 15,300 psi at the inside surface of the hex corners. This deformation imposes no material restriction on the duct. However, definition of an upper limit for calculated creep deformation will require study during preliminary design. This choice must consider the clearance space between ducts, the predicted change in dimension from metal swelling and the required flow area between ducts for maintenance of hydraulic holddown.

It is believed that because the duct material is predicted to increase in volume several percent evaluation of low cycle fatigue damage is not valid. Likewise, any assessment of changes in stress concentration factors with changes in wall thickness are not valid. The embrittlement of the material appears to be applicable only to mechanical strain. Therefore, the deformation associated with metal swelling appears to not be limited by material ductility. Obviously, as more becomes

known about metal swelling the interaction between the differential duct swelling[89,90] and the core radial restraint mechanism must be evaluated. Also, as in-reactor creep data become available[91-94] this effect must be considered for steady-state operation.

3.9.1 Safety Considerations in Duct Design

Higher stresses than allowed for steady-state design can be tolerated during transient conditions depending on the duration of the transient pressures and the increase in temperature. If the yield strength of the duct is used as the upper stress limit, then Figure 3.9.1-1 shows that a pressure differential across the duct wall of 120 psi can be tolerated if the duct temperature remains below approximately 1300 °F. If the pressure differential is 60 psi, then the maximum temperature is slightly above 1500 °F. In the event of a flow blockage near the top of the subassembly, the pressure in the core would approach the pressure in the inlet plenum (120 psi).

However, the coolant temperature at the top of the core reaches 1300 °F for a downstream blockage of only 57% in the average channel and 40% in the peak channel with no orificing. In both these cases, the pressure differential across the duct above the core is substantially below 120 psi. Therefore, downstream blockages below these levels can be tolerated but a more detailed analysis (including the effect of irradiation on the behavior of the duct) is required to determine the maximum duration these blockage conditions can be tolerated.

To determine whether credible accidents can propagate to adjacent subassemblies, it is necessary to postulate the various accident conditions which can lead to failure of the subassembly in which they occur. Analysis or experimental data

will then provide the transient temperatures and pressures which the duct is subjected to as a result of these accidents. However, an analytical model which would use these transient conditions to determine whether duct failure would occur is not available. In addition to the lack of an analytical model, the high-strain-rate data for irradiated stainless steel which would be required as input for the analysis does not exist nor are there experimental programs in existence which would obtain these data.

Some of the accident conditions which may be propagative in nature are: release of fission gas, local blockage, distortions within the fuel bundle, and the fuel-sodium interactions. Out-of-reactor and in-reactor experimental programs are currently in progress at ANL and BNW to investigate these phenomena and assess their consequences. Close surveillance of these programs will be maintained to evaluate the applicability of the data to the design and safety analysis of the duct.

3.10 STRESS RELAXATION AND STRAIN HISTORY OF A TYPICAL FTR FUEL PIN

The fuel pin and wire wrap system as an integral unit will be exposed to high temperatures and high fluences throughout the entire fuel pin life span. The temperatures and fluences will cause changes in the dimensional relationships between the fuel pin, the wire wrap, and the support structure.

Variations in temperature between the wire and fuel pin cladding will cause the wire to tighten during a full power operation and loosen during shutdown periods. Radiation-induced material swelling will also cause variations in dimensional relationships which will induce equilibrium strains in

both the clad and wire. Due to the loading configuration, the stress in the clad will be primarily a bending stress, and the wire will experience primarily in axial stress.

Due to the temperature of the environment and peak temperatures in the clad, thermal creep and stress relaxation will be present. In addition a greatly magnified steady-state radiation induced creep law has been preliminarily identified by several investigators.[91-94] The data for this mechanism is not complete enough to permit a fine definition of the relationship. There is however, a sufficient amount of data that cannot be ignored.[92-94] Figure 3.10-1 shows a typical creep curve of irradiated 304 SS.

The effect of this recently identified creep mechanism is a very substantial input to the overall design analysis. Using this relationship stress will be relaxed to a very low value within the first 20 hr of operation in the FTR in the peak flux regions.

Figure 3.10-2 shows the initial creep rates that were found for irradiated 304 SS. The initial creep strain shown is 1.6 times the elastic strain. Stress relaxation of irradiated 304 SS is shown in Figures 3.10-3 and 3.10-4.

Although the radiation creep is very large, it appears saturated after a fluence of 5×10^{20} n/cm^2. One interpretation of the data presented[92-94] is that an effective stress threshold is developed which appears to limit the relaxation of 15,000 psi. It is at this time that thermal relaxation could again play a significant role.

The relationship at the present has been characterized by:

$$\frac{d\varepsilon}{dt} = K\Phi\sigma$$

where K = constant

ϕ = neutron flux n/cm^2-sec

σ = effective stress

Or in terms of stress:

$$\sigma = \sigma_o \exp(-KE\phi t)$$

where: $\frac{d\sigma}{d\varepsilon} = -E$

t = hours

Figure 3.10-5 shows the comparison of this mechanism between peak flux regions and outer regions of the core along with thermal stress.

The data available concerning radiation creep relationship are not complete. The interpretation of these data can therefore provide only an indication of the effects involved. The form of the equation developed is based on past experience obtained with Zircoloy, the actual relationships are derived based on limited 304 stainless steel data.

Since the amount of relaxation that can occur by using the relationship is so very large compared to thermal creep, thermal creep can largely be ignored in comparison. This may not always be the case for high burnups where the fuel might cause significant yielding of the clad.

Based upon this interpretation of steady-state radiation creep, it is possible to make some predictions of the typical peak strains that will be encountered in the life of a fuel pin. For the numbers quoted, it has been assumed that changes in dimension of the fuel pin are due solely to the material growth and that the fuel was not producing any plastic strain in the clad. In the event that the fuel does plastically strain the clad, a magnification of the clad strains reported would occur.

The external or outside bundle fuel pins will experience different strain histories than will fuel pins located within the fuel bundle, the primary difference being the large temperature gradients that are present in the outer row of fuel pins.

Typical strains that would be present in a fuel pin at power after the first 100 hr of operation would be:

	Clad Bending Strain, %	Ave. Wire Strain, %
External Fuel Pin	0.07	0.023
Internal Fuel Pin	0.028	

Table 3.10-1 shows the contributing factor used to arrive at these values. The associated stress would have been reduced to a very low value due to the very high steady state irradiation stress relaxation capability.

At a later time in the fuel pin exposure, relative material swelling between the fuel pin and clad will begin to cause additional bending stresses to be developed. In addition fission gas pressure buildup will also cause additional straining of the clad. By including these two factors, the strain history can be summarized at an end of life condition as:

	Clad Strain, %		Wire Strain, %
	Axial	Tangential	
External Pins	0.09	0.025	0.038
Internal Pins	0.048		

At this time in the fuel pin life, the lower radiation saturation limit of 5×10^{20} which raised minimum stress threshold from zero to the 15,000 psi threshold would have been reached by all of the pin material. The stresses that are associated

with any additional increase in loading large burnups are below the 15,000 psi effective stress threshold and will not be relaxed appreciably by the steady-state irradiation creep law.

Therefore, any additional stress relaxation in either the clad or wire would have to be based on either thermal creep or some other mechanism which has not been established. Since the thermal creep properties of stainless steel at this exposure are not readily available, it is difficult to evaluate the magnitude of this effect.

TABLE 3.10-1. Fuel Pin Clad Average Stress and Strain

Defection Causes	Ave Center Line Deflection, in.	Ave Clad Stress, psi	Ave Clad Strain, %	Ave Wire Stress, psi	Ave Wire Strain, %
Beginning of Life					
1. After Assembly-Cold	0.0047	4600	0.019	4030	0.017
2. Thermal Bow External Pins[a]	≈0	10000	0.042	≈0	≈0
Internal Pins[a]	≈0	≈0		≈0	
3. Differential Thermal Expansion	0.0023	2300	0.009	2030	0.009
TOTAL Including External Pins	0.007	16900→SN[b]	0.07	6060→SN	0.026
Relaxation Internal Pins	0.007	6900→SN	0.028	6060→SN	0.026
End of Life					
4. Relative Clad Swelling Between the Cladding and Wire Wrap	0.0035	AXIAL[c] 3450 psi; TAN[c] 0.014		3045	0.012
5. Fission Gas (Elastic)		3607	7214 0.006 0.025		
End of Life Subtotal	0.0035	7057	7214 0.02 0.025	3045	0.012
		σEFF = 7135			
TOTAL External Pins	0.0105	7057	7214 0.09 0.025	3045	0.038
Internal Pins	0.0105	σEFF = 7135	0.48 0.025		

(a) = External refers to pins on the duct wall. Internal refers to pins within the bundle.
(b) = Refers to the cylindrical strains in the clad.
(c) = SN refers to some small number that will be approached due to radiation steady-state creep. Due to insufficient data at this time it is not defined.

3.11 BASES FOR THE CORE RESTRAINT-DUCT STRUCTURAL INTERFACE

The duct design is strongly influenced by the core restraint requirements. A one-piece structural duct (Dwg SK-3-14581 in Appendix) compatible with the reference compliant

core restraint system will be used.[95] The compliant restraint is one in which elastic deflections are limited by core packing at reaction pads. A compliant loading member is used to accommodate radial expansion of the core.

Several factors influence the radial restraint system design which in turn effect the duct configuration. Items which must be included in restraint analysis are:

- Thermal camber
- Irradiation induced stainless steel swelling
- Irradiation induced creep
- Thermal creep

Thermal camber results from differential thermal expansion across the duct wall due to the nonlinear power profile across the duct. This effect can be easily analyzed but must be compensated for during transient conditions to assure that reactivity effects are negative.

Irradiation induced swelling is a function of the flux gradient and thermal gradient occurring across the duct. The phenomena is not completely defined at "the present time, but initial analysis of test data indicates a $\Delta L/L$ of as much as about 3% may be attributed to this phenomena. The effect, however, is time (ϕ) and temperature dependent and therefore manifests itself as a function of time in reactor as fuel burnup progresses. The resultant effect of swelling is duct distortion which can result in differential duct swelling such that it can be accommodated by the present reactor core arrangement.

Irradiation induced creep, like stainless swelling, is a time dependent phenomena. Present data indicate that the time regime in which the creep occurs is of much shorter duration than stainless swelling. The data indicate that creep occurs

from time zero and continues to some σ/σ_o value, as yet not defined at a fluence of 1×10^{20} nvt at which time a threshold stress for further creep of 15,000 psi may be imposed.

The completion of the initial or primary creep period extends from about 6 hours to more than a full reactor cycle, depending on the relative distance from the axial core centerline. The restraint system must either adjust for the reduction in applied load due to the creep by built-in additional load at startup or by an adjustable restraint. The former method is more desirable, but due to lack of information on an adjustable system, it is included in CCDD #31 as an alternate. The secondary phase may be neglected by maintaining stress levels below the threshold value--thermal creep does not appear to be a significant factor for the first core due to the lower outlet temperature. Above 900 °F, thermal creep becomes significant.

Factoring all of the above phenomena into the restraint system design indicates that a duct design similar to that shown on SK-3-14581 (Appendix) will fulfill design intent. This design is based on a burnup and outlet temperature limitation as noted above. As additional results of material irradiations become available, the single piece duct must be reviewed to assure that deformations with this design are not excessive due to swelling or irradiation induced creep.

3.12 AXIAL SHIELDING

Radiation from the core to the inlet structure below the core and to the instrumentation probe above the core must be sufficiently attenuated to satisfy irradiation damage criteria. Although the total damage criteria is still under investigation, it appears that a 10% residual ductility at the end of life, along with some method of spectra weighting, can be used for

conceptual design. Figure 3.12-1 shows the allowable fluence as a function of temperature utilizing the total spectra without weighting. At a temperature of 600 °F, the coolant inlet temperature, the fluence limit is 3×10^{21} nvt.

One of the main factors which influences the distance between the bottom of the active core and the hydraulic balance receptacle above the bottom grid plate is the travel length for the control/safety rods. Figure 3.12-2 is a diagram of the control/safety rod geometry showing that for a 38-in. stroke, the total distance from the bottom of the core to the receptacle is 42 in. Figure 3.12-3 shows the flux level as a function of axial distance below the core. Without spectra weighting and without axial shielding between the hydraulic balance receptacle and the core, the fluence limit of 3×10^{21} nvt corresponding to a temperature of 600 °F occurs in the lower end of the receptacle. Use of axial shielding results in the fluence limit for 600 °F still being reached in the upper end of the hydraulic balance receptacle.

By utilizing spectra weighting, the allowable fluence will increase. Figure 3.12-4 shows tentative values for the allowable fluence as a function of temperature using a preliminary estimate for the weighting factor. The fluence limits are sufficiently increased such that the 600 °F limit is reached above the hydraulic balance receptacle both with and without axial shielding. Figure 3.12-5 converts these tentative fluence limits to corresponding allowable distances below the core. The fluence limits distance for temperatures of 500 and 600 °F are also shown.

Although the need for axial shielding below the core will not be definitely settled until preliminary design, a 10 psi pressure drop allowance has been allotted for the potentially

required shielding. Irradiation damage criteria for the instrument probe have not been established and therefore the need for axial shielding above the core must be determined in preliminary design.

3.13 FUEL BUNDLE SUPPORT

The fuel bundle support system has a primary function of providing correct positioning and support of the fuel pins (Drawings SK-3-14582, SK-3-14583, and SK-3-14584, Appendix).

(Upper Support)

- Provide relative positioning of fuel pin within the lattice cell.
- Reduce the potential for vibration of individual fuel pins.
- Provide additional or backup support system for retaining a fuel pin within the bundle in case of local failure of individual fuel pin lower support.
- Provide support for an individual bundle during the assembly period.
- Allow thermal expansion of individual pins without restraining or affecting adjacent fuel pins.
- Allow sufficient compliance to allow relocation of the fuel pin within a lattice due to variations in helical bowing between pins.

(Lower Support)

- Provide axial positioning of the fuel bundle and primary support of hydraulic frictional support.
- Provide individual pin support within a lattice cell.
- Prevent or reduce potential for vibration of individual fuel pins.
- Provide ease of assembly of fuel pin bundle.
- Maintain a high degree of reliability in the assembly process.

Additional work is needed to fully evaluate the forces and reactions acting on the lower and upper support grids. Additional thermal frictional loads caused by the interaction between the pins and fuel duct might require a stiffer lower support structure. The potential for increasing this load will increase later in the fuel pin life when the possibility for increased fuel pin helical deformations exist.

Section 3.7 discusses "Thermal & Support Stress, Strain, Bowing, etc."

3.14 FUEL ASSEMBLY HOLDDOWN

Axial holddown will be accomplished by a hydraulic balance system and assembly weight.[95] Backup holddown and sensing of the loss of hydraulic balance will be furnished by the instrument tree hold down plate.[95] The holddown scheme must be developed in depth in the Preliminary Design.

Since the hydraulic balance is a function of the total reactor configuration it should be tested in a full or part scale core mockup.[96] The possibility of hydraulic induced instabilities as well as the effects of tolerances, structural distortions and wear are of particular interest in such tests. Nonprototypic tests on the hydraulic balance concept have been conducted.[97] Early estimates[98] of pressure surges disclose that the extreme case of a quick-closing checkvalve with resultant fluid hammer can be expected to unseat the fuel subassembly by a distance of no more than 0.001 inches. The damage resulting from this motion should be insignificant.

Possible interplay between the fuel management-orificing scheme and the resistance of the leakage path and thereby the holddown force should be explored. The adverse chemical, radiation and thermal environment will be experimentally studied[99] to determine the extent of the corrosion, erosion and swelling problems.

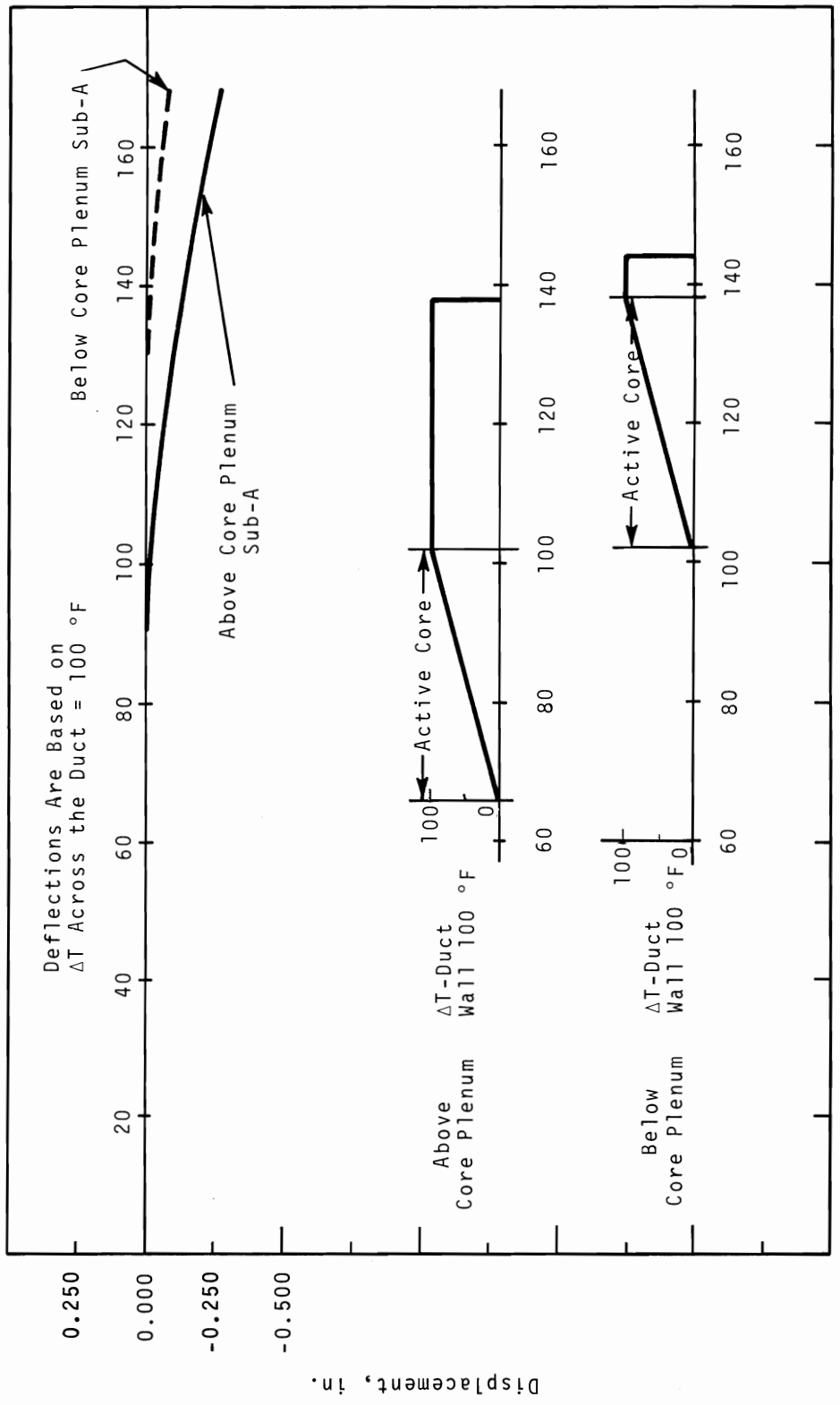

FIGURE 3.4.3-1. A Comparison of the Thermal Deflection in the Above and Below Core Plenum Subassembly - Design

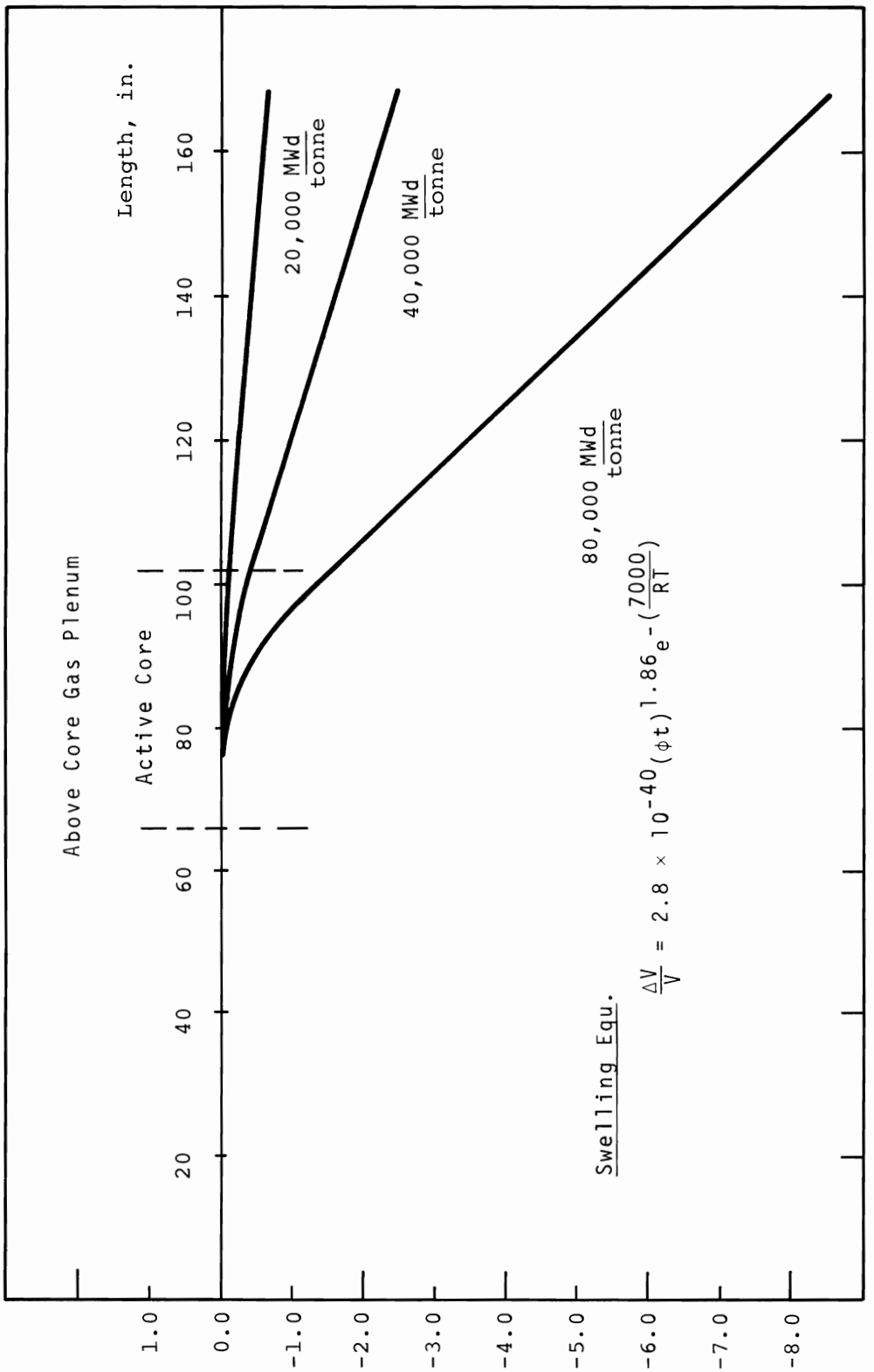

FIGURE 3.4.3-2. Subassembly Deflection Caused by Material Swelling (Above Core Plenum)

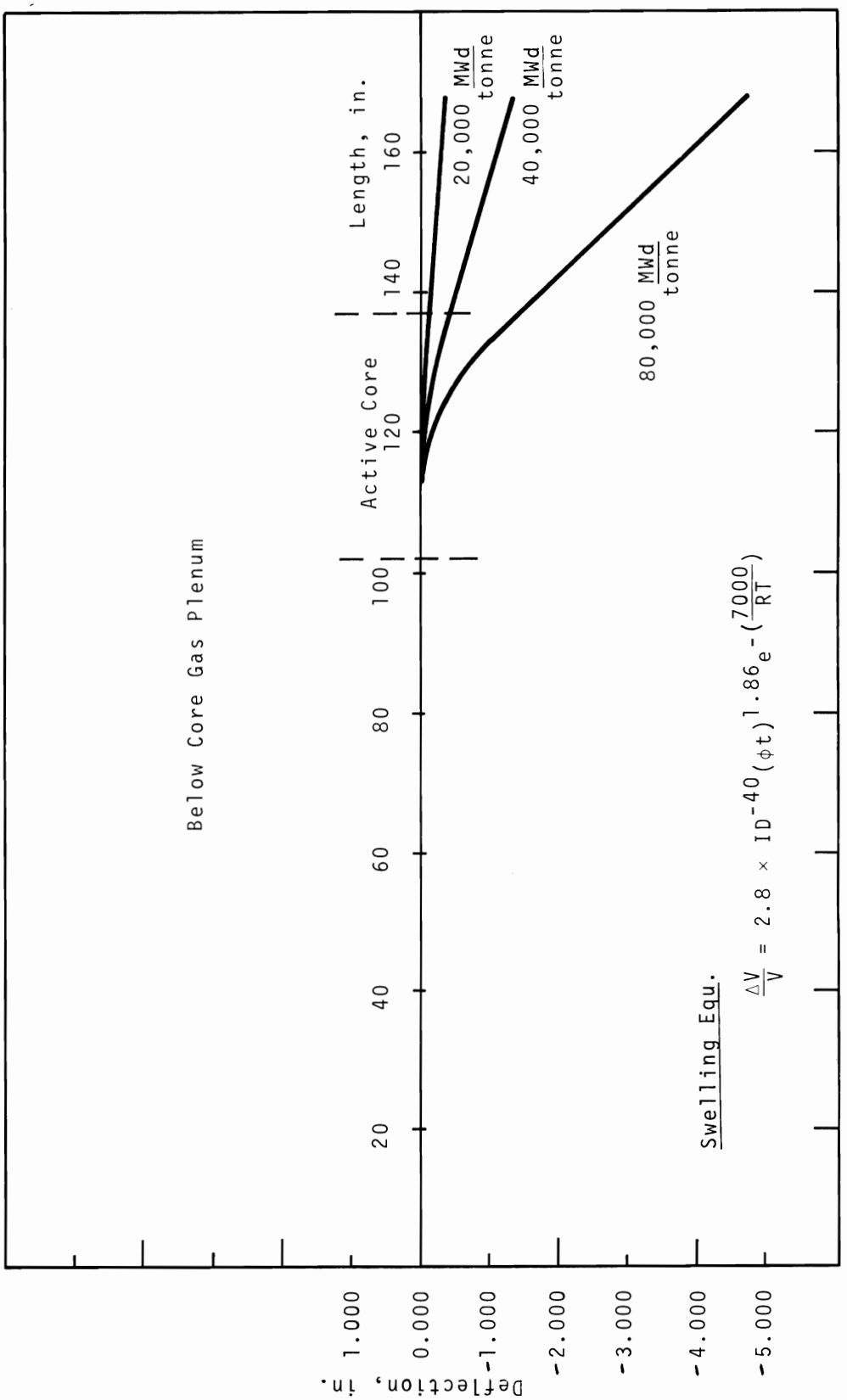

FIGURE 3.4.3-3. Subassembly Deflection Caused by Material Swelling (Below Core Plenum)

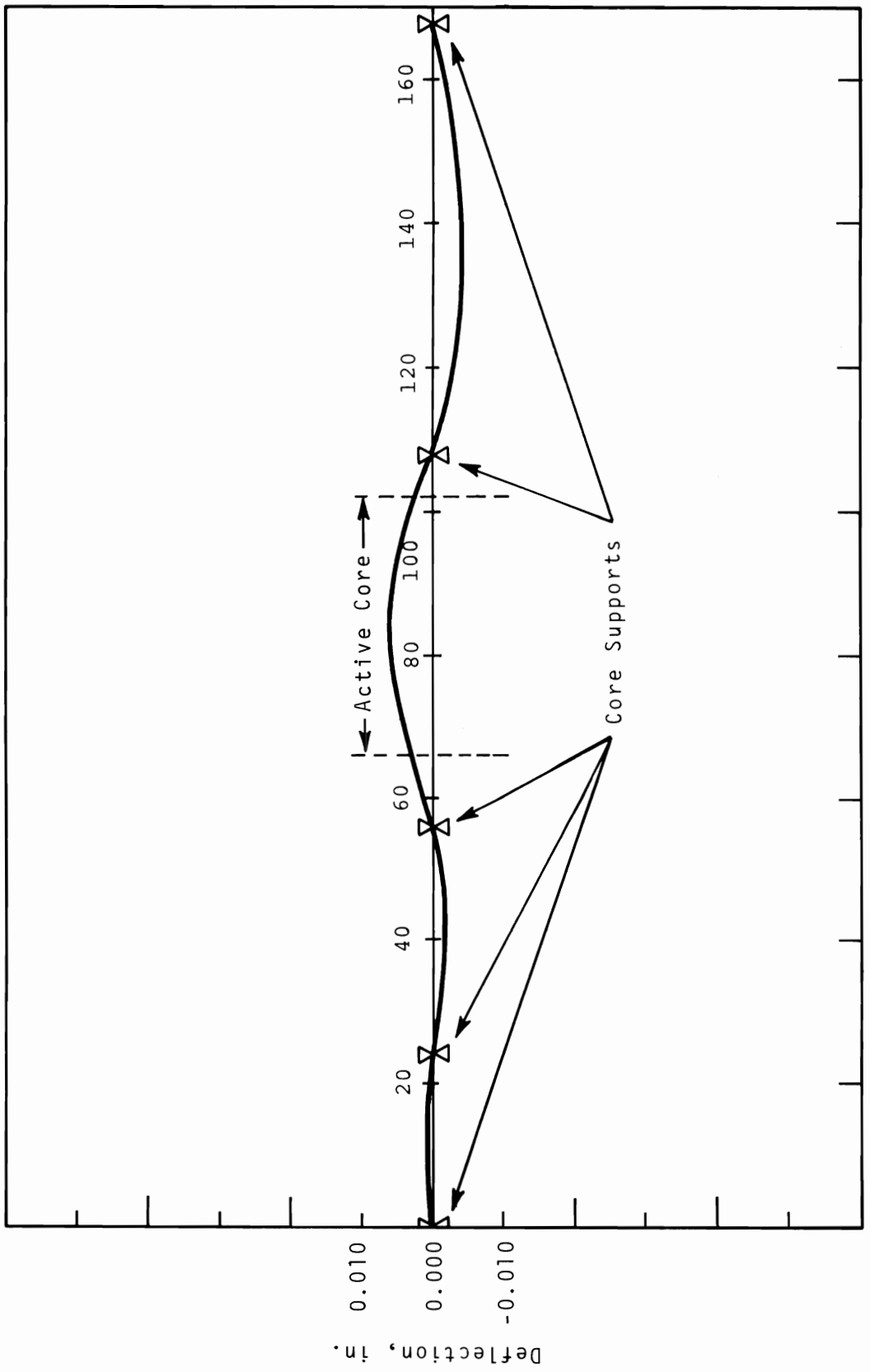

FIGURE 3.4.3-4. Subassembly Deflection After 1st Cycle Using 100% Relaxation of Initial Thermal Stress

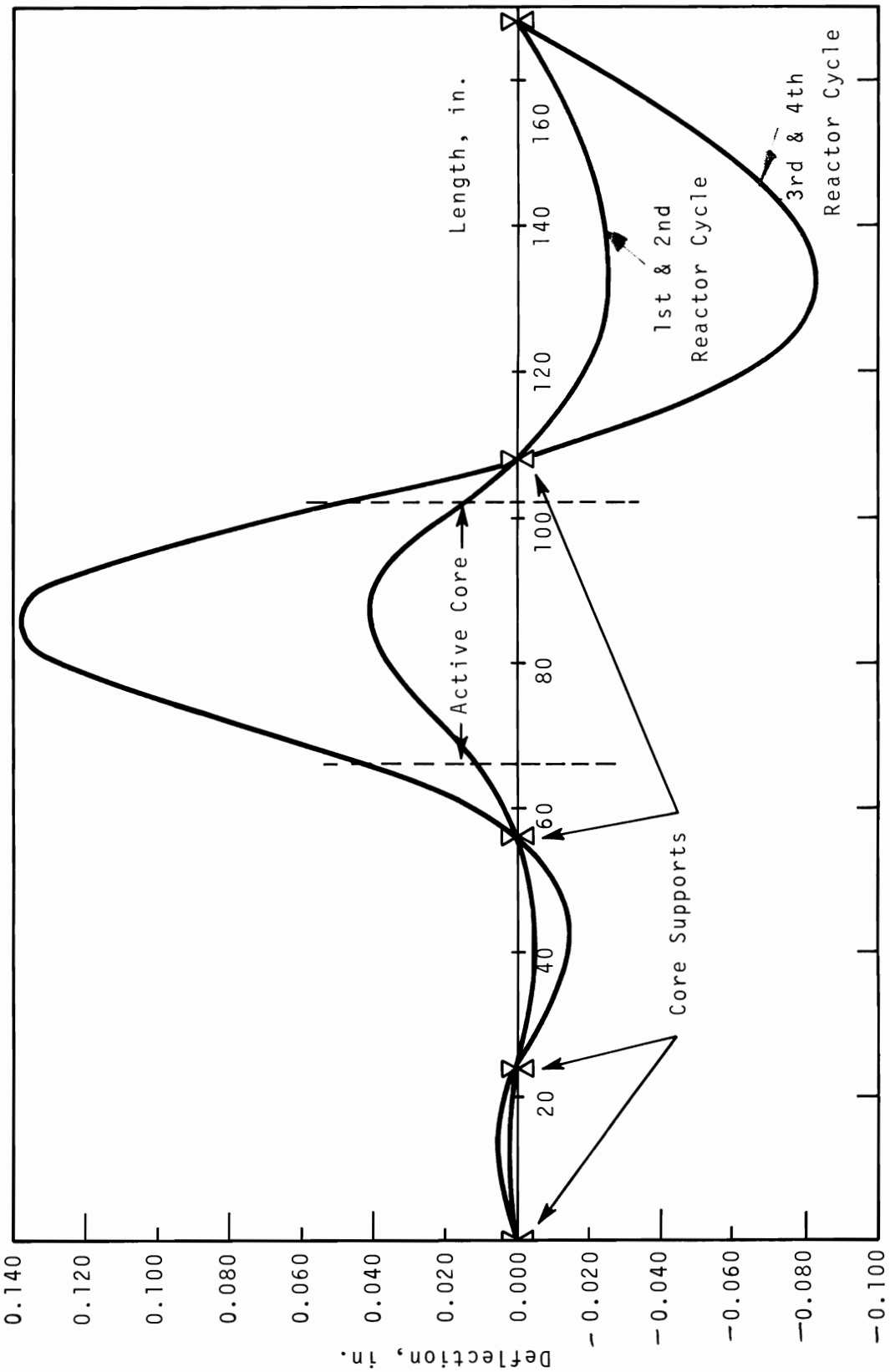

FIGURE 3.4.3-5. Subassembly Deflection for Material Swelling (Subassembly Rotated After Each Cycle)

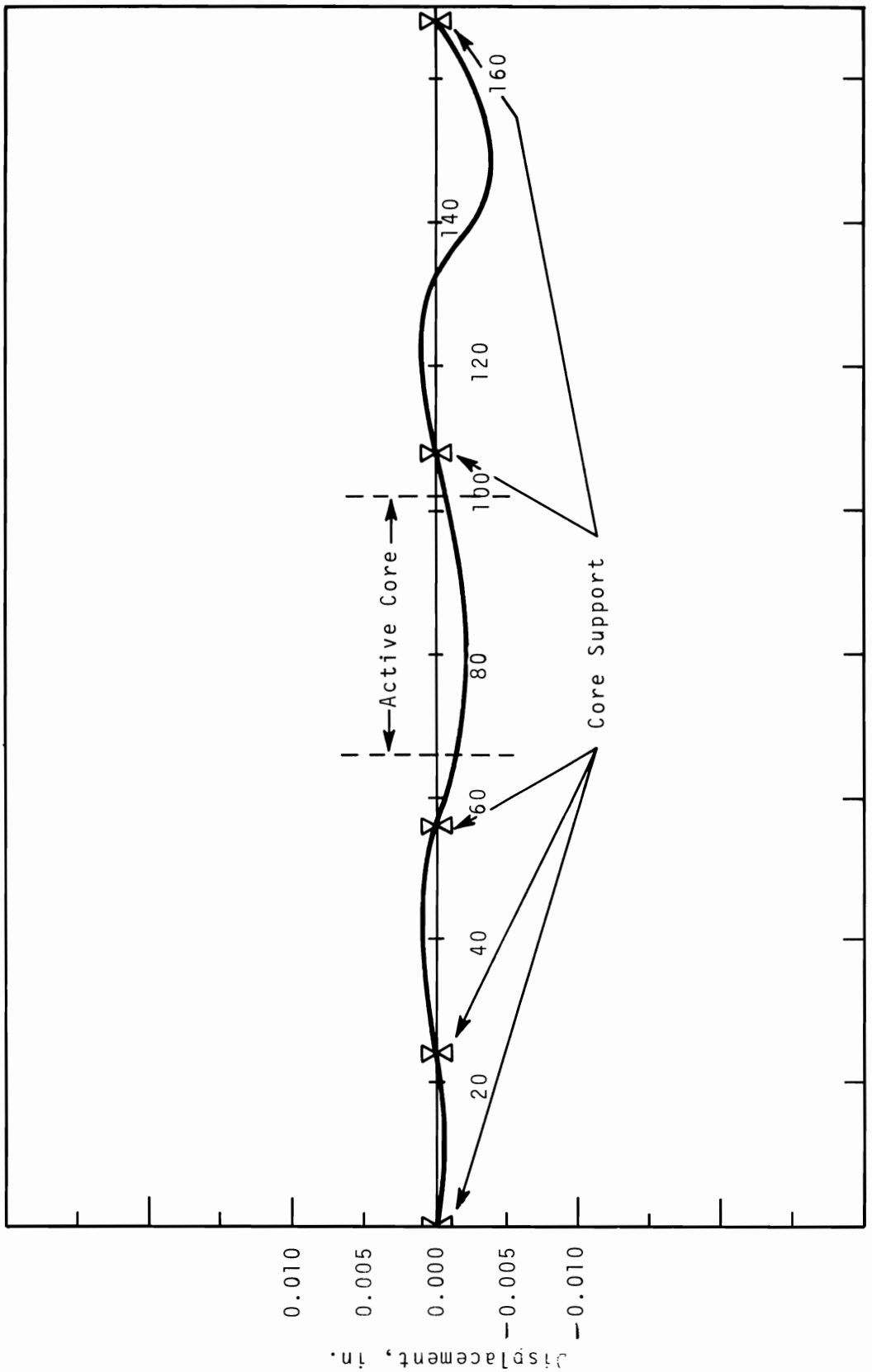

FIGURE 3.4.3-6. Subassembly Thermal Deflection (60 °F-ΔT)

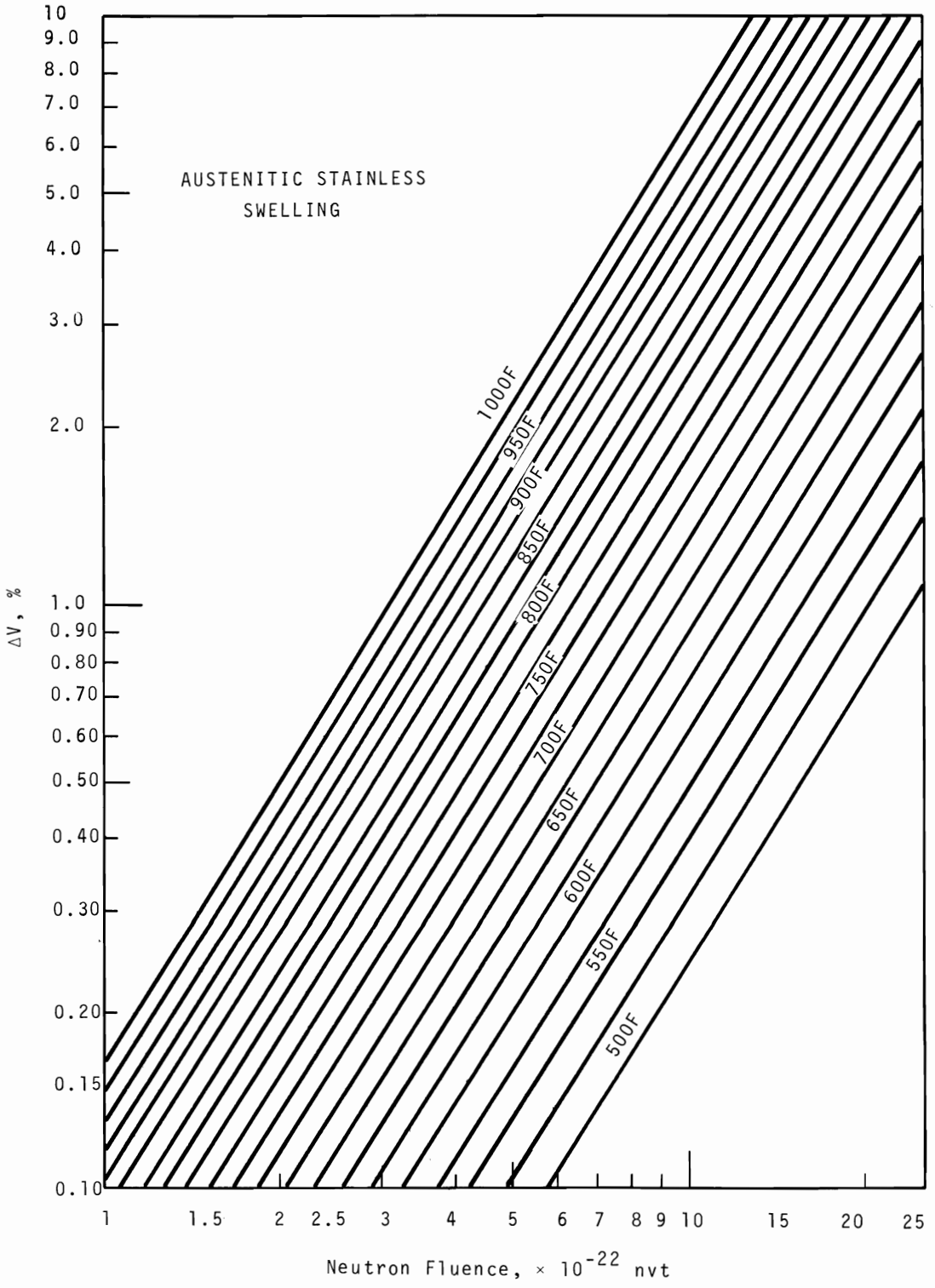

FIGURE 3.5-1. Swelling Model for Solution Treated Austenitic Steel

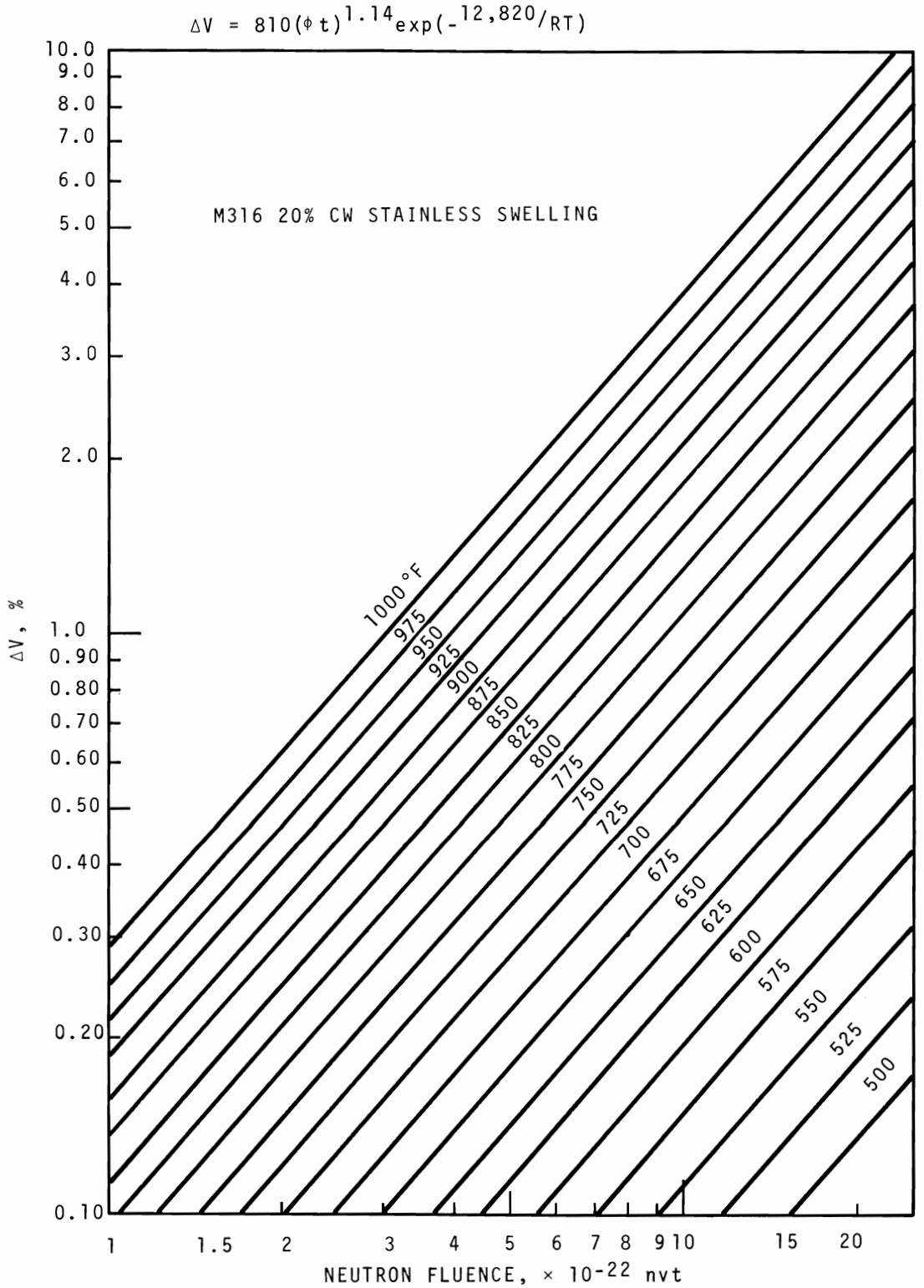

FIGURE 3.5-2. Swelling Model for Cold Worked M-316 Stainless Steel

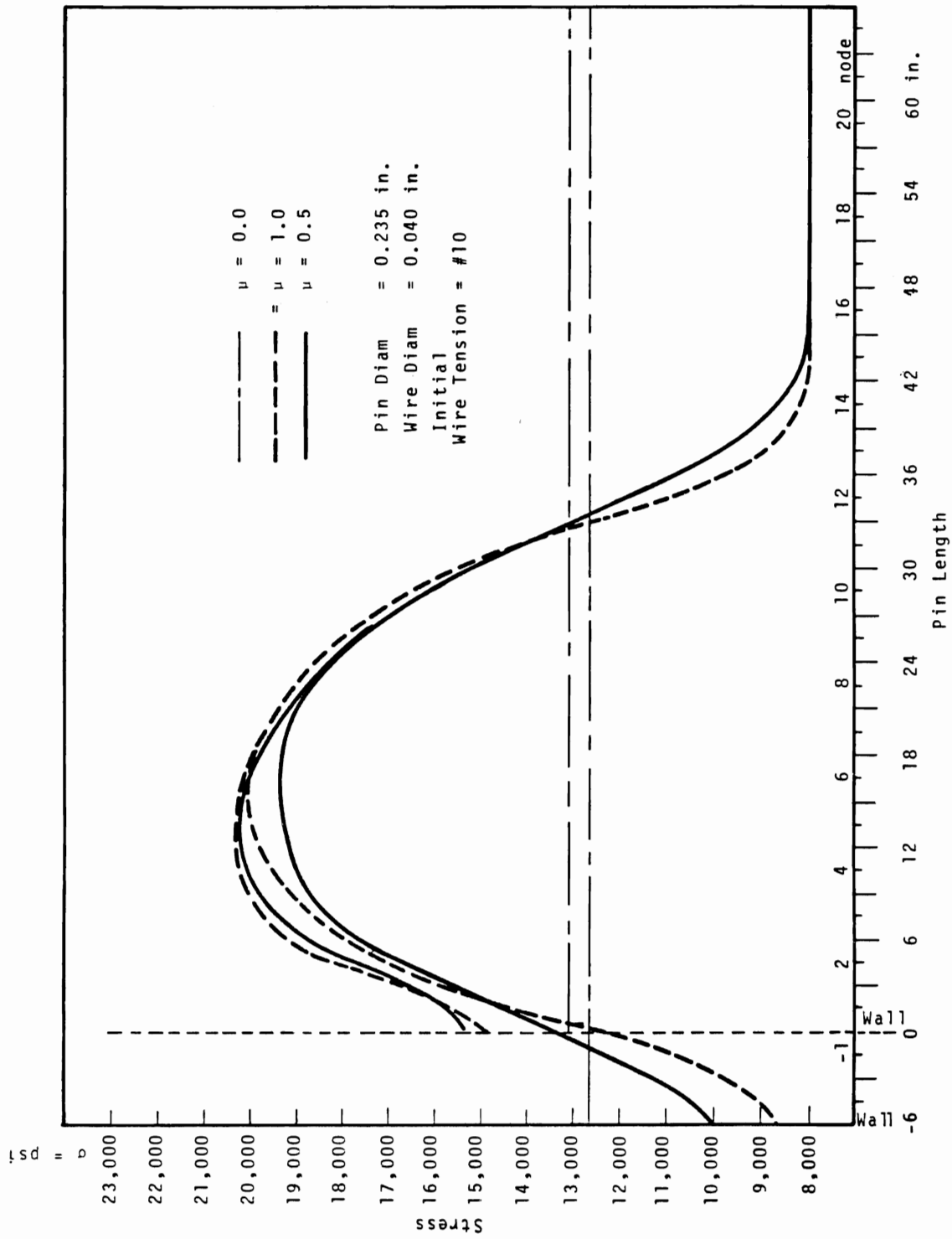

FIGURE 3.7.1-1. Wire Wrap Stress for Standard and 6-in. Reflector Fuel Pin

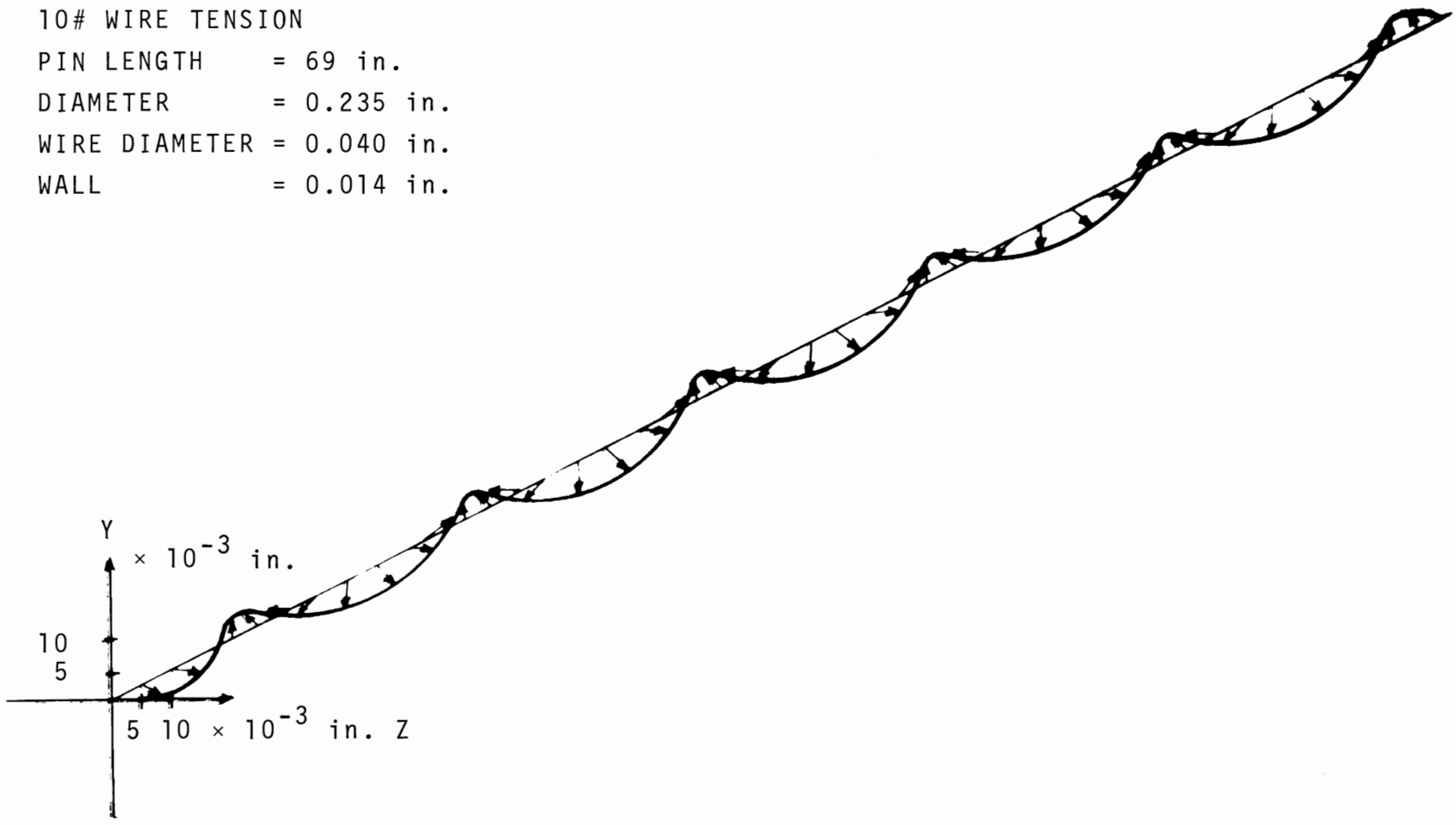

FIGURE 3.7.1-2. Fuel Pin Deflection

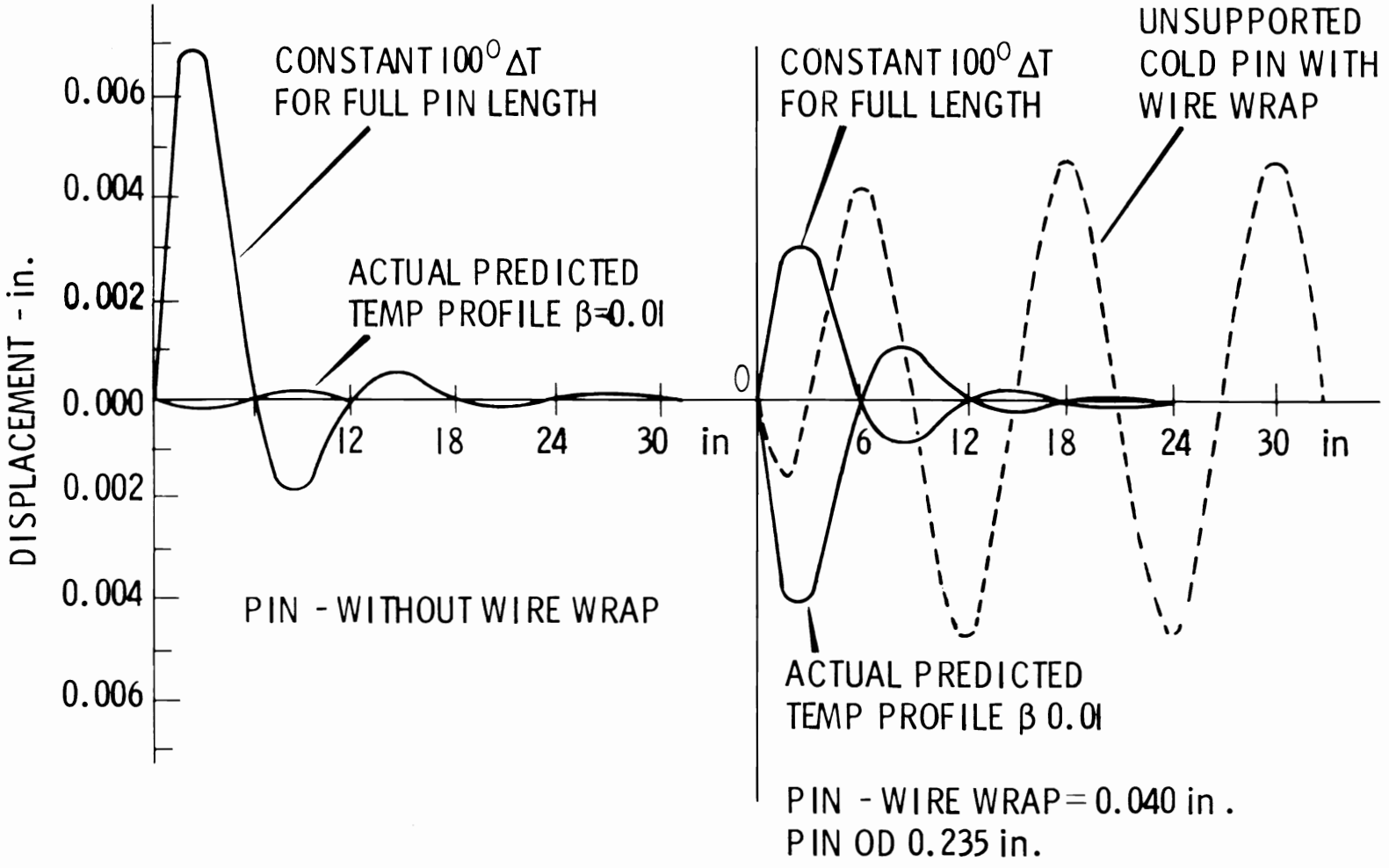

FIGURE 3.7.1-3. Fuel Pin Deformation Patterns for Temperature Gradient of One-Half Pin Segment

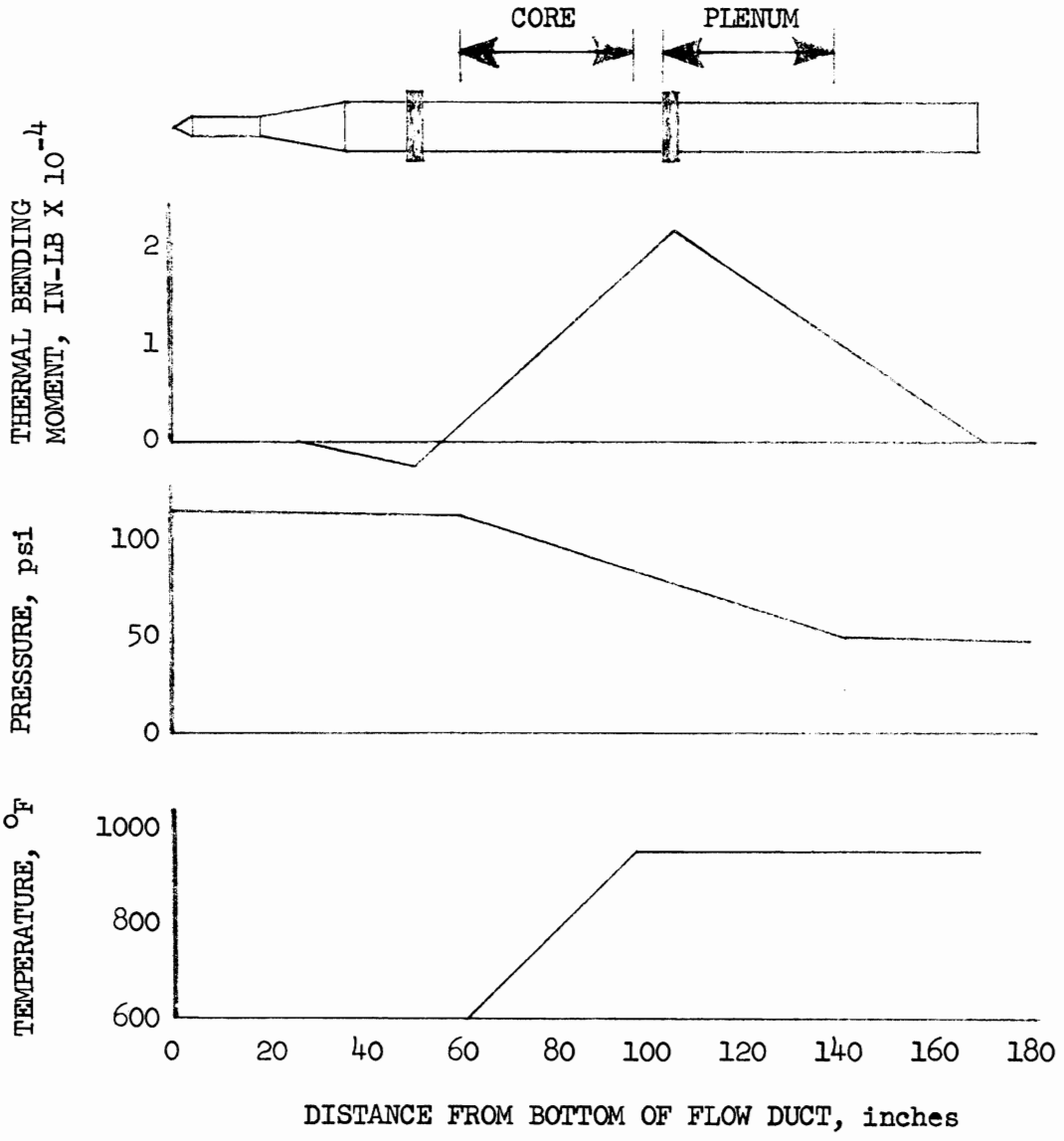

FIGURE 3.9-1. Typical FTR Flow Duct Environment

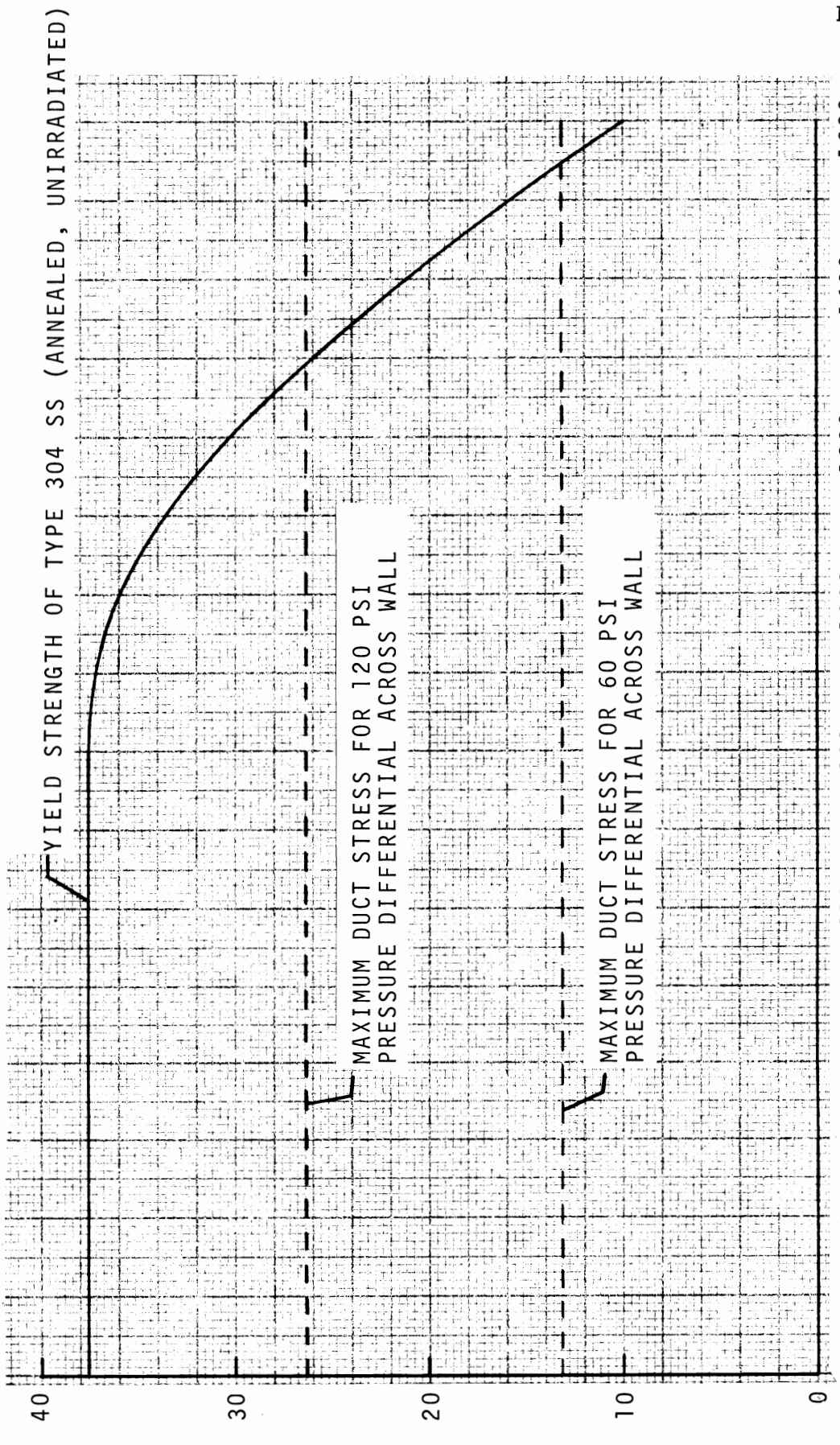

FIGURE 3.9.1-1. Thermal Limits of Driver Fuel Subassembly Duct

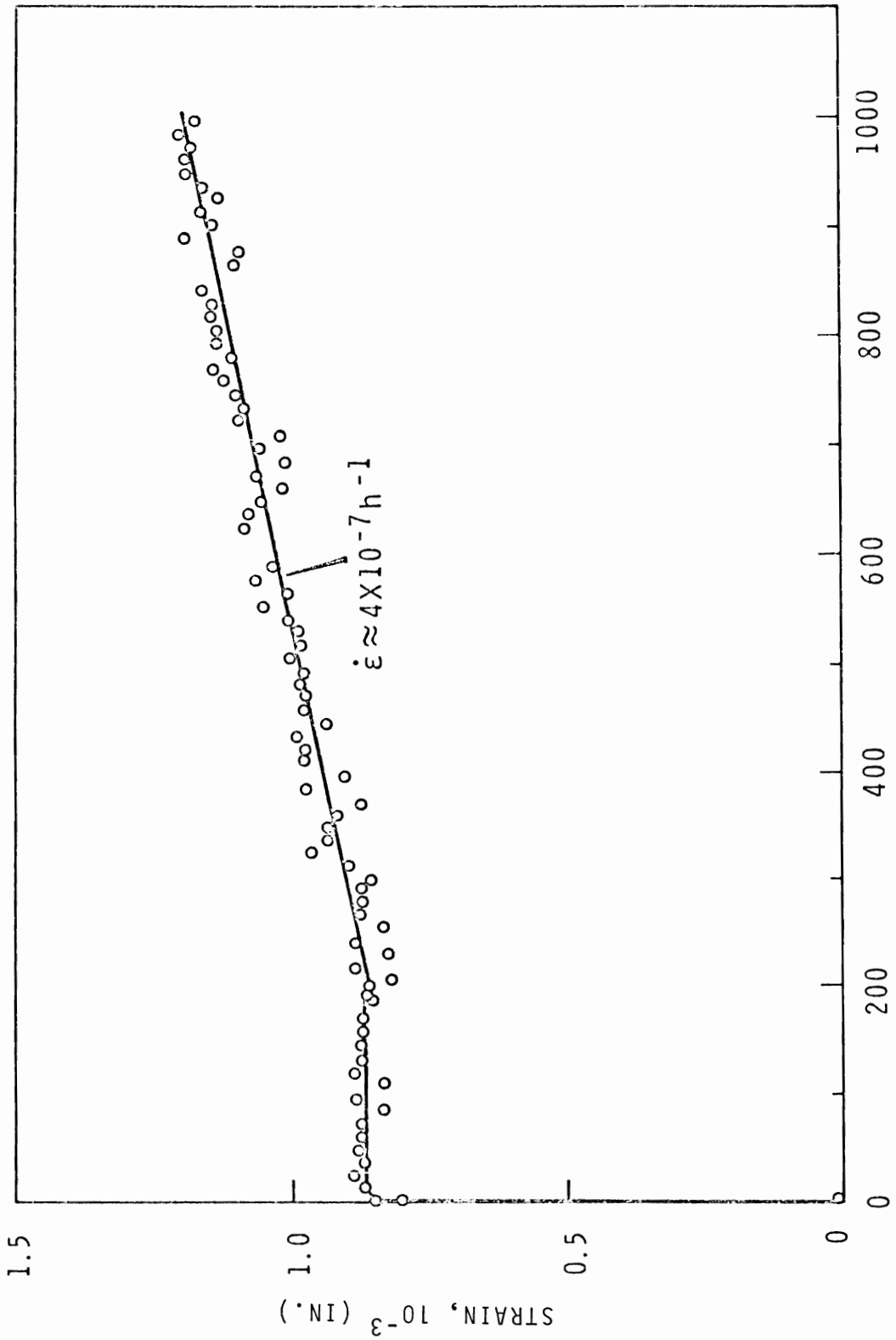

FIGURE 3.10-1. In-Reactor Creep Curve for Annealed 304 SS at 35 ksi Stress and 450 °K Showing the Irradiation Transient Strain and the Radiation Steady-State Creep. All Measurements Taken After the Specimen Was Fully Stressed.

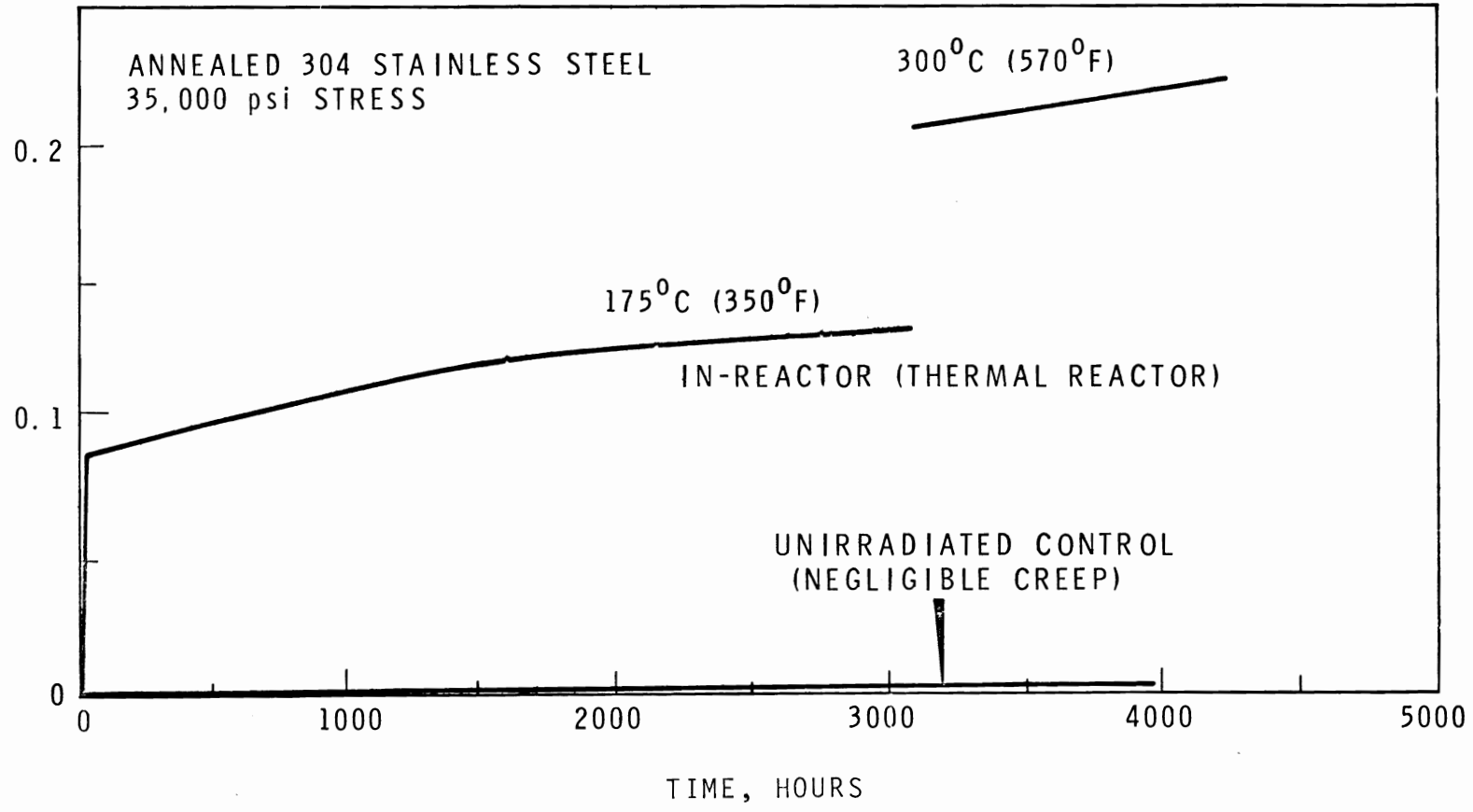

FIGURE 3.10-2. Comparison of Creep Strain for Irradiated and Non-Irradiated 304 Stainless Steel

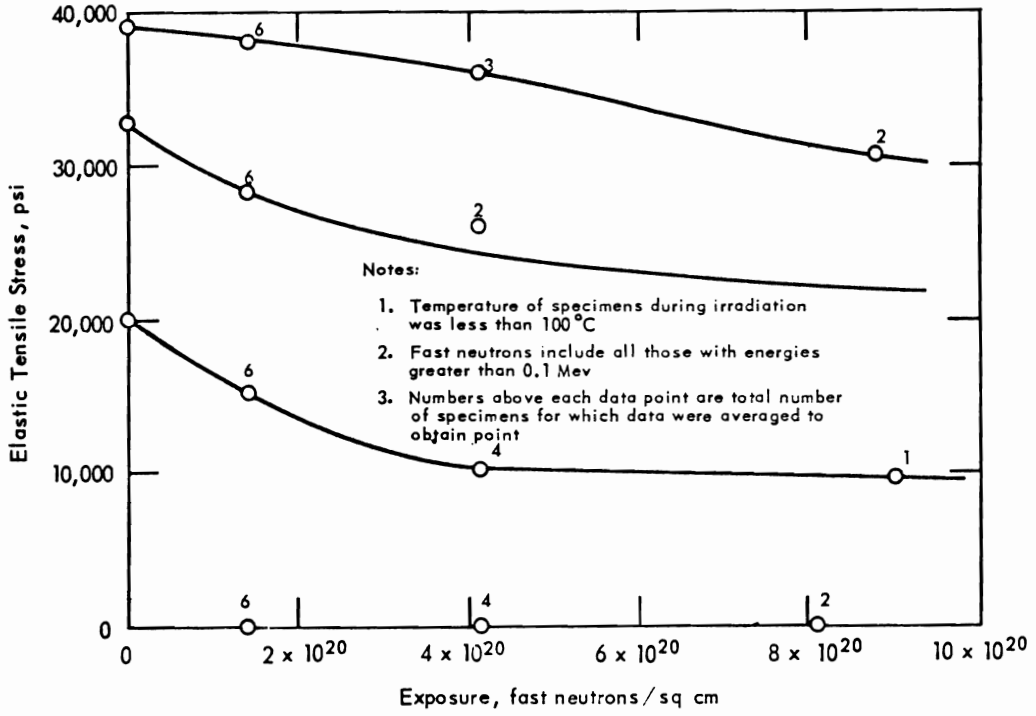

FIGURE 3.10-3. Stress Relaxation in Type 304 SS During Irradiation

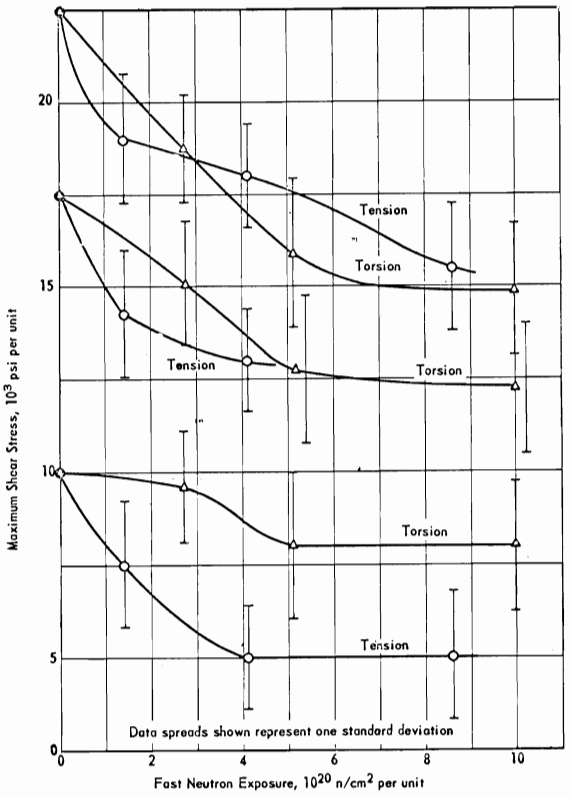

FIGURE 3.10-4. Comparison of Shear Stress Relaxations in Tensile and Torsional Specimens of 304 SS

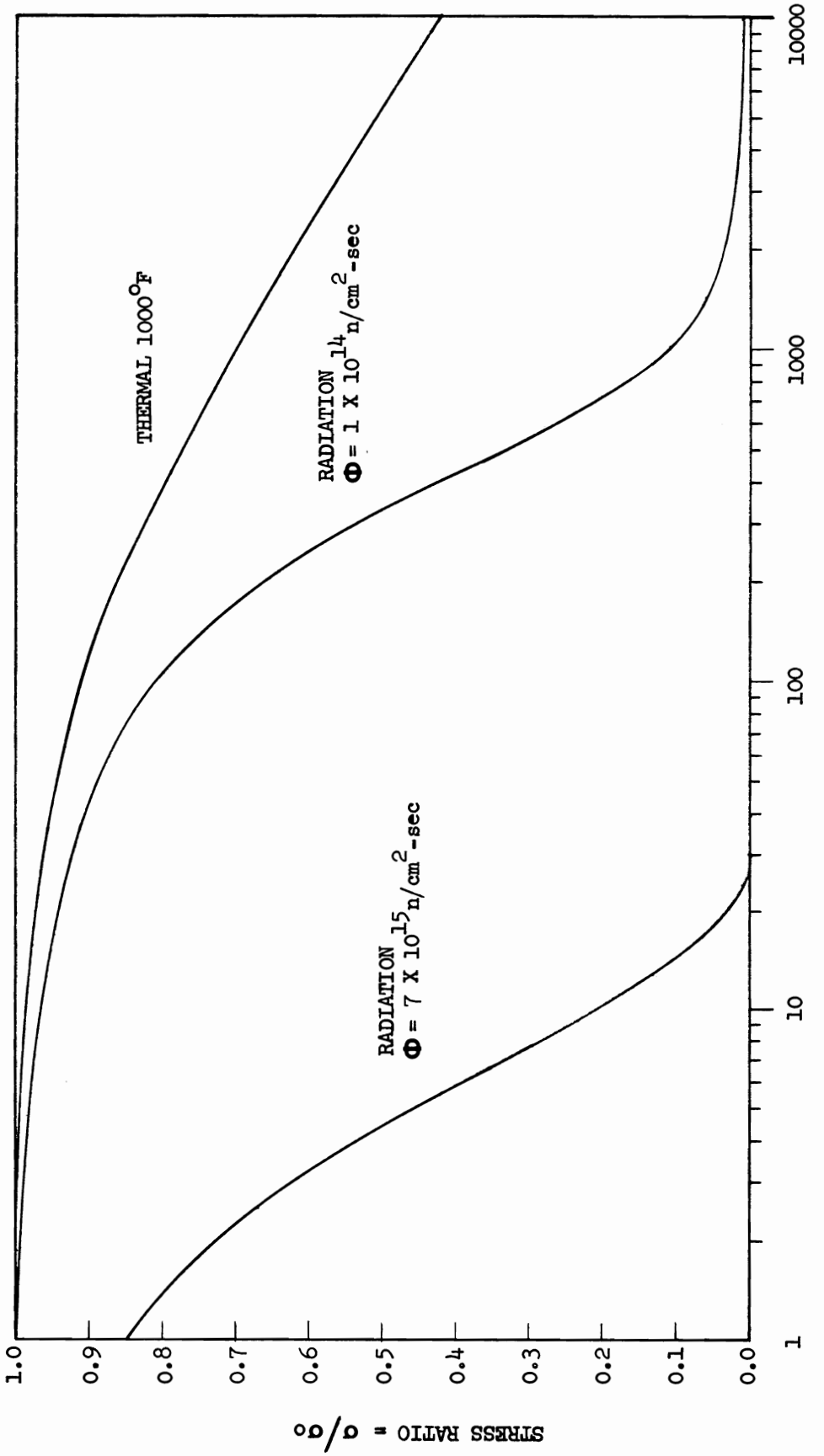

FIGURE 3.10-5. Thermal and Steady-State Stress Relaxation

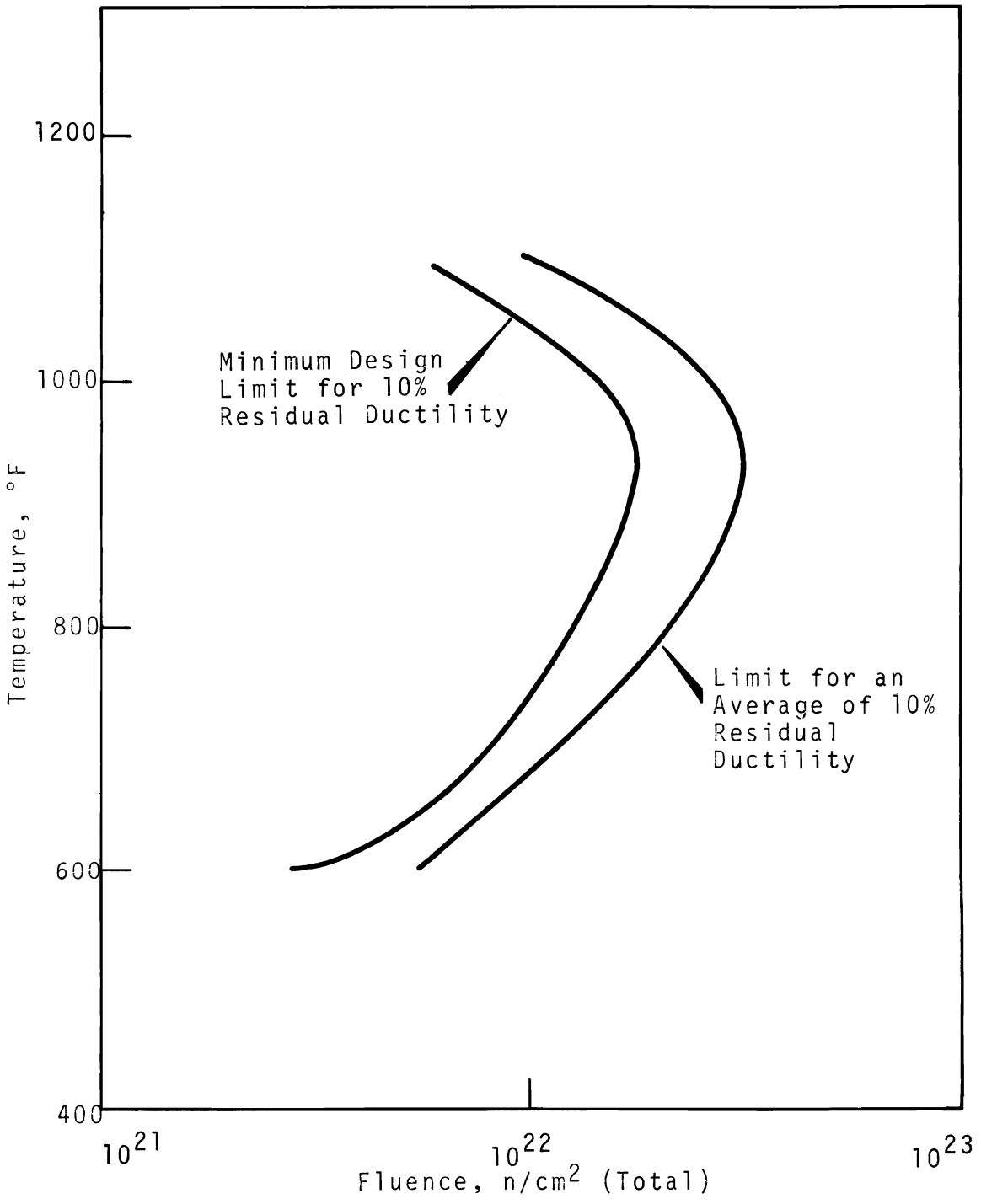

FIGURE 3.12-1. Fluence Limit for FTR Vessel and Core Barrel as a Function of Temperature

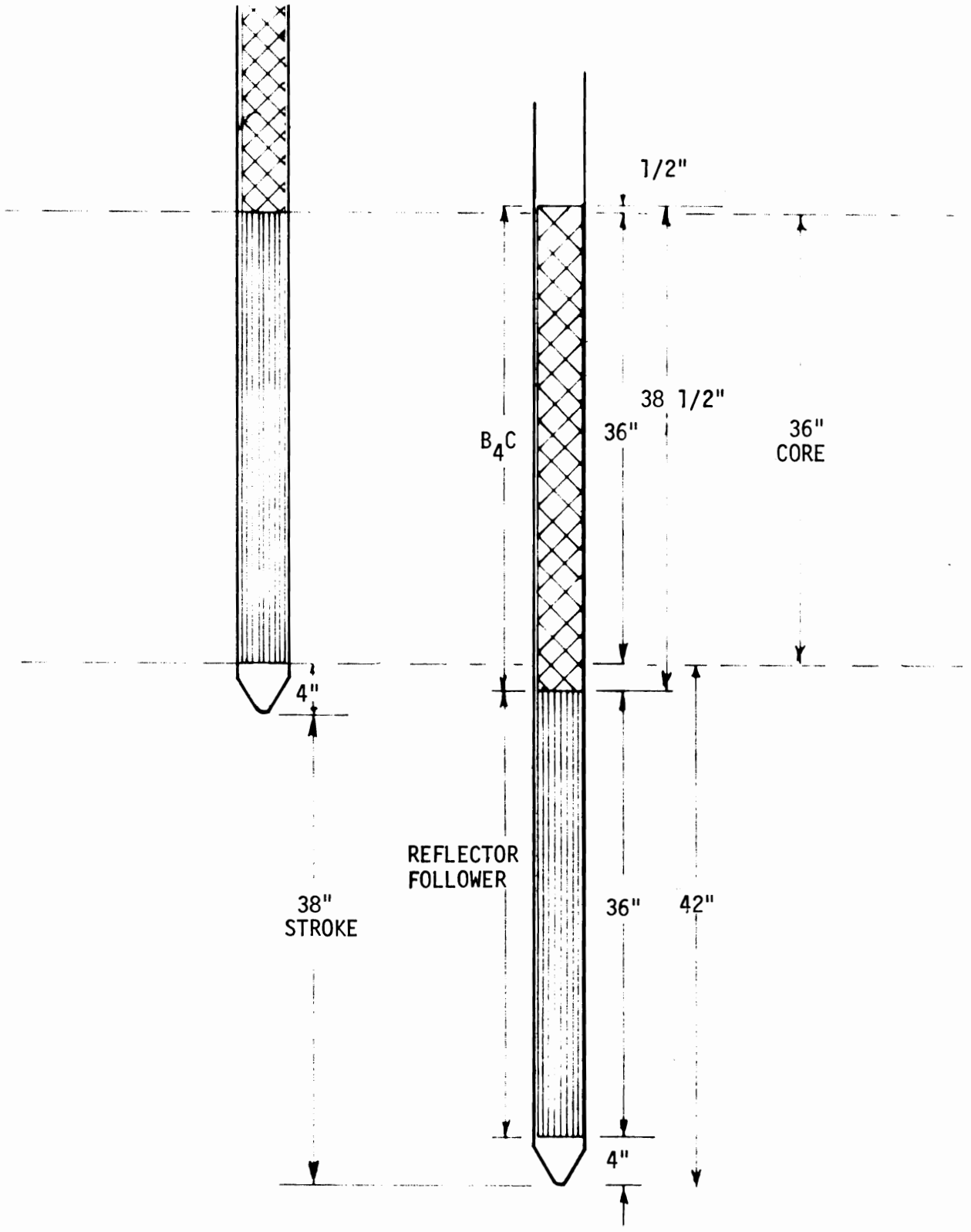

FIGURE 3.12-2. Control/Safety Rod Below Core Lengths

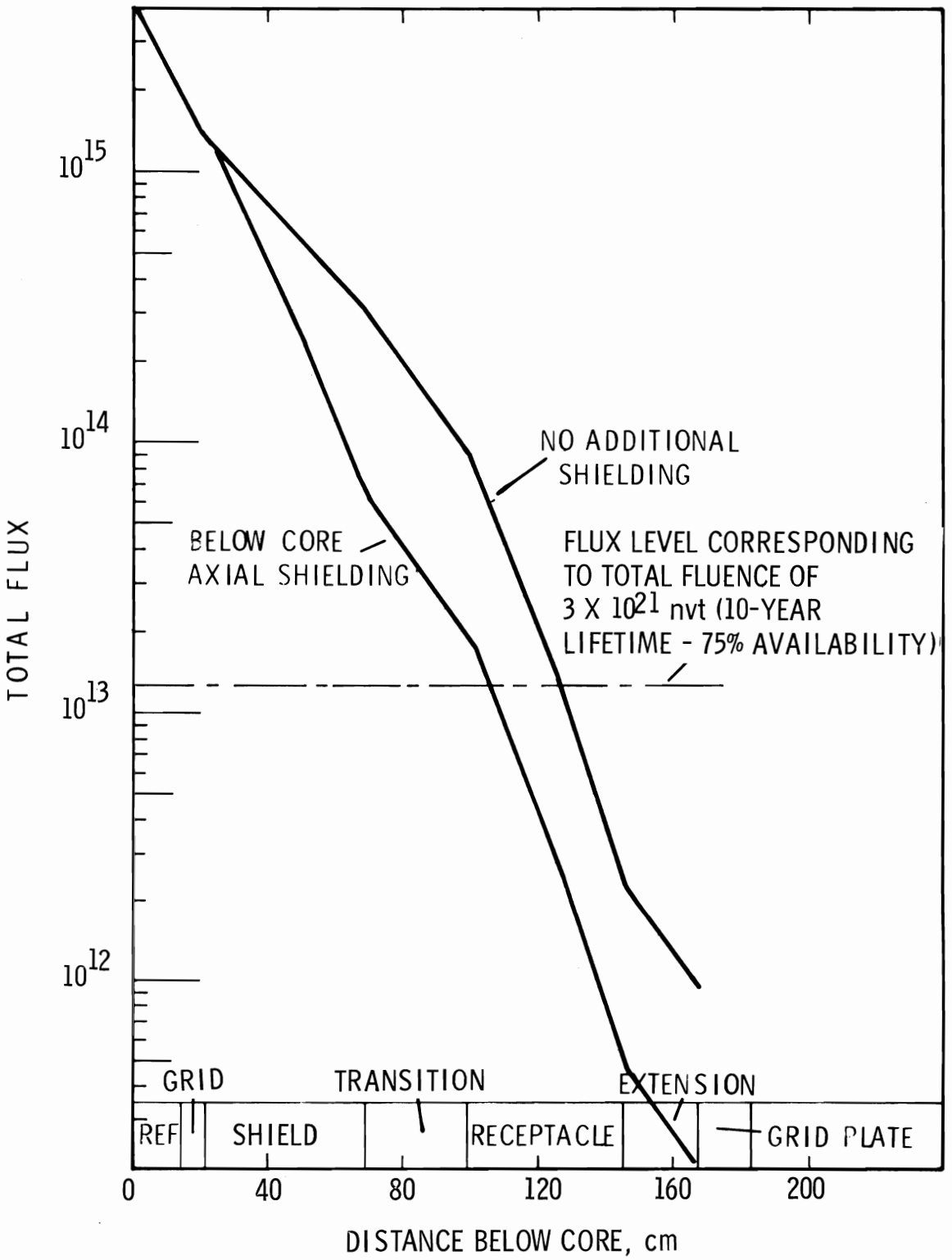

FIGURE 3.12-3. Flux Level as a Function of Axial Distance

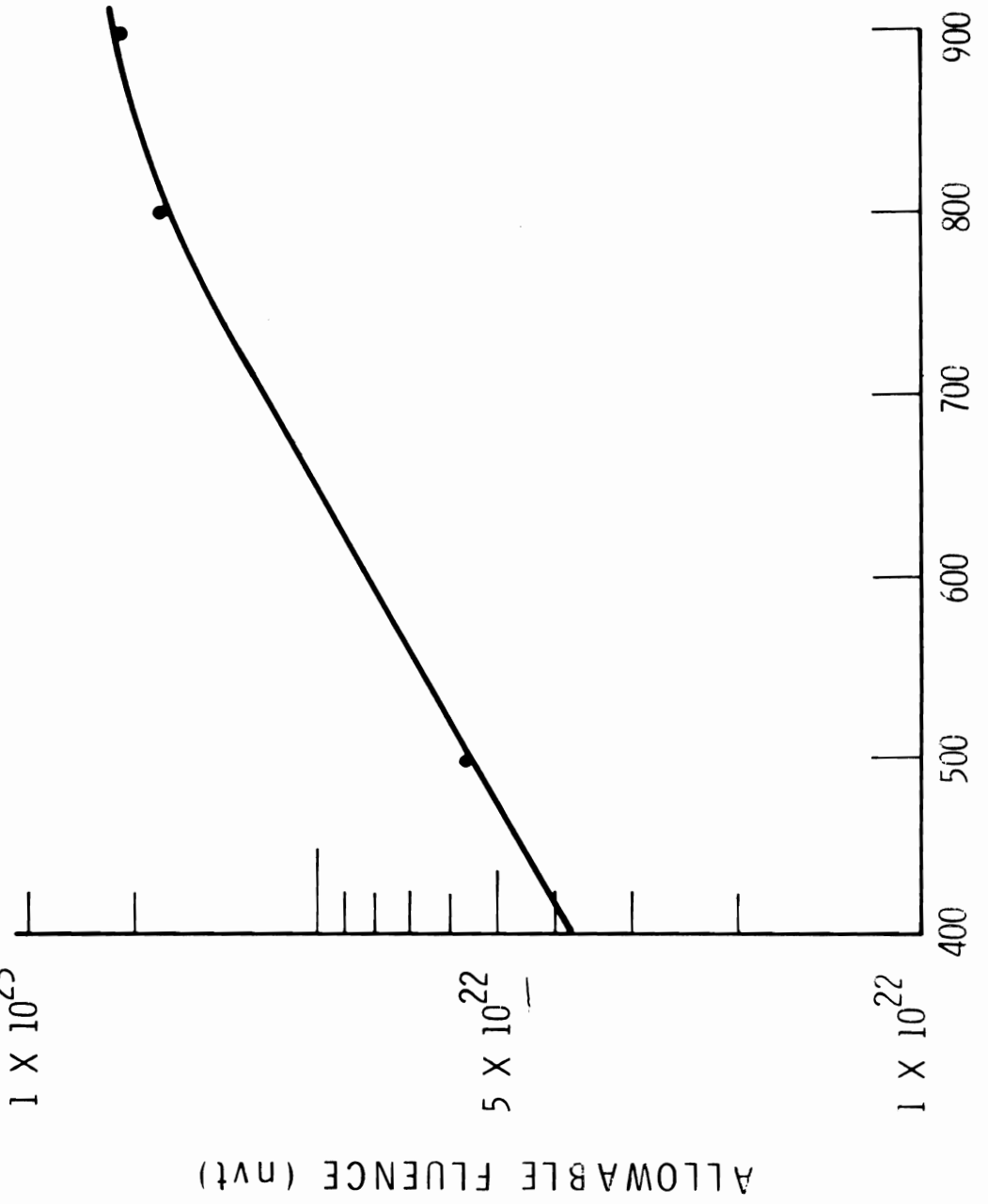

FIGURE 3.12-4. Tentative FTR Receptacle - Fluence Limits for 10% Residual Ductility at End of Life

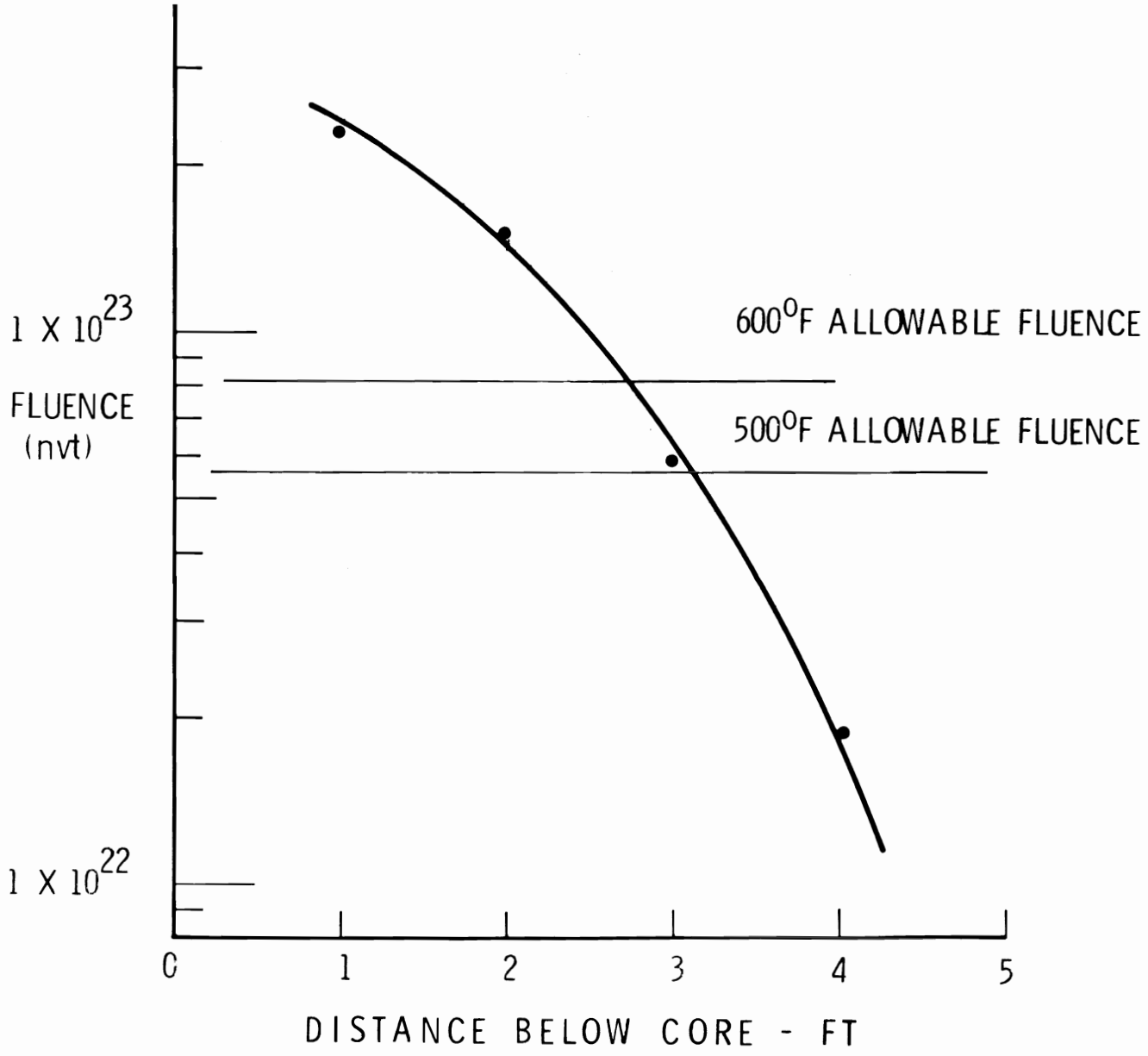

FIGURE 3.12-5. Ten-Year Fluence Without Shielding as a Function of Distance Below Bottom of Active Core

4.0 PERFORMANCE AND MANUFACTURING CHARACTERISTICS

4.1 BURNUP LIMITS - SWELLING

The fuel pins are designed to achieve the desired peak burnup while maintaining clad integrity and without excessive external dimensional changes. The lifetime of the pin depends on fuel management (to achieve desired burnup), operating history (specific power, peak temperature), burnup swelling behavior of the fuel and clad as well as the gas release characteristics of the mixed oxide fuel. Adequate reactivity control can be built into the core to permit fissile loadings in excess of that required for a projected peak burnup of 80,000 MWd/tonne (Pu+U) [Average burnup × radial × axial × hot channel factors affecting burnup]. The limiting factor in attaining this burnup is the uncertainty in the swelling model currently being used beyond the proposed average fuel burnup of 45,000 MWd/tonne (Pu+U). With an adequately sized fission gas plenum (See Section 3.4), the fuel and clad swelling behavior (See Section 3.5) becomes limiting on attainable burnup.

4.2 CORE ZONING

The radial peak-to-average core power is minimized by radial zoning of the core loading. The inner or central zone contains ∿28 driver fuel assemblies and the outer annular zone contains ∿45 assemblies with an enrichment approximately 1.3 times that of the inner zone. The zone boundary can be adjusted to compensate for criticality reactivity requirements. Additional effects of zoning include a reduction of the peak flux when compared to an unzoned core, a slight increase in the required critical mass, a small decrease in the central control rod worths but a significant increase in the peripheral rod worth and a slightly larger overall negative Doppler coefficient.

Distinguishing marks or tests to positively identify fuel rods or assemblies of differing enrichments have not yet been firmed.

4.3 FUEL CYCLE COSTS

Total fuel cycle costs at equilibrium operating conditions are presently estimated at $4.5 million/year for wire-wrapped pins or $5.25 million/yr for a grid-type spaced core, based on a cycle of approximately 12,000 36-inch fueled length, 0.23 inch OD pins/year. The cycle has a fissile throughput of roughly 425 kg ^{239}Pu/year, based on a 75% plant use factor. Complete fuel replacement in the core would occur in approximately 1.3 years, with a quarter of the fuel being replaced every 4 months under one proposed fuel management scheme. The fuel cycle cost is nearly directly proportional to flux and may be expected to vary as the core design is firmed and uncertainties in the fuel fabrication costs are settled. Present fabrication costs of 225 to $300 per pin have been estimated. Assembly costs of 8,000 to $10,000 per fuel assembly have been tentatively estimated for the wire wrapped design, and 27,000 to $33,000 each for grid-type design. Total core costs are estimated at 5 to $6 million for the former and 6.2 to $7.3 million for the latter. However, final fuel cycle costs cannot be firmed until manufacturing techniques have been tried and established and material, shipping and scrap recovery costs are related to the core design and projected operation.

4.4 PROCESS VARIABLE AND DIMENSIONAL CONTROLS

Process variable controls are based upon the product tolerance specifications. Desirable tolerances for all of the components which make up the FTR driver fuel assembly have been set, based upon operational considerations and general engineering practices. However, they must be coordinated with the final manufacturing and assembly process capabilities.

The methods of achieving the desired control over process or product variables are: (1) design reliability and (2) conformance testing. The latter is the least preferred method and is used where satisfactory results cannot be achieved principally by design. Heavy reliance upon conformance testing could be caused by inability to confine, by design, process capability limits within specified tolerances, thereby necessitating inspection of every part. In deriving the variable process controls for the FTR driver fuel assembly, capabilities relating to every product specification must be analyzed. Where heavy reliance upon conformance testing appears necessary, both the product tolerances and the relevant manufacturing process will be re-examined. The criteria for such a study must be overall optimization. More stringent process controls, alternate processes or the widening of product tolerances may be required. The effects on core operations of allowed deviations from the product nominal design values are accounted for the Hot Channel Factor (Section 1.4).

The initial fuel smeared density influences the maximum allowable pin power level, core safety and some data suggest the pin swelling rate with burnup. Smeared density tolerances are directly affected by the design allowances on the clad ID, pellet OD and pellet density. The 0.230 in. OD pin has the following design dimensions:

Clad ID	0.200 ± 0.001 in.
Pellet OD	0.194 ± 0.0015 in.
Pellet Density	93 ± 2% TD

The consequent smeared density and 99.73% confidence level (3σ) deviation is:

Smear Density 87.6 ± 2.1% TD

The dimensional tolerance between the total fuel pin bundle and the flow duct wall must be carefully considered because it affects the coolant velocity distribution, fuel pin restraint and initial assembly procedures. The first two considerations favor minimal spacing from the standpoint of heat transfer and potential fretting of unrestrained fuel pins, while the latter requires sufficient tolerance to permit assembly and free axial movement during full power operations. An analysis of the tolerance stack-up from the pin OD (0.230 in. ± 0.001), spacer wire OD (0.056 in. ± 0.0005) and flat-to-flat hexagonal flow duct dimension (4.335 in. ± 0.005) indicated a preferred mode of assembly would be to compensate for any change in lot average clad OD by using a different lot average diameter spacer wire. (Fuel pins clad and wire will be received in 1/2 mil lot groupings.) This approach maintains a nearly constant rod-to-rod pitch and assures a pin bundle to duct assembly diametral clearance near the design value of 30 mils. A preliminary statistical analysis of this approach indicates the probability of the diametral tolerance being between 20 and 40 mils is at the 98% confidence level. However, because flow streaming around the bundle perimeter must be kept at a minimum, the assembly bundle-to-duct clearance will be controlled to 25 to 30 mils.

4.5 FUEL MANAGEMENT

Preliminary burnup analyses indicate that the design allowance of 1.8 to 2.0% reactivity loss due to fuel burnup will occur after approximately 80 full power days at 400 MW_{th}. The average fuel burnup will be approximately 11,000 MWd/tonne at the initial shutdown for partial refueling. Replacement of one quarter of the driver fuel subassemblies with fresh fuel will provide the required fissile inventory for another 80 day reactivity cycle. Four of these cycles yield

the design average core burnup of 45,000 MWd/tonne, making the core lifetime approximately one full power year.

The optimum fuel management scheme which provides reasonably uniform power profiles across the core with lifetime, balanced by acceptable downtimes for refueling has not been firmed. Several fuel shuffling schemes have been investigated but coordination with the capabilities of the fuel handling machine and goal plant factor must be made.

4.6 AXIAL REFLECTOR MATERIAL AND HEIGHT

Axial reflectors above and below the active fuel region will increase the flux and decrease the critical loading. Figure 4.6-1 shows the effect of axial reflector length on the flux and critical loading for both stainless steel and Inconel. For stainless steel axial reflectors 6 in. long, the flux is increased by 2% and the critical loading decreased by 2% over the unreflected core. For Inconel reflectors of the same length, the benefits to flux and critical loading is twice as great. Use of only 6 in. of either reflector material at each end of the core results in approximately two thirds of the total benefit from an infinite reflector length.

Although stainless steel is only half as effective as Inconel, it has been chosen as the reference reflector material because of uncertainties in the swelling characteristics of Inconel. Until additional exposure data for Inconel becomes available, stainless steel provides greater assurance that irradiation swelling of the reflector will not block the passage of fission gas from the fuel to the gas plenum or endanger clad integrity. Figure 4.6-2 shows current data[101] which indicates that Inconel swells at an acceptable and predictable rate out to a fluence of 5×10^{21} nvt. Allowance

should be made for substitution of Inconel or any other reflector material with better neutronic properties if future irradiation swelling data indicate its acceptability.

It is estimated that use of stainless steel instead of Inconel for the reflector material would cause about a 2% increase in the axial peaking factor (resulting in a 2% decrease in total power) and a maximum decrease of about 5% in the Doppler coefficient.

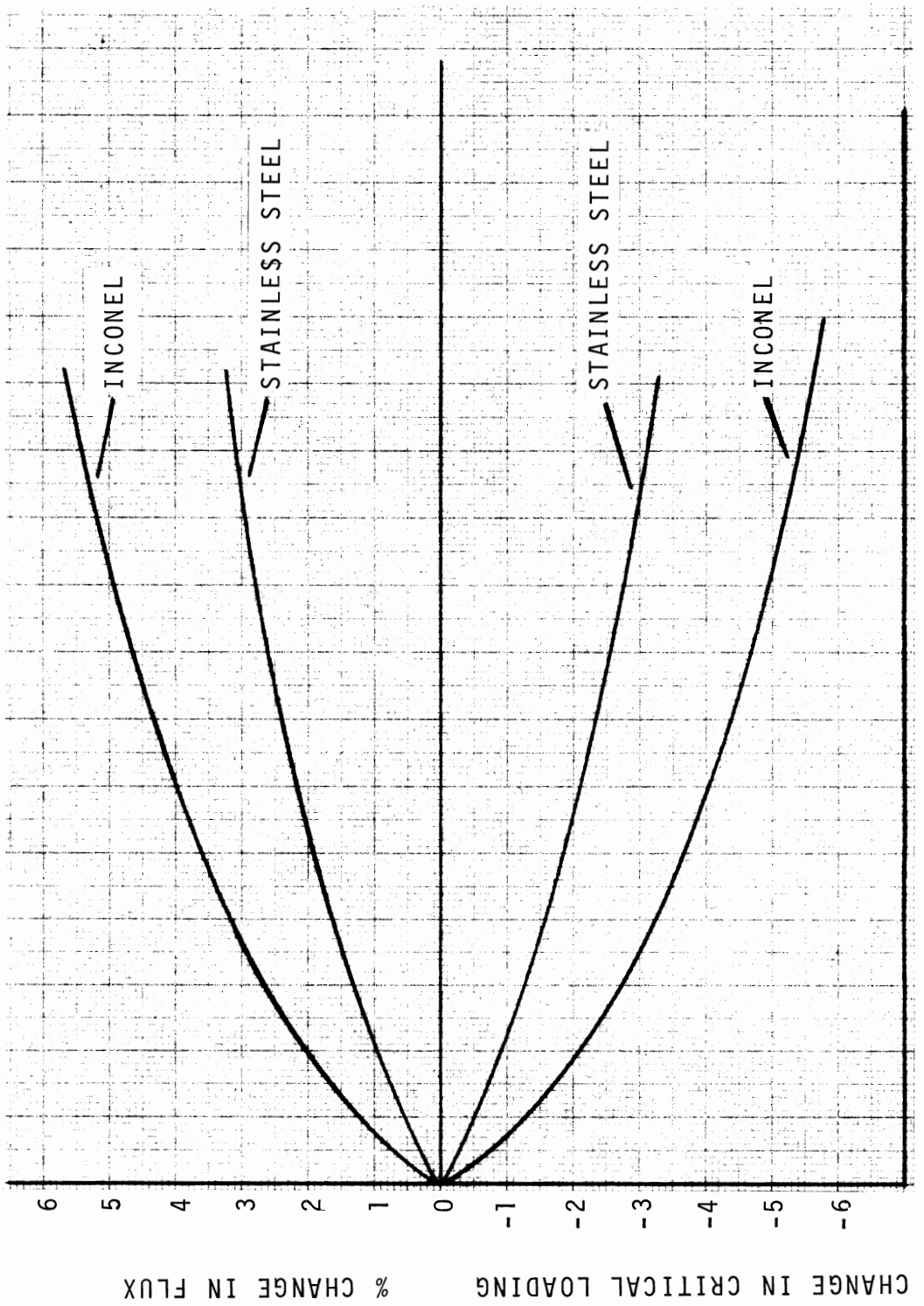

FIGURE 4.6-1. Effect of Reflector Length and Material Versus Change in Flux and Critical Loading

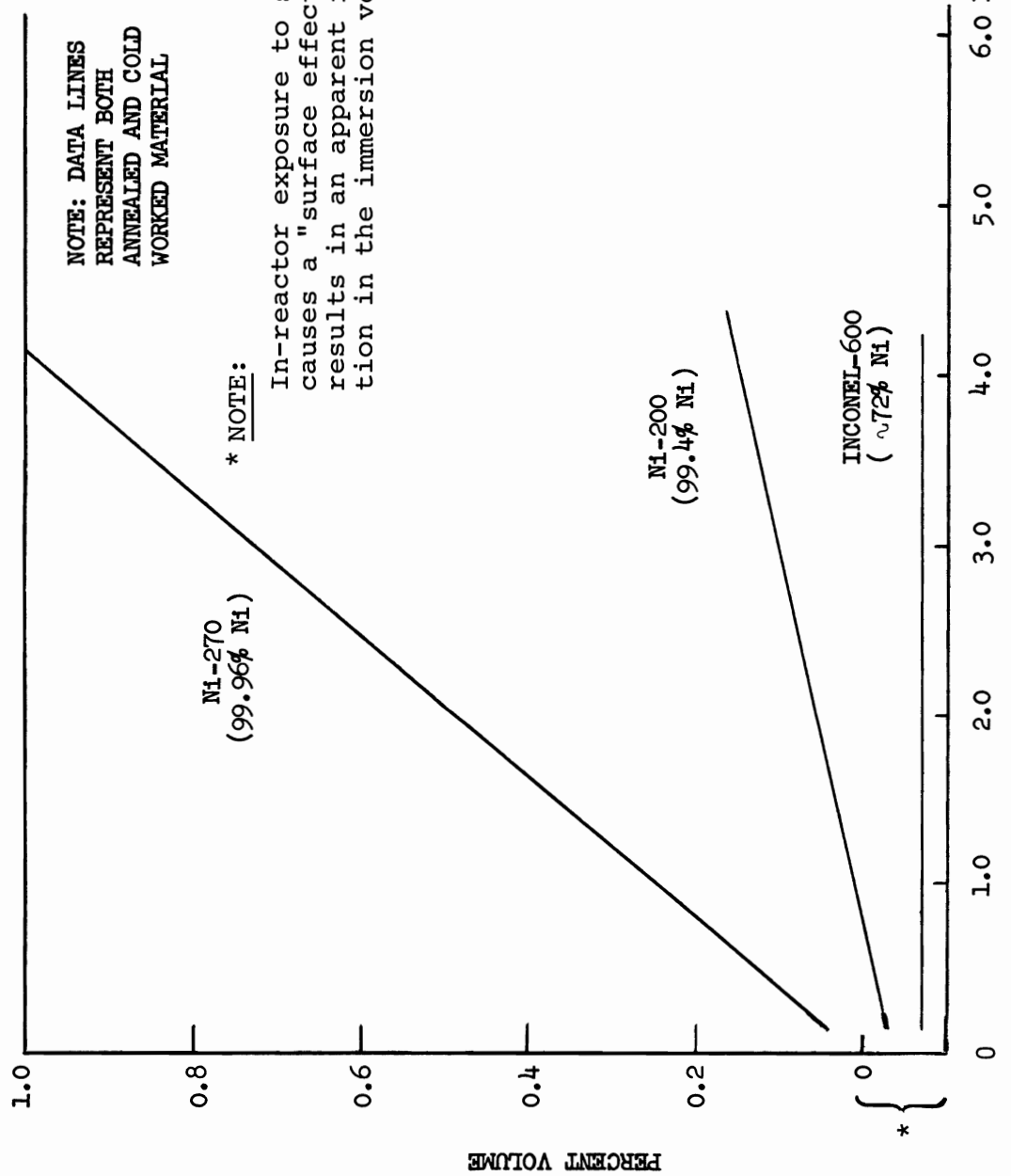

FIGURE 4.6-2. Swelling in Nickel Base Alloys

REFERENCES

1. E. G. Stevens. Revised $\int$kdT Curves, FFTF Monthly Informal Technical Progress Report, BNWL-712, p. 3.63-3.72, February 1968.

2. J. L. Krankota and C. N. Craig. Melting Point of High Burnup PuO_2-UO_2, ANS Transactions 11, 1, p. 132, June 1968.

3. J. A. Christensen. Stoichiometry Effects in Oxide Nuclear Fuels, I. Power Rating Required for Melting and Oxygen Redistribution in Molten Center $UO_{2\pm x}$ Fuels, BNWL-563, December 1967.

4. G. L. Fox and K. R. Mercks, SINTER-A Program for Calculating Radial Temperature Distributions in Oxide Fuel Pins Undergoing Sintering, BNWL-1241, January 1970.

5. E. G. Stevens. A Correction Factor for In-Reactor Sintering of Fast Oxide Fuels, Nuclear Applications, 5, 6, 410-416, December 1968.

6. R. A. Hein and P. M. Flagella. Enthalpy Measurements of UO_2 and Tungsten to 3260 K, GEMP-578, February 16, 1968.

7. L. F. Epstein. Ideal Solution Behavior and Heats of Fusion from the UO_2-PuO_2 Phase Diagram, J. of Nuclear Materials, 22, p. 340, 1967.

8. A. E. Ogard and J. A. Leary. High Temperature Heat Content and Heat Capacity of UO_2 and PuO_2 Solid Solution, IAEA Proceedings of the Symposium on Thermodynamics of Nuclear Materials, Vienna, September 4-8, 1967.

9. T. G. Godfrey et al. Thermodynamic Functions of Nuclear Materials: UC, UC_2, UO_2, ThO_2 and UN, ONNL-TM-1596, December 1967.

10. J. Roth et al. Thermal Expansion of Coprecipitated (U, Pu)O_2 Powders by X-Ray Diffraction Techniques, NUMEC-2389-9, October 1965.

11. G. Berggren and R. S. Forsyth (A. B. Atomenergi, Sweden). Some Studies of the High Temperature Behavior of PuO_2 and PuO_2-UO_2 Mixtures, PLUTONIUM 1965, p. 828, A. E. Kay and M. B. Waldron (Eds.), Chapman and Hall, LTD, London.

12. J. Roth et al. The Effects of Stoichiometry on the Thermal Expansion of 20% w/o PuO_2-UO_2 Fast Reactor Fuel, ANS Trans., 10, 2, 457, November 1967.

13. R. R. Asamoto et al. The Effective Axial and Diametral Thermal Expansion of UO_2 Under Radial Temperature Gradient, GEAP-5284, October 1966 or ANS Transactions, 8, 383, November 1965.

14. T. J. Bennett. Average FTR Core Expansion During 25% Overpower Transient, FFTF Monthly Informal Technical Progress Report, p. 3.68, BNWL-603, October 1967.

15. M. F. Lyons et al. UO_2 Fuel Rod Operations with Gross Fuel Melting, GEAP-4264, October 1963.

16. J. A. Christenson. Thermal Expansion and Change in Volume on Melting for UO_2, HW-75148, October 1962.

17. H. Hausner et al. Correlation of UO_2 Microstructures from In-Pile and Out-of-Pile Experiments, GEAP-4535, June 1964.

18. J. E. Hanson et al. FTR Driver Fuel Design Bases, p. 4-7, BNWL-CC-1777, August 1968.

19. F. Anselin et al. Irradiation Behavior of Plutonium Mixed Oxide Driver Fuel of RAPSODIE, ANS Transactions, 11, 2, 514, November 1968.

20. Sodium Cooled Reactors Fast Ceramic Reactor Development Program, 27th Quarterly Report, GEAP-5677, p. 71, August 1968.

21. J. E. Hanson et al. Unpublished Data (Fuel Smeared Density), 1968.

22. W. E. Baily et al. Effect of Diametral Gap Size on the In-Pile Performance of Fast Ceramic Reactor Mixed-Oxide Fuel, ANS Transactions, 9, 1, 40, June 1966.

23. I. Cohen et al. Measurement of the Thermal Conductivity of Metal-Clad Uranium Oxide Rods During Irradiation, WARD-228, August 1960.

24. A. M. Ross et al. Heat Transfer Coefficient Between UO_2 and Zircaloy-2, CRFD-1075 (AECL-1552), June 1962.

25. E. G. Stevens. Revised Design SCF and h_{gap}, FFTF Monthly Informal Technical Progress Report, p. 3.77 BNWL-742, March 1968.

26. FFTF Monthly Informal Technical Progress Report, BNWL-863, Battelle-Northwest, Richland, Washington, July 1968.

27. O. E. Dwyer. Analytical Study of Heat Transfer to Liquid Metals Flowing In-Line Through Closely Packed Rod Bundles, Nuclear Science and Engineering 25, 343-358 (1966).

28. R. C. Deissler and M. F. Taylor. Analysis of Fully Developed Heat Transfer and Flow in an Annulus with Various Eccentricities, NACA Tech. Note 3451, 4-8, May 1955.

29. K. W. Cook. Velocity Distribution Around Fuel Pins in Sodium-Cooled Fast Reactors with Triangular Fuel Pin Arrays, GEAP-5725, (Preliminary) December 1968.

30. D. J. Bander et al. Tubulent Velocity Distribution in a Rod Bundle, GEAP-5411, October 1967.

31. H. Fenech and H. M. Gueron. The Synthesis Method of Uncertainty Analysis in Nuclear Reactor Thermal Design, Nuclear Science and Engineering, 31, 505-512 (1968).

32. W. G. Blessing et al. Summary of the APDA Fuel Development Programs, APDA-143, April 1961.

33. L. J. Koch et al. Addendum to the Hazard Summary Report of the Experimental Breeder Reactor, EBR-II, ANL-5719, p. 55, January 27, 1964.

34. Liquid Metal Fast Breeder Reactor Design Study, Design Analysis, p. IV-51, Vol. II of II, CEND-200, Combustion Engineering, January 1964.

35. G. H. Farbman and J. H. Jacobs. PWR's - How They've Grown to Today's Size, POWER, p. 69, April 1968.

36. D. C. Kolesar. Temperature Peaking Under the 30 Mil Wire Wrap, FFTF Monthly Informal Technical Progress Report, BNWL-722, April 1968.

37. C. A. Strand. Critical Component-Driver Fuel Pin Fuel Pellet, A-0080A-R (HWS-1002), November 6, 1968.

38. R. L. Gibby. The Thermal Diffusivity and Thermal Conductivity of Stoichiometric $(U_{0.8}Pu_{0.2})O_2$, BNWL-704, May 1968.

39. A. Padilla. "Transient Scram Analyses," Fast Flux Test Facility Monthly Informal Technical Progress Report, BNWL-915, pp. 3.52-3.58, October 1968.

40. Technical Bases for FFTF Driver Fuel Instrumentation, Compiled by J. J. Regimbal, BNWL-916, October 1968.

41. A. Padilla et al. Overheating Factor, FFTF Monthly Informal Technical Progress Report, BNWL-512, p. 0.1, July 1967.

42. J. W. Hagan et al. Parametric Scram Transient Analysis for the FFTF, BNWL-657, November 1967.

43. J. E. Hanson and J. H. Field. Experimental Studies of Transient Effects in Fast Reactor Fuels-Series III, Pre-Irradiated Mixed Oxide (PuO_2-UO_2) Irradiations Final Report, Transient Irradiations, GEAP-4469, General Electric Co., July 1967.

44. A. E. Waltar et al. Considerations on the Use of Fuel Motion Restrictors in FTR Fuel Pins, BNWL-623, Battelle-Northwest, Richland, Washington, November 1967.

45. J. E. Hanson et al. Unpublished Data (Fuel Smeared Density), 1968.

46. D. E. Simpson et al. Preliminary Analysis of Postulated Maximum Accidents for the FFTF, BNWL-760, November 1968.

47. Unpublished Data (FFTF Informal Monthly Progress Report), 1966.

48. J. C. Ringle. Private Communication to R. E. Peterson, BWN, January 1968.

49. J. L. Jaech. Sodium Mass Transfer: XIV, Statistical Analysis of 1961 to 1964 Sample Weight Change Data, GEAP-4830, October 1965.

50. J. F. W. Bishop et al. Design and Development of Fuel and Fuel Elements for PFR, London Conference on Fast Breeder Reactors, 4B/1, BNES, May 1966.

51. T. J. Bennett et al. Seven Rod Sodium Flow Test, FFTF Monthly Informal Progress Report, BNWL-937, p. 4.62, November 1968.

52. M. P. Paidoussis. The Amplitude of Fluid Induced Vibration of Cylinders in Axial Flow, AECL-2225, Chalk River, Ontario, Canada, March 1965.

53. P. D. Cohn et al. Thermal-Hydraulic and Mechanical Aspects of FTR Fuel Pin Spacer Design, BNWL-750, Battelle-Northwest, Richland, Washington, October 1968.

54. T. C. Reihman and F. F. Rotan. Unpublished Data (Leakage Tests), 1969.

55. C. N. Craig et al. In-Pile Comparison of Effective Thermal Conductivity of (PuO_2-UO_2) Mixed Oxides, GEAP-5556, January 1968.

56. A. E. Waltar et al. Considerations on the Use of Fuel Motion Restrictors in the FTR Fuel Pins, BNWL-623, November 1967.

57. J. E. Hanson et al. Experimental Studies of Transient Effects in Fast Reactor Fuels, GEAP-4469, July 1967.

58. A. Ridal et al. Irradiation of UO_2 Fuel Elements to Study Circumferential Ridging of the Sheath, CRFD-1074, (AECL-1463), February 1962.

59. R. M. Berman et al. Irradiation Behavior of Zircaloy-Clad Fuel Rods Containing Dished-End UO_2 Pellets, WAPD-TM-629, July 1967.

60. R. R. Asamoto et al. The Effective Axial and Diametral Thermal Expansion of UO_2 Under a Radial Temperature Gradient, GEAP-5284, October 1966.

61. W. R. Morten et al. Dimensional Behavior of the Experimental Gas - Cooled Reactor Fuel Element at Elevated Temperatures, ORNL-3103, August 1961.

62. M. J. F. Notely et al. The Length Changes of Zircaloy Sheathed UO_2 Fuel Elements During Irradiation, CRFD-1174 (AECL-1846), August 1963.

63. R. E. Skavdah et al. U. S. Experience on Irradiation Performance of UO_2-PuO_2 Fast Reactor Fuel, AIME Nuclear Metallurgy Symposium, Phoenix, Arizona, October 1967.

64. K. M. Swanson et al. Mark II Subassembly - Report on the Examination of DRF-114 at 7.3% Maximum Burnup, TRG Memo 4073-D, July 1967.

65. O. D. Kazachkovskii et al. Study of the Operation of an Assembly of Fuel Elements Containing Plutonium Dioxide Fuel in the BR-5 Reactor (6.1% Burnup), Atomnaya Energiya, 24, 2, pp. 136-143, February 1968 (Translation JPRS 45,100, April 1968), Nuclear Reactors in the Soviet Union, Wash-1060, December 11-22, 1964.

66. Sodium Cooled Reactors Fast Ceramic Reactor Development Program, 27th Quarterly Report, Task F, Integral Fast Flux Irradiations, GEAP-5677, August 1968.

67. J. Veeder. Thermo-Elastic Expansion of Finite Cylinders, AECL-2660, January 1967.

68. A. S. Bain. Comparison Between Elements with Flat and Dished Pellet Ends, Experiment NRX-51000, Chalk River Quarterly Progress Report, PR-CM-49, (Sect. 4.5.4) January-March, 1967.

69. H. Fenech et al. Circumferential Clad Ridging at Fuel-Pellet Interfaces, NUCLEAR APPLICATIONS, 3, p. 406, July 1967.

70. S. J. Stachura (AI, attached to RAPSODIE). Potential Mechanisms for Observed Reactivity Effects in RAPSODIE, Memo S.E.T.R. 67.705, Clt: 1219, Cadarache, November 10, 1967.

71. E. G. Stevens. Pellet End Configuration: Flat Versus Dished Ends, FFTF Monthly Informal Technical Progress Report, BNWL-712, p. 373, February 1968.

72. E. G. Schechtendahl et al. Safety Features of a 300 MWe Sodium Cooled Fast Breeder Reactor (Na-2), KFK-611, Kernforschung-mbh, Karlsruhe, June 1967.

73. A. M. Judd. Loss-of-Coolant Accidents in a Large Sodium Cooled Fast Reactor. Proceedings of the Conference on Safety, Fuels and Core Design in Large Fast Power Reactors, October 11-14, 1956, ANL-7120, Argonne National Laboratory.

74. K. Bagley. UKAEA, Private Communication to T. T. Claudson, BNW, May 1968.

75. A. E. Addal et al. ANS Transactions, Vol. II, No. 2, November 1968, p. 651.

76. A. E. Waltar. Considerations of the Use of Fuel Motion Restrictors in the FTR Fuel Pin, BNWL-623, November 1967.

77. E. L. Zebroski et al. Oxide Fuel Status and Stretch Capabilities, BNWL-268, June 1966.

78. J. M. Yatabe. FTR Thermal-Hydraulic Testing, FFTF Monthly Informal Progress Report, BNWL-1006, p. 4.21, February 1969.

79. C. E. Leach and K. R. Merckx. Unpublished Data, (FFTF Monthly Informal Technical Progress Report), 1966.

80. G. L. Fox and K. R. Mercks, SINTER-A Program for Calculating Radial Temperature Distributions in Oxide Fuel Pins Undergoing Sintering, BNWL-1241, January 1970.

81. R. J. Melosh, P. A. Diether, and M. Brennan. Jet Propulsion Technical Memorandum 33-307, Rev. 1, Structural Analysis for Matrix Interpretive Systems Program Report, December 1966.

82. C. M. Friedrich. SEAL-SHELL-2, A Computer Program for the Stress Analysis of a Thick Shell of Revolution with Axisymmetric Pressures, Temperatures and Distributed Loads, WAPD-TM-398, December 1963.

83. J. W. Hagan. Design Safety Criteria for the First Core Fuel Assembly Component, Section 16, BNWL-823, Battelle-Northwest, Richland, Washington, April 8, 1969.

84. W. J. Freede et al. Static and Sliding Contact Behavior of Materials in Sodium Environments at Elevated Temperatures, NAA-SR-12446, LMEC-AI, September 29, 1967.

85. C. D. Flowers. Structural Analysis of Hexagonal Tube or Ring Under Internal Pressure, BNWL-263, June 1966.

86. FFTF Monthly Informal Technical Progress Report, BNWL-964, P. 1.3, Battelle-Northwest, Richland, Washington, December 1968.

87. W. H. Sutherland. AXICRP - A Finite Element Computer Code for Creep Analysis of Plane Stress, Plain Strain and Axisymmetric Bodies, (Unpublished Data), May 1969.

88. FFTF Monthly Informal Progress Report, BNWL-915, p. 4.127, Battelle-Northwest, Richland, Washington, October, 1968.

89. C. Cawthorne and E. J. Fulton. Voids in Irradiated Stainless Steel, NATURE, Vol. 216, p. 675, November 1967.

90. J. J. Holmes. Fast Reactor Induced Swelling in Austenitic Stainless Steel, BNWL-SA-2126, December 1968.

91. R. W. Hesketh. Collapse of Vacancy Cascades to Dislocation Loops, BNL-50083, September 1967, pp. 389-401.

92. J. W. Joseph, Jr. Stress Relaxation in Stainless Steel During Irradiation, Dp-369, June 1959.

93. E. R. Gilbert (BNW). Stress Dependence of the In-Reactor Uniaxial Creep Rate of Zr-2 and Zr-2.5 Nb, ANS Meeting, Seattle, Washington, June 1969.

94. R. E. Schreiber. Relaxation of Torsional Stresses in Stainless Steel During Irradiation, DP-669, April 1962.

95. G. R. Waymire. Conceptual System Design Description for the Reactor Core - No. 31, A-0036-R2, Battelle-Northwest, Richland, Washington, (Preliminary Report, April, 1969)

96. Development and Testing Program-Hydraulic Core Mockup - 1/2 scale vessel, BNW (In preparation).

97. P. M. Jackson. Hydraulic Balance Concept and Tube Sheet Leakage FFTF Hydraulic Feature Model, BNWL-883, November 1968.

98. E. H. Novendstern. Hydraulic Analyses of the PNL Hydraulic Balance System, WARD-FRT-23, January 31, 1969.

99. Memo, D. L. Condotta to R. W. Dickinson. PNL/FFTF-68765, LMEC Testing in Support of the FFTF Project - Flow Duct/Tubesheet Erosion-Flow Test Part B Sodium Erosion - Flow Leakage Test (T-1B), dated 8-19-68.

100. E. G. Stevens and P. D. Cohn. Conceptual Component Design Description for the First Core Fuel Assembly Component, No. 35, A-0035-R2, Battelle-Northwest, Richland, Washington, (Preliminary Report, April 1969)

101. J. L. Straalsund and H. R. Brager. Cladding Evaluation-Damage Analysis, FFTF Monthly Informal Progress Report, p. 5.8, BNWL-1043, Battelle-Northwest, Richland, Washington, March 1969; also J. J. Holmes, Irradiation Induced Swelling in Nickel Alloys, ANS Transaction, Vol. 12, No. 1, June, 1969.

102. R. J. Jackson et al., Metal Swelling Effects on FTR Core Components, BNWL-1286, March 1970.

APPENDIX

DRAWINGS

SK-3-14581	DRIVER FUEL ASSEMBLY
SK-3-14582	DRIVER FUEL SUBASSEMBLY
SK-3-14583	DRIVER FUEL PIN ASSEMBLY AND DETAILS
SK-3-14584	DRIVER FUEL LOCKING AND SPACER GRID DETAILS

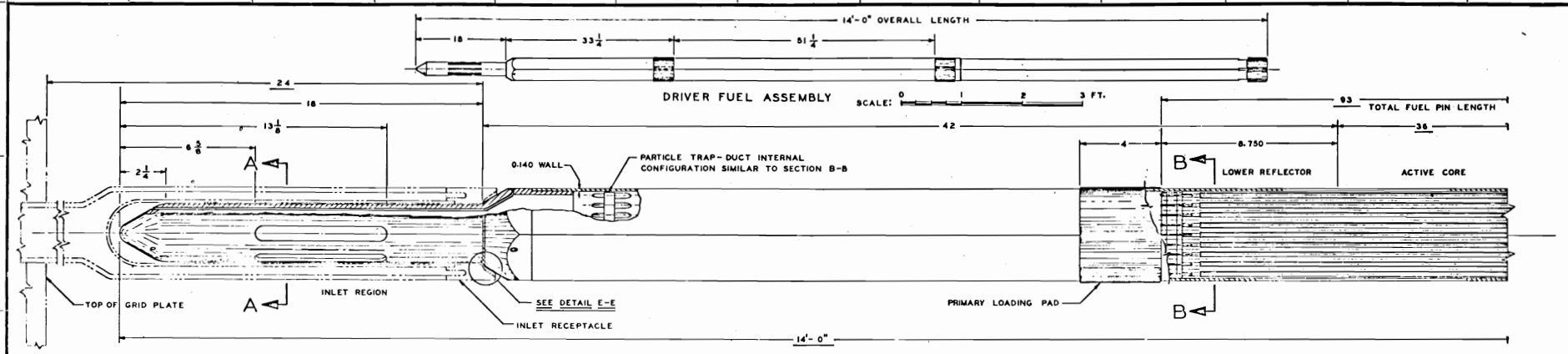

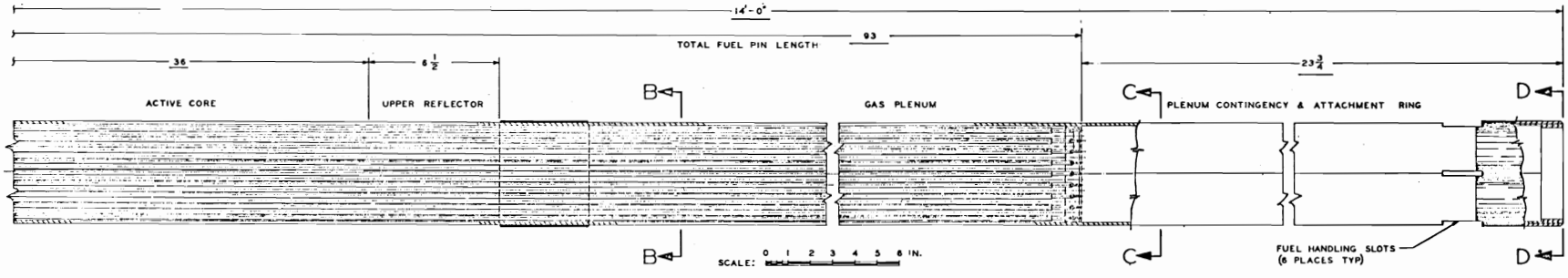

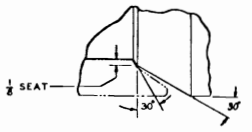

DETAIL E-E

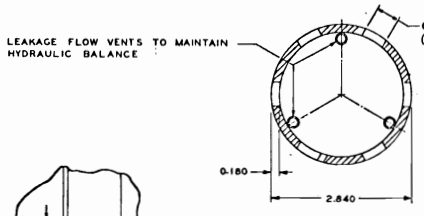

SECTION A-A

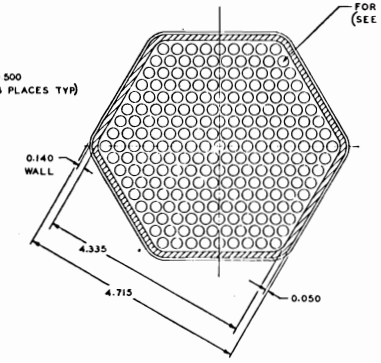

SECTION B-B

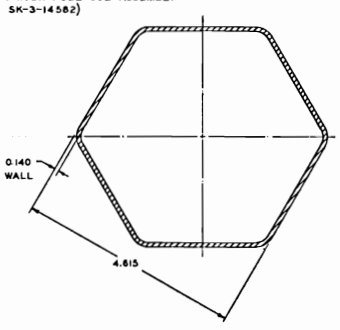

SECTION C-C

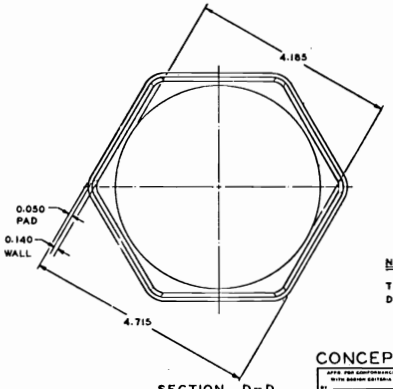

SECTION D-D

SCALE: 0 1 2 3 IN.

NOTE

THIS DRAWING COMPLIES WITH THE DECEMBER 1968 CONCEPT GUIDELINES.

5TH	ISSUE	5-14-69
4TH	ISSUE	3-27-69
3RD	ISSUE	3-3-69
2ND	ISSUE	2-19-69
1ST	ISSUE	2-6-69

CONCEPTUAL

DRAWN	G.R. WAYMIRE	2-6-69
CHECKED	W.U. JACKSON	2-6-69
SCALE	NOTED	
APPROVED		2-6-69

U. S. ATOMIC ENERGY COMMISSION
RICHLAND OPERATIONS OFFICE
PACIFIC NORTHWEST LABORATORY
OPERATED BY BATTELLE MEMORIAL INSTITUTE

DRIVER FUEL ASSEMBLY

FAST FLUX TEST FACILITY

CLASSIFICATION	NONE	DWG NO	SK-3-14581
PROJECT NO	300 GEN	MODEL NO	2200.01

REFERENCE DRAWINGS

NEXT USED ON

REVISIONS

DRAWING STATUS

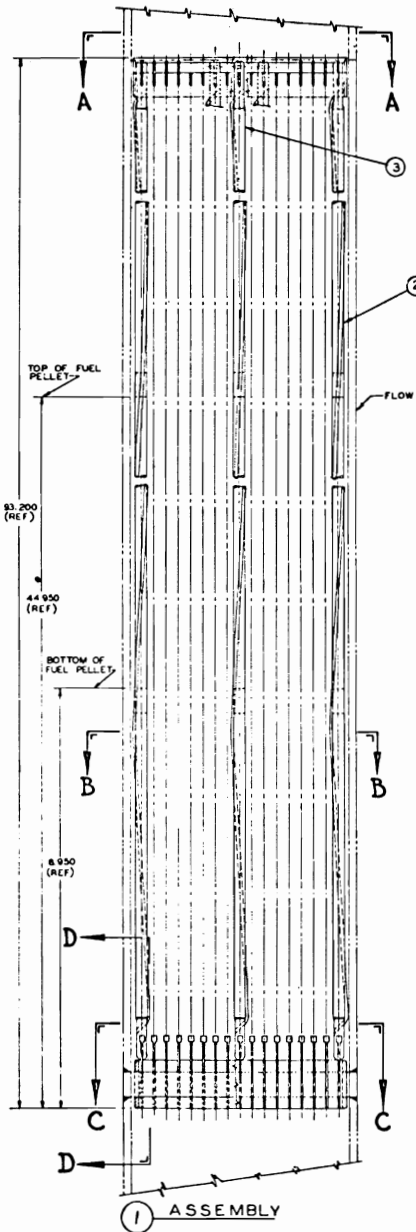

1 ASSEMBLY

SCALE 1 0 1 2 3 IN.

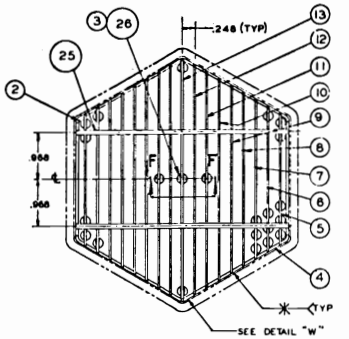

SECTION A-A

(TOP LOCKING GRID)

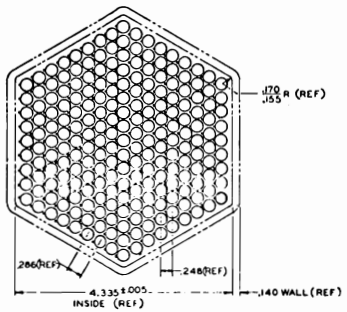

SECTION B-B

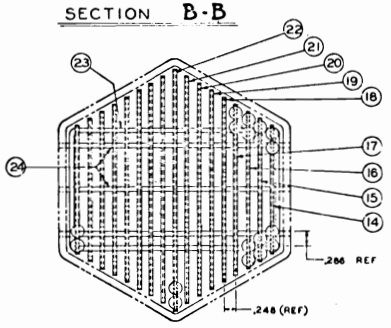

SECTION C-C

(LAYER SPACING GRID)

STEEL STAMP OR ELECTROETCH IN ⅛ CHARACTERS-NUMBERS SUPPLIED BY CUSTOMER.

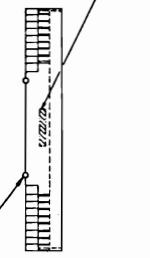

NOTE

1- ASSEMBLE PARTS (5) THRU (13) IN (4) AND WELD.

2- SLOT TOP OF WELD ASSEMBLY WITH $\frac{3}{32}$ X $\frac{3}{64}$ DEEP SLOT 2 PLACES.

3- PLACE PARTS (2) IN SLOTS AND WELD TO ASSEMBLY.

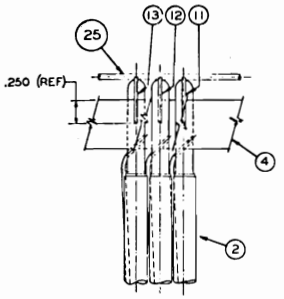

DETAIL "W"

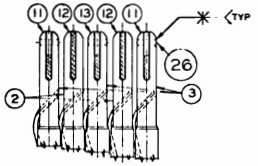

SECTION F-F

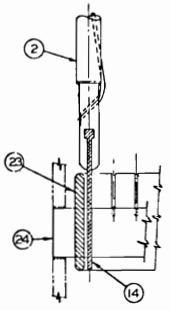

SECTION E-E

SCALE 0 1 IN.

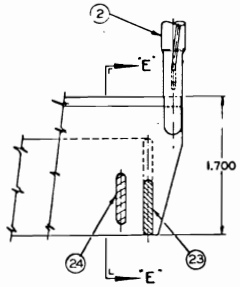

SECTION D-D

SCALE 0 1 IN.

QTY	PART NO.	DESCRIPTION	MAT'L	REF
X	1	FUEL CLUSTER ASSY		
214	2	FUEL PIN ASSEMBLY		SK-3-14583 P-1
3	3	FUEL PIN ASSEMBLY		P-2
1	4	RETAINER BAND		SK-3-14584 P-1
2	5	STRIP- TOP		P-2
2	6			P-3
2	7			P-4
2	8			P-5
2	9			P-6
2	10			P-7
2	11			P-8
2	12			P-9
1	13			P-10
2	14	LAYER SPACING GRID		P-11
2	15			P-12
2	16			P-13
2	17			P-14
2	18			P-15
2	19			P-16
2	20			P-17
2	21			P-18
1	22			P-19
1	23	LAYER LOCKING GRID		P-20
3	24	ELEMENT SUPPORT		P-21
2	25	ROD $\frac{3}{32}$ DIA x 4.142 LG	316 S.S.T.	
3	26	PIN 0.050 $^{+.001}$ DIA x 0.200 $^{\pm.005}$ LG.	316 S.S.T.	

GENERAL NOTES

ALL PARTS, UNLESS OTHERWISE SPECIFIED, SHALL CONFORM TO THE FOLLOWING;

1- TOLERANCES, FRACTIONAL ± $\frac{1}{64}$ DECIMAL ± .005 ANGULARITY ± 0° 30'

2- REMOVE ALL BURRS AND BREAK ALL SHARP EDGES AND CORNERS TO $\frac{1}{64}$ MIN RADIUS.

3- ALL MACHINE SURFACES ▽ SURFACE ROUGHNESS SHALL BE IN ACCORDANCE WITH U.S.A.S.I B 46.1 (LATEST REV)

4- ALL MATERIAL TO BE AS SPECIFIED, OR APPROVED EQUAL QUALITY.

5- MATERIAL 316 S.S.T. TO BE A.S.T.M. SPEC MODIFIED A 213-65 (CARBON 0.04-0.08)

6- SPACER DESIGN UNSPECIFIED PENDING AGREEMENT BETWEEN B.N.W. AND WESTINGHOUSE.

NOTE THIS DRAWING COMPLIES WITH THE DECEMBER 1968 CONCEPT GUIDELINES.

CONCEPTUAL

2ND ISSUE 4-10-69

1ST ISSUE 2-14-69

U. S. ATOMIC ENERGY COMMISSION
RICHLAND OPERATIONS OFFICE
PACIFIC NORTHWEST LABORATORY
OPERATED BY BATTELLE MEMORIAL INSTITUTE

F. F. T. F. DRIVER FUEL SUB-ASSEMBLY

FAST FLUX TEST FACILITY

APPD P. D. COHN

SCALE AS NOTED

300 GEN 300-40

NONE

SK-3-14582 1 1

REFERENCE DRAWINGS

NEXT USED ON

REVISIONS

DRAWING STATUS

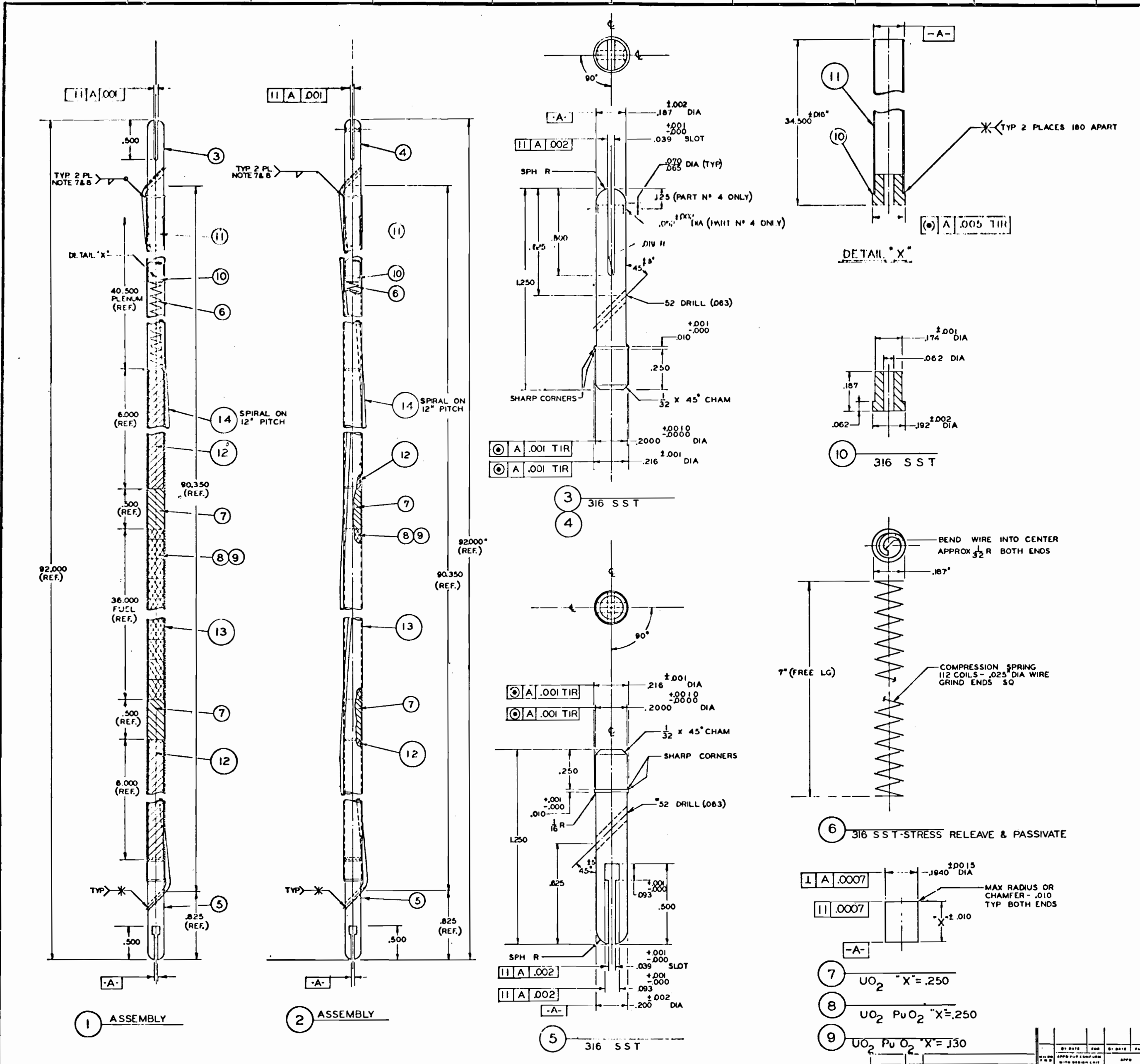

QTY		PT NO	DESCRIPTION	MAT'L
	X	1	ASSEMBLY	
X		2	ASSEMBLY	
	1	3	END CAP - TOP	
1		4	END CAP - TOP	
1	1	5	END CAP - BOTTOM	
1	1	6	SPRING	
AR	AR	7	INSULATOR PELLET	
AR	AR	8	FUEL PELLET	
AR	AR	9	SHIM PELLET	
1	1	10	PLUG	
1	1	11	TUBE - 0.187 ±.002 O.D. x .005 ±.0005 WALL x 34.438" LG	316 SST
1	1	12	ROD - 0.194 ±.001 O.D. x 6.000 LG	316 SST
1	1	13	TUBE - 0.230 ±.001 OD x 0.200 ±.001 I D x 90.000 LG	316 SST
AR	AR	14	WIRE 0.056 ±.001 DIA	316 SST

GENERAL NOTES

ALL PARTS, UNLESS OTHERWISE SPECIFIED, SHALL CONFORM TO THE FOLLOWING:

1. TOLERANCES, FRACTIONAL $\pm\frac{1}{64}$, DECIMAL ±.005, ANGULAR ± 0° 30'
2. REMOVE ALL BURRS AND BREAK SHARP EDGES TO $\frac{1}{64}$ MIN RADIUS, EXCEPT WELD PREP AREA (TUBE ENDS & LIPS)
3. ALL MACHINED SURFACES 32√ SURFACE ROUGHNESS SHALL BE IN ACCORDANCE WITH U S A S I B 46.1 (LATEST REV)
4. ALL MATERIAL TO BE AS SPECIFIED, OR APPROVED EQUAL QUALITY.
5. MATERIAL 316 S S T TO BE A S T M SPEC. MODIFIED A 213-65 (CARBON 0.04-0.06).
6. FUEL PIN SHALL SHOW A MAXIMUM BOW NOT TO EXCEED .010 PER LINEAL FOOT. TOTAL FOR PIN NOT TO EXCEED .025.
7. END CAP WELD DIAMETER SHALL NOT PROJECT MORE THAN .0010 BEYOND THE TUBE DIA.
8. CENTER LINE IN END CAPS SHALL BE SYMMETRICAL TO THE CENTER LINE OF THE SLOTS WITHIN A TOLERANCE OF .001.

NOTE THIS DRAWING COMPLIES WITH THE DECEMBER 1968 CONCEPT GUIDELINES.

CONCEPTUAL

4TH ISSUE 4-18-69
3RD ISSUE 4-10-69
2ND ISSUE 3-10-69
1ST ISSUE 2-14-69

U. S. ATOMIC ENERGY COMMISSION
RICHLAND OPERATIONS OFFICE
PACIFIC NORTHWEST LABORATORY
OPERATED BY BATTELLE MEMORIAL INSTITUTE

F. F. T. F. DRIVER FUEL
FUEL PIN ASSEMBLY & DETAILS

P. D. COHN
W. H. DAVIDSON
SCALE NONE
FAST FLUX TEST FACILITY
300 GEN 490040
NONE SK-3-14583

REFERENCE DRAWINGS
REVISIONS
DRAWING STATUS
NEXT USED ON SK-3-

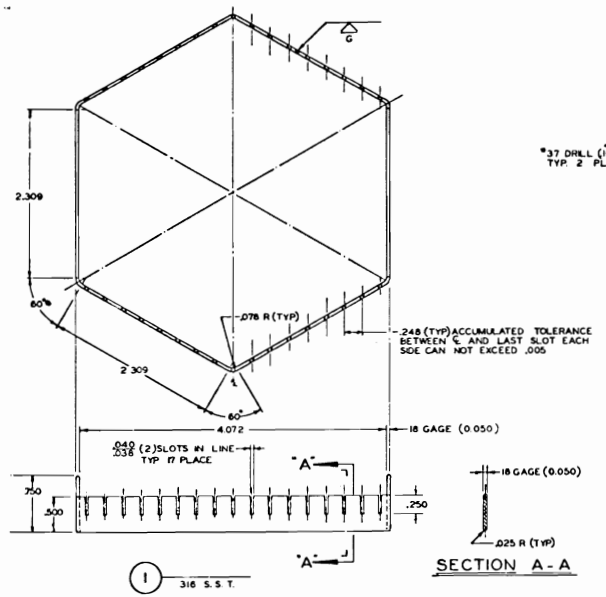

(1) 316 S.S.T.

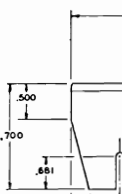

SECTION A-A

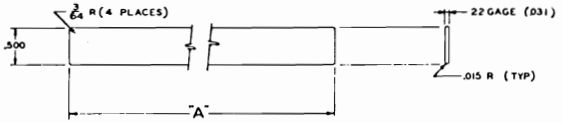

PART Nº	"A"	MATERIAL
2	2.629	316 S S T
3	2.915	
4	3.201	
5	3.487	
6	3.773	
7	4.059	
9	4.531	

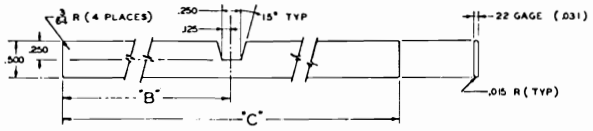

PART Nº	"B"	"C"	MATERIAL
8	2.172	4.345	316 S S T
10	2.395	4.790	

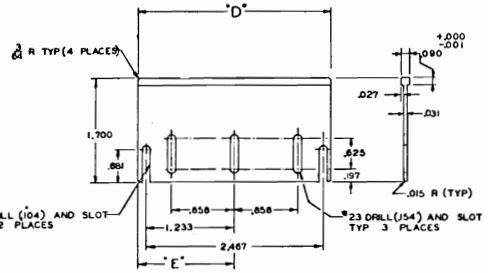

NOTE: ACCUMULATED TOLERANCE BETWEEN FIRST AND LAST HOLES IN ANY CASE CAN NOT EXCEED .005

PART Nº	D	E	MATERIAL
11	2.562	1.281	316 S S T
12	2.848	1.424	

NOTE: ACCUMULATED TOLERANCE BETWEEN FIRST AND LAST HOLES IN ANY CASE CAN NOT EXCEED .005

PART Nº	F	G	MATERIAL
13	3.096	1.548	316 S S T
14	3.382	1.691	
15	3.668	1.834	
16	3.954	1.977	
17	4.240	2.120	
18	4.526	2.263	
19	4.812	2.406	

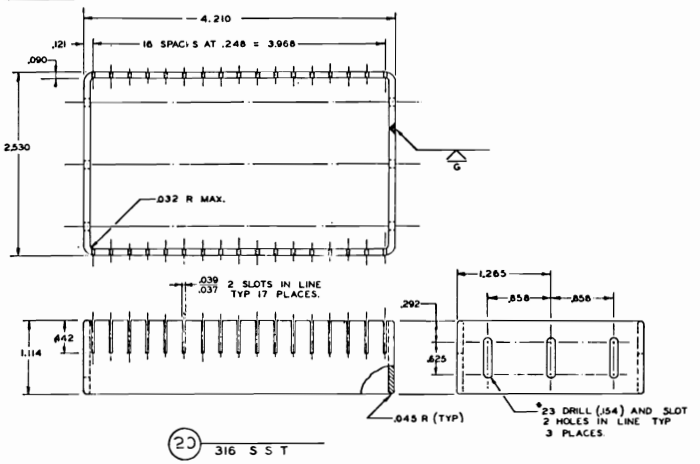

(20) 316 S S T

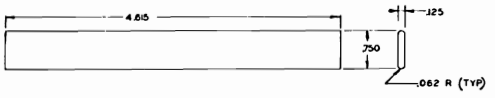

(21) 316 S S T

NOTE THIS DRAWING COMPLIES WITH THE DECEMBER 1968 CONCEPT GUIDELINES.

CONCEPTUAL

1/2ND ISSUE 4-9-69
1ST ISSUE 2-12-69

APPD FOR CONFORMANCE WITH DESIGN CRITERIA		DATE
BY		
FOR		
APPD		
APPD		
APPD	P. D. COHN	12/16/68
DATE APPD		
CHECKED		
DRAWN	W. H. DAVENPORT	11/13/68
SCALE	1/2" = 1"	
CLASSIFICATION	UNCLASSIFIED	DATE 12/16/68

U. S. ATOMIC ENERGY COMMISSION
RICHLAND OPERATIONS OFFICE
PACIFIC NORTHWEST LABORATORY
OPERATED BY BATTELLE MEMORIAL INSTITUTE

F. F. T. F. DRIVER FUEL LOCKING & SPACER GRID DETAILS

FAST FLUX TEST FACILITY
300 GEN | PLNG NO. 4900.40 | SHEET NO. 1 | SHEETS IN SET 1

DWG NO. SK-3-14584 REV NO. 1

DWG NO	REV NO	DRAWING TITLE OR INDEX NO
REFERENCE DRAWINGS		
NEXT USED ON		

BY	DATE	FOR	BY	DATE	FOR	REV BY	DESCRIPTION	REV NO

REVISIONS

COMMENT PRT ISSUE NO	DATE	CHECK PRT ISSUE NO	DATE	LAST REV

DRAWING STATUS

NONE

DISTRIBUTION

No. of Copies

OFFSITE

1 AEC Chicago Patent Group

G. H. Lee

26 AEC Division of Reactor Development and Technology

Director, RDT
Asst Dir for Nuclear Safety
Analysis and Evaluation Br, RDT:NS
Asst Dir for Plant Engrg, RDT
Facilities Br, RDT:PE
Components Br, RDT:PE
Instrumentation & Control Br, RDT:PE
Liquid Metal Systems Br, RDT:PE
Asst Dir for Program Analysis, RDT
Asst Dir for Project Mgmt, RDT
Liquid Metals Projects Br, RDT:PM
FFTF Project Manager, RDT:PM
Asst Dir for Reactor Engrg, RDT
Control Mechanisms Br, RDT:RE
Core Design Br, RDT:RE (2)
Fuel Engineering Br, RDT:RE
Fuel Handling Br, RDT:RE
Reactor Vessels Br, RDT:RE
Coolant Chemistry Br, RDT:RT
Fuel Recycle Br, RDT:RT
Fuels & Materials Br, RDT:RT
Reactor Physics Br, RDT:RE
Special Technology Br, RDT:RT
Asst Dir for Engrg Standards, RDT
EBR-II Project Manager, RDT:PM

215 AEC Division of Technical Information Extension

1 AEC Idaho Operations Office
Nuclear Technology Division

C. W. Bills, Director

1 AEC San Francisco Operations Office
Director, Reactor Division

No. of Copies	
5	AEC Site Representatives Argonne National Laboratory - CH Atomics International General Electric Co. Westinghouse Electric Corporation Argonne National Laboratory - ID
3	Argonne National Laboratory R. A. Jaross LMFBR Program Office N. J. Swanson
1	Atomic Power Development Associates Document Librarian
5	Atomics International FFTF Program Office
2	Babcock & Wilcox Co. Atomic Energy Division S. H. Esleeck G. B. Garton
1	Bechtel Corporation J. J. Teachnor
1	BNW Representative R. M. Fleishman (ZPPR)
1	Combustion Engineering 1000 MWe Follow-On Study W. P. Staker, Project Manager
1	Combustion Engineering 911 West Main Street Chattanooga, Tennessee 37401 Mrs. Nell Holder, Librarian
3	General Electric Company Advanced Products Operation Karl Cohen
1	General Electric Company Nucleonics Laboratory P.O. Box 846 Pleasanton, California 94566 Dr. H. W. Alter

No. of Copies	
2	Gulf General Atomic Inc. General Atomic Division D. Coburn
1	Idaho Nuclear Corporation J. A. Buckham
1	Liquid Metal Engineering Center R. W. Dickinson
2	Liquid Metal Information Center A. E. Miller
1	Oak Ridge National Laboratory W. O. Harms
1	Stanford University Nuclear Division Division of Mechanical Engrg R. Sher
1	United Nuclear Corporation Research and Engineering Center R. F. DeAngelis
10	Westinghouse Electric Corporation Atomic Power Division Advanced Reactor Systems D. C. Spencer

ONSITE-HANFORD

1	AEC Chicago Patent Group R. K. Sharp
3	RDT Assistant Director for Pacific Northwest Laboratories T. A. Nemzek
2	AEC Richland Operations Office J. M. Shivley
3	Battelle Memorial Institute

No. of Copies	
1	Bechtel Corporation
	W. A. Smith (Richland)
4	WADCO
	W. H. Esselman
	W. M. Gajewski
	J. M. Norris
	B. G. Rieck
1	Westinghouse Electric Corporation
	J. D. Herb
46	Battelle-Northwest
	A. L. Bement
	W. L. Chase
	J. C. Cochran
	P. D. Cohn
	J. F. Erben
	E. A. Evans
	P. L. Hofmann
	R. J. Jackson
	D. C. Kolesar
	F. J. Leitz
	W. B. McDonald
	J. S. McMahon
	C. L. Mohr
	A. Padilla, Jr.
	R. E. Peterson
	J. M. Seehuus
	R. J. Squires
	E. G. Stevens (5)
	J. H. Westsik
	C. L. Wheeler
	B. Wolfe
	Legal-703 Bldg.
	Legal-ROB, 221-A
	BNW-Technical Information (5)
	BNW-Technical Publication (3)
	FFTF File (703) (10)
	FFTF TPO (703)